Università di Genova | PhD IMEG
Dottorato in Ingegneria meccanica, energetica e gestionale

PhD Thesis
Department of Mechanical, Energetics and Management Engineering (IMEG)
Curriculum: Building Physics and Building Energy Systems
Cycle: XXXVIII

Eng. Juliana Peshku

Port and Port Hinterlands Environmental Sustainability
Analysis, Impact, and Mitigation

Supervisor:
Prof. Eng. Corrado Schenone

Co-Supervisor 1:
Prof. Eng. Davide Borelli
Co-Supervisor 2:
Dr. Augusto Bocanegra

Reviser 1:
Prof. Eng. Vincenzo Bianco
Reviser 2:
Prof. Eng. Marina Neophytou
Reviser 3:
Prof. Eng. Tania Rodriguez
Reviser 4:
Dr. Petros Mouzourides

April 2026

Abstract

European ports are key nodes in global supply chains and energy systems, yet their close integration with urban environments increasingly gives rise to environmental and social challenges. Environmental noise, building energy consumption, and greenhouse gas emissions represent key sustainability issues affecting port–city systems, including port operational areas, hinterlands, and surrounding urban environments. Despite growing attention, mitigation strategies are often addressed separately, while coordinated approaches remain limited.

This doctoral research proposes a multidisciplinary framework structured around three complementary pillars: environmental acoustics, renewable energy integration, and building energy efficiency, addressing key dimensions of environmental sustainability. While energy efficiency and renewable energy are directly coupled, environmental acoustics is addressed as a parallel and complementary domain; however, acoustic mitigation interventions, particularly through material solutions at building and urban scales, can directly or indirectly influence building energy performance, an interaction to be explored in subsequent phases of the research.

The first pillar investigates port noise through regulatory analysis, measurement techniques, and source identification, with particular focus on transport-related contributions. Acoustic measurements, including acoustic camera analysis and phonometric monitoring, are combined with noise perception assessment through Willingness to Pay (WTP) method. Mitigation strategies are explored through experimental characterization of novel sound-absorbing materials. Mitigation strategies are explored through experimental characterization of novel sound-absorbing materials. Multilayer systems achieve absorption coefficients up to 1.0, while perforated 3D-printed panels combined with porous materials reach peaks of 0.96 in the 1000–2200 Hz range, due to combined resonant and porous dissipation mechanisms. The second pillar addresses renewable energy integration through photovoltaic systems and Renewable Energy Communities (RECs), proposing an inclusive configuration that enables participation of economically, socially, and regulatorily constrained stakeholders. Results show that REC performance strongly depends on the temporal alignment between energy production and consumption. The third pillar focuses on building energy efficiency, using dynamic modelling (EnergyPlus and certified Italian software) to determine optimal insulation thickness based on annual energy cost balance. Results highlight the importance of occupancy schedules and internal gains, and show that energy efficiency measures significantly modify consumption profiles, directly influencing REC performance and economic benefits.

Overall, the study demonstrates that coordinated but distinct interventions across acoustics, energy efficiency, and renewable energy can support more sustainable,

resilient, and socially inclusive port–city systems, providing a transferable framework combining experimental, modelling, and socio-economic approaches.

Acknowledgements

The PhD journey has been dynamic and demanding, marked by both challenges and achievements. I am grateful to have reached its conclusion and to present the results of the work developed throughout this period. I also acknowledge the institutional support of the University, which provided the academic framework for the completion of this research.

I would like to express my gratitude to my supervisor for the guidance provided throughout the development of this PhD research. I am also thankful to my co-supervisors for their feedback and insightful discussions during the course of this work.

I would like to thank the external reviewers for their time and for their independent evaluation of this thesis, which I greatly appreciate as an important contribution to the validation and improvement of the research.

Several aspects of this work were developed within a stimulating academic and collaborative environment, particularly through the scientific activities carried out within the European projects in which I was involved. These activities offered valuable opportunities for interdisciplinary exchange and discussion. I am grateful to the colleagues of the research group and to the many professionals and researchers encountered during conferences, training activities, and project meetings, whose perspectives and interactions have contributed to shaping this research. I also wish to acknowledge the professors and former employers who, at different stages of my academic and professional path, provided guidance, inspiration, and opportunities that supported the development of this work.

Finally, I would like to express my deepest gratitude to my family for the values they instilled in me and for their continuous support throughout my journey. I am deeply grateful to my husband, whose unwavering presence, understanding, and constant support gave me strength and balance throughout the years of this PhD journey, and to my friends for their constant encouragement.

Table of Contents

List of Figures

List of Tables

List of Abbreviations

Acoustic Abbreviations

α – Sound Absorption Coefficient
R – Reflection Coefficient
Z_c – Acoustic Impedance
k_c – Complex Wave Number
c – Speed of Sound
ρ – Air Density
dB – Decibel
dB(A) – A-weighted Sound Pressure Level
SEL - Sound Exposure Level
L_{Aeq} - A-weighted Equivalent Continuous Sound Level

Renewable Energy and REC Abbreviations

GHG – Greenhouse gas emissions
PV – Photovoltaic
REC – Renewable Energy Community
RES – Renewable Energy Sources
POD – Point of Delivery
SCS – Self-Consumption Scheme
ISC – Individual Self-Consumption
ToR – Terms of Reference
KFI – Knowledge Facility Instrument
NBS – Nature-Based Solutions
SDG – Sustainable Development Goals

Energy Efficiency and Building Physics Abbreviations

HVAC – Heating, Ventilation and Air Conditioning
HDD – Heating Degree Days
DHW – Domestic Hot Water
U-value – Thermal Transmittance Coefficient
S/V – Surface-to-Volume Ratio
BEM – Building Energy Model
UHI – Urban Heat Island

Institutional and Data Source Abbreviations

ARPAL – Regional Agency for Environmental Protection of Liguria
ARERA – Italian Regulatory Authority for Energy, Networks and Environment
ISTAT – Italian National Institute of Statistics
GSE – Energy Service Manager

1. Introduction

1.1 Research context and Motivation

Ports in Europe serve as vital gateways to global markets and play a central role in international supply chains, making them a cornerstone of national and regional infrastructure systems [1, 2]. Within the European Union, ports display a wide range of operational profiles, including passenger, cruise and ferry terminals, offshore and energy hubs, urban ports, island ports, as well as large industrial and logistics platforms. As such, ports are key drivers of economic development, facilitating international trade, supporting industrial activity, and creating employment opportunities [3]. By connecting maritime transport with inland logistics and industrial networks, ports strengthen supply chains across multiple sectors and enhance the competitiveness of national economies. In addition, ports increasingly function as energy hubs, playing a strategic role in ensuring Europe's energy security and supporting the transition toward low-carbon energy systems. Through the development of renewable energy infrastructures, alternative fuels, and energy distribution networks, ports contribute not only to economic growth but also to broader societal and environmental objectives [4, 5].

However, the economic benefits associated with port activities are accompanied by significant environmental impacts and social challenges, particularly affecting public health and the quality of life of nearby communities [6, 7]. Shipping and port-related operations represent major sources of greenhouse gas emissions (GHG) [8, 9] and environmental noise [10, 11]. Emissions generated by vessel propulsion systems, auxiliary engines, cargo handling operations, and hinterland transport contribute significantly to air pollution and climate change [12]. At the same time, port infrastructures are often located in close proximity to densely populated urban areas and historical city centers, intensifying the impact of noise on human health, quality of life, and social acceptance of port activities [13, 14]. Beyond atmospheric and acoustic concerns, port expansion and increased maritime traffic pose risks to coastal and marine ecosystems, including habitat loss, pollution, and biodiversity degradation [15]. These issues highlight the need to reconsider the role of ports within contemporary society, recognizing that while the ports of today have been essential to economic development, the ports of tomorrow must evolve toward sustainable, resilient, and socially integrated systems [16-17].

In response to these challenges, the European Union has developed a comprehensive policy framework aimed at guiding ports toward greater environmental sustainability. Key initiatives include the European Green Deal which provides the overarching policy reference for this thesis, as well as the Fit for 55 Package, the Green Ports Initiative, EcoPorts, the Ports and Maritime Decarbonization (PMD) strategy, the Trans-European Transport Network (TEN-T), and the EU Emissions Trading System (EU ETS). Collectively, these initiatives aim to reduce emissions, enhance energy efficiency, and protect ecosystems while preserving the economic competitiveness of the European port sector. The European Green Deal sets ambitious long-term objectives, including a 90%

reduction in emissions from the transport sector by 2050, while the International Maritime Organization (IMO) targets at least a 40% reduction in GHG from international shipping. Within this evolving regulatory landscape, European ports are expected to attract net-zero industries, integrate renewable energy systems, and balance decarbonization goals with operational efficiency and economic viability.

The environmental priorities of European ports are regularly assessed by the European Sea Ports Organization (ESPO). According to the ESPO, climate change remains the foremost concern for port authorities, followed by a set of closely interrelated priorities, including air quality, energy efficiency, port development (land-related), noise, water quality, ship waste, port waste, and relationships with local communities [18]. Noise continues to be identified as a relevant environmental issue, particularly in ports characterized by strong spatial interaction with urban environments. These priorities are firmly embedded in the strategic and operational agendas of European ports and reflect the increasing need to address environmental impacts in an integrated manner [19].

Addressing these environmental challenges requires significant financial resources. ESPO's Port Investments Study, published in April 2024, estimates that European ports will need approximately 80 billion euros in investments over the period 2024–2034. Investments related to sustainability and energy transition represent the second largest category, accounting for approximately 24% of total planned investments, following investments in the expansion of port basins, quays, or terminals, which account for 26% [20]. In parallel, a growing number of European co-funded research and innovation projects have been launched to support port–city systems in managing environmental issues and achieving sustainability objectives. Among these, the Interreg Maritime project CLASTER [21] as well as the Interreg Euro-MED EnerCmed project [22], are directly linked to the research activities presented in this thesis and provide practical frameworks for testing and validating mitigation measures in real port and port-hinterland contexts.

Despite the extensive body of research and the increasing number of funded initiatives addressing port and port hinterland sustainability, the results achieved so far remain insufficient to meet the ambitious targets set by European policies. Existing studies have primarily focused on noise assessment and mitigation [23-26], reduction of energy consumption through targeted interventions [27], and lowering CO_2 emissions through the integration of renewable energy systems [28, 29]. Despite the progress achieved in noise assessment and mitigation, as well as in advancing the transition toward climate neutrality through energy efficiency measures and the integration of renewable energy systems, recent evaluations of the implementation of the European Green Deal indicate that further acceleration is still required. This highlights the persistence of important gaps and the need for additional efforts to effectively achieve its objectives [30]. These include standardized methodologies for noise assessment in port areas, the limited availability of lightweight, thin, and fire-resistant sound-absorbing materials capable of providing effective acoustic absorption over a wide frequency range, as well as the lack of integrated methodologies that simultaneously address energy efficiency in buildings and the balance between energy consumption and renewable energy production through appropriate Renewable Energy Community (REC) configurations. Moreover, the inherent uniqueness

of each port and its hinterland composition defined by specific operational, geographical, and regulatory conditions complicates the standardization and scalability of proposed solutions.

1.2 Methodological approach

To address the environmental challenges associated with port–city systems, this PhD thesis adopts a multidisciplinary methodological framework structured around three main phases: analysis through experimental measurements, impact assessment through modelling and social perception, and mitigation through material-based solutions, building-scale interventions, and community-level strategies (REC). The methodology integrates advanced acoustic measurements, including acoustic camera analysis and phonometric monitoring, combined with the evaluation of noise perception among exposed populations through Willingness to Pay (WTP). These approaches support both the identification of dominant noise sources and the definition of mitigation strategies. In parallel, a framework for Renewable Energy Community (REC) configuration is developed, based on energy modelling and electricity demand profiles, explicitly incorporating economically, socially, and regulatorily constrained stakeholders to promote a more inclusive energy transition. Building energy modelling is employed to determine the optimal insulation thickness, accounting for operational characteristics such as occupancy schedules and internal gains. The resulting electricity demand profiles are then used to re-simulate REC configurations, enabling the assessment of how energy efficiency measures influence energy balance, self-consumption, and shared energy within the community, as well as the associated economic performance.

1.3 Objectives and Contributions of the Thesis

The main objective of this doctoral research is to contribute to the environmental sustainability of port–city systems, including port operational areas, hinterlands, and surrounding urban environments where port activities interact with the rest of the city. The study develops coordinated methodologies to address key challenges related to port noise impact, building energy consumption, and renewable energy integration, while supporting a more sustainable environment and socially inclusive energy transition.

Research Questions

The research is structured around the following questions:

- RQ1. *How can environmental noise in complex port–city environments be robustly characterized through the integration of advanced acoustic measurements and perceptual indicators, and how can this combined approach improve the interpretation of noise impact on exposed populations?*

- RQ2. *To what extent can novel multilayer, polyimide foam, and perforated acoustic materials, experimentally characterized under controlled conditions, achieve high sound absorption performance, and what potential applicability can be identified for noise mitigation?*
- RQ3. *How can photovoltaic-based Renewable Energy Communities be optimally configured to integrate economically, socially, and regulatorily constrained stakeholders, and what is the resulting impact on energy sharing efficiency and socio-economic benefits?*
- RQ4. *How does the determination of optimal insulation thickness based on annual energy cost balance (heating and cooling) vary with building use, occupancy schedules, and climatic conditions, and how does this differ from conventional regulatory approaches?*
- RQ5. *How do energy efficiency interventions alter electricity consumption profiles in both magnitude and temporal distribution, and how do these changes influence the energy balance, self-consumption rates, and economic performance of Renewable Energy Communities?*

Main Contributions

The main contributions of the thesis are summarized as follows:

1. *Integrated noise assessment combining physical and perceptual dimensions*
   The thesis proposes an integrated framework for port noise characterization that integrates advanced acoustic measurements, including acoustic camera analysis and phonometric monitoring with perceptual indicators based on Willingness to Pay (WTP). This approach enables a more comprehensive interpretation of environmental noise by linking objective sound levels with their socio-economic impact, supporting more informed mitigation strategies.
2. *Experimental characterization of novel sound-absorbing materials for port environments*
   The work provides experimental characterization of the acoustic performance of multilayer systems, mechanically reticulated polyimide foams, and perforated configurations, showing high absorption coefficients (up to 0.95–1) under controlled conditions and identifying their potential applicability for compact noise mitigation solutions.
3. *Inclusive Renewable Energy Community (REC) configuration methodology*
   A methodological framework for photovoltaic-based Renewable Energy Communities is developed, explicitly incorporating economically, socially, and regulatorily constrained stakeholders. This contribution extends conventional

REC approaches by enabling a more inclusive energy transition and improving the distribution of energy and economic benefits.

4. *Dynamic determination of optimal insulation thickness*
   The thesis introduces a dynamic methodology for defining optimal insulation thickness based on the minimization of annual energy costs for heating and cooling, explicitly accounting for building use, occupancy schedules, and internal gains. The results highlight the non-linear response of energy demand to increasing insulation, with decreasing heating needs and increasing cooling demand, enabling the identification of an optimal insulation level for the analyzed building typology.

5. *Quantification of the interaction between energy efficiency and REC performance*
   The research demonstrates that energy efficiency measures significantly modify electricity consumption profiles, affecting both magnitude and temporal distribution. Through re-simulation of REC configurations, the study evaluates how these changes influence self-consumption, energy balance, and economic performance at the community level.

Validated Methodologies and Case-Study Applications

The thesis combines methodological developments with applied case studies.

- Validated methodologies include:
  - (i) the integrated framework for noise assessment combining measurements and perception analysis;
  - (ii) the approach for inclusive REC configuration;
  - (iii) the dynamic modelling methodology for hourly consumption profile and optimal insulation thickness definition.

- Case-study applications include:
  - (i) the identification and characterization of truck traffic and railway noise within the port area;
  - (ii) the experimental acoustic characterization of sound-absorbing materials;
  - (iii) the evaluation of photovoltaic-based REC scenarios;
  - (iv) the analysis of building energy performance under different insulation configurations and their impact on demand profiles.

1.4 Structure of the Thesis

The thesis is organized into several chapters that progressively present the research context, methodological framework, and the experimental and modelling analyses

developed throughout the study. The overall structure of the work related to the three research pillars and the corresponding chapters, is schematically illustrated in Figure 1.

Chapter 1 introduces the research context related to the sustainability challenges of port–city systems and presents the methodological approach, the objectives, and the main contributions of the thesis.

Chapter 2 focuses on environmental acoustics in port-city environments. It reviews the regulatory framework governing environmental noise, describes the measurement methodologies adopted for outdoor noise assessment, and identifies the main noise sources associated with port activities, including shipping, port machinery, focusing on truck traffic, and rail operations. The chapter also investigates noise perception among exposed populations and introduces the principles of sound absorption materials and their acoustic characterization. Finally, it discusses noise mitigation strategies based on novel sound-absorbing materials, including multi-layer porous absorbers and 3D printed perforated systems.

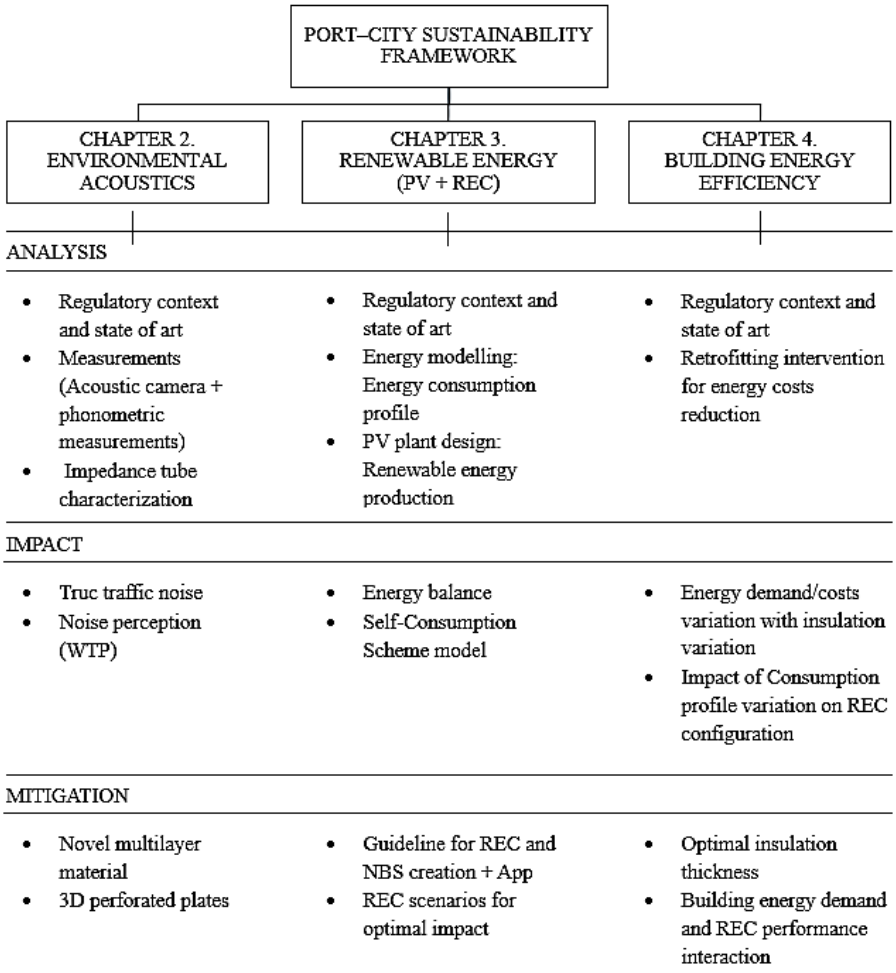

Figure 1. Conceptual framework of the thesis

Chapter 3 addresses renewable energy integration in port and port-hinterland contexts, with particular reference to the EnerCmed project. It presents the regulatory framework and state of the art and introduces the methodological framework for the development of RECs, including energy modelling, photovoltaic system assessment, and scenario analysis. The chapter further presents an original contribution consisting of the development of a guideline and a support tool (app) for the implementation of RECs and Nature-Based Solutions (NBS), followed by the configuration and evaluation of REC scenarios in terms of energy balance and socio-economic performance.

Chapter 4 focuses on building energy efficiency, presenting the development of the building energy model and the evaluation of the optimal insulation thickness based on the annual energy balance considering both heating and cooling costs. The chapter also discusses the Incentives for the implications of insulation strategies for public administrations and their potential interaction with RECs through the modification of electricity consumption profiles.

Chapter 5 summarizes the main findings and discusses their limitations, transferability, and future research directions, structured according to the three pillars of the proposed methodologies for improving the environmental sustainability of port–city systems.

2. Sustainability of ports and port hinterlands in terms of noise reduction

2.1 Regulatory framework

Noise pollution remains a significant environmental health issue in Europe. Scientific research has demonstrated that prolonged exposure to elevated levels of noise pollution can result in serious health consequences, particularly affecting extensive regions of the human endocrine system and brain [31, 32]. Several countries use surveys to assess the perception of noise in the general population. The last European Quality of Life survey, carried out 2016–2017, found that 32% of more than 30.000 participants across Europe reported problems with noise in the immediate neighborhood of their home [33].

Regulatory frameworks governing noise pollution exist at various levels. Both European and national legislative instruments address the noise generated by roadways, railways, airports, and industrial activities. However, these regulations do not specifically target the noise produced by port operations [34].

2.1.1 European framework

At the European level, the regulatory framework on environmental noise is well developed for transport and industrial sectors but remains incomplete with regard to port activities. Existing legislation addresses noise from road traffic, railways, airports and major industrial facilities, yet no specific provisions explicitly target port noise. Consequently, the acoustic impacts generated by port operations, including cargo handling, ship maneuvering and related logistics, are only indirectly covered within broader environmental noise policies.

The cornerstone of European legislation on environmental noise is Directive 2002/49/EC, commonly known as the Environmental Noise Directive. This directive establishes a common approach for the assessment and management of environmental noise with the overarching objective of preventing, avoiding, or reducing the harmful effects of noise exposure on human health and the environment. It focuses primarily on major noise sources, including road traffic, railways, airports, and large industrial facilities, and requires Member States to produce strategic noise maps and action plans for agglomerations and key transport infrastructures [35]. However, despite its comprehensive scope, the directive does not explicitly regulate port activities as a distinct noise source. Instead, port-related noise emissions are generally subsumed under the broader category of industrial noise, which fails to fully capture the operational complexity and multimodal nature of ports.

In an effort to ensure consistency and comparability in noise assessment across Member States, the European Commission launched in 2008 the CNOSSOS EU project, coordinated by the Joint Research Centre (JRC). The initiative aimed to harmonize

methodologies for determining noise exposure and to provide a shared technical and scientific basis for policy making. By standardizing the calculation procedures, input data requirements and modelling approaches, CNOSSOS EU enabled the production of comparable noise indicators across Europe, thus supporting more coherent environmental noise management strategies. The outcomes of the CNOSSOS EU project were formally integrated into EU legislation through Directive (EU) 2015/996, which amended Annex II of Directive 2002/49/EC. This directive established common assessment methods to be used by all Member States for strategic noise mapping, thereby strengthening the technical robustness and harmonization of noise evaluation across Europe [36].

Nevertheless, even with the adoption of these advanced methodological tools, the regulatory framework still does not specifically address the peculiarities of port-generated noise. The acoustic impacts associated with shipping operations, cargo handling equipment, and intermodal freight flows remain largely embedded within the broader classification of industrial noise, leading to a partial and sometimes inadequate representation of port-related environmental pressures.

Consequently, despite the significant progress achieved at the European level in terms of methodological harmonization and environmental noise governance, a dedicated policy framework tailored to the specific characteristics of port activities is still lacking. This gap highlights the need for more targeted regulatory instruments capable of capturing the multifaceted nature of port noise and supporting more effective mitigation strategies within coastal and urban port areas.

2.1.2 National Framework: Italy

In Italy, the regulation of noise pollution is structured through a combination of civil, criminal and environmental legislation. However, similarly to the European context, these provisions address noise in a general manner and do not establish a specific regulatory framework dedicated to port activities.

At the civil law level, Article 844 of the Italian Civil Code governs nuisances between neighboring properties. According to this provision, individuals exposed to noise emissions may seek legal protection when such disturbances exceed the threshold of "normal tolerability," which is assessed case by case by the competent judicial authority. This article is frequently invoked in disputes related to industrial or transport noise, including those associated with port areas, especially where residential zones are located in close proximity to port operations [37].

Instead, Article 659 of the Italian Criminal Code addresses the disturbance of public peace and people's rest [38]. The provision penalizes anyone who, through noise or other disturbances, disrupts the rest or occupations of a large number of people. Although not specifically designed for environmental noise management, it can be applied to severe noise emissions originating from port operations when they cause widespread disturbance.

The primary legislative reference for environmental noise in Italy is Law No. 447 of 26 October 1995 [39], known as the "Framework Law on Noise Pollution," together with its implementing decrees. Article 2 of this law defines noise pollution as the introduction of noise into the living or external environment that causes annoyance, disturbance to rest and human activities, risks to human health, or deterioration of ecosystems, material goods and cultural heritage. The law establishes the fundamental principles for the protection of both the living and external environment from noise generated by major sources such as road, rail and airport traffic, as well as industrial activities. Nevertheless, it does not provide a specific regulatory discipline for noise produced by port operations, which are generally assimilated to industrial sources within the broader environmental noise framework.

In order to align national legislation with European requirements, Legislative Decree No. 42 of 17 February 2017 amended Legislative Decree No. 194/2005, which transposed Directive 2002/49/EC on environmental noise [40]. The decree redefined procedures and institutional responsibilities for strategic noise mapping and the preparation of action plans aimed at reducing environmental noise exposure, while also strengthening provisions on public information and participation. In particular, it mandated the replacement of Annex II on methods for determining acoustic descriptors with the common European assessment methods introduced by Directive (EU) 2015/996, thereby ensuring methodological harmonization with the CNOSSOS-EU framework.

Within this evolving regulatory and technical context, the technical specification UNI/TS 11844:2022 provides complementary guidance on the measurement and analysis of intrusive noise in indoor environments [41]. The document establishes standardized procedures for identifying and quantifying noise events penetrating buildings from external or internal sources, defining measurement conditions, instrumentation requirements, data acquisition and analysis methods, and reporting criteria. By enabling consistent and repeatable assessments of indoor acoustic disturbance, the specification supports the evaluation of noise impact on occupants and the verification of compliance with applicable acoustic comfort and regulatory limits.

More recently, the Ministerial Decree of 5 August 2024 introduced technical criteria concerning the acoustic emission of road pavements, published in the Official Gazette of the Italian Republic on 23 August 2024 [42]. The measure applies to bituminous mixtures used in closed-type wearing course layers in accordance with the UNI EN 13108 standard and is relevant for road sections included in Noise Containment and Reduction Plans established under Law 447/95. The decree requires that, for both new roads and those subject to maintenance or upgrading, pavement materials must guarantee not only the required mechanical performance but also a specified acoustic emission level, expressed as LCPX and measured using the Close Proximity (CPX) method in accordance with UNI EN ISO 11819-2 [43]. The verification tests must be carried out within a defined timeframe after the opening of the road section to traffic, as detailed in the relevant technical specifications. Although primarily focused on road infrastructure, this provision is indirectly relevant to port contexts, where road transport constitutes a major source of noise within and around port areas.

Overall, the Italian regulatory framework provides several legal and technical instruments to address environmental noise, but it lacks a dedicated, sector-specific discipline for port noise. Consequently, noise generated by port activities continues to be managed through a combination of general environmental noise legislation, civil and criminal provisions, and infrastructure-related technical standards.

Regional Framework

At the dock level, port noise emissions are emerging as a significant and cross-cutting issue across various Italian contexts.

The year prior to the entry into force of Framework Law 447 of 1995, the Liguria Region, based on the administrative norms established by the Decree of the President of the Council of Ministers of March 1, 1991, "Maximum Noise Exposure Limits in Residential and External Environments" [44], had already enacted its own law (Regional Law 31/1994 "Guidelines for the Containment and Reduction of Noise Pollution"), which was reviewed and updated by the subsequent Regional Law No. 12/1998, setting standards for the protection of both the external and residential environments from noise pollution [45].

Subsequent investigations into the issue, conducted through specific noise measurement campaigns across the Liguria region, identified vehicle traffic as the main source of environmental noise. The areas most affected are in the cities of Genoa, Savona, and La Spezia, which are characterized not only by high traffic density but also by the presence of railway and motorway crossings, long stretches of port activities, and heavy industrial settlements. Particularly in the areas adjacent to commercial and tourist ports, an increase in noise pollution levels has been observed in recent years, caused not only by the noise from ships but also by the traffic of cars and heavy vehicles coming to and from the ports.

In Liguria, the Municipality of Genoa carried out systematic noise measurement campaigns from 2008 to 2011 with two main objectives: to verify the sound levels present in certain residential areas near major port infrastructures, and to identify a suitable method for characterizing the port-related noise in densely populated urban areas intersected by important infrastructures such as roads and railways. The most critical sites correspond to urban areas near noisy port zones.

ARPAL (Regional Agency for Environmental Protection of Liguria) has been monitoring the noise caused by activities at the Genoa port for about twenty years, establishing a rather stable scenario. The multi-year analysis experience has allowed the identification of the main noise sources: ship noises (including ventilation systems) during the berthing phase, loudspeakers for announcements related to the boarding and disembarking operations at the ferry and tourist terminals, and the movement of cars, trailers, and container transfer vehicles.

The Tuscany Region, in the field of noise pollution, adopted Regional Law No. 89 of December 1, 1998, which sets rules for the protection of the environment and public health from noise pollution caused by anthropogenic activities, regulating their operation to limit noise levels within legally established limits [46].

The main objective of a noise control policy in its various aspects is to keep exposure to noise as low as possible, protecting the health and well-being of the population. The specific objectives of such a policy are the development of criteria for protection from noise exposure and the promotion of noise evaluation as part of the process of safeguarding citizens' health.

Among the main responsibilities of the Tuscany Region are defining technical criteria and guidelines for municipalities to follow when drafting Municipal Acoustic Classification Plans and Municipal Noise Abatement Plans, identifying the priority timing for noise remediation interventions, and defining the procedures for drafting noise impact assessment and acoustic climate documentation, as well as the procedures for issuing municipal permits for temporary and/or outdoor activities. Additionally, since January 1, 2016, the Tuscany Region has been responsible for maintaining and updating the regional list of Certified Environmental Acoustic Technicians.

The Regional Implementation Regulation, approved by Decree of the President of the Regional Government No. 2/R of January 8, 2014, under Article 2, paragraph 1 of Regional Law No. 89/1998, "Rules on Noise Pollution" [47], was elaborated with the technical support of ARPAT (Regional Agency for Environmental Protection of Tuscany). This regulation replaces and updates the guidelines issued by the Regional Council Resolution No. 77/2000. The structure of the guidelines is maintained, divided into several sections, which have become separate parts of the regulation: acoustic classification of territory, coordination of municipal acoustic classification plans with municipal urban planning instruments, procedures for issuing permits for temporary activities or public events, and municipal noise abatement plans. A new section has been added concerning the methods for controlling the noise impact prediction documentation required in the procedures outlined in Article 12 of Regional Law No. 89/98 [46] and its amendments (the criteria for drafting noise impact documentation and the acoustic climate prediction report were defined by Regional Government Resolution No. 857/2013).

2.2 Noise Measurement Methods in Outdoor Environments

Ports located along the Mediterranean coastline are frequently embedded within densely populated urban areas, where port-related noise represents significant environmental

pressure. The outdoor acoustic environment in these contexts is characterized by pronounced spatial and temporal variability, resulting from the coexistence of multiple stationary and mobile noise sources, heterogeneous emission patterns, complex propagation paths, and variable operational schedules. As a consequence, effective noise assessment in port areas cannot rely on a single measurement technique, but requires a structured and integrated methodological approach.

As already mentioned in the previous chapter, within the European regulatory framework, port noise is commonly assimilated to industrial noise, despite its distinctive characteristics. This simplification does not fully reflect the complexity of port soundscapes, where ship operations, cargo handling equipment, road and rail traffic, and auxiliary systems coexist, and where sound propagation is strongly influenced by meteorological conditions and waterfront geometries. This regulatory gap has practical implications for the selection and integration of appropriate noise measurement methodologies in outdoor port environments.

Recent multidisciplinary initiatives, such as the NoMEPorts [48], RUMBLE [25], MON ACUMEN [49], DECIBEL [26], REPORT [50], CLASTER project [21], have highlighted the need for an integrated and harmonized approach to port noise assessment, combining technical and socio-economic perspectives. From a measurement standpoint, this translates into the coordinated use of complementary techniques, including phonometric measurements, real-time monitoring stations, and advanced diagnostic tools such as acoustic cameras. Each method captures different aspects of the outdoor acoustic environment and addresses specific assessment objectives (see Table 1).

Table 1. Comparison of Environmental Noise Measurement Techniques

Measurement Method	Temporal Coverage	Typical Cost	Main Output	Main Advantages	Limitations
Short-term phonometric measurements	Short duration (minutes to hours)	Low	Sound pressure levels (e.g., L_{Aeq}, L_{max}) at specific locations	Standardized measurements; suitable for regulatory verification and localized exposure assessment	Limited representativeness of long-term conditions; sensitive to temporary events
Continuous monitoring stations	Long-term, real-time monitoring (days, weeks, months, years)	Medium–High	Time-series noise indicators (e.g., L_{den}, L_{night}), statistical indicators	Captures temporal variability; enables evaluation of cumulative exposure and operational patterns	Limited capability for precise identification of individual noise sources
Acoustic camera measurements	Short targeted campaigns	High	Spatial noise maps and source localization	Enables identification and visualization of dominant noise sources in complex environments	High equipment cost; limited temporal representativeness; requires expert for measurements and data interpretation

Short-term phonometric measurements provide standardized and repeatable sound pressure level data for regulatory verification and localized exposure assessment, but they are limited in their ability to represent long-term trends and operational variability [51-54]. Continuous monitoring systems overcome this limitation by supplying statistically robust datasets over extended periods, enabling the evaluation of temporal patterns and cumulative exposure, particularly during nighttime or irregular port activities [55-57]. However, continuous monitoring alone offers limited capability for precise source attribution. Acoustic camera measurements complement these approaches by enabling spatial localization and identification of dominant noise sources in complex outdoor scenarios, thereby supporting targeted mitigation strategies [58].

International guidelines explicitly recommend the combined use of complementary noise measurement techniques in complex environments. The World Health Organization emphasizes that comprehensive environmental noise assessment should be based on multiple data sources to adequately evaluate exposure and related health impacts. Similarly, European technical guidance for strategic noise mapping highlights the importance of integrating short-term measurements, long-term monitoring, and diagnostic analyses to obtain representative and reliable noise.

By addressing both methodological and regulatory limitations, integrated noise measurement strategies contribute to a more accurate characterization of outdoor port noise, support harmonization across cross-border maritime regions, and enable the development of effective and transferable noise mitigation measures. In this context, advances in measurement methodologies and data integration represent essential components of sustainable port noise management.

2.2.1 Phonometric measurements

Phonometric measurements, defined as systematic recordings of sound pressure levels using precision instruments, represent the core methodology for the characterization, monitoring, and management of environmental noise in outdoor environments. They provide objective and quantifiable data necessary to assess noise exposure, identify major sources of disturbance, and verify compliance with applicable legal thresholds.

As already mentioned in Italy, noise monitoring is regulated by Law No. 447/1995 [39] and related technical decrees, including D.M. 16 March 1998, which establish the national framework for environmental noise measurements. These provisions are consistent with international electroacoustic standards, particularly the IEC 61672 series for sound level meters. Further details on the measurement procedures adopted in this study are provided in 2.1.2**.**

IEC 61672-1:2013 defines three categories of sound measuring instruments: time-weighting sound level meters, integrating-averaging sound level meters, and integrating sound level meters for sound exposure level (SEL) measurements. IEC 61672-2 classifies instruments into Class 1 and Class 2, with Class 1 meters required for high-accuracy

environmental monitoring and compliance assessments due to stricter tolerance limits [59]. IEC 61672-3 establishes requirements for periodic testing and measurement uncertainty, including provisions for automatic and continuous measurements without an operator present [60].

Phonometric measurements support multiple objectives. From a regulatory perspective, they ensure compliance with national and regional acoustic zoning plans. From a public health standpoint, they enable identification of areas exposed to noise levels associated with adverse effects such as sleep disturbance, cardiovascular stress, and reduced cognitive performance. Moreover, phonometric data constitute the basis for noise mapping, long-term acoustic planning, and the design of mitigation measures. In modern port governance, these measurements also support transparency and stakeholder engagement by informing environmental reporting and responding to public complaints.

Measurements may be conducted as short-term surveys or structured assessments. Indicative surveys can be performed using handheld instruments; however, for representative and legally valid measurements, standardized configurations are required. To reduce operator influence and ensure repeatability, microphones are typically mounted on tripods and positioned according to prescribed geometrical criteria. In façade measurements, the microphone is placed at a standardized distance from the building surface and at a height representative of the most exposed openings, using extendable supports when necessary.

While phonometric measurements provide essential indicators of environmental noise exposure based on sound pressure levels, perceived disturbance is not determined solely by global A-weighted values. In complex acoustic environments, disturbance is often influenced by the intrusiveness of specific noise sources relative to the background noise.

To address this aspect, the Italian technical specification UNI/TS 11844:2022 defines procedures for the objective assessment of intrusive noise [41]. A sound source is considered intrusive when it is perceptibly distinguishable from the surrounding environmental noise, a condition that can be described in terms of the signal-to-noise ratio. From a psychoacoustic perspective, perception is governed by masking phenomena occurring within critical frequency bands, whose bandwidth increases with frequency and is comparable to one-third-octave bands above approximately 500 Hz.

UNI/TS 11844 adopts concepts derived from Signal Detection Theory to interpret intrusive noise using spectral data obtained from phonometric measurements. The methodology involves measuring environmental noise with the specific source operating and background noise under comparable conditions with the source inactive. The equivalent sound level of the specific source L_s is estimated as:

$$L_{Aeq,s} = 10\log_{10}\left(10^{L_{Aeq,a}/10} - 10^{L_{Aeq,r}/10}\right) \quad [dB(A)] \tag{1}$$

where $L_{Aeq,a}$ and $L_{Aeq,r}$ are the equivalent A-weighted levels of environmental and background noise, respectively. This estimation is considered reliable when:

$$\Delta L = L_{Aeq,a} - L_{Aeq,r} \geq 3 \text{ dB(A)} \quad (2)$$

To account for spectral and temporal characteristics not captured by global indicators, UNI/TS 11844 introduces the Detectability Level D'_L. For each frequency band, the detectability index d'_i is defined as:

$$d'_i = \eta \sqrt{BW_i \cdot \frac{10^{L_{s,i}/10}}{10^{L_{r,i}/10}}} \quad (3)$$

where $\eta = 0.4$, $L_{s,i}$ and $L_{r,i}$ are the band levels of the source and background noise, and BW_i is the bandwidth of the i-th band. The cumulative detectability is obtained as:

$$d'_c = \sqrt{\sum_{i=1}^{n} (d'_i)^2} \quad (4)$$

and the corresponding detectability level is:

$$D'_L = 10\log_{10}(d'_c) \quad [dB] \quad (5)$$

Higher values of D'_L indicate greater intrusiveness. By explicitly accounting for spectral differences between the source and background noise, this approach enhances the interpretation of phonometric measurements and supports targeted noise mitigation strategies in complex outdoor environments.

2.2.2 Real-time monitoring stations

Real-time monitoring stations represent a key tool for the planning, management, and control of acoustic conditions in commercial ports and for the assessment of their impact on adjacent urban areas. The implementation of real-time noise monitoring systems typically follows a structured methodology articulated in four consecutive phases:

- Analysis of the state of the art of port noise monitoring technologies;
- Development of noise maps to describe the spatial distribution of sound levels;
- Identification and configuration of appropriate monitoring systems;
- Verification and validation of monitoring system performance.

Real-time monitoring stations are fixed or semi-permanent installations equipped with calibrated Class 1 sound level meters (in accordance with EN 61672), an environmental protection box, and data transmission systems. These stations are often powered by photovoltaic panels to ensure autonomous operation. They are strategically located within

port areas and in nearby residential zones to enable continuous acquisition and transmission of noise data over extended periods, ranging from days to several months.

Such systems typically provide continuous measurement of key acoustic indicators, including equivalent continuous sound levels (L_{Aeq}), maximum levels (L_{max}), and composite indices such as L_{den}. Additional functionalities include real-time access to data, automatic alerts for threshold exceedances, integration with meteorological sensors for the identification and exclusion of invalid measurements, and secure data storage for long-term trend analysis.

Real-time monitoring enables longitudinal assessment of noise exposure and facilitates temporal correlation between measured sound levels and port operational activities. This approach is particularly effective for capturing nighttime operations, irregular or intermittent events, and seasonal variations, and for supporting compliance documentation and responses to community complaints.

As example, within the MON ACUMEN project [49], in the Port of La Spezia, four real-time noise monitoring stations were installed (see Figure 2). Each station was equipped with 01 dB CUBE Smart Noise Terminal/sound level meters, capable of acquiring detailed information on environmental noise levels and typologies. The instruments, certified as Class 1 (uncertainty 0.5 dB) in accordance with EN 61672, also integrate meteorological sensors, automatic event detection algorithms, and audio recording capabilities. The monitoring units are fully remotely managed, allowing real-time data acquisition as well as remote control, configuration, and maintenance of the system.

Or lately, within the CLASTER project [21], other monitoring stations were installed in the Toulon port (see Figure 3). The instruments are certified as Class 2 (uncertainty up to 1.5 dB) according to EN 61672.

Figure 2. Monitoring station in La Spezia port

Figure 3. Monitoring station in Toulon port

2.2.3 Acoustic camera measurements

Acoustic cameras are advanced measurement systems designed for the spatial identification and analysis of noise sources in complex outdoor environments. They are based on microphone arrays combined with beamforming algorithms, which allow the reconstruction of the spatial distribution of sound energy as a function of direction and frequency. Unlike conventional sound level meters, acoustic cameras provide directional and spatially resolved acoustic information, enabling the localization of individual sound sources within multi-source scenarios.

In outdoor and port environments, noise assessment is often complicated by limited access to sources, safety constraints, and the simultaneous operation of heterogeneous equipment. Under these conditions, acoustic cameras represent an effective complementary tool to conventional phonometric measurements. By coupling acoustic signal processing with optical imaging, these systems allow the identification and relative quantification of noise sources without the need for direct proximity measurements.

Figure 4 shows the acoustic camera used [61] during the measurements conducted at the La Spezia port by the UNIGE team within the framework of the CLASTER project.

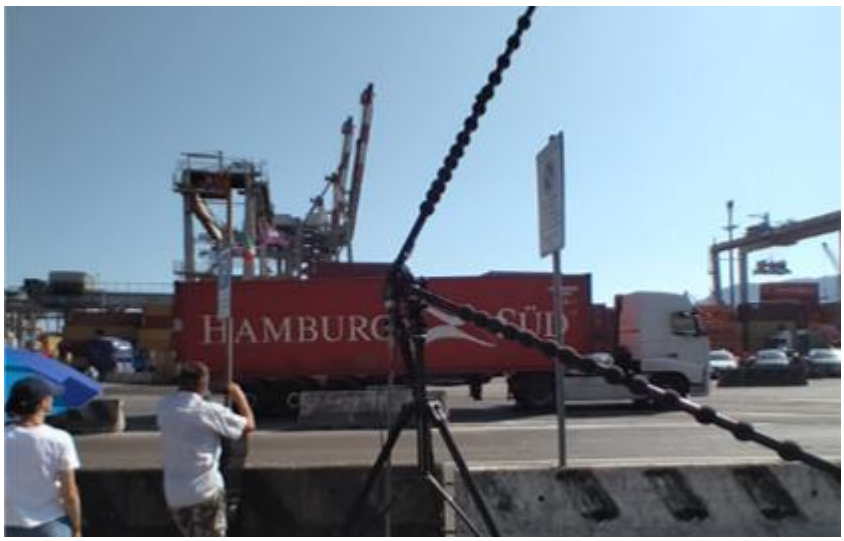

Figure 4. Acoustic camera used for measurement in La Spezia port

The output of an acoustic camera consists of acoustic maps overlaid on visual images, representing sound pressure levels or sound intensity distributions across selected frequency bands. This approach supports the identification of dominant noise sources, the analysis of spectral contributions, and the separation of direct sound radiation from reflections or background noise [62, 63].

Due to their diagnostic nature, acoustic camera measurements are primarily used for source attribution, investigation of noise generation mechanisms, and evaluation of

mitigation measures, rather than for routine compliance monitoring. When integrated with phonometric measurements and real-time monitoring systems, acoustic cameras contribute to a more detailed and reliable characterization of outdoor noise in acoustically complex environments.

2.3 Noise sources in port Areas

Port areas are characterized by a high density and diversity of noise sources operating simultaneously and often continuously over a 24-hour cycle. Unlike conventional industrial or urban environments, ports host a combination of stationary, mobile, and intermittent sources associated with maritime operations, cargo handling, internal logistics, and transport connections. The resulting acoustic environment is highly heterogeneous in both spatial and temporal terms and is strongly influenced by operational schedules, traffic flows, and meteorological conditions.

From an environmental noise assessment perspective, port-related noise sources can be grouped into four main categories: naval sources, port handling equipment, internal road traffic, and railway activities. Each category is characterized by distinct emission mechanisms, spectral content, and temporal behavior, requiring specific measurement and modeling approaches. A correct classification and characterization of these sources represent a fundamental prerequisite for reliable noise mapping, exposure assessment, and the definition of effective mitigation strategies, as highlighted in recent literature on port noise assessment.

2.3.1 Naval sources (Ships)

Naval sources comprise airborne noise emissions generated by commercial vessels during maneuvering, berthing, and stationary conditions at berth. For port noise assessment and mapping purposes, the primary contributors are cargo and passenger ships, including container vessels, ferries, Ro-Ro ships, tankers, and cruise ships, whereas recreational and service craft are generally excluded unless locally significant [62], [64].

In port environments, ship noise is dominated by auxiliary engines, generators, ventilation systems, and exhaust outlets during hoteling phases, while propulsion-related emissions become relevant during maneuverings and low-speed navigation. These sources typically exhibit broadband spectra with possible tonal components and quasi-stationary temporal behavior, resulting in prolonged exposure, particularly during nighttime operations.

Standardized procedures for ship noise characterization in ports are currently limited. Existing methodologies proposed by ISO standards such as ISO 2922:2020 [65] and ISO 14509-1:2008 [66], require controlled measurement conditions, low background noise levels, and, in some cases, direct access to vessels. These constraints limit their

applicability at operational ports, where measurements must be conducted without interfering with port operations.

Consequently, port noise mapping practices generally rely on indirect noise characterization based on measurements performed at the berth or quay side, with onboard measurements considered only in exceptional cases. In noise models, ships are commonly represented as fixed point or area sources during stationary phases and as line sources during maneuvers.

2.3.2 Port machinery sources

Port machinery sources include equipment used for cargo handling and internal logistics within terminal areas, such as forklifts, front lifts, reach stackers, dock tractors, mobile harbor cranes, stacking cranes, rubber-tired gantry cranes (RTGs), container cranes, trailers, and bulk-handling systems. These sources operate in close proximity to quay edges, storage yards, and internal traffic corridors and represent a major contribution to operational noise levels within port areas [10], [53], [67].

Noise emissions originate from propulsion systems (internal combustion engines or electric drives), hydraulic circuits, cooling and ventilation units, mechanical impacts during cargo handling operations, and rolling noise during displacement. Depending on the operational phase, port machinery behaves either as a mobile source during transit or as a quasi-stationary source during loading and unloading. The emitted noise is predominantly broadband, frequently characterized by impulsive components and, in some cases, tonal features associated with engine or generator operation.

Field measurements conducted in operational port environments indicate that large handling equipment, such as reach stackers, container cranes, and mobile harbor cranes, typically exhibits A-weighted sound power levels in the range of 105–115 dB(A) during loading and unloading operations. Smaller mobile equipment, including forklifts, dock tractors, and front lifts, generally produces lower emission levels, with sound power levels of approximately 95–105 dB(A) during displacement [10]. Fixed auxiliary sources, such as generators and refrigerated containers, may contribute continuous noise emissions of comparable magnitude, particularly during nighttime periods.

From a noise assessment and modelling perspective, port machinery is characterized by high spatial localization and strong temporal variability. In strategic noise mapping, these sources are commonly represented as point or area sources during stationary operations and as moving point or line sources during transit phases. Due to the heterogeneity of equipment types and operating conditions, source characterization is generally based on representative field measurements and consolidated literature data rather than standardized laboratory procedures.

2.3.3 Truck Traffic noise source

Introduction

This section is based on a peer-reviewed publication developed within the framework of the CLASTER project [21], to which the PhD candidate contributed as co-author, with primary responsibility for the measurements, data analysis and interpretation. The section addresses transportation-related noise within port areas, focusing on truck movement, which represents a critical contribution to the overall environmental noise level.

Among the various noise sources present in port areas, transportation-related activities, such as truck and train movements within and around port boundaries, play a critical role in contributing to overall environmental noise levels. Traffic noise is typically continuous and spatially widespread, affecting both port operations and the quality of life of nearby communities. A regulatory gap exists regarding transport-related noise within port areas.

The research paper "Identifying optimal areas for sound-absorbing asphalt in the port of La Spezia using acoustic camera measurements", presents an innovative methodology based on Acoustic Camera technology for the evaluation of transport-related noise and mitigation strategies inside the Port of La Spezia (Italy). The application of this advanced measurement technique proved effective for the characterization and monitoring of port noise, particularly in environments characterized by multiple, dynamically moving sound sources. Acoustic Cameras, which combine optical imaging with advanced sound analysis algorithms [58], have been previously employed for ship noise measurements during docking operations in the ports of Genoa [64], Nice [68], and Livorno [62], demonstrating their suitability for complex port environments.

Addressing port-related traffic noise through effective monitoring and mitigation strategies is therefore essential to ensure a sustainable coexistence between port activities and surrounding urban communities.

Methodology

Based on the real time database developed during the MON ACUMEN project and the periodical noise monitoring, elevated noise levels are identified in between the junction leading to the 'Molo Garibaldi', highlighted in red in Figure 5, and the entrance to the 'Varco Canaletto', railway crossing at the Fornelli connection highlighted in blue. These junctions are particularly sensitive, as they represent critical nodes within the internal port road network.

Figure 5. Identification of the measurement areas

Daytime Acoustic Camera measurements in a normal daily port activity when cargo handling and transportation activities were ongoing, are conducted at these two junctions (see Figure 6) to qualitatively assess the rolling noise levels generated during the trucks movements and to evaluate the need for the installation of sound-absorbing asphalt in the following positions:

- P1_Entrance 'Varco Canaletto'
- P2_Juction 'Molo Garibaldi'

Figure 6. Measurement position P1 and P2

The measurement setup comprised an Acoustic Camera (gfai tech GmbH Star48 AC Pro microphone array), a 48-channel data acquisition system (mcdRec), and a laptop for data processing. This specific microphone array is optimized for environmental acoustics and long-distance noise measurements.

Results

For each measurement station, detailed results are provided separately, including the temporal progression of perceived sound levels, representative acoustic images, frequency spectra, and spectrogram analyses.

At position P1, the time history of the perceived sound levels in the measurement station P1 is presented in Figure 6. The acoustic camera was placed at a distance of 10 m from the sound source. From the measurement (see Figure 7) can be observed different peaks when the trucks are driving by, and it's of course worse when more trucks are passing simultaneously, resulting in high sound levels.

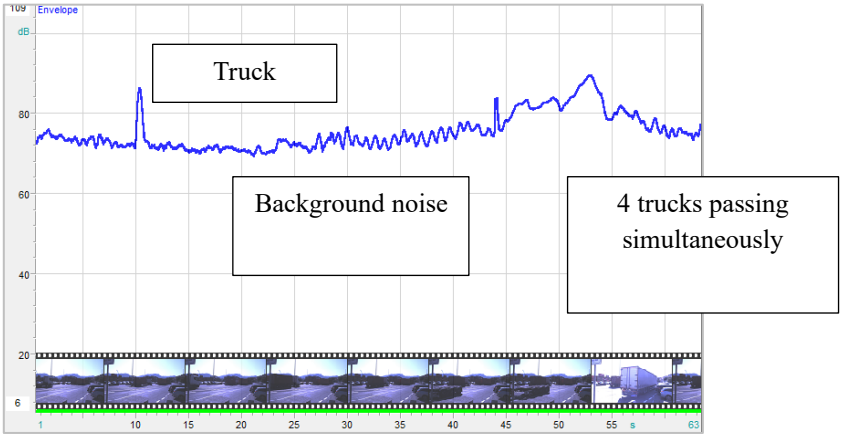

Figure 7. Time history [dB(A)]. Measurement position P1

The coloured acoustic picture presented in Figure 8, in frequency range: 63 Hz -13 kHz shows that even the other port activities are ongoing, the trucks movement represent the predominant noise sources at the measurement locations. Despite the noise produced from the engine, at this specific time the noise is generated due to the interaction of the tires and the road surface.

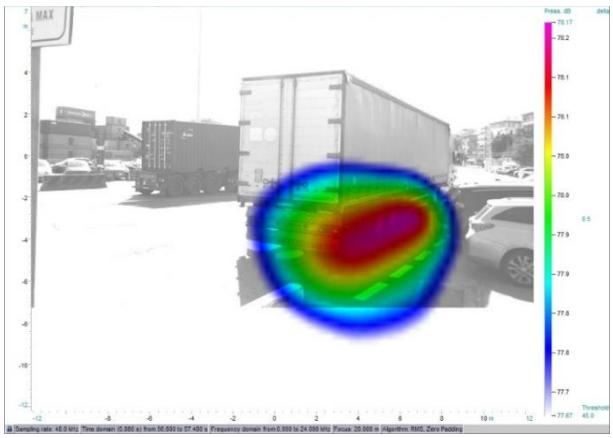

Figure 8. Colored acoustic picture. Measurement position P1

Figure 9 displays the spectral analysis of the recorded sound levels. The results are presented in octave bands up to 13 kHz, with observed levels reaching a maximum of 72 dB. The spectrogram illustrates the measurement results over a 64-second time window, encompassing the total noise contribution from all sources within the port area.

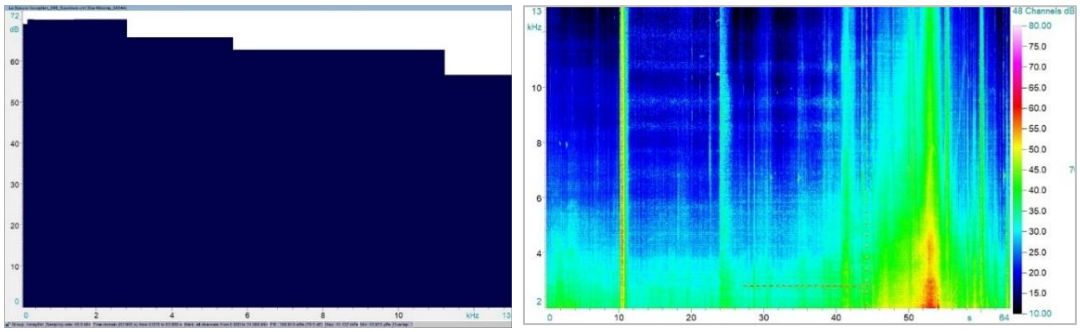

Figure 9. (a) Spectrum; (b) linear spectrogram. Measurement position P1.

At position P2, measurements recorded at a distance of 12 m from the traffic flow yielded average sound pressure levels exceeding 60 dB(A), with clear peaks associated with truck pass-by events (see Figure 10).

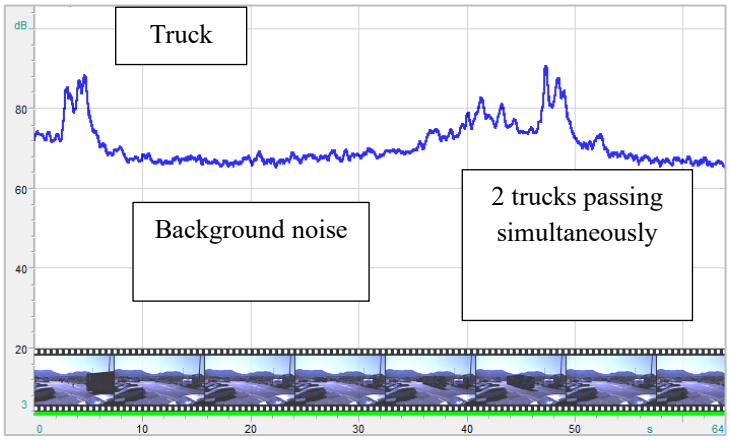

Figure 10. Time history [dB(A)]. Measurement position P2

The colored acoustic picture presented in Figure 11, covering frequencies up to 13 kHz, clearly delineates the rolling noise generated by tire-road interaction.

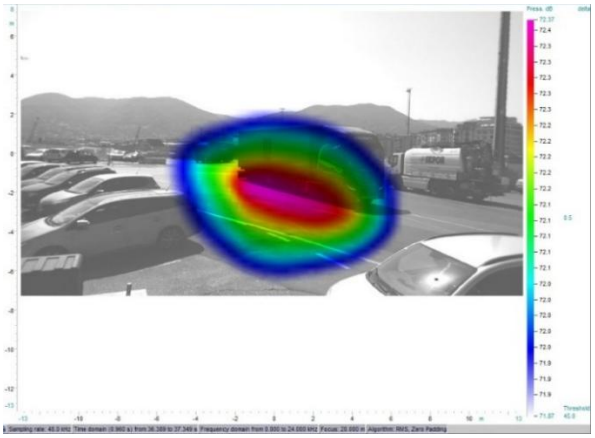

Figure 11. Colored acoustic picture. Measurement position P2

Figure 12 presents spectral information. Again, the results are presented octave bands up to 13 kHz and the spectrogram represents results of the measurement for a time window of 64s considering the overall noise generated from all port sources.

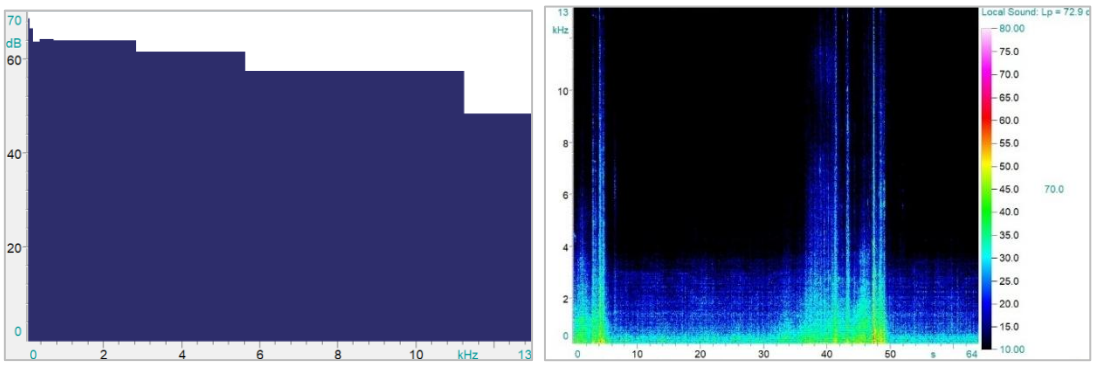

Figure 12. (a) Spectrum; (b) linear spectrogram. Measurement position P1.

Conclusions

This study, conducted within the framework of the CLASTER project, employed Acoustic Camera technology to qualitatively investigate and characterize rolling noise generated by truck movements within the Port of La Spezia. The complex acoustic environment, characterized by multiple and dynamic noise sources, posed significant challenges for accurate noise identification and analysis.

Through the utilization of the Acoustic Camera, this investigation successfully identified the rolling noise generated by truck movements within the Port of La Spezia, distinguishing it from other noise sources in the area.

The application of the Acoustic Camera as a qualitative measurement technology proved invaluable, enhancing the understanding of rolling noise produced by tire-road interaction

and enabling the identification of specific areas where mitigation measures could be implemented to reduce its impact.

However further measurements and verifications are required in accordance with the new Italian Ministerial Decree of 5/8/24 under criterion: "2.2.4 Acoustic Emission of Pavements," published on August 23, 2024 [69], which mandates that bituminous mixtures used for both new roads and those undergoing maintenance must meet the required mechanical properties and ensure compliance with acoustic emission levels (L_{CPX}), measured using the Close Proximity (CPX) method as per the UNI EN ISO 11819-2 standard [70].

The outcomes of this research offer valuable perspectives for the design of efficient noise reduction measures, such as the adoption of noise-dampening materials rather than reflective asphalt, to mitigate the impact of rolling noise. Given the critical economic role of ports and their typical proximity to residential areas, the implementation of effective noise reduction measures is essential to ensuring the sustainable development of port cities. The noise mitigation measure addressing tire–road interaction, based on the use of acoustically optimized asphalt, is described 0.

2.3.4 Rail Activity noise source

Railway activity within port areas represents a relevant source of environmental noise, particularly where rail infrastructure is directly integrated into terminal operations and located in close proximity to urban areas. Rail noise in ports is characterized by a combination of continuous and transient contributions associated with train movements, shunting operations, braking, acceleration, and wagon coupling or decoupling.

The dominant noise components originate from wheel–rail interaction, traction systems, and mechanical impacts occurring during low-speed manoeuvres typical of port environments. Rolling noise generated at the wheel–rail contact interface constitutes the primary contribution during train passages, while impulsive events may occur at track discontinuities or during coupling operations, resulting in marked temporal variability and potential perceptual intrusiveness.

Acoustic Camera measurements performed within the Port of La Spezia indicate that rail traffic noise can reach sound pressure levels of 78-79 dB (see Figure 13), comparable to those produced by heavy road vehicles. The spatial localization capability of the Acoustic Camera confirms the predominance of rolling noise during train passages and enables clear discrimination of rail-related sources from adjacent port activities, even in acoustically complex operational conditions.

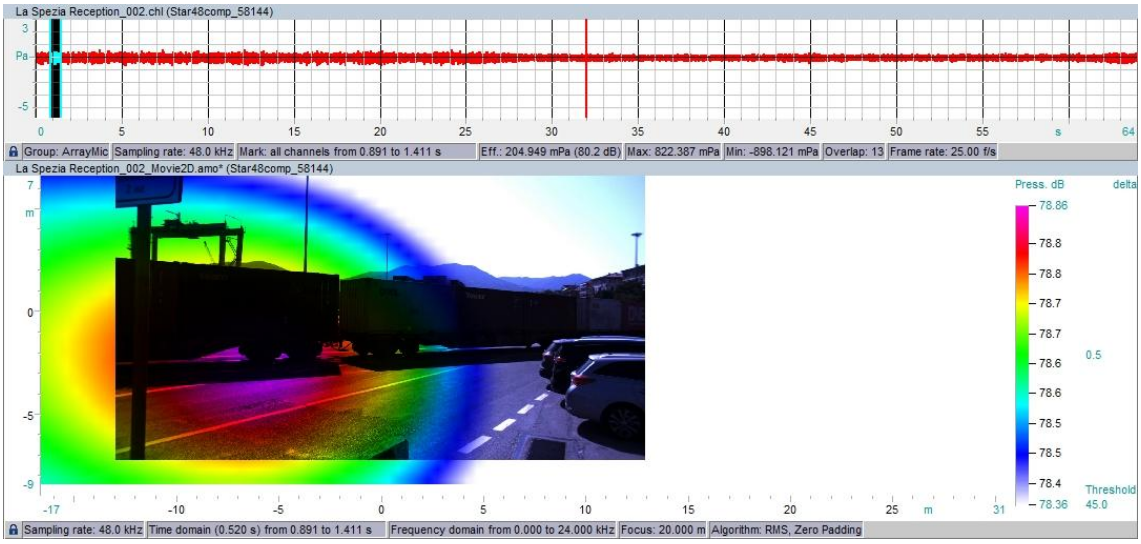

Figure 13. Acoustic camera image when the train was passing

Due to the limited distance between the railway infrastructure and nearby building façades, approximately 8 m, an acoustic barrier has been installed between the railway line and the adjacent roadway. This mitigation measure aims to reduce direct sound propagation toward sensitive receivers and to partially decouple railway noise from road traffic noise. However, the close spatial arrangement of rail, road, and built environments continues to pose challenges for noise assessment and source attribution.

From a noise assessment perspective, railway activity in port environments presents specific challenges, as standard railway noise models are generally developed for open-line conditions and do not fully represent the low-speed operations, shielding effects, and complex geometries typical of port rail networks. For this reason, integrated measurement approaches combining conventional phonometric techniques with advanced diagnostic tools, such as Acoustic Cameras, are particularly effective for accurate noise characterization and the evaluation of mitigation measures. In addition, as discussed in 2.2.2, a real-time noise monitoring station has been installed at the closest railway–building receiver location, providing continuous sound level data that complement short-term diagnostic measurements and support long-term assessment of railway noise impact.

2.4 Noise perception from the population

While physical noise indicators provide an objective description of environmental exposure, the impact of port-related noise cannot be fully assessed without considering population perception, which is influenced by individual sensitivity and socio-economic factors. For this reason, the evaluation of residents' responses to noise exposure represents an essential component of comprehensive port noise assessment.

To complement technical noise analyses, socio-economic approaches are increasingly adopted in complex environments such as ports. Within this framework, noise perception is commonly investigated through stated preference methods that allow the quantification of perceived disturbance in monetary terms and support decision-making related to mitigation strategies. This socio-economic evaluation represents one of the activities developed within the framework of the CLASTER project, in parallel with the investigation of truck traffic noise, and was intended to integrate technical and population-based indicators of port-related noise.

In this study, noise perception is assessed by estimating residents' Willingness to Pay (WTP) for a reduction in port-related noise using the Contingent Valuation Method (CVM), based on structured surveys following the methodological framework proposed by Portney in 1994 subsequently adopted in related studies by Ciucci, L. at al [71] and Instamto at al [72].

2.4.1 Methodology

The method proposed by the University of Corsica [71] involves administering surveys in which residents are first asked a series of screening questions related to demographic and contextual variables, such as age, gender, educational background, and their level of exposure or connection to port-related activities or noise. Following this, participants are asked to listen to two audio recordings: one featuring unmitigated port noise and the other featuring port noise reduced by 10 dB. After listening, respondents are invited to state their willingness to pay for achieving the noise reduction presented in the second recording.

The identification of the areas in which the questionnaires are to be administered represents a critical step of the methodology and therefore required a dedicated preliminary analysis. In the case of the Port of La Spezia, time constraints prevented the execution of on-site surveys and preliminary consultations with municipal authorities and local stakeholders, leading to the adoption of an indirect approach based on the collection and integration of documentary and project-based data. The identification and definition of suitable areas for survey administration were carried out by the PhD candidate.

To this end, the following data sources were considered:

- Municipal Institutional Portal: The municipal acoustic zoning map (generated as required by Italian Law No. 447/1995) was consulted. This document constitutes a fundamental tool for territorial noise planning and management and provides an official classification of areas according to their acoustic sensitivity.
- Acoustic monitoring campaigns by competent authorities: Noise data provided by ARPAL [73], the authority responsible for environmental monitoring, were taken

into account. Since 2019, ARPAL has conducted periodic measurements at key receptor locations within both the port area and the surrounding urban environment.

- Data from the Italian National Institute of Statistics (ISTAT): Socio-demographic data and thematic maps related to population distribution by age group, economic status, and level of education or professional training were extracted and used to support the selection of representative survey areas [74].

2.4.2 Target zones

The target area of La Spezia port corresponds to the urban zone immediately adjacent to the port boundary (see Figure 14) and was selected to assess noise perception among residents most exposed to port-related acoustic emissions. The focus on this area ensures that the analysis reflects population responses primarily influenced by port activities at the port–city interface.

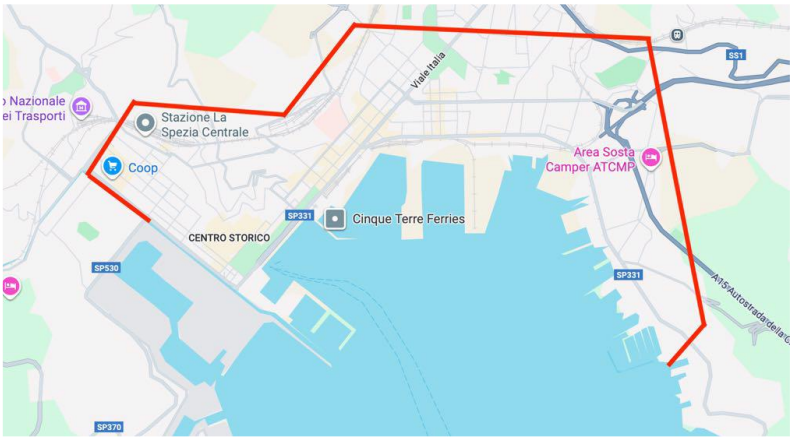

Figure 14.Target zone in the port of La Spezia

La Spezia is a medium-sized Italian city with approximately 100,000 inhabitants. It hosts a strategically important intermodal system consisting of the commercial port of La Spezia and the Santo Stefano Magra hinterland logistics platform. The city is also home to one of Italy's most significant naval arsenals, highlighting its strategic role in both commercial maritime activities and national defense.

2.4.3 Data acquisition

The data acquisition phase integrates regulatory, acoustic, and socio-demographic information in order to support the selection of representative areas for the assessment of noise perception among the population. The adopted approach combines official acoustic zoning, measured noise levels, and population characteristics, ensuring coherence between physical noise exposure and social context.

Acoustic Zoning

According to the Municipal Acoustic Classification Plan of the Municipality of La Spezia, published in December 2021 [75], as shown in Figure 15, the port area falls within Class VI – Exclusively industrial areas. The surrounding urban areas are classified as Class V – Predominantly industrial areas and Class IV – Areas with intense human activity.

The applicable emission, immission, and differential noise limits for each acoustic class are defined by Framework Law No. 447 on Noise Pollution and are summarized in Table 2. These limits provide the regulatory reference for the interpretation of measured noise levels and the assessment of compliance in both port and surrounding urban areas.

Table 2. Applicable emission, immission, and differential noise limits for each acoustic class

Acoustic Class	Absolute Emission Limit – Daytime [dB(A)]	Absolute Emission Limit – Nighttime [dB(A)]	Absolute Immission Limit – Daytime [dB(A)]	Absolute Immission Limit – Nighttime [dB(A)]	Differential Immission Limit – Daytime [dB(A)]	Differential Immission Limit – Nighttime [dB(A)]
I	45	35	50	40	5	3
II	50	40	55	45	5	3
III	55	45	60	50	5	3
IV	60	50	65	55	5	3
V	65	55	70	60	5	3
VI	65	65	70	70	Not applicable	Not applicable

The acoustic zoning of the Port of La Spezia and the adjacent urban areas is illustrated in Figure 15, which also identifies the locations of the acoustic monitoring stations used during the measurement campaigns, indicated by black rectangles and circles. It provides a spatial overview of the regulatory acoustic context within which the measurements were performed.

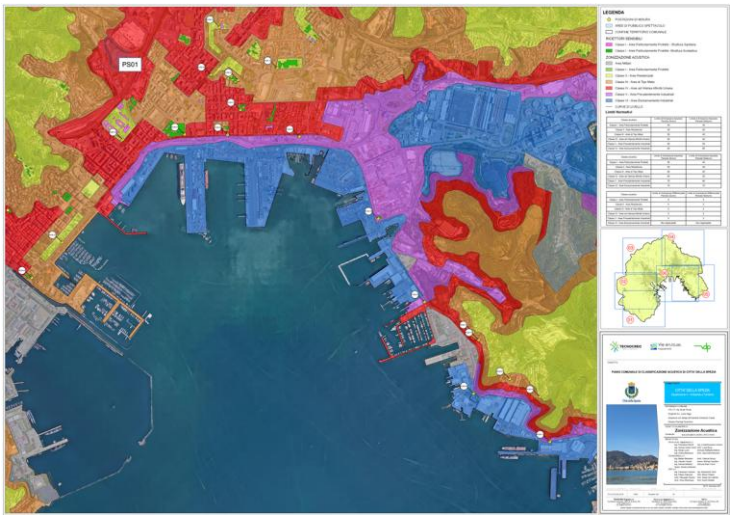

Figure 15. Acoustic zoning port of La Spezia [75]

Based on this zoning framework, Table 3 summarizes the types of receptors located in the vicinity of each monitoring station and the corresponding regulatory noise limits associated with the updated acoustic classification. The table also indicates the presence or absence of nearby road infrastructures and their respective buffer zones, which are relevant for interpreting the measured sound levels.

Table 3. Results of the phonometric measurements during the day measurements

Postazione Di Misura	Tipologia Ricettore	Denominazione	Fascia Di Pertinenza			Nome Strada	Limite Classe Proposta		Classe Proposta
			Periodo Diurno	Periodo Notturno	Categoria		Periodo Diurno	Periodo Notturno	
Rum-01_Diu	Casa Di Cura	Alma Mater	Non Presente				65	55	IV
Rum-02_Diu	Scuola	Istituto Maria Ausiliatrice	50	55	Db	Viale Italia Viale Amendola	65	55	IV
Rum-03_Diu	Edificio Residenziale	Viale San Bartolomeo	65	55	Db	Viale San Bartolomeo	65	55	IV
Rum-04_Diu	Scuola	Istituto Tecnico Industriale Giovanni Capellini	50	55	Db	Viale San Bartolomeo	60	50	III
Rum-05_Diu	Scuola	Scuola Materna Statale	50	55	Db	Viale San Bartolomeo Via Delle Casermette	60	50	III
Rum-06_Diu	Caserma	Caserma A Ruffino	65	55	Db	Viale San Bartolomeo	70	60	V
Rum-07_Diu	Edificio Amministrativo	Fincantieri Divisione Costruzioni Militari Stabilimento Muggiano	Non Presente				55	45	II
Rum-08_Diu	Edificio Residenziale	Salita Ruffino					55	45	II
Rum-09_Diu	Edificio Industriale	Viale San Bartolomeo	65	55	Db	Via Ugo Botti	65	55	IV
Rum-10_Diu	Edificio Residenziale	Via Luigi Rizzo	65	55	Db	Via Luigi Rizzo	55	45	II
Rum-11_Diu	Edificio Residenziale	Via Enrico Toti	65	55	Db	Via Enrico Toti	55	45	II
Rum-12_Diu	Edificio Industriale	Viale San Bartolomeo	65	55	Db	Viale San Bartolomeo	70	70	VI
Rum-13_Diu	Scuola	Scuola Pia Casa Misericordia	Non Presente				65	55	IV
Rum-14_Diu	Ospedale Militare	Dipartimento Militare Di Medicina Legale	50	40	Db	Via Nicolo' Fieschi	60	50	III
Rum-15_Diu	Scuola	Scuola Media Statale Jean Piajet	50	55	Db	Via A. Benedicenti	60	50	III
Rum-16_Diu	Ospedale/Casa Di Cura	Ospedale Civile Santandrea	50	40	Db	Via Vittorio Veneto	55	45	II
Rum-17_Diu	Scuola	Istituto Scolastico I.S.A. 2	Non Presente				65	55	IV
Rum-18_Diu	Scuola	Ipsia 'D. Chiodo I.T.S. 'N.Sauro'					65	55	IV
Rum-19_Diu	Scuola	I.T.C.T. A.Fossati-M.Da Pasano					65	55	IV

The noise levels recorded during the acoustic monitoring campaign, conducted at the identified sites during the daytime period (06:00–22:00). All values are expressed in dB(A); the L_{eq} values have been rounded to the nearest half decibel (0.5 dB). These acoustic indicators and the positioning provide a quantitative characterization of noise exposure and constitute the reference dataset intended for future comparison with population noise perception outcomes within the framework of the ongoing project activities.

Measurements conducted by ARPAL

ARPAL carried out a multi-year campaign that began in 2011. This campaign consists of a systematic and exploratory monitoring of noise emissions of port origin affecting the residential areas of La Spezia.

- Methodology

Environmental noise measurements were conducted using a combination of continuous monitoring and short-term assisted phonometric measurements in order to capture both temporal variability and localized acoustic conditions. Continuous monitoring was performed over a multi-week period to assess long-term noise trends associated with port

activities, particularly during nighttime when port-related noise is typically more perceptible due to reduced road traffic. Complementary short-term measurements (approximately 10–60 minutes) were carried out at selected locations during both daytime and nighttime using Class 1 (uncertainty 0.8) sound level meters (Brüel & Kjær models 2250 and 2270). The measurements included the measurement of the equivalent continuous sound level (L_{Aeq}). All measurements were conducted under meteorological conditions compliant with D.M. 16 March 1998, with instruments calibrated before and after each measurement campaign. The long-term monitoring setup for continuous measurements included a sound level meter installed within a weather-protected enclosure, with the microphone mounted on a fixed support at the monitoring location.

- Measurements 2023 [73]

The acoustic monitoring was conducted during the months of November and December 2023, focusing measurements near residential buildings located along the central-eastern arc of the port. The monitoring campaign was carried out through a continuous, multi-week (21-day) monitoring program, as well as six assisted short-term measurements (lasting less than one hour) conducted at five different sites. Figure 16 schematically illustrates the monitored areas over the past three years, highlighting the measurement sites in red.

Figure 16. Measurement points 2023

Table 4 presents a summary of equivalent sound levels at the monitoring stations identified on the map.

Table 4. L_{Aeq} e L_n [dB(A)] measured values

Measurement point	Acoustic Class	Position	Identification ID	Date	L_{eq} [dB(A)]
S. Bartolomeo Street, 1st floor terrace	V	Latitude North: 4.884.582 Longitude Esat: 1.568.056	SP206	08/11/2023	58
S. Bartolomeo Street, 2nd floor terrace	V	Latitude North: 4.884.583 Longitude East: 1.568.056	SP207	14/11/2023	56.1
S. Bartolomeo Street, 2nd floor balcony	V	Latitude North: 4.884.577 Longitude East: 1.568.129	SP208	14/11/2023	56.7
Del Canaletto Street– 1st floor balcony	III	Latitude North: 4.885.055 Longitude East: 1.567.631	SP209	15/11/2023	47.7
Pagliari locality	III	Latitude North: 4.883.758 Longitude East: 1.569.058	SP212	07/12/2023	52.7
Ruffino locality	III	Latitude North: 4.882.586 Longitude East: 1.569.908	SP213	07/12/2023	48

Measurements 2024 [73]

The analysis of sound level measurements conducted by ARPAL in 2024, including both short-term and continuous monitoring at three locations within the urban area of La Spezia during nighttime (see Figure 17), led to the following observations (see

Table 5).

Figure 17. Measurement positions 2024

Table 5. L_{Aeq} e L_n [dB(A)] measurement values (short time measurements)

Measurement point	**Area**	**Location / Period**	**L_{Aeq} [dB(A)]**	**Reference value [dB(A)]**	**L_1 [dB(A)]**	**L_{10} [dB(A)]**	**L_{50} [dB(A)]**	**L_{90} [dB(A)]**	**L_{95} [dB(A)]**	**L_{99} [dB(A)]**
SP276	Corso Nazionale	Roadside / Nighttime	55.4 ± 0.8	55	67.0	58.1	49.8	45.1	44.2	41.3
SP277	Viale S. Bartolomeo	Roadside / Nighttime	69.3 ± 0.8	55	79.4	72.9	60.7	52.2	50.6	48.4
SP278	Viale S. Bartolomeo	Roadside / Nighttime	67.7 ± 0.8	55	80.0	71.6	59.9	49.7	48.2	44.4

The short-term measurements of L_{Aeq} and percentile levels (in dBA) show that noise levels are significantly influenced by road traffic, particularly along Viale S. Bartolomeo, which represents the dominant contributor to the highest measured L_{Aeq} values. The L_1, L_{10}, L_{50}, L_{90}, L_{99} presented in Table 5 are used to describe statistical noise levels over time (were L_n = the sound level exceeded for n% of the measurement time). L_{99}, more representative of continuous sources such as port-related noise, range between 41 dBA and 48 dBA depending on the measurement location.

Spectral analysis of the measurements highlights a prominent low-frequency component at 31.5 Hz across all sites, suggesting the presence of a measurable contribution from port-related noise sources, particularly within the background noise.

- Measurements 2025 [73]

The 2025 measurement campaign was financed within the framework of the CLASTER project and was primarily focused on noise assessment inside the port area. Most of the measurements were conducted at internal port locations to evaluate sound pressure levels associated with rolling noise generated by truck traffic, particularly in correspondence with the areas identified for the installation of sound-absorbing pavement.

In addition to the internal port measurements, two supplementary monitoring points were selected along Viale San Bartolomeo, an urban road adjacent to the port area, in order to assess noise propagation towards nearby residential receptors. The locations of these external measurement points are illustrated in the Figure 18 and the most representative results of measurements to the receivers are reported in Table 6.

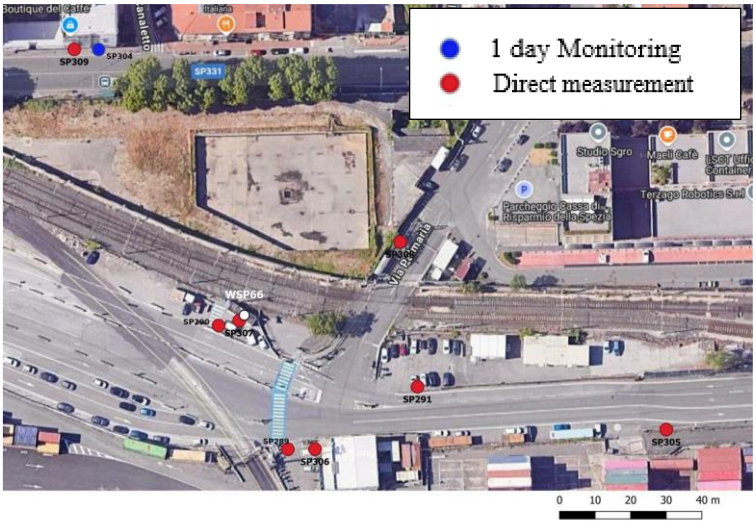

Figure 18. Measurement positions 2025

Table 6. L_{Aeq} e L_n [dB(A)] measurement values

Measurement point	Acoustic class	Identification ID	Date	Leq [dB(A)]
In proximity to Fornelli Pier - street level	IV	SP309	04/03/2025	64.4
In proximity to Fornelli Pier – 6th floor balcony of the residential building	IV	SP 304	03/04-24/04/2025	62.1

ISTAT data analysis

Socio-demographic data provided by the Italian National Institute of Statistics (ISTAT) [74] were analyzed to characterize the population potentially exposed to port-related noise and to support the interpretation of noise perception outcomes. For the purposes of this study, the analysis was interpreted in relation to the main urban contexts of the Municipality of La Spezia, including the historic center, central residential and commercial areas, eastern districts such as Migliarina and La Scorza, semi-peripheral and hilly neighborhoods (e.g., Pegazzano, Fabiano, Marinasco, Valdellora, Termo, and Montalbano), the port and industrial zone (Canaletto and Fossamastra), and the outer hilly and coastal settlements (such as Pitelli, Ruffino, and Cadimare).

Figure 19 illustrates the population distribution based on the 2011 census. Higher population densities are mainly observed in residential areas located in semi-peripheral and hilly zones. Although these areas are not directly adjacent to the port, they may still be affected by port-related noise propagation, particularly under specific meteorological and topographical conditions.

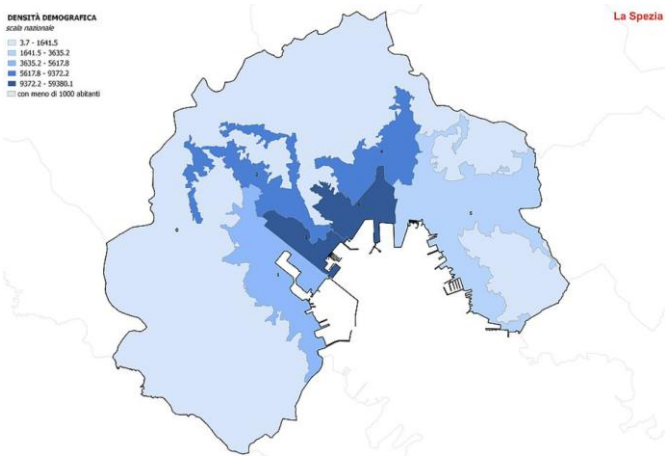

Figure 19. Population distribution of La Spezia

Population Distribution by Age Groups

The analysis of population age structure highlights significant spatial differences. According to ISTAT data, central areas are mainly characterized by a working-age population (15–64 years), while peripheral and semi-peripheral zones show a higher proportion of elderly residents (65+), who are generally considered more sensitive to environmental stressors such as noise. The port and industrial area, by contrast, exhibits a predominance of working-age adults and a limited residential function.

Distribution of employment in medium–high specialization professions

The incidence of employment in medium–high specialization professions was used as an indicator of the socio-economic profile of the population. As shown Figure 20, higher values are concentrated in a limited inland urban sector, while areas near the port mostly show low to intermediate levels, with only localized portions exhibiting higher values. The remaining parts of the municipality generally display low to intermediate values. This spatial pattern provides context for interpreting potential differences in noise perception among residents exposed to port-related noise.

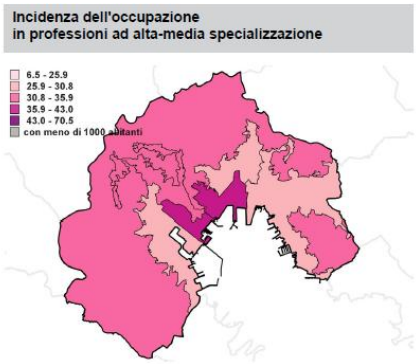

Figure 20. Incidence of employment in medium- and high-skilled occupations

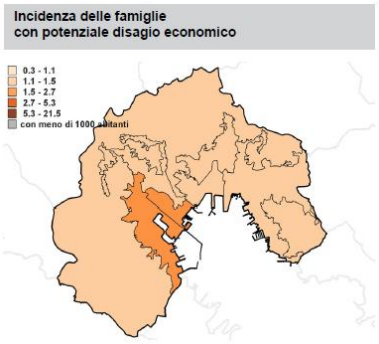

Figure 21. Incidence of households at risk of economic disadvantage

Incidence of households with potential economic hardship

The incidence of households with potential economic hardship was analyzed as an indicator of social vulnerability (Figure 21). Higher values are observed in urban sectors closer to the port and along major transport corridors, where residential areas coexist with industrial and logistics activities.

Economic vulnerability may increase exposure to environmental stressors such as noise and influence both noise tolerance and the capacity to support mitigation measures. This indicator therefore contributes to the socio-acoustic interpretation of port-related noise impacts.

Area definition

The selection of the most appropriate areas for the social experiment aimed at evaluating the perceived impact of port-related noise pollution, an integrated analysis of available acoustic measurement data and socio-demographic information provided by ISTAT was carried out. This approach allows measured noise exposure levels to be interpreted within their territorial and social context. The study areas, shown in Figure 22, correspond to urban zones most exposed to port-related noise and associated transport activities.

The analyzed areas are characterized by medium to high population density and a heterogeneous demographic structure, with a predominance of working-age residents but also a significant presence of children and elderly people, who represent sensitive

receptors to environmental noise. Several areas adjacent to the port also exhibit high levels of skilled employment and low-medium economic hardship, factors that may influence noise sensitivity and expectations regarding environmental quality.

For each area, it is therefore essential to account for the distribution of sensitive receivers, such as residential buildings, hotels, and places of worship, schools and universities as well as for the presence of major noise sources. Particular attention is given to key urban corridors and port-adjacent zones, including San Bartolomeo Street, Canaletto Street, Nazionale Street, Manzini Street (near the Cruise Terminal), Italia Street (affected by both cruise and railway activities), and the Terminal del Golfo, which represent critical interfaces between port operations and the urban environment.

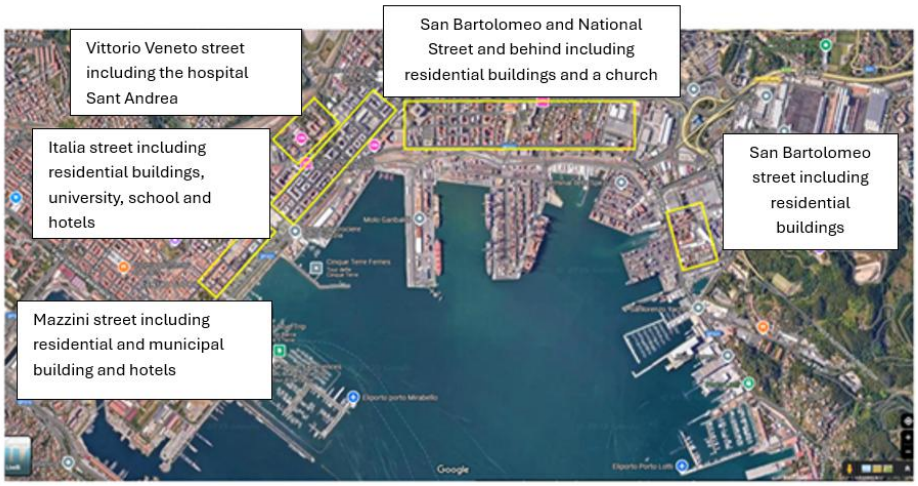

Figure 22. Areas selected for questionnaire administration

2.4.4 Results

A representative sample of 268 questionnaires was collected in La Spezia as part of the survey conducted across the study cities. Participants were exposed to audio samples representing typical port activities (40 and 50 dB) and to a series of monetary bids ranging from €1 to €50 to evaluate their willingness to pay (WTP) for noise reduction. This experimental design allowed the estimation of residents' WTP for a 10 dB reduction in environmental noise.

The results indicate that La Spezia exhibits a relatively high proportion of positive responses, suggesting a significant willingness among residents to financially support measures aimed at reducing port-related noise pollution (see Figure 23).

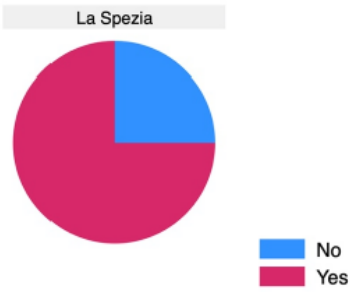

Figure 23. Distribution of positive responses [76]

However, the median WTP value still requires further post-processing to assess the influence of additional factors, such as sample heterogeneity and respondents' spatial distribution, etc. A more comprehensive analysis of these aspects is currently ongoing, and the results are expected to be presented by the end of February 2027 on the project website. Moreover, the results of the noise perception will be compared with the results of the measurements gathered from the data acquisition and presented in a map.

2.5 Sound absorption/insulation materials

2.5.1 Introduction

Sound absorption refers to the ability of materials to reduce the energy of sound waves incident on their surface. When a sound wave encounters a material, part of its energy is reflected, part is transmitted, and the remaining portion is dissipated within the material. The absorbed fraction is quantified by the sound absorption coefficient, defined as the ratio between absorbed and incident acoustic energy. This coefficient depends on sound frequency and angle of incidence and is commonly averaged over multiple directions for practical applications.

Sound absorption represents a fundamental strategy in noise control and is widely applied in industrial, architectural, and transport-related contexts. For instance, in the automotive sector, sound-absorbing materials are routinely employed within passenger cabins and engine compartments to mitigate both interior and exterior noise emissions [77].

The effectiveness of sound absorption is governed by three primary physical mechanisms:

- Viscous (frictional) losses, generated by the interaction between oscillating air particles and the internal surfaces of porous or fibrous materials, converting acoustic energy into heat;
- Thermal exchange, caused by pressure fluctuations that induce heat transfer between air and solid surfaces, particularly relevant at low frequencies;
- Internal structural damping, occurring in certain materials where acoustic excitation induces mechanical vibrations within the material structure itself.

Understanding these mechanisms is essential for classifying sound-absorbing materials and selecting the right type for a specific application. The following sections will explore the main categories of sound absorption materials, based on their structure and the dominant physical phenomena they utilize.

2.5.2 Porous absorbers

Sound-absorbing systems can be broadly classified into porous absorbers, resonant absorbers, and sound-insulating elements, each characterized by distinct physical mechanisms and frequency-dependent behavior.

Absorption mechanisms and characteristics

Porous sound absorbers are widely employed in acoustic treatments due to their capacity to dissipate acoustic energy through viscous and thermal losses within an interconnected pore structure. Typical examples include fibrous materials and open-cell foams, which allow air and sound waves to penetrate the material volume. As sound propagates through these narrow air paths, energy is lost primarily due to viscous boundary layer effects. Because air is a viscous fluid, the oscillating air particles interact with the internal surfaces of the pores, leading to frictional losses. This friction dissipates the sound energy in the form of heat, particularly within a very thin boundary layer adjacent to the pore walls, typically on the sub-millimetre scale at audible frequencies. Additionally, thermal conduction occurs between the vibrating air particles and the material itself, which becomes increasingly significant at lower frequencies, where there is more time per sound wave cycle for heat to transfer. Changes in airflow direction and velocity within the irregular pore structure also cause momentum losses, further contributing to sound attenuation [78].

For porous absorbers to function effectively, the pore structure must be open and interconnected. Closed-cell materials, which trap air inside sealed pockets, do not allow sufficient interaction between the sound wave and the material and therefore absorb very little sound. Vibrational energy losses within the material itself are generally minor compared to the losses caused by air movement through the pores.

The sound absorption performance of porous materials is strongly influenced by their physical thickness and their pore shape. Typically, porous absorbers behave like high-pass filters: they are most effective at mid to high frequencies, while absorption at low frequencies improves as the material becomes thicker. A commonly cited rule of thumb is that the material thickness should be at least one-tenth of the wavelength of the target frequency to begin absorbing sound significantly, and about one-quarter of the wavelength to achieve near-total absorption. Because particle velocity in a sound wave is zero at a rigid boundary, such as a wall, the part of the porous absorber closest to that surface contributes very little to absorption. The most effective absorption occurs in the

material layers farthest from the backing surface, which is why increased thickness is especially important for low-frequency performance. Alternatively, spacing a thinner absorber away from the wall can enhance its effectiveness by placing it in a region of higher particle velocity [78].

Finally, sound absorption is affected by the angle of incidence, with porous materials generally exhibiting increased absorption for oblique sound incidence due to longer effective propagation paths within the absorbing medium. Overall, the effectiveness of porous absorbers depends on the combined influence of pore structure, flow resistivity, thickness, mounting configuration, and incident sound field characteristics.

Typologies of Porous Absorber Materials

Mineral wool

Mineral wool is among the most widely used porous absorbers in noise control applications. It is typically manufactured from basalt, sand, or recycled glass, melted and spun into fibrous structures. Its absorption performance depends on fibre diameter, orientation, density, and binder content, and may exhibit anisotropic behavior depending on the direction of sound incidence [79].

The experimental characterization of a mineral wool sample with a thickness of 40 mm and a density of 80 kg/m³ (Figure 24), was conducted by the author at the Acoustic Laboratory of the University of Genoa. The normal-incidence sound absorption coefficient was measured using a three-microphone impedance tube in accordance with ISO 10534-2. For the adopted setup, characterized by an internal tube diameter of 45 mm and a 30 mm spacing between microphones, the valid measurement frequency range was 250–4300 Hz, ensuring plane-wave propagation inside the tube.

Prior to the measurement campaign, the system was calibrated using a 25 mm reference sound-absorbing sample, performing sequential measurements with different microphone pair configurations (1–2, 2–1, 1–3, 3–1) to verify the stability of the transfer functions; calibration was repeated twice per day. Measurements were conducted in a controlled laboratory environment (approximately 20 °C temperature and 60% relative humidity) to minimize environmental influences. Samples were carefully cut to match the tube diameter (45 mm) and mounted without compression, ensuring no air gaps between the sample and the tube wall; sealing paste was applied when necessary to prevent leakage.

For each sample, five repeated measurements were performed to evaluate repeatability and measurement uncertainty, showing negligible deviations between tests. The obtained absorption curves were finally compared with reference measurement results provided by the Materiacustica laboratory (University of Ferrara), which also designed and built the impedance tube used in the experiments.

As expected, the mineral wool sample exhibits high sound absorption performance in the mid-to-high frequency range, with absorption coefficients approximately between 0.6 and 0.8, while showing reduced effectiveness at low frequencies.

Material typology		Thickness [mm]	Density [kg/m^3]
Mineral wool		40	80

Figure 24. Mineral wool sample

Additionally, inverse characterization techniques by were applied to estimate the Biot–Allard macroscopic parameters, enabling the reconstruction of the absorption coefficient. As shown in the Figure 25, measured, reconstructed, and reference curves show good agreement across the investigated frequency range, confirming the reliability of the experimental and inverse modeling approach.

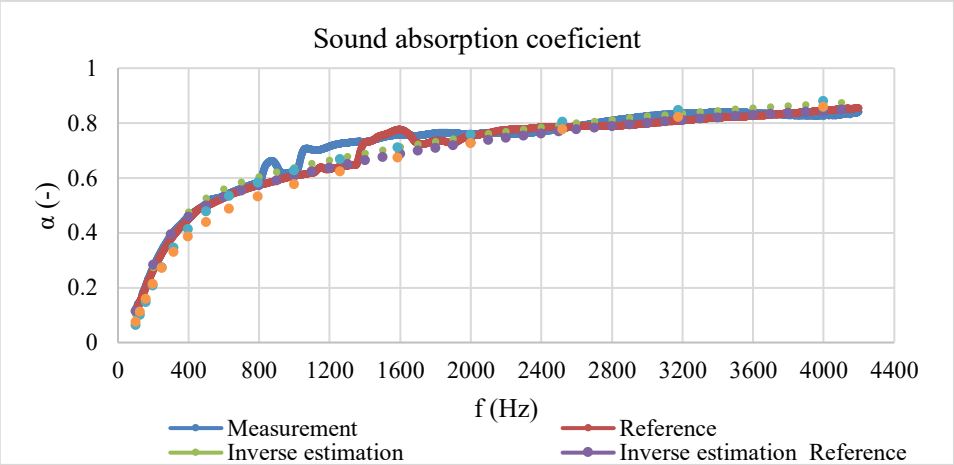

Figure 25. Sound absorption coefficient of the mineral wool sample

Foams

Foam materials, particularly open-cell polyurethane foams, represent another common class of porous materials for sound attenuation. Their interconnected pore structure allows effective sound absorption (better than mineral wool previously described) through viscous and thermal losses, whereas closed-cell foams exhibit negligible absorption unless mechanically perforated.

Even the acoustic experimental characterization of a mineral foam sample with a thickness of 19 mm and a density of 25 kg/m³ (see Figure 26) was carried out by the

author in the acoustic laboratory of the University of Genoa following the same methodology previously described. The measured sound absorption coefficient exhibits the typical behavior of porous absorbers, with increasing effectiveness at mid-to-high frequencies (0.8-1) and reduced performance at low frequencies due to limited thickness and airflow resistivity.

Material typology		Thickness [mm]	Density [kg/m^3]
Polyurethane Foam		19	25

Figure 26. Polyurethane foam sample

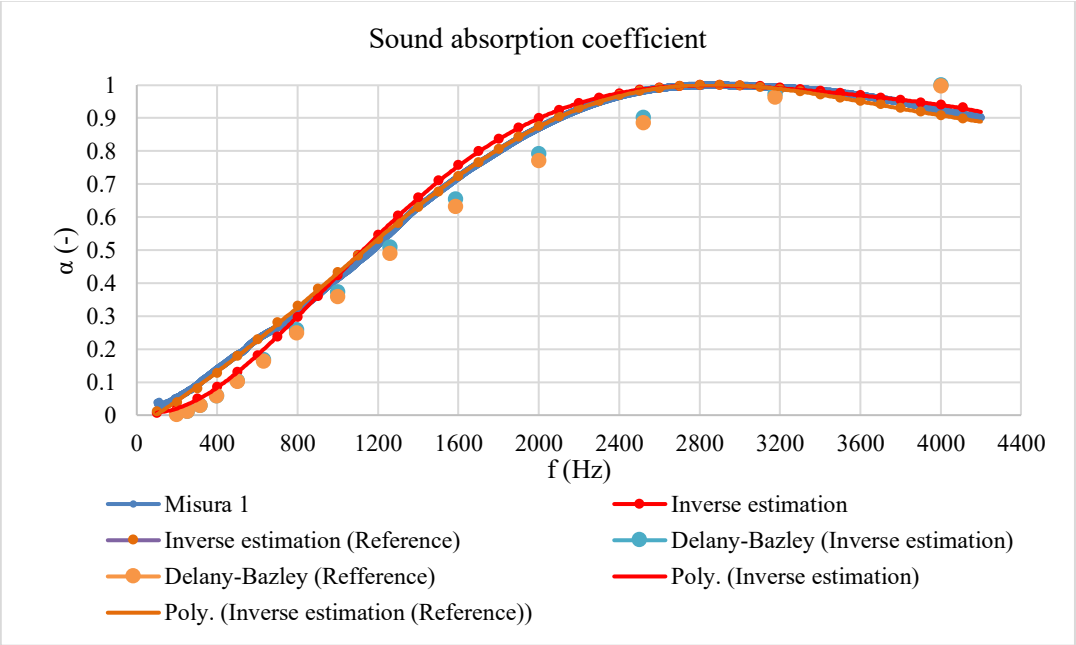

Figure 27.Sound absorption coefficient of the polyurethane foams

In addition to direct measurements, the absorption coefficient was estimated using the Delany–Bazley empirical model, assuming a rigid frame and equivalent fluid behavior. The model predictions were computed within the validity range prescribed for porous materials and using airflow resistivity as the primary input parameter. The results obtained from experimental measurements, inverse parameter estimation, and Delany–Bazley predictions were then compared with the reference datasets.

As presented in Figure 27, a quite good level of agreement was observed among measured, modeled, inversely estimated, and reference absorption coefficients, particularly in the mid-high frequency range, while deviations occurred at low and high

frequencies due to the limited thickness of the sample and the intrinsic limitations of empirical models.

Sustainable material

Sustainable porous absorbers are designed to reduce environmental impact while maintaining adequate acoustic performance. From an acoustic perspective, these materials rely on the same dissipation mechanisms as conventional porous absorbers namely viscous and thermal losses induced by air motion within an interconnected pore network but differ in raw material origin, manufacturing processes, and end-of-life characteristics. Sustainability criteria typically include the use of recycled or renewable resources, reduced energy consumption during production, low-emission binders, and recyclability or biodegradability.

Natural fibrous materials, such as sheep wool, represent renewable alternatives to mineral wool. While their porous structure enables sound absorption through viscous and thermal mechanisms, their relatively low density and airflow resistivity generally result in reduced absorption efficiency compared to mineral fibers. Consequently, increased material thickness is required to achieve comparable performance, particularly at low frequencies and in cavity-based applications.

Granular porous absorbers produced from recycled rubber, waste foams, or glass constitute another class of sustainable materials. In contrast to fibrous absorbers, their acoustic behavior is governed by intergranular air flow and contact losses between particles, leading to a more pronounced frequency-dependent absorption response. For a given thickness, absorption performance improves with decreasing grain size and optimized packing density. Geometric shaping or graded configurations can further enhance performance. Although their maximum absorption coefficient is typically lower than that of fibrous materials (α generally below 0.8), granular absorbers offer advantages in mechanical durability, moisture resistance, and environmental sustainability. Commercial solutions based on sintered recycled glass demonstrate that non-fibrous, fire-resistant, and fully recyclable absorbers can achieve a balanced compromise between acoustic efficiency and ecological performance.

Aerogels

Aerogels are ultra-lightweight porous materials characterized by extremely high porosity and low solid-phase density. From an acoustic standpoint, their large internal surface area favors viscous and thermal dissipation, making them potentially effective porous absorbers, particularly at mid-to-high frequencies.

However, monolithic aerogels present practical limitations for acoustic applications. Low-density aerogels are mechanically fragile, while denser variants often exhibit airflow

resistivity values that are not optimal for efficient sound absorption. To overcome these constraints, aerogels can be employed in granular form, improving mechanical stability and enabling better acoustic coupling with incident sound waves. When combined with impedance-matching layers or suitable backing configurations, granular aerogel systems can achieve measurable absorption while retaining the benefits of low density and high porosity.

Activated carbon

Activated carbon represents a special class of granular porous absorbers with distinctive low-frequency acoustic behavior. In addition to conventional viscous and thermal losses, sound attenuation is enhanced by adsorption–desorption processes occurring within the material's extensive microporous structure. During acoustic pressure fluctuations, gas molecules are temporarily adsorbed and released from pore surfaces, dissipating acoustic energy in a time-dependent manner.

The coexistence of macropores, which facilitate sound penetration, and micropores, which enable adsorption mechanisms, results in increased low-frequency attenuation compared to conventional porous materials. This makes activated carbon particularly suitable for applications where enhanced absorption at low frequencies is required.

2.5.3 Resonant absorbers

Absorption mechanisms and characteristics

Resonant absorbers are acoustic treatments specifically designed to provide efficient sound absorption at low to mid frequencies, where conventional porous absorbers become ineffective or require impractically large thicknesses. Their operating principle is based on resonance phenomena, whereby acoustic energy is converted into mechanical motion of a mass–spring system and subsequently dissipated through damping mechanisms. Unlike porous absorbers, resonant devices are inherently narrowband, exhibiting peak absorption around a tuned resonance frequency; therefore, extending their effective bandwidth represents a key design challenge [80-81].

Two principal categories of resonant absorbers are commonly distinguished: membrane (panel) absorbers and Helmholtz-type resonators. In both cases, the system response is governed by the interaction between an oscillating mass and the compliance of an enclosed air volume, with additional losses introduced to control resonance sharpness and increase absorption efficiency.

Typologies of Resonant Absorber Materials

Membrane absorbers

Membrane absorbers consist of a flexible panel (e.g., plywood, rubber, metal sheet, or mass-loaded vinyl) mounted in front of a sealed or semi-sealed air cavity. The panel acts as the oscillating mass, while the enclosed air volume provides the restoring stiffness. The resonance frequency is primarily controlled by the surface mass of the panel and the depth of the cavity [82]. Acoustic energy is dissipated through viscous losses in the air cavity and, more effectively, by incorporating porous damping layers behind the membrane. These absorbers are particularly effective for targeting discrete low-frequency modes and are commonly applied near rigid boundaries, where porous absorbers perform poorly due to low particle velocity.

Helmholtz resonators

These devices consist of a cavity with a narrow neck where a plug of air acts as a mass vibrating against the air spring inside the cavity. Resonance occurs at a specific frequency, allowing strong absorption in a narrow band. Damping is typically introduced via porous materials in the neck or cavity, or by viscous losses in microperforated designs. Helmholtz resonators are effective at low frequencies and are often used near boundaries where porous absorbers are less efficient [83].

Perforated panel absorbers

Building on these basic principles, recent innovations include clear absorbers and microperforated panels that leverage viscous and thermal losses without porous materials. These designs aim to broaden absorption bandwidth or improve aesthetic integration while maintaining resonant absorption principles [84].

2.5.4 Sound Insulators (Barriers)

Sound insulators, commonly referred to as acoustic barriers or sound-reflecting materials, are designed to reduce the transmission of airborne sound between a source and a receiver. Unlike absorptive materials, which dissipate acoustic energy within their porous structure, barriers primarily act by reflecting and attenuating sound waves, thereby limiting their propagation into surrounding areas.

The effectiveness of acoustic barriers is mainly governed by the Mass Law, according to which the sound transmission loss increases with the surface density of the barrier and with frequency. Consequently, barriers are typically constructed from dense and non-porous materials such as concrete, masonry, steel, laminated glass, gypsum boards, or mass-loaded vinyl or recycled materials for example demolition waste [85], ensuring high airborne sound insulation.

In outdoor environments, and particularly in port areas, barrier performance depends not only on material properties but also on geometric and installation parameters, including height, length, continuity, and the relative positioning between source and receiver.

Diffraction over the top edge and around the sides of the barrier can significantly reduce the achievable attenuation, especially at low frequencies.

Acoustic barriers are therefore widely applied in port contexts to mitigate noise generated by road and rail traffic, cargo handling activities, and stationary equipment located close to sensitive receptors.

2.6 Acoustic Characterization of Porous Sound-Absorbing Materials

Building on the overview of the main typologies of sound-absorbing materials presented in the previous chapter, this section introduces the theoretical framework required to describe their acoustic behavior.

2.6.1 Definition of acoustic parameters

The propagation of plane acoustic waves within a porous material whose solid frame is assumed to be rigid can be described using the same fundamental principles governing sound propagation in air. Under this assumption, the acoustic response of the material is fully characterized by the characteristic acoustic impedance Z_c and the complex wave number k_c.

The characteristic impedance Z_c is defined as the ratio between acoustic pressure and particle velocity at any point inside the material. The complex wave number k_c plays a role analogous to that of the wave number in air but includes an imaginary component associated with dissipative mechanisms within the porous structure, accounting for the attenuation of acoustic energy as the wave propagates through the medium.

For a plane wave propagating along the x-direction, the acoustic pressure p and particle velocity v fields can be expressed as:

$$p(x,t) = \hat{p}\, e^{-\alpha' x} e^{i(\omega t - k_0 x)} = \hat{p}\, e^{i(\omega t - k_c x)} \qquad (6)$$
$$v(x,t) = \hat{v}\, e^{i(\omega t - k_c x + \phi)}$$

where:
α' is the attenuation constant [m^{-1}],
$k_c = k_0 - i\alpha'$ is the complex wave number [m^{-1}],
$k_0 = \omega / c_0$ represents its real part and is related to the phase velocity of sound in the porous medium [m^{-1}], and
ϕ denotes the phase shift between particle velocity and acoustic pressure [rad].
For a homogeneous porous material, the ratio between acoustic pressure and particle velocity defines the characteristic acoustic impedance Z_c, which is assumed to be spatially constant.

$$Z_c = \frac{p(x,t)}{v(x,t)} = \frac{\hat{p}}{\hat{v}}\, e^{-i\varphi} = \mathrm{Re}[Z_c] + i\,\mathrm{Im}[Z_c] \qquad [\mathrm{Ns/m}] \tag{7}$$

Consider now a homogeneous porous layer of thickness l. Starting from the characteristic parameters of the medium, the acoustic response at the surface exposed to an incident plane-wave field can be evaluated. To determine the surface acoustic impedance, a boundary condition must be imposed at the opposite face of the layer. A widely adopted configuration is that of a porous material backed by a rigid, perfectly reflecting surface. Under this assumption, the particle velocity at the backing surface is zero, corresponding to an infinite surface impedance.

As a result, the surface acoustic impedance at the exposed face depends on the characteristic impedance Z_c, the complex wave number k_c, and the layer thickness l, and can be written as:

$$Z_1 = -\,i\,Z_c \cot(k_c l) \qquad [\mathrm{N\backslash cdotps/m^3}] \tag{8}$$

Once the surface impedance is known, the reflection and absorption properties of the material can be determined. The complex pressure reflection coefficient R_p, defined as the ratio between the reflected and incident acoustic pressure amplitudes, is given by:

$$R_p = \frac{Z_1 - \rho_0 c_0}{Z_1 + \rho_0 c_0} \qquad [-] \tag{9}$$

where $\rho_0$denotes the air density and c_0 the speed of sound in air. From the reflection coefficient, the apparent normal-incidence sound absorption coefficient is obtained as:

$$\alpha_n = 1 - |\,R_p\,|^2 \qquad [-] \tag{10}$$

This coefficient represents the fraction of incident acoustic energy that is not reflected and is commonly used to characterize the sound-absorbing performance of porous materials under normal-incidence conditions.

In practical applications, porous materials are often exposed to diffuse or reverberant sound fields rather than to plane-wave incidence. Assuming a perfectly diffuse acoustic field and a locally reacting material, it is possible to estimate the absorption coefficient under random-incidence conditions starting from the surface impedance derived for plane-wave propagation. According to the analytical formulation proposed by Paris [86], the random-incidence absorption coefficient α_{rnd}can be expressed as:

$$\alpha_{\mathrm{rnd}} = 2\int_0^{\pi/2} \alpha(\theta)\,\sin\,\theta\cos\,\theta\,d\theta \qquad [-] \tag{11}$$

A closed-form analytical expression for α_{rnd}can be obtained as:

$$\alpha_{\mathrm{rnd}} = \frac{8}{\zeta}\left[\cos\ \mu + \frac{\sin\mu}{2\mu} - \frac{\cos\ (2\mu)}{2\mu} + \frac{\sin\ (2\mu)}{2\mu}\right] \quad [-] \tag{12}$$

where the parameters μ and ζ depend on the surface impedance and on the acoustic properties of the porous medium.

The theoretical relationships introduced in this section [87] define the acoustic parameters associated with porous sound-absorbing materials, whose typologies were discussed in the previous chapter. These parameters will be investigated through experimental characterization in the remainder of this work.

The next chapter is therefore devoted to the description of the Experimental Measurement Method adopted to evaluate the acoustic properties introduced herein. Subsequently, a dedicated chapter presents the experimental characterization of selected materials, representing the original contribution of this study.

2.6.2 Experimental Measurement Methods

Following the definition of the acoustic parameters governing the behavior of porous materials and the classification of sound-absorbing material (SAM) typologies presented in the previous subchapter, this chapter addresses the experimental methodologies employed for their acoustic characterization. As schematically summarized in Figure 28, the available measurement techniques for sound-absorbing materials can be grouped into three main categories according to the properties under investigation.

The first group comprises methods for the determination of surface acoustic properties, such as surface impedance, complex reflection coefficient, and apparent absorption coefficient. These properties may be measured using standing wave tube techniques under normal incidence, in-situ methods based on impulsive excitation for oblique incidence, or reverberation room measurements under diffuse-field conditions.

The second group includes methodologies aimed at the evaluation of the complex intrinsic acoustic properties of materials, namely the characteristic acoustic impedance and the complex wavenumber. These quantities are typically determined in a standing wave tube using either indirect approaches, such as the double thickness and double cavity methods, or direct approaches based on transfer matrix formulations with multiple microphones.

The third group concerns the experimental determination of physical parameters required for the theoretical modelling of acoustic behavior, including airflow resistivity, open porosity, tortuosity, and viscous and thermal characteristic lengths. These properties are measured using dedicated laboratory techniques specifically developed for rigid-frame porous materials.

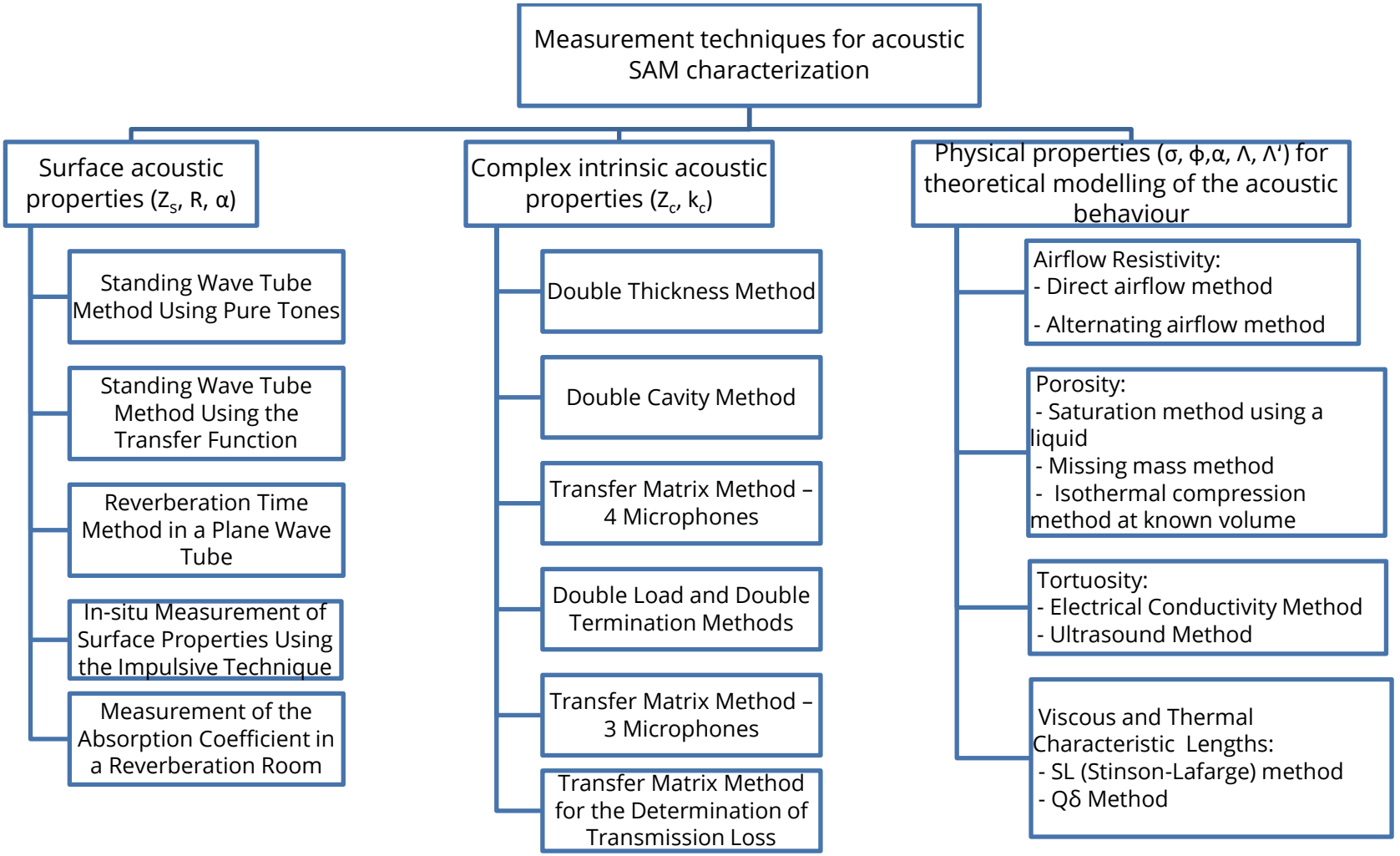

Figure 28. Measurement techniques for acoustic SAM characterization

Within this general framework, the present work focuses on normal-incidence measurements performed in a standing wave tube, with particular emphasis on the Transfer Function Method as defined by UNI EN ISO 10534-2 [88]. Furthermore, an extension of this methodology based on the transfer matrix approach using three microphones is adopted in order to experimentally determine intrinsic acoustic properties [89]. These techniques (which are later reported [90], [91], form the basis for the experimental characterization of the materials investigated in this study and represent the core methodological contribution of the present work.

2.6.3 Experimental Measurement Methodology

Standing wave measurements using the transfer function method by UNI EN ISO 10534-2

The transfer function method under normal-incidence conditions, standardized by UNI EN ISO 10534-2 [88], constitutes the reference experimental technique adopted in this work for the determination of the surface acoustic properties of porous sound-absorbing materials. In particular, this method enables the experimental evaluation of the surface acoustic impedance, the complex pressure reflection coefficient, and the normal-incidence sound absorption coefficient.

The measurement apparatus, as shown in Figure 29 consists of a rigid impedance tube with smooth internal walls, terminated at one end by a sound source and at the other by a rigid sample holder. Two microphones are flush-mounted along the tube wall at known distances $x_1$and x_2 from the sample surface, allowing the measurement of the sound pressure field generated by the superposition of incident and reflected plane waves. Within the impedance tube, a plane-wave acoustic field is generated under normal-incidence conditions.

Figure 29. Measurement setup for the transfer function method [91].

This method is based on the fact that the complex pressure reflection coefficient R_p can be determined from the measurement of the transfer function H_{12} between two positions located at distances $x_1$and x_2 from the test sample. The reflection coefficient is obtained as:

$$R_p = \frac{H_{12} - H_i}{H_r - H_{12}} e^{2ik_0x_1} \tag{13}$$

from which the normal-incidence absorption coefficient is calculated as:

$$\alpha_n = 1 - |R_p|^2 \tag{14}$$

The transfer functions associated with the incident and reflected waves are defined as:

$$H_i = \frac{p_{2i}}{p_{1i}} = e^{-ik_0(x_1 - x_2)} = e^{-ik_0 s} \tag{15a}$$

$$H_r = \frac{p_{2r}}{p_{1r}} = e^{ik_0(x_1 - x_2)} = e^{ik_0 s} \tag{15b}$$

where $s = x_1 - x_2$ represents the distance between the two microphones and k_0 is the wave number in air.

In addition to the reflection coefficient and absorption coefficient, this method allows the determination of the specific surface acoustic impedance of the tested material, which is given by:

$$Z_s = \rho_0 c_0 \frac{1 + R_p}{1 - R_p} \tag{16}$$

where ρ_0 is the air density and c_0 is the speed of sound in air.

Transfer matrix method using three microphones

The three-microphone transfer matrix method, originally proposed by McIntosh, Zuroski, and Lambert [89] represents a direct extension of the two-microphone transfer function method defined in UNI EN ISO 10534-2 [88]. The same impedance tube, sound source, sample mounting conditions, and plane-wave excitation are retained; the extension consists solely in the introduction of a third microphone along the tube axis. The measurement configuration adopted for the three-microphone method is illustrated in Figure 30, which highlights the positions of the microphones along the impedance tube.

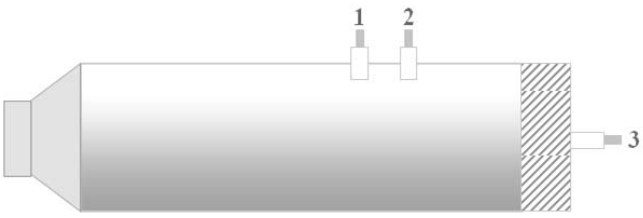

Figure 30. Measurement setup for determining characteristic acoustic properties using the three-microphone method [91]

This methodological continuity ensures consistency between the measurement of surface acoustic quantities, obtained using the standard two-microphone configuration, and the determination of the intrinsic acoustic properties of the material.

The three-microphone method uses a simplified transfer matrix that takes the following form:

$$\begin{pmatrix} p \\ v \end{pmatrix}_{x=0} = \begin{pmatrix} T_{11} & T_{12} \\ T_{21} & T_{22} \end{pmatrix} \begin{pmatrix} p \\ 0 \end{pmatrix}_{x=d} \tag{17}$$

Considering the measurement layout shown in Figure 30, the sound pressure is measured at three axial positions. The transfer functions between microphones 1–2 and 1–3 are defined as:

$$H_{12} = \frac{p_2}{p_1}, H_{13} = \frac{p_3}{p_1} \tag{18}$$

From these measured transfer functions, the elements of the transfer matrix can be analytically determined as following:

$$T_{21} = \frac{v(x_0)}{p(x_d)}, T_{22} = \frac{v(x_0)}{v(x_d)} \tag{19}$$

with:

$$p(x_0) = H_{12}\, p(x_1), v(x_0) = \frac{1}{\rho_0 c_0} \frac{\sin(kx_1)\sin(kx_2)}{\sin(k(x_2 - x_1))} p(x_1) \tag{20}$$

$$p(x_d) = H_{13}\, p(x_1), v(x_d) = \frac{1}{\rho_0 c_0} \frac{\cos(kx_1)\cos(kx_2)}{\sin(k(x_2 - x_1))} p(x_1)$$

where H_{12} and H_{13} are the transfer functions between the microphone positions (1–2) and (1–3), respectively. Once the matrix coefficients are known, the characteristic acoustic impedance Z_c and the complex wave number k_c of the porous material can be calculated using the same theoretical relations introduced for the two-microphone method:

$$Z_c = \sqrt{\frac{T_{12}}{T_{21}}} \tag{21}$$

$$k_c = \frac{1}{l} \cos^{-1}(T_{11})$$

where l is the sample thickness.

So, using the three-microphone transfer matrix method enables a comprehensive acoustic characterization, linking surface properties and intrinsic material parameters within a

unified experimental framework. This approach constitutes a central element of the experimental contribution of the present work.

Measurement limits of the tube [88]

The frequency limits depend on the diameter of the tube and are given:

$$f_{max} \leq \frac{200}{D} \; ; f_{min} \geq \frac{250}{l-3D} \tag{22}$$

It can also be defined as a function of the distance between the two microphones as given by the standard:

$$s < \frac{0{,}45c_0}{fmax} \tag{23}$$

The standard suggests a distance between the two microphones higher than 5% of the maximum wavelength measured for the inferior frequency. In Table 7 are summarized these limits.

Table 7. Frequency limits based on the impedance tube diameter and microphone distance [84]

Diameter [mm]	**Microphone spacing [mm]**	**f_{min} [Hz] (Standard)**	**f_{max} [Hz] Standard (Diameter)**	**f_{max} [Hz] Standard (Spacing)**	**f_{min} [Hz] (Practice)**	**f_{max} [Hz] (Practice)**
100	50	343	2000	3087	**100**	**1600**
100	100	172	2000	1544	**50**	**1300**
45	30	572	4444	5145	**250**	**4300**
45	100	172	4444	1544	**50**	**1300**
30	20	858	6667	7718	**400**	**6400**

The tube should be at a certain length in order to permit plane wave development between the source, sample, and microphones. The source produces waves close to the plane ones and the closest microphone should be positioned at a distance three times the diameter of the source. As the sample can produce distortion of the acoustic field, the second microscope should be positioned at least at a distance of two times the diameter of the tube from the sample.

2.7 Noise mitigation through Sound-Absorbing Materials

Following the identification of the main noise sources and the discussion of sound-absorbing material typologies and their acoustic characterization presented in the previous chapters, this section addresses noise mitigation measures based on the use of sound-absorbing materials. The focus is not on the definition of comprehensive noise control strategies, but on the discussion of material-based solutions whose acoustic performance has been experimentally investigated and documented in the literature.

In this chapter, the reviewed studies are organized according to the typology and acoustic behavior of the sound-absorbing materials investigated, rather than according to source–path–receiver noise control schemes. This choice reflects the scope of the works considered, which are primarily concerned with the experimental characterization and analysis of materials, while the specific fields of application are explicitly defined within each individual study and are therefore discussed on a case-by-case basis.

The first group of works addresses porous sound-absorbing materials and multilayer acoustic configurations, focusing on their absorption performance and suitability for applications where reduced thickness, high density, mechanical robustness, and fire resistance are required. These aspects are investigated through experimental studies on polyimide foams and multilayer acoustic materials, whose acoustic behavior is analyzed under controlled laboratory conditions. The results provide insight into the potential of such materials for noise mitigation in enclosed and semi-enclosed environments, such as ships (multilayer double porosity materials and polyimide foam) and industrial buildings (polyimide foams).

A second group of studies is devoted to perforated sound-absorbing systems, with particular attention to the influence of geometric parameters on sound absorption performance. These works investigate 3D printed perforated plates with elliptical holes as stand-alone and in multilayer configuration, highlighting how perforation geometry and configuration affect the acoustic response of surface-based absorbers. Owing to their versatility, such systems are applicable in a wide range of contexts, including architectural environments, transport infrastructures, and industrial settings, as detailed in the respective studies.

In addition, a dedicated case study is presented later in the 0 concerning the selection of an appropriate sound-absorbing asphalt typology for rolling-noise reduction, introduced as a specific application example based on the acoustic principles and material properties.

The studies discussed in the following subsections are based on peer-reviewed publications developed by the author in collaboration with other researchers. In all cases, the experimental activities, data analysis, and interpretation of the results were carried out jointly, and the specific contributions of each co-author are acknowledged in the corresponding publications.

2.7.1 Porous Sound-Absorbing Materials and Multilayer Acoustic Configurations

Laboratory characterization of a multilayer acoustic material

Innovative materials to accomplish thermal and sound insulation are constantly emerging from the industry. In this paper one of those innovative materials, mainly destinated to

applications in environments such as yachts and ships, is characterized by means of a three-microphones impedance tube. Several samples were tested, and their properties were found comparable to commonly used foams and porous materials, showing the applicability of this composite material to sound insulation problems in particular environments such as the ones of transportation systems, where non-combustibility, effectiveness, and low weight are essential characteristics.

Introduction

Innovation in materials is a never-ending pursuit and the industry continues to evolve each day. One such innovation is the development of acoustic materials that provide both thermal and sound insulation. These materials find applications in various industries, including transportation systems, where noise and vibration reduction are crucial. Yachts and ships are examples of such environments where noise reduction and vibration control are not just a luxury but a necessity.

In this paper, we present the characterization of a multilayer composite acoustic material specifically designed for use in yachts and boats. By measuring its acoustical properties, we aim to establish the suitability of this material for noise control in those transportation systems where low weight, low thermal conductivity, high thermal temperature range, and effectiveness are key characteristics.

Multilayer materials have been widely used due to their improved acoustic properties compared to single-layer materials. These materials consist of a combination of different layers, each with unique acoustic properties. Kundt tube measurements are commonly used to evaluate the acoustic properties of these materials, e.g., [90], [92]. This technique involves placing a sample in a tube and measuring the sound waves that pass through it. The tube allows for the measurement of the sound absorption coefficient, impedance, and depending on the specific tube configuration (2, 3, or 4 microphones), the normal incidence of sound transmission loss [93], which are important parameters in the evaluation of acoustic materials [94]. Previous studies have shown that the thickness and composition of the layers in multilayer materials can greatly affect their vibrational and acoustic properties, making it important to carefully select and design these materials for specific acoustic applications [95-98]. One of the layers studied corresponds to a double porosity material. A double porosity material could be obtained by drilling holes or slits in a microporous matrix, which can modify its acoustical properties [99]. By implementing such modifications, it is possible to increase and adjust the absorption coefficient of the microporous matrix [100, 101].

This study aims to characterize the acoustic properties of a multilayer composite material designed for applications in the yacht and ship industry. The focus is on the material's sound absorption coefficient and surface impedance when measured from both sides of

the material. The results of this study can provide valuable information for the selection and design of materials for sound insulation and noise and vibration reduction in transportation systems where non-combustibility, effectiveness, and low weight are essential characteristics.

Method

Acoustic measurements were carried out using an experimental setup, as shown in Figure 31. Six multilayer material samples were tested in a Kundt's tube following the standard methodology outlined in ISO 10534-2. The Kundt tube used is suitable for measurements in the frequency range of 100 Hz to 4300 Hz. The setup consisted of an aluminum tube with a diameter of 45 mm, three PCB Piezotronics 378C10 microphones, and a National Instruments USB-4431 data acquisition system [94].

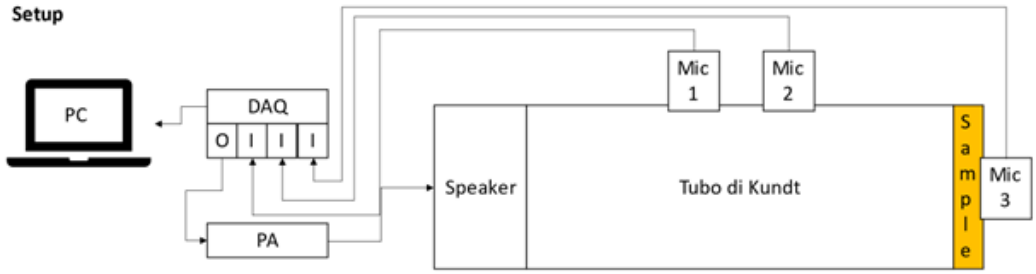

Figure 31. Experimental setup

The multilayer material is composed of three different layers: a thin metal sheet, a rubber sheet, and a porous material. Three types of polyurethane, PTSD-8, PTSD-10, and PTSD-16 were tested, each with two different lengths. The metal and rubber layers have a thickness of approximately 2 mm, while the porous layer has two different thicknesses of 12.5 mm and 25 mm, resulting in total sample lengths of L=14.5 mm and 27 mm, respectively. Some characteristics of the polyurethane foam are presented in Table 8. Porosity, although not reported in the table, is higher for PTSD 8 and decreases for higher formulations (PTSD 10 and PTSD 16). This difference is associated with the foam chemical formulation, the details of which are proprietary and were not disclosed by the material developer.

The samples are depicted in Figure 32, which includes a) a sketch of the layer structure and b) photos of the actual samples.

Table 8. Polyurethane foam characteristics

Material properties	**PTSD-8 Blue**	**PTSD-10 Red**	**PTSD-16 Orange**
Static Elastic module, N/mm^2	0.036	0.048	0.111
Dynamic Elastic module, N/mm^2	0.11	0.144	0.328

Thermal conductivity, W/(m·K)	0.04	0.05	0.05
Operative temperature range, °C	-30 to 70	-30 to 70	-30 to 70
Maximum temperature, °C	120	120	120

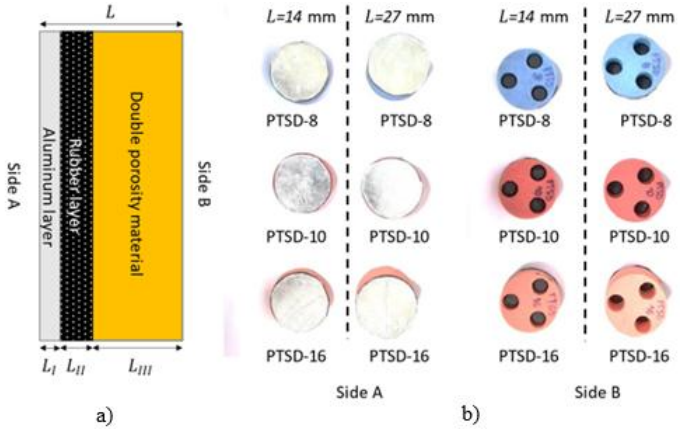

Figure 32. Acoustic material samples. a) Sketch of the layers and b) photos of the samples

Results

This section presents the sound absorption coefficient (for normal and random incidence) and the surface impedance for both sides of the multilayer material.

Figure 33 shows the sound absorption coefficient for both sides, with side A having a lower absorption coefficient than side B. The low absorption coefficient value is because the first two layers of side A have closed pores and exhibit a resonant behavior due to mass-spring interaction; instead, side B exposes the open-cell porous material directly to the sound.

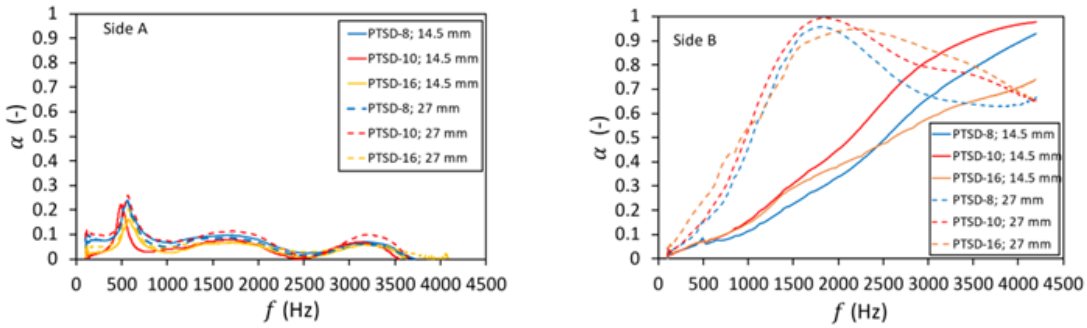

Figure 33. Normal incidence sound absorption coefficient for both sides.

Figure 34 presents the random incidence sound absorption obtained from the experimental values of the normal incidence sound absorption. As can be seen, the values for random incidence are higher than those for normal incidence. The fine-tuning of the absorption peak, observed around 500 Hz for side A, can be done by changing the

polyurethane foam and its thickness, but it is evident that the performance is very similar for all the measured samples.

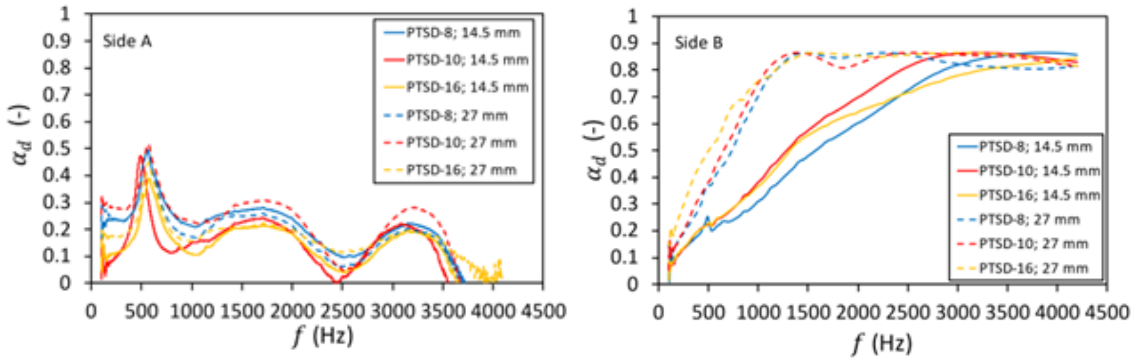

Figure 34. Random incidence sound absorption coefficient for both sides.

Instead, Figure 35 shows the normalized surface impedance for sample PTSD-10 (only one sample is depicted for clarity, the other samples have a similar behavior). The resonant behavior is observed for side A. On the other hand, side B presents typical impedance curves of a porous material.

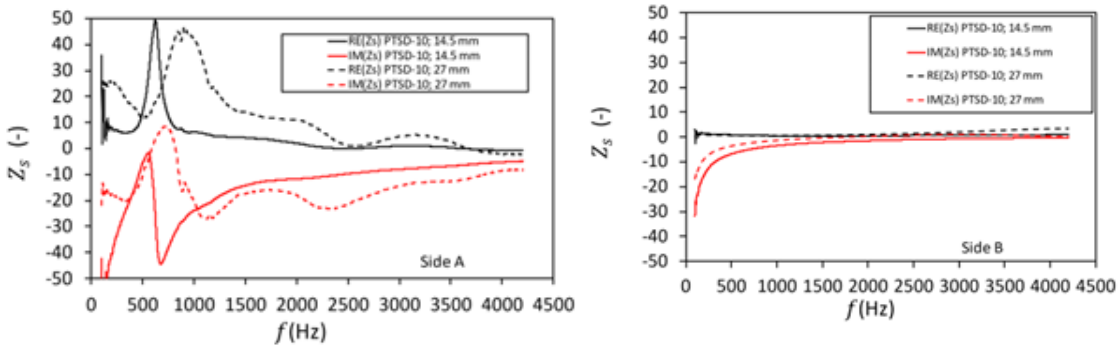

Figure 35. Normalized surface impedance. Sample PTSD-10.

The sound absorption coefficient and surface impedance were measured for both sides of the material. The acoustic behavior of the material changes significantly depending on which side is exposed to sound. While the three porous materials tested show slight differences, thickness is a key determinant of performance. The selection of a particular material should consider the characteristics presented here and other factors such as thermal insulation needs, weight, and cost (the polyurethane foam cost is proportional to density).

Based on the results presented, it is evident that the multilayer composite material tested in this study is a promising solution for noise and vibration control in particular environments, such as naval transportation systems, where thermal, mechanical, and acoustical properties are essential characteristics. However, further research is needed to

investigate the transmission loss and the material's behavior under different conditions as well as to optimize its performance for specific applications.

Conclusions

This study presented the characterization of a multilayer material using an impedance tube. The results showed that the face that exposed the aluminum layer presented a low absorption with a resonant peak at low frequencies, which could be suitable for acoustic insulation. On the other hand, the face that exposed the double porosity material (polyurethane foam) presented a higher absorption; the thicker polyurethane foam layer provided a higher absorption, especially at low frequencies. This orientation (polyurethane foam) could be used for noise absorption. However, it should be noted that in the yacht industry, this type of panel is typically involved in solving vibrational, acoustic, and thermal insulation problems of the machinery room and occasionally acoustic absorption inside the cabins. Therefore, a balance between the thermal and the acoustic characteristics must be considered when selecting a specific material. Overall, the findings of this study provide useful insights into the acoustic performance of the multilayer material and could contribute to developing more effective acoustic and thermal insulation solutions for the yacht and ship industry.

Sound absorption of polyimide foams, an experimental study

Polyimide foam panels have emerged as advanced solutions in naval, nautical, aeronautical, and railway industries, overcoming limitations associated with the high densities and thicknesses of traditional thermal and acoustic insulation materials. This study aims to experimentally characterize the sound absorption coefficient of both standard and mechanically crushed polyimide foams within the 200-4300 Hz frequency range, utilizing the Standing Wave method with three microphones. Thermally cut samples, designed for thermal insulation, show significant absorption in high-frequency ranges but are less effective at lower frequencies. Remarkably, the mechanical compression of these samples transforms closed pores into open and interconnected structures, substantially enhancing absorption at lower frequencies. This phenomenon is also observed in acoustically cut samples. Polyimide foam shows tunable sound absorption, with the degree of enhancement dependent on variables such as the number of compression cycles, the applied force magnitude and rotational forces (not evaluated in this paper). Further investigation into these mechanical influences promises insights into optimizing the acoustic performance of polyimide-based solutions.

Introduction

Polyimide foams in comparison with other polyurethane foams exhibit excellent behavior in terms of thermal resistance, high working temperatures, fire resistance, low smoke and no toxic gas emission [102]. Different investigations through scanning electron microscopes (SEM) concerning the microstructure of the polyimide foam shows that their structure can be considered as interlinked struts forming packing of cells interconnected to others through pores. Based on their microstructure composition, polyimide foams can be characterized by closed cells which make them rigid and perfect material to be used as a thermal insulator due to their capacity to snare the air passing through it or open cell (partially or fully reticulated) structures which usually are less rigid and great sound absorbers [103]. But this depends on the fabrication process or other subsequent applied processes upon them.

Over the years different fabrication processes have been invented and still used such as the powdered foaming method [104], polycondensation method [105], closed mold foaming method [106], freeze-drying method [107-108] and 3D printing method [109]. From the powder forming method can be obtained polyimide foams with high densities and nonuniform structures. On the other hand, closed mold forming permits obtaining low-density foams with a uniform structure. The polycondensation method remains the widely used due to the low costs of production. Freeze-drying has the advantage of producing foams with integral 3D structures and adjustable shapes. Moreover, 3D printing allows to create arbitrary shapes but with high costs [110]. Thanks to their high mechanical strength, fire resistance, heat resistance, sound absorption, etc, polyimide foams are emerging in different field such as naval, nautical, aeronautical, and railway industries, so that, lot of studies are conducted in order to characterize and improve their properties. It was seen that sound absorption of the foams is directly affected by the foam microstructure and the service environment. An increase in thickness lead to an increase of the sound absorption in low frequency range and in contrary a decrease in density (through increasing the amount of the blowing agent) lead to increase of α. Moreover, as cell size decreases, the interfacial area between the solid frame and the fluid resistance increases, so that the viscosity dissipation of sound wave increases and the value of α increases in the mid and low frequency region. The ambient temperature increase causes a decrease in α [111]. On the contrary, the increase of the slurry temperature from 0◦C to 40◦C led to increase of the window opening rate from 6.85% to 58.46%, with a double increase of the sound absorption coefficient and even more for high frequency range over 10^3 [112].

Producing closed-cell foams is generally cheaper and simpler than open-cell foams. The airflow resistivity of these foam is so high and have to be decreased to an acceptable level to have sound absorption. For this reason, further optimization methods as thermal or chemical reticulating methods which consists in the destruction of the membranes and obtaining fully or partially reticulated materials. Chemical reticulation means that the

destruction of the membranes is reached by using chemical agent. It ensures higher absorption coefficient 0.6 at 2 kHz and 0.8 at 4 kHz but air flow resistivity and tortuosity are greatly decreased [113].

Instead, mechanical reticulation or mechanical compression makes possible to obtain a sound absorption coefficient 0.9 at 2 kHz but it decreases above 2 kHz to reach 0.6 at 4 kHz [113]. Also in other studies, the mechanical compression from 20-90% of the original thickness of the polyimide foams leads to a relevant increase in sound absorption performance. Furthermore, the measurement of double wall sound transmission loss application of mechanically crashed polyimide was consistent with the prediction of the poroelastic material model modeled by Statistical Energy Analysis (SEA) software [114]. Shock wave treatment is another method to remove the membranes closing the pore cells and though to improve the absorption performance of the polyimide foams. By increasing the shock wave amplitude Ms<1,58 the amount of the destroyed membranes increases and consequently, the sound absorption increases too. For 1,53<Ms>1,73 the sound absorption decreases after a plateau due to the increase of the plastic deformation and so a strong increase of the airflow resistivity [115].

This paper is focused on acoustical characterization based on the standard methodology outlined in ISO 10534-2 of the pristine and mechanically crashed polyimide foams in a wide frequency range of 200-4300 Hz. The first round of measurements consists in the measurement of the sound absorption coefficient of the 8 samples of the pristine 'Soliboard' originating from expanded polyimide already treated in a previous study and widely used in the naval industry [116], but in a more extended frequency range. Instead, the second round of measurement refers to the definition of the α of mechanically reticulated samples corresponding to 10%, 20% and 40% decrease of its original length. Higher mechanical compression led to lower absorption in frequency range 200-700 Hz and a relevant increase 700-1700 Hz with α close to 1 but again decreases in high frequencies compared to the α of the pristine one.

Materials and Method

As already mentioned, the present study is focused on the experimental characterization of the standard polyimide foam samples and mechanically compressed ones. In Figure 36, the images of different samples of polyimide foams treated in this study are represented. Data about the sample thicknesses and the surface finishers are given in Table 9.

Uncoated polyimide foam | Polyimide foam with RMW thin coating layer | Polyimide foam with VBD thin metal coating layer

Figure 36. Images of polyimide samples with and without covering layers

The pristine samples S1 to S8 differ from each other in thickness (25 cm and 50 cm), coating layer (naked, RMW or VBD) and microstructure (based on the production process they can be with open or closed cell structures). Some of them are designed as thermal insulation materials and the remaining ones as sound-absorbing materials. Based on their use, the Soliboard panels can be reinforced with polyester film (RMW) which provides a barrier to vapours and chemical agents used in machineries and living spaces in ships, or with fiberglass scrim and aluminized polyester film (VBD) which provides a vapour barrier as well that is also highly fire resistant. These polyimide foams are mostly used in air conditioning ducts on ships. Polyimide foams reinforced with the aluminized film are used also in the commercial buildings sector as duct liners as they satisfy the requirements about fire resistance, thermal and acoustical performance, resistance to mold growth, etc.

Table 9. Properties of the tested samples

Sample ID	Thickness [mm]	Cutting method	Surface finish
S1	25	Thermal	–
S2	25	Thermal	RMW
S3	25	Thermal	VBD
S4	50	Thermal	RMW
S5	25	Acoustic	–
S6	25	Acoustic	RMW
S7	25	Thermal	RMW
S8	50	Acoustic	RMW

Mechanical compression is then applied to two samples, the S1 uncoated polyimide foam (25 mm thick) and the S4 polyimide foam sample with RMW coating (50 mm thick), causing a decrease of their original thickness of about 10%, 20% and 40% (see Figure 37).

Original sample | 10% thickness reduction | 20% thickness reduction | 40% thickness reduction

Figure 37. Example of the mechanically compressed samples

As already mentioned, the compression led to the crushing of the membranes interlinking the pores which led the samples to become partially open-cell. The sample ID and their thicknesses are presented in the following Table 10.

Table 10. Mechanically reticulated samples

Original sample	Sample ID	Thickness [mm]	Surface finish
S4	SC9	45	RMW
S4	SC10	40	RMW
S4	SC11	30	RMW
S1	SC12	22.5	–
S1	SC13	20	–
S1	SC14	15	–

The experimental setup shown in Figure 38 consists of a standing wave tube based on the standard methodology outlined in ISO 10534-2 [88]. The impedance tube used is suitable for measurements in the frequency range from 200 Hz to 4300 Hz. The apparatus consists in an aluminum tube with an internal diameter of 45 mm, three PCB Piezotronics 378C10 microphones, and an NI USB 4431 data acquisition system. All the measurements are conducted by maintaining a rigid end.

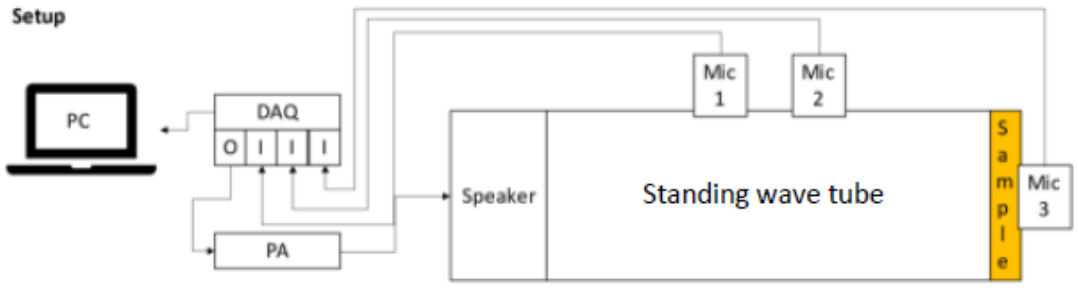

Figure 38. Experimental set-up

Results and Discussion

The results of the measurements for the samples S1 to S8 are summarized in Figure 39 and Figure 40. The sample S1, designed as a thermal insulation material without any covering layer presents a considerable absorption, reaching a peak of the absorption coefficient between 2900 Hz and 3200 Hz. A shift towards the 2600 Hz - 2900 Hz range is observed for sample S7 reaching an absorption coefficient close to 1 and a second peak with lower absorption at about 3800 Hz. Instead, the samples S2 and S3, both with surface finishings, provide lower absorption if compared to sample S1. A shift of sound absorption towards lower frequencies is noticed for sample S4 (50 mm thick), having two peaks with α around 0.9 in the frequency range between 1300 Hz and 1500 Hz, and the second peak covering a very wide frequency range from 2400 Hz to 4300 Hz.

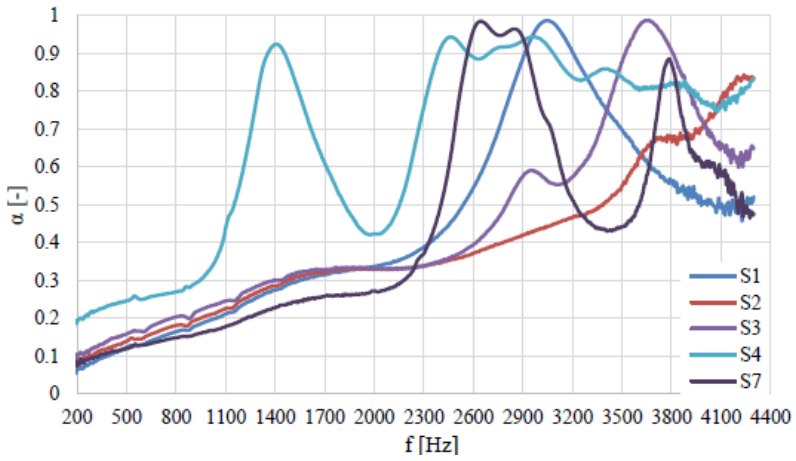

Figure 39. Sound absorption coefficient of the thermal samples S1 to S4 and S7

The samples designed as sound absorption materials show higher absorption as expected, having an open porous structure. The uncoated S5 sample reaches a coefficient of about 0.4 at 1200 Hz and of about 0.9 around 2400 Hz.

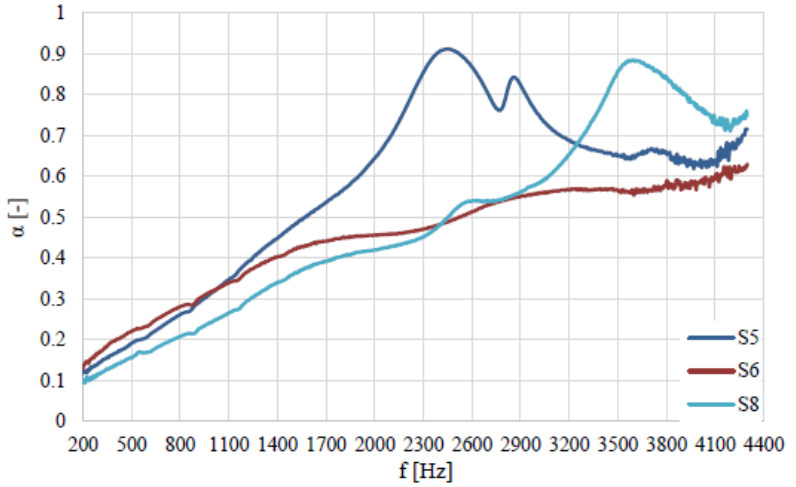

Figure 40. Sound absorption coefficient of the acoustic samples S5, S6 and S8

On the other hand, sample S6 which has a reinforced RMW layer but is of the same thickness as the S5, shows lower absorption. The increase in thickness of sample S8 from 25 mm to 50 mm led to a slight increase in absorption for higher frequencies ranges over 3000 Hz.

In Figure 41 is shown that, after mechanically crushing the samples by applying compression cycles to them, as expected and witnessed in different studies [114-115], the sound absorption was greatly improved. With just a 10% reduction of the original thickness, i.e. the SC9 sample, it can be observed that the absorption is tuned and shifted towards lower frequencies but with a slight decrease of the peak from about 0.9 to 0.85. The increase of compression reaching the 20% of the original thickness (sample SC10) highlights more this effect. Furthermore, sample SC11 being compressed and having a reduction of the original length of 40% led to further shift towards lower frequencies, increase of the first peak and extension in wide frequency range. Instead, a decrease of the absorption in higher frequencies is obtained for such compression.

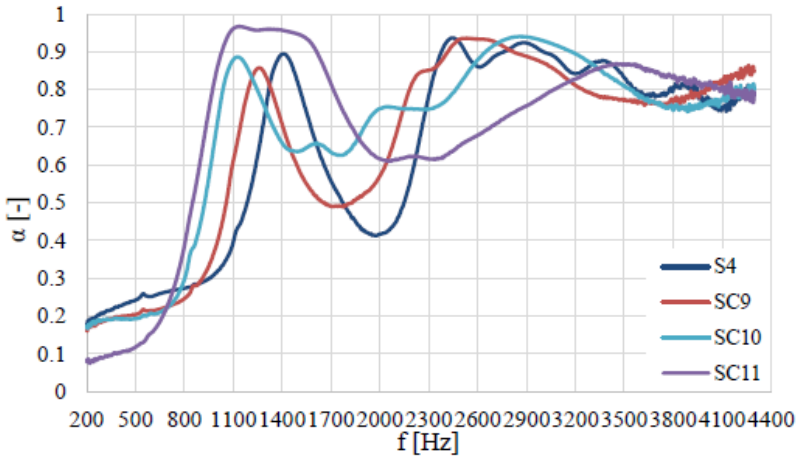

Figure 41. Sound absorption coefficient of mechanically compressed samples S9 to S11 and the original S4

Referring to the sample S1, after 10% reduction of its original thickness (sample SC12), the sound absorption enhances having two peaks where the first one is shifted towards lower frequency ranges, but the peak is lower if compared to the peak reached by S1 sample (see Figure 42).

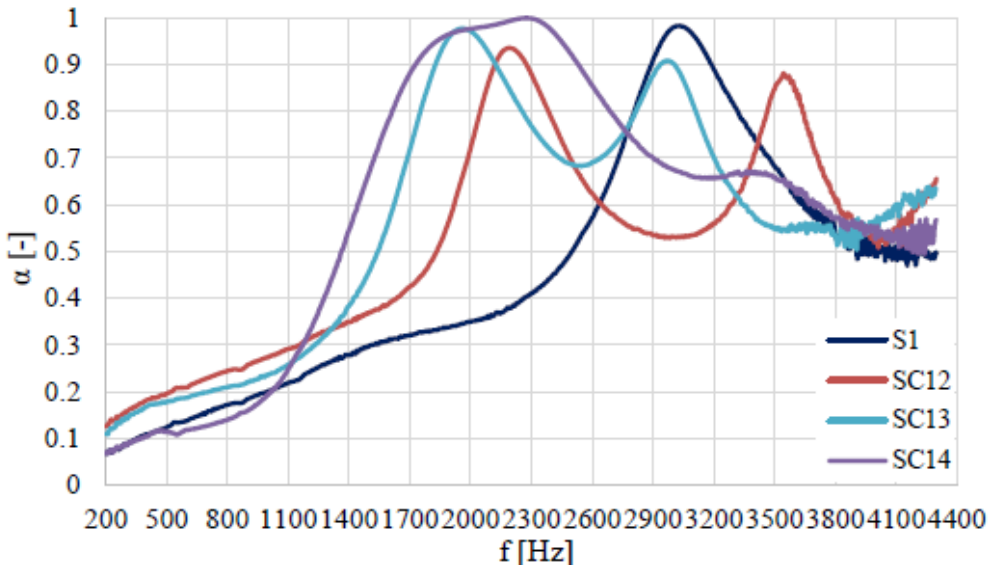

Figure 42. Sound absorption coefficient of mechanically compressed samples S12 to S14 and the original S1

By increasing the compression cycles, passing from 10% to 20% reduction of the original thickness, the progression is the same of sample SC12 but with higher peaks and displaced towards lower frequencies. After 40% reduction of the thickness, the absorption is increased and spread in a wide frequency range.

The mechanically crushed samples at the beginning reduce their thickness, but after one day it is observed that the samples tend to return to their initial shape by increasing their thickness of at least 2 mm up to 5 mm, as showed in Table 11.

Table 11. Samples thickness after 1 day

Sample ID	Initial thickness [mm]	Thickness after 1 day [mm]	Surface finish
SC9	45.0	47.0	RMW
SC10	40.0	44.0	RMW
SC11	30.0	35.0	RMW
SC12	22.5	25.0	–
SC13	20.0	24.0	–
SC14	15.0	19.0	–

Conclusions

This paper focuses on the acoustical characterization of polyimide foams using the ISO 10534-2 methodology and is based on two measurement campaigns. The first extends the frequency range of sound absorption measurements previously performed, while the second investigates mechanically reticulated samples obtained through controlled compression cycles (10%, 20%, and 40%), showing partial thickness recovery after one day and reduced low-frequency absorption accompanied by a significant increase between 700 Hz and 1700 Hz. From this study the following aspects were observed:

1. For most of the samples from 100Hz to 2000 Hz the sound absorption coefficient increases linearly with the increase of the frequency. But after that each one presents different behaviors with different peaks achieved at different frequencies. The uncoated samples present better behavior than the ones with RMW or VBD surface finish, reaching peaks of α close to 1 and covering more frequencies, for both thermal and acoustic designed samples.

2. Higher mechanical compression led to a relevant absorption increase from 700 Hz to 1700 Hz, whereas it decreases at higher frequencies if compared to the α of the non-crushed one.

3. The samples tend to recover their initial thickness one day after the mechanical compression.

Further research is needed to explore optimization strategies for compression parameters and investigate long-term stability post-compression.

2.7.2 Perforated Sound-Absorbing Systems

Effect of geometrical parameters of elliptically perforated plates on the sound absorption performance

The integration of perforated plates in acoustic applications has gained interest for their effectiveness in noise mitigation, especially in low to mid-frequency ranges, while keeping a lightweight and compact design. However, significant absorption at lower frequencies remains challenging, as performance is closely tied to pore geometry. This study investigates the effect of geometric parameters, namely, the shape factor (β) and pore area, on sound absorption performance in two configurations: one with an airgap backing layer and the other with melamine foam. The plates were fabricated using stereolithography 3D printing, and sound absorption testing was conducted between 200-4300 Hz via impedance tube tests, following ISO standard 10534-2. Results indicate that increased shape factor enhances absorption rates at mid to high frequencies, particularly in micro-perforated plates (equivalent diameter < 1mm). The inclusion of the melamine foam layer significantly boosts absorption in the mid-low frequency range. In conclusion, modest shape factor (β) and pore area changes can substantially improve sound absorption, indicating potential for future research on optimal configurations to maximize performance in lower frequency ranges.

Introduction

Since the 1960s, acoustic perforated plates have been meticulously engineered to control sound transmission through precisely arranged apertures that promote absorption and

diffusion [117, 118]. Research in this area remains dynamic, with continued advancements in design and analysis methodologies [119]. Perforated plate absorbers operate based on acoustic resonance, wherein each aperture acts as a resonator that, when excited at its natural frequency, induces amplified air motion within the cavity, enhancing viscous and thermal dissipation and thereby maximizing sound absorption. Perforated acoustic systems are conventionally categorized by aperture dimensions: macro-perforated systems possess hole diameters ranging from 1 mm to 1 cm, whereas micro-perforated panels (MPP) feature sub-millimetric apertures [120]. The fundamental acoustic characteristics of these systems are governed by parameters such as porosity and flow resistivity, both of which are intrinsically correlated with the size, geometry, and distribution of the perforations [121]. Over the years, numerous analytical models have been developed to characterize the acoustic behavior of perforated plates. Early contributions by Rayleigh and Crandall described sound propagation in narrow tubes [122-123], later extended by Ingard to include viscous losses, multi-aperture interactions, and backing cavities [120]. Maa further refined the model in the 1970s for micro-perforated panels (MPPs) by incorporating thermo-viscous boundary layer effects into a lumped mass-spring system, enabling accurate high-frequency absorption predictions [124]. Perforated plates can also be modeled by the Johnson-Champoux-Allard model, which introduces frequency-dependent formulations for effective density and bulk modulus based on porosity, tortuosity, and characteristic lengths, later enhanced by Atalla and Sgard to include rigid-frame effects [125]. Contemporary models integrate complex geometries, material anisotropies, and computational methods to meet modern engineering demands.

Due to their compact form factor, low mass, and high effectiveness in attenuating low to mid frequency noise, perforated plates are increasingly deployed as standalone absorbers and components within multilayer acoustic systems. Their performance is predominantly influenced by the perforation geometry and area, given that the plate thickness is typically limited to the millimeter scale. The advent of additive manufacturing technologies, particularly 3D printing, has enabled the fabrication of intricate geometrical configurations, thereby broadening the scope of design possibilities [126]. Numerous investigations have examined multilayer acoustic absorbers incorporating 3D-printed MPPs with varying pore geometries, air gap thickness, and porous backing materials. The influence on the sound absorption of the hole diameter, perforated plate and air gap thickness of circular perforated panels was studied, resulting in absorption peak shifts in low-mid frequencies due to air gap increase and hole area decrease [127]. The experimental measurement results agree pretty well with results coming from the Maa theoretical model. The effect of the perforation ratio and the air gap thickness was also confirmed in the study, where perforated plates with circular and quadratic holes were considered [128]. In another study, multilayer systems composed of circular perforated

plates and porous materials confirmed, once again, the absorption increase with the increase in airgap layer [129]. Innovative investigations into non-circular perforation geometries, such as maze-like, hexagonal, and star-shaped apertures, fabricated from titanium and paired with porous media, have revealed that star-shaped perforations yield superior absorption performance. Theoretical predictions for these configurations were validated through experimental measurements conducted using impedance tube techniques [130].

Despite these advancements, the literature addressing elliptically perforated plates remains sparse [131, 132]. The present study seeks to bridge this gap by systematically investigating the acoustic performance of elliptically perforated panels. The configurations examined include panels backed by a 24 mm air gap as well as those combined with a melamine foam layer to achieve broadband sound absorption. This investigation focuses specifically on the influence of geometrical parameters, including the shape factor (β=b/a) and area of elliptical apertures, while maintaining all other design variables constant. The analysis spans both the micro and macro perforation regimes, corresponding to the area of equivalent circular pore diameters below, equal to, and above 1 mm. The perforated plates were fabricated using Stereolithography (SLA) 3D printing with a photopolymer resin as the base material. Acoustic characterization is performed in accordance with ISO 10534-2, using impedance tube measurements across the frequency range of 200 to 3800 Hz [88].

Materials and methods

The perforated plates (see Figure 43) were produced using Stereolithography 3D printing employing photopolymer resin as a printing material. Their thickness, d, is 2 mm with a diameter of 45 mm. In total, 25 perforated plates were printed with elliptic hole dimensions that vary according to the elliptic area (A_e) and shape factor (β) variation in the range [0.2-1] with an increasing step of 0.2. To evaluate the acoustic behavior of the elliptic macro and micro perforated plates, elliptic areas lower and higher than the circle area (A_c) of 1mm diameter, as it is the cutoff point between the micro and macro perforation, are considered. More precisely A_e = 0.5, 0.75, 1, 1.25, 1.5 A_c. Perforated plates with elliptic hole areas 0.5 and 0.75 A_c are considered microperforated plates (MPP), instead, for elliptic hole areas 1, 1.25, and 1.5 A_c are considered as macroperforated plates (PP).

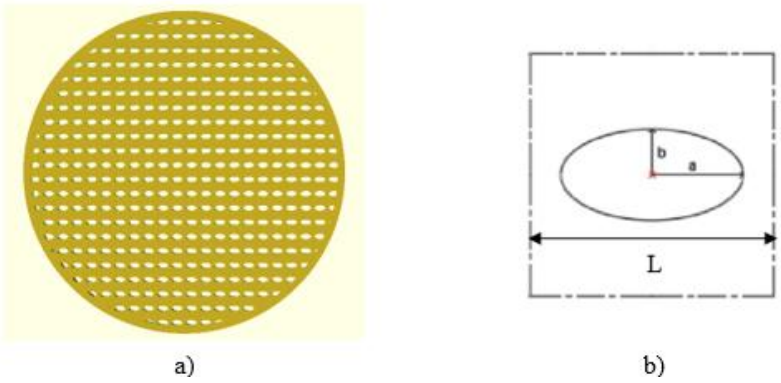

Figure 43. (a) Elliptic perforated plate configuration and (b) cell detail

For simplicity in Table 12 are given the sample geometrical properties just for 10 samples instead of 25, corresponding to A_e equal to 0.75 and 1.25 A_c.

Table 12. Perforated plates dimensions

	MMP A_e = 0.75 A_c of 1 mm diameter					**PP A_e = 1.25 A_c of 1 mm diameter**				
β	**a [mm]**	**b [mm]**	**A_e [mm^2]**	**ϕ [-]**	**L [mm]**	**b [mm]**	**a [mm]**	**A_e [mm^2]**	**ϕ [-]**	**L [mm]**
0.2	0.87	0.22	0.59	0.2	1.73	1.12	0.28	0.98	0.2	2.24
0.4	0.68	0.27	0.59	0.2	1.73	0.88	0.35	0.98	0.2	2.24
0.6	0.56	0.34	0.59	0.2	1.73	0.72	0.43	0.98	0.2	2.24
0.8	0.48	0.39	0.59	0.2	1.73	0.63	0.50	0.98	0.2	2.24
1	0.43	0.43	0.59	0.2	1.73	0.56	0.56	0.98	0.2	2.24

where:
a – major diameter
b – minor diameter
β – represents the shape factor (b/a); ratio between the minor and major diameter
A_e – area of the ellipse
A_c – area of the circle
ϕ – sample porosity
L – cubic cell dimension

Instead, the porous material used for the configuration 'perforated plate + porous material' is 24 mm melamine foam with a density of 10 kg/m^3 and physical parameters as shown in Table 13.

Table 13. Physical properties of the 24 mm melamine foam

Material	**Air flow resitivity σ [Pa·s/m]**	**Porosity ϕ [-]**	**Tortuosity α_∞ [-]**	**Viscous characteristic length Λ [-µm]**	**Thermal characteristic length Λ′ [-µm]**
Melamine	10550	0.99	1.01	100	188

The adopted methodology entailed determining the normal incidence sound absorption coefficient (α) of the 3D-printed perforated plates in different configurations using a three-microphone standing wave impedance tube in accordance with ISO 10534-2 [88].

The configurations examined in this study (see Figure 44) consist of:

i) elliptically perforated plate with an airgap backing layer of 24 mm;

ii) elliptically perforated plates paired with 24 mm melamine foam layer to enhance sound absorption in broadband frequencies.

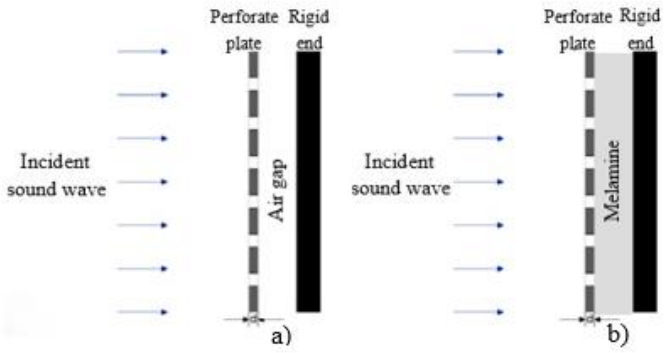

Figure 44. a) Configuration 1. Elliptic perforated plate + air gap; b) Configuration 2. Elliptic perforated plate + melamine foam

Results and discussion

Starting with the first configuration, which considers a multilayer system composed of the perforated plate and 24 mm constant air gap, the effect of shape factor (β) variation from 0.2 to 1 with an increasing step of 0.2 and ellipse area variation from 0.5-1.5 A_c of 1 mm diameter with increasing step of 0.25 (while all the other parameters are kept constant) on sound absorption is studied.

As shown in Figure 45, increasing the shape factor from 0.25 to 0.4 results in a noticeable reduction in the peak sound absorption coefficient, from 0.6 to 0.5. Further increases of β led to a continued but marginal decline of the absorption coefficient of 0.05, beyond which no significant variation in absorption is observed. This suggests that shape factor has no diminishing influence on absorption beyond a certain threshold, corresponding to the β 0.6.

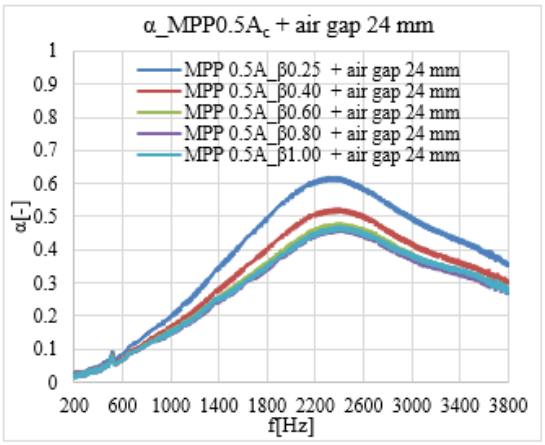

Figure 45. Sound absorption coefficient of the MMP(Ae=0.5Ac) + air gap 24 mm

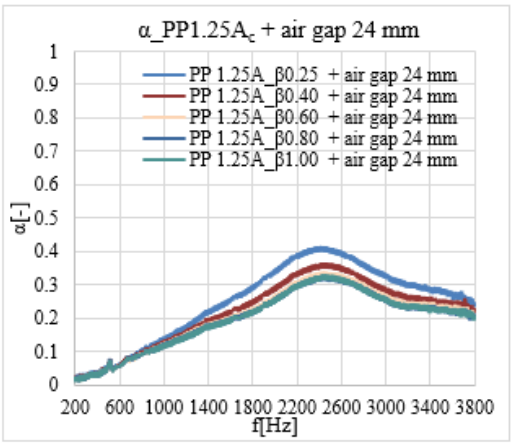

Figure 46. Sound absorption coefficient of the MMP(Ae=1.25Ac) + air gap 24 mm

For ellipse area $1.25A_c$ (see Figure 46), a similar trend is observed as in the case with $0.5\,A_c$. The sound absorption coefficient declines with increasing the shape factor; however, the peak absorption reaches 0.4 for shape factor (β) of 0.25, and the rate of decrease is more gradual compared to the previous configuration. This indicates a less pronounced sensitivity to the shape factor at higher aperture areas.

Figure 47 shows how the absorption coefficient changes, varying the A_e while keeping constant the shape factor (0.25) and porosity (0.2). As A_e increases, the overall absorption profile retains a similar shape, with reduced peak values. This trend underscores the positive effect of the smaller perforation area on enhancing the sound absorption performance.

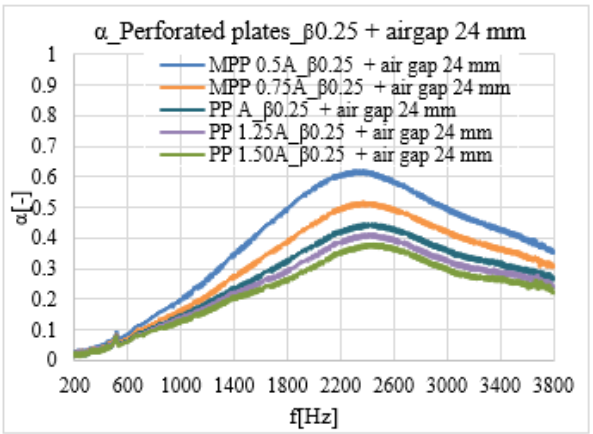

Figure 47. Sound absorption coefficient of the MMP and PP with β 0.25 + air gap 24 mm

The second configuration comprises a perforated plate backed by a 24 mm layer of melamine foam, terminated by a rigid boundary. It is well established that porous materials such as melamine foam exhibit high absorption efficiency in the mid-to-high

frequency range [133], whereas perforated plates predominantly enhance absorption in the low-to-mid frequency domain.

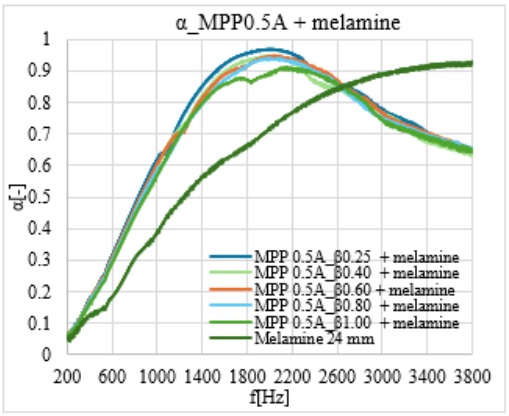

Figure 48. Sound absorption coefficient of the MMP(Ae=0.5Ac) + melamine 24 mm

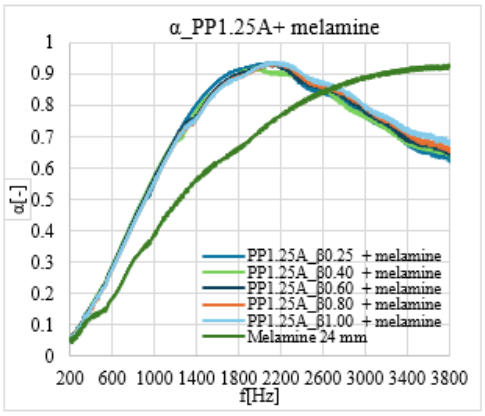

Figure 49. Sound absorption coefficient of the MMP(Ae=1.25Ac) + melamine 24 mm

As illustrated in Figure 48, for micro-perforated panels (MPPs) with an elliptical aperture area equivalent to 0.5 A_c, the incorporation of the perforated plate significantly enhances low-frequency absorption across all the shape factors. Specifically, absorption coefficients reach 0.4 at 700 Hz, in contrast to the melamine foam alone, which achieves comparable performance only at 1000 Hz. The effect of β is evident in the magnitude of peak absorption: lower β values correspond to higher peak absorption.

In contrast, for an elliptical aperture area of 1.25 A_c, the peak sound absorption remains consistent across all β values, as illustrated, as shown in Figure 49.

A comparative analysis of all perforated plates with a fixed β of 0.25, presented in Figure 50, reveals that smaller elliptical apertures yield marginally higher peak absorption coefficients. However, this variation exerts a negligible influence on the absorption behavior at lower frequencies.

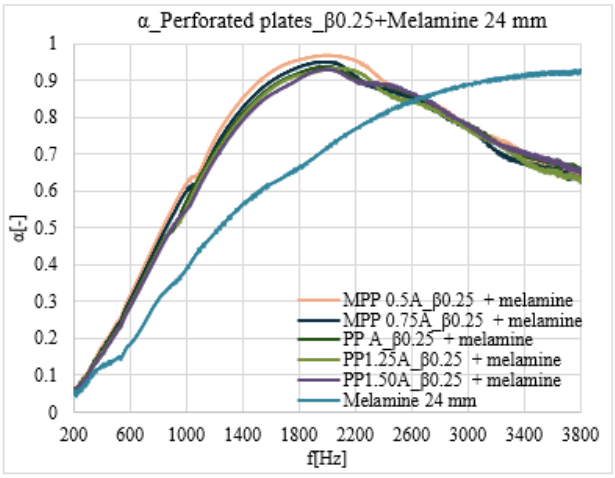

Figure 50. Sound absorption coefficient of the MMP and PP with β 0.25 + melamine 24 mm

Conclusions

The experimental findings related to the initial configuration, characterized by a perforated plate with an air gap, demonstrate a significant enhancement in sound absorption in the mid to high-frequency spectrum as the β parameter is reduced, especially for micro-perforated plates. Notably, a decrease in β from 0.4 to 0.25 results in a marked increase in the absorption coefficient, peaking at approximately 0.6 within the 2100 to 2500 Hz range. This effect is diminished in elliptical pore regions larger than 1 mm, leading to a decline in overall absorption with the transition to macro-perforated plates, where reduced β yields minimal benefits.

In a multilayer configuration comprising an elliptical perforated plate and melamine foam, the absorption coefficient shows considerable improvement, particularly with micro-perforated plates of 0.25 β value. The coefficient begins at 0.3 at 600 Hz and rises almost linearly to 0.95 within the 1800 to 2200 Hz interval, contrasting with melamine foam alone, which starts at 0.2 at 600 Hz and peaks at 3400 Hz. The impact of the β parameter is increasingly evident when the porous material is integrated with the micro-perforated plate, as reductions in β enhance peak absorption in the low to mid-frequency ranges. In summary, these findings highlight that slight adjustments to the β parameter can lead to significant improvements in sound absorption, particularly in the lower and mid-frequency domains influenced by the perforated plate, while melamine foam primarily affects higher frequency ranges. Future research should explore alternative configurations to further enhance sound absorption in lower frequency ranges and incorporate numerical simulations or analytical models for a deeper understanding of the underlying mechanisms.

2.7.3 Summary of Acoustic Materials and Performance

This chapter provides a comparative summary of the acoustic materials investigated in this work, bringing together their main characteristics, sound absorption performance, and underlying mechanisms. The results are synthesized in a unified table (see Table 14) to facilitate direct comparison between different material typologies and configurations. The results show that hybrid and optimized porous systems provide the highest performance. Micro-perforated plates combined with melamine foam achieve peak absorption of $\alpha \approx 0.96$ due to the combined effect of resonance and porous dissipation. Reticulated polyimide foams also perform well ($\alpha \approx 0.9$–1.0), with enhanced mid-frequency absorption resulting from improved pore interconnectivity. Multilayer polyurethane systems are effective when the porous side is exposed, with thickness shifting the absorption peak toward lower frequencies (~1500–2200 Hz). Conversely, macro-perforated plates ($\alpha \approx 0.4$) and coated foams ($\alpha < 0.8$) show lower efficiency due to reduced dissipation. These materials are suitable for applications such as ship cabins, ducts, and lightweight acoustic panels depending on the target frequency range.

Table 14. Summary of the acoustic materials investigated in this work

Material / Sample ID	Configuration (layers & backing)	Thickness [mm]	Density [kg/m²]	Perforation parameters [mm]	Frequency band α > 0.6 [Hz]	Peak freq. [Hz]	Peak α [-]	Absorption mechanism	Port applicability
Multilayer (PTSD-8)	Metal side exposed (Al + rubber front+PU), rigid backing	27	–	d=13	None (α < 0.6)	~400–600	~0.2–0.25	Resonant (mass–spring system due to metal + elastic layer)	Structural insulation or technical rooms (low-frequency vibration control)
Multilayer (PTSD-8)	Foam side exposed (PU+rubber+Al), rigid backing	14.5	–	d=13	2500–4200	~3800	~0.9–0.97	Porous (viscous losses in open-cell polyurethane)	Ship panels (high-frequency noise control)
Multilayer (PTSD-8)	Foam side exposed (PU+rubber+Al), rigid backing	27	–	d=13	1000–2500	~1500–2200	0.95~1.0	Porous + thickness effect (enhanced dissipation + quarter-wavelength shift)	Machinery rooms / cabins
Polyimide (S1-thermal)	Uncoated foam, rigid backing	25	–	–	2600–3200	~3000	~0.9–1.0	Porous (mainly closed pore structure)	Naval / HVAC ducts
Polyimide (S2_RMW)	Coated foam (polyester), rigid backing	25	–	–	3600-4300	~4100–4300	<0.8	Porous (limited by surface coating reducing permeability)	Machineries, living spaces in ships
Polyimide (SC12 – reticulated S1)	Reticulated (~10% compression), rigid backing	~22–25	–	–	1900–2700	~2200-2300	~0.92	Partially reticulated porous (incomplete pore opening)	Transport / naval systems/industrial buildings
Polyimide (SC11 – best reticulated S4)	Reticulated (~40% compression), rigid backing	~30–35	–	–	900–4300	~1000–1600	~0.95–1.0	Enhanced porous (fully reticulated → improved tortuosity & dissipation)	Transport / naval systems / industrial buildings
Perforated plate (worst)	PP (Ae = 1.25Ac) + 24 mm air gap	2	–	Ae = 1.25Ac	None (α < 0.6)	~2400	~0.4	Resonant (low viscous losses due to large perforations)	Lightweight panels (limited efficiency)
Perforated plate (best)	MPP (Ae = 0.5Ac, β = 0.25) + 24 mm air gap	2	–	Ae = 0.5Ac, β = 0.25	2100–2500	~2300	~0.6	Resonant (Helmholtz-type with enhanced viscous losses)	Architectural environments/ transport infrastructures
Melamine foam	Melamine foam alone, rigid backing	24	10	–	1500–4300	3400–4300	~0.92	Porous (low density, high porosity material)	Buildings / Indoor liners / transport
Perforated + foam (best)	MPP (Ae = 0.5Ac, β = 0.25) + melamine 24 mm	26	10	Ae = 0.5Ac, β = 0.25	1000–2500	1800–2200	~0.96	Hybrid (resonant + porous → broadband enhancement)	Buildings / transport
Perforated + foam	PP (Ae = 1.25Ac, β = 0.25) + melamine 24 mm	26	10	Ae = 1.25Ac, β = 0.25	1150–2500	1900–2200	~0.94	Hybrid (resonant + porous, less efficient than MPP)	Buildings / transport

2.8 Noise Mitigation Intervention through Acoustically Optimized Asphalt

The proposed intervention for the selected section of the port road network in La Spezia (Figure 51) is based on the outcomes of the ante operam acoustic assessment. Measurements indicate that the acoustic environment is predominantly influenced by heavy vehicle traffic operating at low speeds (30–60 km/h), with rolling noise associated with tire–road interaction, identified as the dominant source through acoustic camera analysis and confirmed by phonometric measurements.

With the entry into force of the updated *CAM Strade* regulation in December 2024 (Minimum Environmental Criteria for the design, construction, maintenance, and upgrading of road infrastructures), the identification of the intervention area required revision. In particular, the originally selected road section was modified, so the length was increased to comply with the new regulatory requirements, which prescribe a minimum length of 200 m (100 m per direction) to enable acoustic performance assessment through Close Proximity (CPX) measurements.

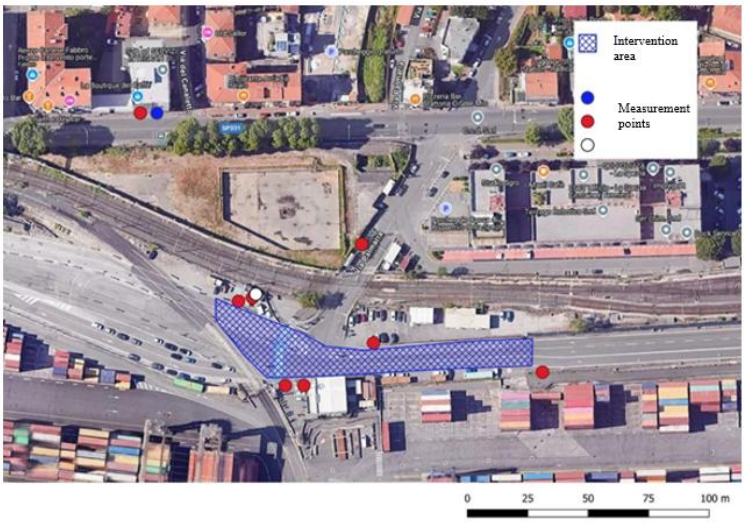

Figure 51. Identification of the intervention area

The adopted solution consists of a low-noise dense-graded bituminous mixture, specifically designed for port environments characterized by heavy traffic loads and low vehicle speeds. The mixture is a closed-graded, impermeable wearing course (thickness ≥ 30 mm), combining natural aggregates with a minimum of 10% recycled materials, in compliance with UNI EN 13043. Acoustic and mechanical performance are achieved through an optimized granulometric distribution and the use of a highly polymer-modified bitumen (high SBS content), ensuring enhanced resistance to rutting, fatigue, and

deformation. Production is carried out using warm mix asphalt technology (≤140°C), reducing energy consumption and emissions while maintaining performance.

This typology represents a balanced solution between durability and noise reduction, particularly suitable where porous pavements are not applicable due to high mechanical stress. The mixture complies with CAM Strade (D.M. 05/08/2024) requirements and its acoustic performance will be evaluated before and after intervention through CPX measurements.

2.9 Conclusions

This chapter presented an integrated framework for the assessment and mitigation of port-related environmental noise, combining measurement methodologies, source characterization, perception analysis, and material-based solutions. The results confirm that port–city environments are characterized by complex and dynamic soundscapes, where stationary sources (ships and machinery) coexist with mobile sources such as road and rail traffic, requiring integrated measurement approaches combining short-term and long-term monitoring techniques.

Measurement campaigns in the Port of La Spezia demonstrated the effectiveness of combining short and continuous monitoring with acoustic camera analysis. In particular, acoustic camera measurements enabled the localization of rolling noise generated by truck traffic, highlighting the significant contribution of tire–road interaction at the port–city interface and supporting the identification of targeted mitigation areas. These findings emphasize the importance of transport-related noise sources.

From a mitigation perspective, the experimental characterization of sound-absorbing materials confirmed the potential of advanced solutions. Multilayer double-porosity systems achieved absorption coefficients up to 1.0, with peaks in the 1500–2200 Hz range (and 0.9–0.97 at higher frequencies for thinner configurations), due to enhanced viscous and thermal dissipation within the porous structure and thickness-related effects, making them suitable for transportation applications (e.g., yachts and ships). Perforated and micro-perforated configurations combined with porous materials reached values up to 0.96, with effective absorption from 1000 Hz and peaks between 1800 and 2200 Hz, resulting from the combined action of resonant (Helmholtz-type) and porous dissipation mechanisms. As standalone systems, they can be applied as acoustic barriers or in building applications. Polyimide foams showed tunable behavior, with mechanical compression enhancing absorption in the 700–1700 Hz range, with peak values up to 0.95–1.0, due to increased pore interconnectivity and improved viscous dissipation, while also providing high fire resistance and low emission of smoke and toxic gases.

These results highlight the application-oriented relevance of the investigated materials. In particular, polyimide foams and double-porosity multilayer systems, due to their fire

resistance and mechanical robustness, are suitable for naval and transport applications, while perforated systems combined with porous layers are effective for building, road barriers and infrastructure applications requiring compact solutions.

The analysis of noise perception through WTP indicators shows that residents are aware of port-related noise and willing to support mitigation measures, highlighting the socio-economic relevance of the issue and the need for more targeted regulatory frameworks. However, the monetary estimates still require further post-processing to account for heterogeneity and spatial variability.

Overall, effective port noise management requires:
(i) integrated measurement strategies;
(ii) robust source identification; and
(iii) application-oriented acoustic materials capable of delivering effective mitigation.

Another key outcome of this chapter is the transferability of the proposed methodological framework. The integrated approach combining acoustic measurements, source localization, perception analysis, and material characterization can be applied to different port–city contexts, providing a scalable and replicable basis for sustainable noise management strategies.

2.10 Limitations

While the proposed methodology is transferable, the quantitative results, particularly source contributions, measured noise levels, and mitigation performance, are site-specific, as they depend on local operational conditions and infrastructure layout. From a measurement perspective, acoustic cameras provide effective qualitative source identification and spatial localization, but cannot be used as standalone tools. They must be integrated with phonometric measurements and monitoring systems to obtain standardized and regulatory-compliant acoustic indicators.

Finally, although the investigated materials demonstrated high performance at mid–high frequencies, their effectiveness at low frequencies remains limited, indicating the need for further development of advanced acoustic solutions

2.11 Future Work

Future research will focus on the optimization and validation of noise mitigation strategies in port environments, with particular emphasis on truck rolling noise. This includes the identification and design of suitable low-noise asphalt typologies and mixtures, beyond the one already investigated, as a function of vehicle speed and operational conditions. Their acoustic performance will be evaluated through CPX measurements and in-situ assessments, with the aim of supporting the implementation of effective low-noise pavement solutions.

In parallel, further work will investigate the optimization of sound-absorbing materials, including the geometry of perforated plates and of the porous configurations, with particular attention to improving low-frequency and broadband performance.

Future activities will aim to demonstrate the transferability of the developed methodologies and mitigation solutions to similar port–city contexts, taking into account site-specific operational and environmental conditions. This will contribute to the definition of good practices and adaptable noise mitigation strategies.

3. Sustainability of ports and port hinterlands in terms of Renewable Energy

Mediterranean port cities are increasingly exposed to combined environmental and socio-economic pressures, particularly in peripheral and socially marginalized neighborhood's located within port hinterlands. These areas are often characterized by ageing building stock, higher levels of energy poverty and limited access to green and open spaces, which amplify their vulnerability to extreme climatic events and to the urban heat island (UHI) effect [134, 135]. Consequently, improving the energy performance of public and social infrastructures becomes essential not only for reducing greenhouse gas emissions but also for enhancing resilience, environmental equity and quality of life in port-city territories [136].

At the European level, the transition towards a low-carbon energy system is framed by the European Green Deal, which aims to achieve climate neutrality by 2050 and reduce net greenhouse gas emissions by at least 55% by 2030 compared to 1990 levels. The production and use of energy account for more than 75% of the EU's greenhouse gas emissions, making the decarbonization of the energy system a critical step toward meeting these climate objectives. The Green Deal is built upon three key principles guiding the clean energy transition: ensuring a secure and affordable energy supply, developing a fully integrated and interconnected energy market, and prioritizing energy efficiency, particularly through the improvement of building energy performance and the large-scale deployment of renewable energy sources. To achieve these objectives, the European Commission promotes the development of interconnected and digitalized energy systems, innovative technologies and modern infrastructure, enhanced energy efficiency and eco-design, decarbonization of the gas sector, smart sector integration, and the empowerment of consumers in tackling energy poverty [137].

In this framework, energy system integration plays a fundamental role by creating stronger links between different energy carriers (electricity, heat, gas and fuels), infrastructures and consumption sectors, enabling a more flexible and decentralized system capable of efficiently absorbing higher shares of renewable energy. Electrification of demand through solutions such as heat pumps, electric mobility and renewable-based heating and cooling together with digitalization, flexibility markets and energy storage, are recognized as key enablers of an optimized, reliable and resource-efficient energy system. These strategies are further supported through the implementation of the revised Renewable Energy Directive [138], the reform of electricity market design, and the updated Energy Efficiency and Energy Performance of Buildings Directives, which collectively aim to deliver decarbonized energy services at the lowest societal cost while accelerating the transition towards a climate-neutral European energy system [139].

Within port cities and their hinterlands, these policy objectives acquire specific relevance due to the coexistence of energy-intensive infrastructures, dense urban settlements and complex socio-economic dynamics. In this context, public buildings such as schools and municipal facilities represent strategic nodes within local energy systems, combining relatively high and predictable energy demand with public ownership structures that facilitate the implementation of renewable energy solutions and community-based governance models.

In this perspective, the EnerCmed project [22] addresses these challenges by exploring an integrated approach combining Renewable Energy Communities (RECs) [140] or Self Consumption schemes (SCSs) [141] with Nature-Based Solutions (NBS) [142] to support sustainability and climate resilience in vulnerable urban areas. Although REC and NBS are addressed in the literature as separate domains [143], they actually have important synergies in addressing climate mitigation. The simultaneous deployment of renewable energy systems and green infrastructures can reduce carbon emissions through clean energy production while improving microclimatic conditions via vegetation-based interventions [144]. Moreover, NBS can facilitate the energy transition by increasing social acceptance thanks to visible co-benefits, such as improved thermal comfort, health conditions and aesthetic quality, while also contributing to cleaner air and low-carbon urban environments [145, 146].

Despite these opportunities, Renewable Energy Communities face several implementation barriers. Literature identifies three main categories: regulatory barriers related to the legal framework and PV system sizing, technical barriers associated with spatial constraints and structural capacity of buildings, and financial barriers linked to investment costs and economic feasibility [147, 148]. Within this context, the EnerCmed project explicitly analyses these constraints and develops context-specific solutions, with the aim of proposing a transnational model that combines decentralized renewable energy governance with nature-based interventions to reduce CO_2 emissions and foster more sustainable energy production. This integrated approach is also intended to improve living conditions in disadvantaged areas of Mediterranean port hinterlands, which are often inhabited by economically vulnerable populations. The project goals are aligned with the European Commission's priorities under the Green Deal and the "just transition" principle of leaving no one behind, and are supported by the Interreg Euro-MED programme, which promotes green development and climate-resilient, energy-positive neighborhoods [149].

The integration of renewable energy systems within ports and their hinterlands therefore represents a critical pathway for addressing both climate change mitigation and energy efficiency enhancement. According to the ESPO and EcoPorts assessment of environmental priorities identified by European port authorities, these aspects correspond to Priority 1 (Climate Change) and Priority 3 (Energy Efficiency), underscoring their

strategic relevance for sustainable port development. In alignment with these priorities, initiatives such as EnerCmed (Testing energy-community & climate-resilient integrated paradigm for carbon neutrality and energy poverty shielding in MED city-port hinterlands) contribute to advancing renewable energy deployment and promoting resilience, thereby supporting the transition of port ecosystems towards greater environmental, economic and social sustainability.

Against this background, the present chapter investigates the sustainability of port hinterland environments in terms of renewable energy by focusing on the energy performance of a representative school building located within the municipal context. The analysis begins with the development of a dynamic energy model to determine the building's electricity demand profile, followed by the dimensioning of a photovoltaic (PV) system based on the load characteristics and local solar resource. Subsequently, the degree of energy coverage provided by the PV system and the resulting individual self-consumption levels are evaluated, highlighting the seasonal interaction between electricity demand and renewable generation. Finally, different Renewable Energy Community scenarios are analyzed to assess how the integration of the building within a local REC configuration can influence the balance between self-consumed, shared and grid-injected energy. Through this integrated approach, the chapter aims to demonstrate how building-scale renewable energy integration can contribute to the broader sustainability of port hinterlands, supporting local decarbonization pathways while aligning with European objectives related to renewable energy expansion, climate neutrality, the mitigation of energy poverty and the promotion of social engagement.

3.1 EnerCmed Project and beyond

3.1.1 Introduction

The Clean Energy for All Europeans Package places citizens at the center of the energy transition, providing a framework that empowers them to actively participate in and benefit from clean energy initiatives. Building on this foundation, the EnerCmed project introduces an innovative approach to fostering sustainable and climate-resilient urban areas, starting with marginalized neighborhoods in port cities that are often affected by energy poverty [150]. Central to this approach is the activation of RECs and SCSs, which organize collective, citizen-driven energy actions and deliver environmental, social and economic benefits to their members.

In line with RSO2.4, EnerCmed proposes a new paradigm for energy-positive and climate-resilient port hinterlands, targeting vulnerable groups such as the elderly, low-income households, and immigrants. The approach will be implemented through six pilot

RECs/SCSs in Genova, Valencia, Patras, Pula, and Novigrad, involving about 345 households affected by energy poverty (see Figure 52). Each community will be complemented by a NBS to reduce cooling demand and mitigate the Urban Heat Island effect.

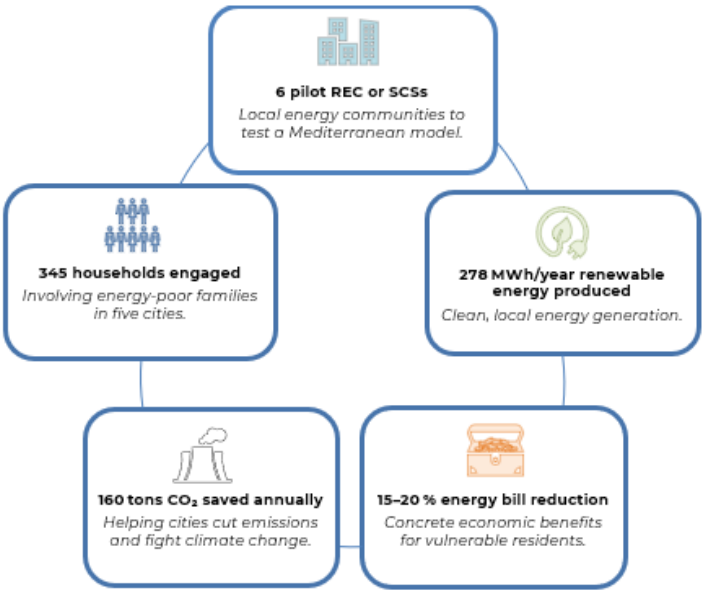

Figure 52. Project targets

The project integrates three pillars: REC/SCS, NBS, and energy poverty mitigation. EnerCmed extends the REC/SCS framework, covering citizen engagement, governance, and system engineering, by embedding it within micro-scale energy planning that accounts for local climatic and social conditions. The objective is to demonstrate a fair, inclusive, and scalable energy transition across diverse European contexts [151]. The transnational cooperation is supported by the Knowledge Facility Instrument (KFI), which provides technical expertise to implement the Hinterland Renewables Communities Action Plan.

The KFI was conceived as a core component of the EnerCmed project from the proposal stage. The partnership was structured by assigning scientific and technical partners to thematic roles aligned with the project's key dimensions, enabling the development of a multi-level framework integrating technical, legal, social, environmental, and digital aspects for coherent and interdisciplinary implementation (see Figure 53).

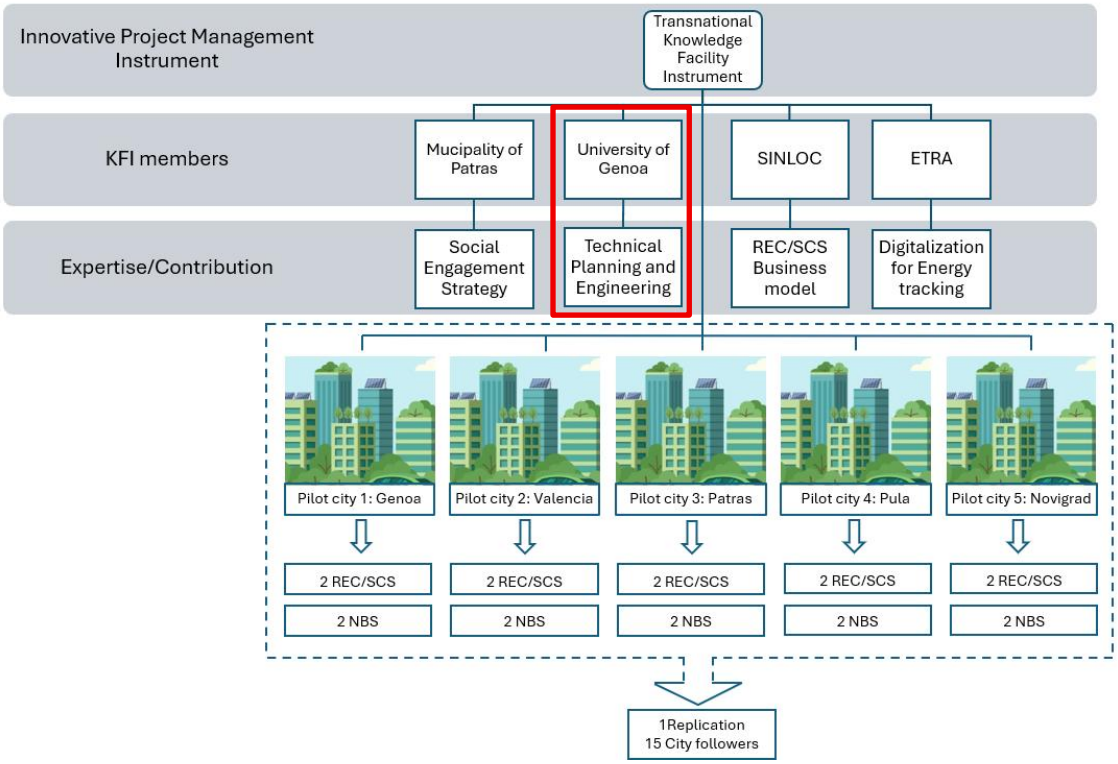

Figure 53. KFI definition in the EnerCmed Project

The Knowledge Facility Instrument (KFI) provides coordinated technical support and mentorship to pilot cities through a co-design approach that integrates partner expertise with local knowledge. Within this framework, the University of Genoa leads technical planning and engineering activities (Figure 53), supporting the optimal sizing of PV systems and addressing regulatory and spatial constraints. A Knowledge Sharing Helpdesk Platform was also developed to provide continuous guidance and disseminate best practices across Mediterranean contexts. The PhD candidate was actively involved in these activities, directly contributing to the development of the Terms of Reference (ToR), the preparation of training materials (including video tutorials), and the provision of technical support to pilot partners.

The project is structured into three work packages: WP1 defines the methodological framework, including the KFI and ToR; WP2 implements the pilot actions (REC activation, business models, PV systems, and NBS deployment); and WP3 focuses on replication through Action Plans and support services for broader replication.

3.1.2 Guideline for REC and NBS creation

As previously introduced, Work Package 1 (WP1) focused on the preparation of the Terms of Reference (ToR), a strategic document providing a comprehensive framework for the development of RECs or SCSs and NBS.

The main objective of the ToR is to conceptualize a transnational guideline for Renewable Energy Communities in marginalized neighborhoods. This guideline is conceived as an innovative multi-criteria decision-making protocol that integrates key dimensions of REC development, including social engagement, technical and energy-related aspects, and economic, financial and governance considerations. In addition, it incorporates microclimate-oriented actions through the implementation of Nature-Based Solutions (NBS), with the aim of delivering an efficient planning paradigm for energy-positive and climate-resilient hinterlands centered on the REC concept.

Recognizing the need for a shared methodological approach among the different pilot sites involved in the project, and considering the previously identified technical, social and economic factors, a common transnational guideline was developed. This guideline provides a clear, step-by-step methodological framework that explains the process to be followed for the establishment and operation of RECs in disadvantaged urban contexts.

The document, already available on the project website [152], offers a common diagnosis and feasibility assessment framework for the pilot actions implemented under Work Package 2 (WP2). Furthermore, it serves as a reference model for the first city replicator and for subsequent follower cities, ensuring consistency and coherence in the transnational implementation of the EnerCmed approach. The author was one of the main contributors to the drafting of this document, particularly with respect to the definition of the methodological framework and the integration of the technical-energy, social and governance dimensions.

ToR Composition

The ToR guideline is subdivided into the following sections (4 pillars), and checklists are provided for each of them to check whether all the necessary information is included in the document:

I. ToR for Social Engagement of Vulnerable Populations
II. ToR for energy community technical Design & Digitalization of the RECs/SCSs
III. ToR to build a legal, administrative and management structure of the RECs/SCSs
IV. ToR for the application of Nature-Based Solutions (NBS) to mitigate Urban Heat Island (UHI) effects.

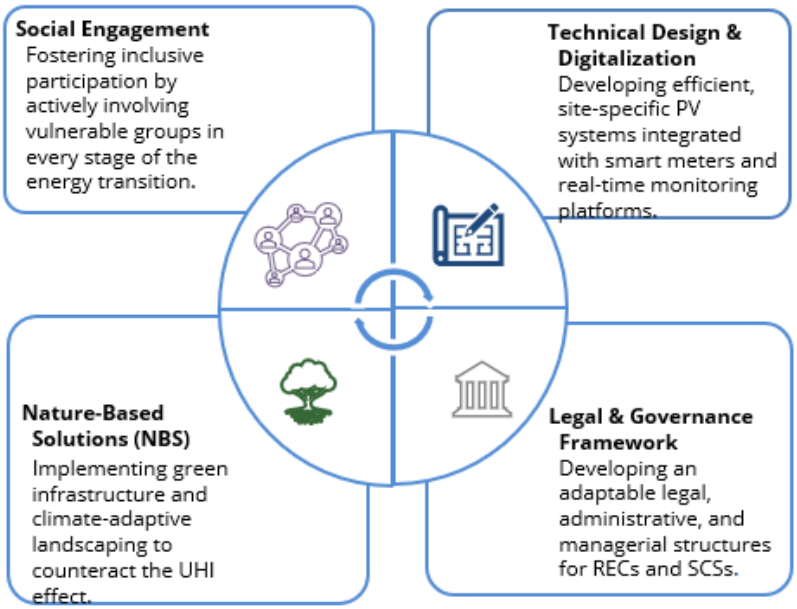

Figure 54. ToR guideline pillars

In order to effectively develop the four main pillars of the project previously mentioned, the process illustrated in Figure 54, delineates a comprehensive and iterative process comprising the key interlinked steps.

ToR organization

Each ToR is systematically structured into chapters, serving as a clear, step-by-step guideline. Within each section, clearly defined tasks are articulated, accompanied by comprehensive explanations to ensure clarity of purpose and methodological coherence.

Figure 55. Process Flow for the Implementation of RECs and Self-Consumption Models

As shown in Figure 55, the process begins with Project Planning, where the strategic vision, goals, and scope of the RECs or SCSs are defined. This is followed by the Identification of Economic Resources, ensuring that the necessary financial means, both public and private, are mapped and mobilized to support the initiative.

Next, project management must be established as a cross-cutting function to coordinate activities, timelines, and responsibilities across all stakeholders involved. With the project structure in place, the process moves into Social Engagement, which focuses on building awareness, participation, and trust among local communities, particularly targeting vulnerable populations. This step ensures that the energy transition is inclusive and community-driven.

Following social engagement, the Technical Design and Digitalization phase lays out the necessary engineering, including the integration of renewable energy sources (RES), smart metering, and grid compatibility. At this point, the Constitution of RECs or SCS is addressed, involving the legal formation of the community or scheme, as well as the development of governance, administrative procedures, and business models suited to local legislative contexts.

In parallel, the Design of NBS is carried out, contributing to the environmental pillar of the project. This step focuses on selecting and integrating interventions that mitigate the Urban Heat Island (UHI) effect and enhance urban resilience, thereby fostering energy-positive and climate-adaptive neighborhoods.

Once the structural and technical foundations are in place, the Implementation phase commences. This includes the physical deployment of energy infrastructure, digital tools, and the activation of community governance structures. Post-implementation, the Monitoring stage ensures continuous evaluation of performance, social impact, and environmental benefits, enabling data-driven adjustments where necessary.

Finally, insights and lessons from the initial cycle are used to inform the Future Expansion of the REC or SCS. This stage supports scalability and replicability, extending the project's benefits to additional areas or communities and reinforcing its long-term sustainability.

By following this structured and interconnected process, the project ensures that all technical, financial, legal, social, and environmental dimensions are not only addressed but harmonized. This integrated approach enables the robust, inclusive, and scalable implementation of RECS and SCSs across diverse urban contexts. Each step of the process will be further detailed and analyzed in the following chapters, providing methodological guidance and operational tools for their effective implementation.

Moreover, the guideline is accompanied by checklists to support pilots in validating procedural adherence and confirming that all process steps are executed.

The following subchapters present a synthesis of the main contents of the guideline and the associated checklists, while the complete document is available on the EnerCmed project website under the "What we achieve" section [152].

ToR for Social Engagement of the vulnerable population

In urban neighborhoods near Mediterranean ports, vulnerable populations such as low-income families, older residents, migrants, and marginalized groups face significant energy poverty and climate challenges. They often lack access to reliable, affordable energy and have little influence over decisions that affect their lives [153]. In order to ensure reliable identification, awareness and inclusion of the vulnerable population, it was developed a Social engagement strategy that consists in the following action presented in Figure 56.

These initiatives are designed not only to foster a sense of belonging and social inclusion but also to empower these groups by ensuring their perspectives are acknowledged, their needs are effectively addressed, and they are meaningfully included in decision-making processes that shape the policies and services impacting their daily lives. Such engagement promotes equity, enhances community cohesion, and supports the creation of more inclusive societies.

Figure 56 outlines the key elements of the social engagement strategy targeting vulnerable populations, which is examined in detail in the corresponding subchapters in the ToR guideline [152]. These elements include contextual understanding of the vulnerable population aimed at understanding community profiles, identifying specific vulnerabilities and their cultural values; forms of social engagement designed to promote inclusive and participatory approaches; mechanisms for monitoring, evaluation, and feedback to assess impact and ensure continuous improvement; and the integration of engagement strategies with national and regional policies to maintain alignment with broader regulatory and governance frameworks.

The EnerCmed initiative begins with context-sensitive assessments that map demographic, cultural, and socioeconomic profiles to identify energy-related vulnerabilities. This approach ensures that project strategies are grounded in real lived experiences rather than assumptions. Engaging vulnerable populations is a key pillar of the project, making it essential to raise awareness and provide knowledge about the energy transition and their vital role within it. Empowering these residents through accessible education is crucial for achieving transformation.

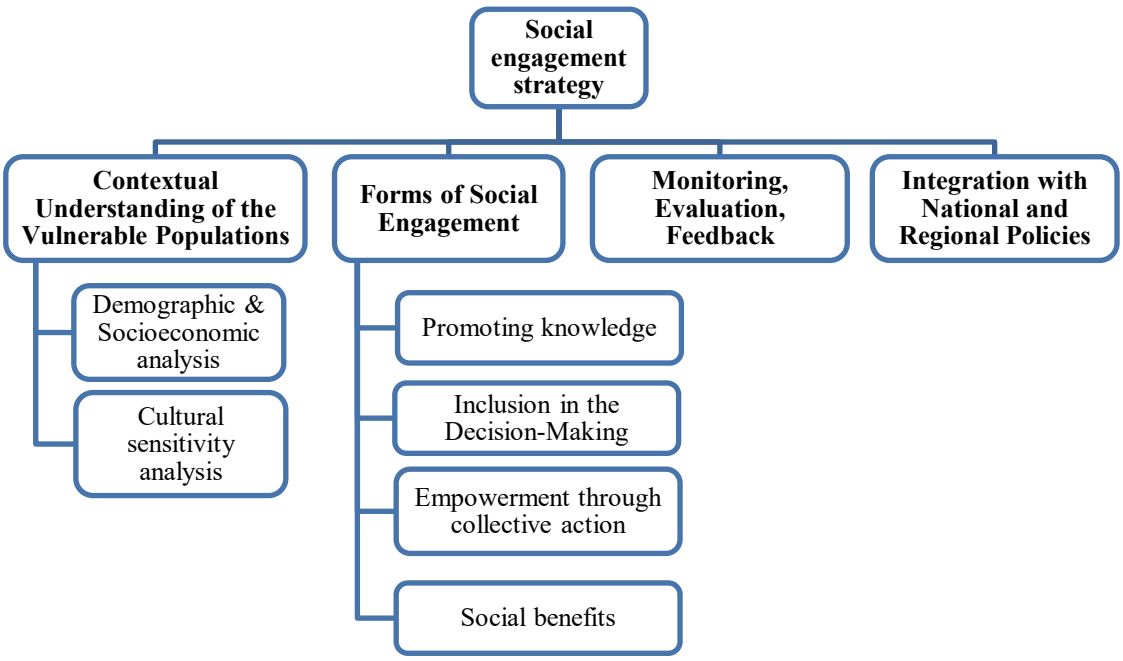

Figure 56. Pillars of Inclusive Social Engagement in Renewable Energy Initiatives

Evidence shows that increasing awareness of energy issues, such as the benefits of renewable energy, individual rights, and efficient usage, can turn passive consumers into active energy citizens. When communities understand their role, they are more likely to engage meaningfully with Renewable Energy Communities (RECs).

Building on this foundation, the project extends into inclusive decision-making and co-design: early involvement through dialogue, consultations, and participatory workshops ensures that energy-sharing schemes and clean energy models reflect community priorities. Collaborative governance platforms, such as community-led committees or advisory bodies, give residents a sustained voice in strategic decisions, reflecting principles of procedural justice and energy democracy.

EnerCmed employs a clear monitoring and feedback framework focusing on KPIs such as participation, satisfaction, energy burden reduction, and behavioral shifts to ensure and adapt its social engagement strategy continually.

This robust engagement strategy is expected to broaden the energy transition by ensuring that community-led RECs evolve from initial involvement into lasting and ensuring continuity and self-formation of new RECs by empowering vulnerable communities.

ToR for Technical Design and Digitalization

The ToR for Technical Design and Digitalization of the RECs or SCSs encompasses the development of a comprehensive methodological framework.

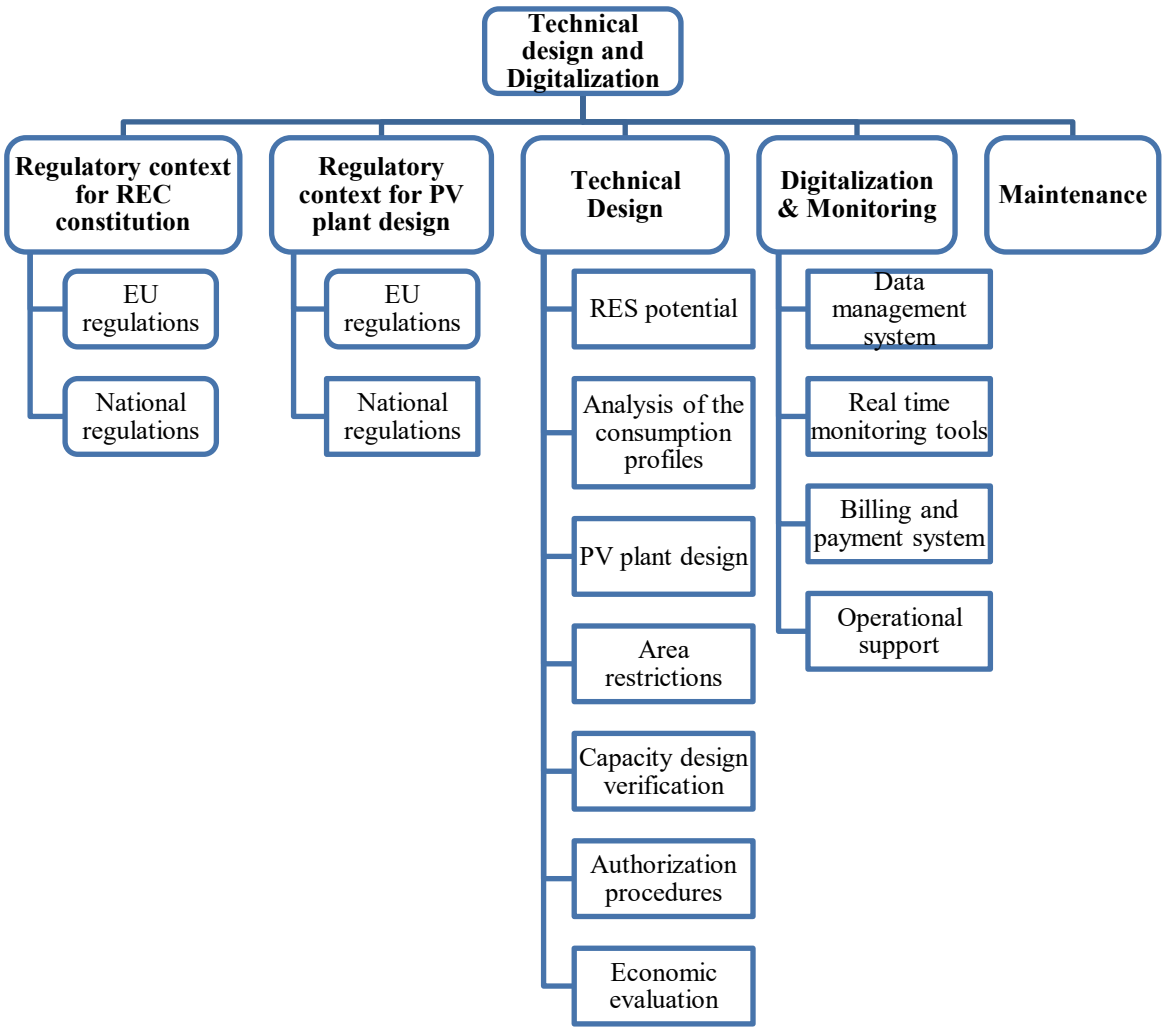

Figure 57. Development Scheme for Technical Design and Digitalization of the RECs or SCSs

As shown in Figure 57, this framework is aimed at guiding the technical configuration, including the verification and assessment of the regulatory context for REC or SCS constitution and PV plant design, the key technical parameters such as the availability and exploitation of endogenous renewable energy sources (RES), the capacity and structure of the existing grid infrastructure, and the compatibility of RECs or SCSs with territorial planning and landscape regulations. Furthermore, the scope includes the strategic integration of digitalization processes, specifically by establishing advanced management systems designed to ensure the efficient operation, monitoring, and maintenance of the Energy Community infrastructure. To better support the pilots and furnish a clear example of the technical design, a training video is provided by the author on the Knowledge Sharing Platform [154]. It treats the examination of the national legislation, the restrictions, the authorization procedure, grid connection), Preliminary and Definitive Design Study of the PV plant including a tutorial for the use of PVsyst software.

ToR for Legal, Administrative and Management structure

This chapter provides a comprehensive framework for the establishment, governance, and implementation of Renewable Energy Communities (RECs) or Self-Consumption Schemes (SCSs), highlighting the critical role of regulatory compliance, structured governance, and integrated technical–economic planning and aligned with six key structural areas (as shown in Figure 58): regulatory context, governance, execution, platform integration, impact assessment, and risk evaluation. It aims to support REC administrators in navigating EU and national regulations, defining juridical entities, preparing statutes and contracts, managing procurement and installation phases, and ensuring grid connection and fiscal compliance.

The chapter first emphasizes the importance of compliance with the European regulatory framework, introduced by Directive (EU) 2018/2001 [155] and Directive (EU) 2019/944 [156], which define Renewable Energy Communities and Citizen Energy Communities. These directives establish the legal foundations, governance principles, participation criteria, and obligations for Member States, including the creation of enabling frameworks, simplified procedures, non-discriminatory market access, and mandatory transposition into national law.

Building on this foundation, the chapter reviews the national regulatory frameworks adopted by selected EU Member States, illustrating how European provisions are implemented through country-specific legal instruments. Particular attention is given to Italy, Spain, Croatia, and Greece, highlighting differences in legal definitions, governance models, geographic constraints, and incentive schemes, as well as their respective responses to EU regulatory requirements.

The chapter then outlines the phases for the constitution of a REC or SCS, starting from preliminary activities such as stakeholder identification, feasibility studies, financial planning, and access to incentives. This is followed by the governance phase, where institutional structures, decision-making mechanisms, and participation rules are defined, and by the selection of the juridical entity, assessing risks and opportunities associated with different legal forms. Associations and cooperatives are identified as the most suitable structures for most community-oriented initiatives, due to their democratic governance and regulatory alignment.

Subsequent sections address the drafting of statutes and internal regulations, which formalize members' rights and obligations, energy-sharing rules, incentive distribution mechanisms, and compliance procedures. The chapter also highlights the strategic role of digital management platforms for handling energy, economic, and data flows, as well as the need to contextualize technical and organizational models to local regulatory, infrastructural, and social conditions.

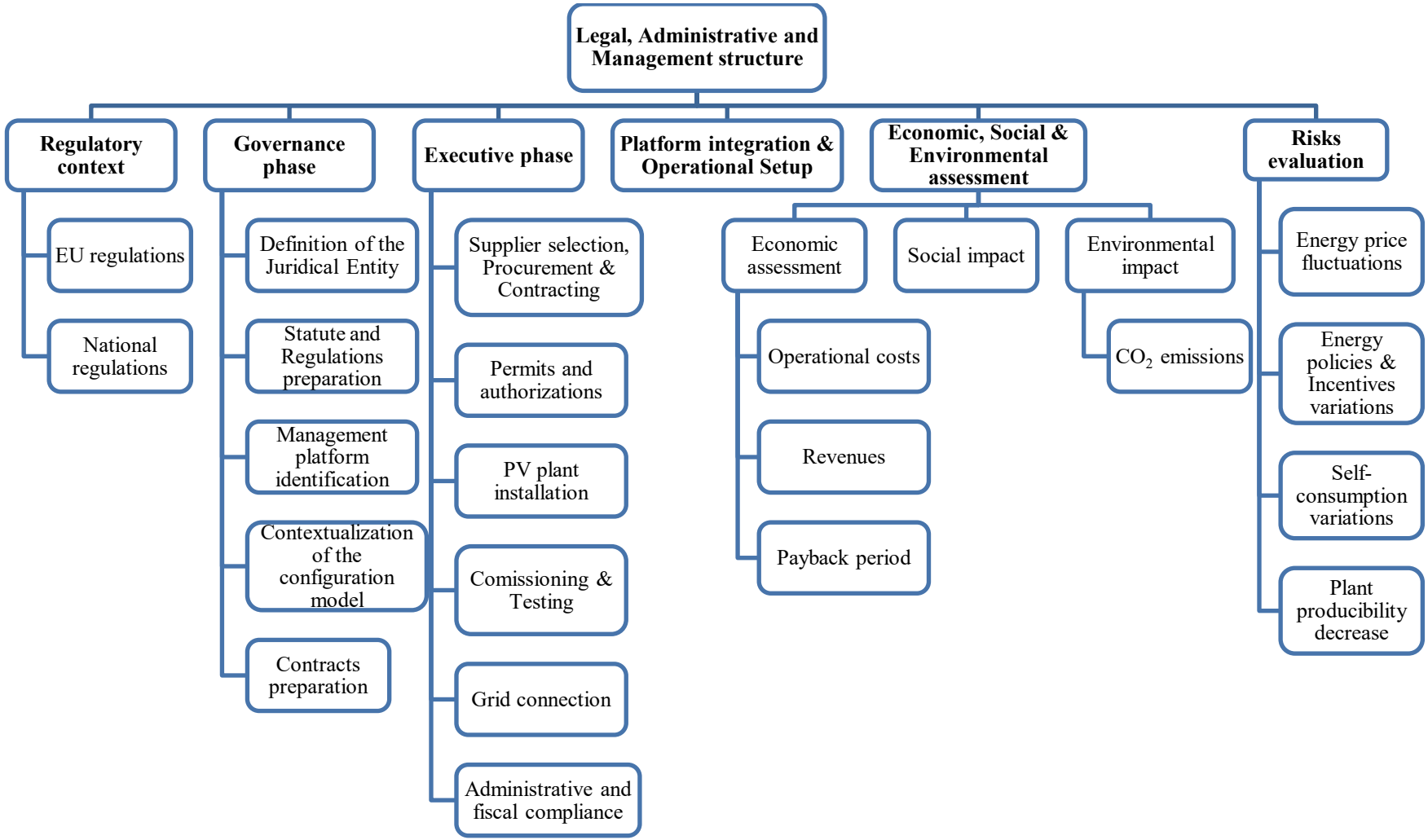

Figure 58. Framework for the Legal, Administrative, and Operational Development of RECs or Self-consumption schemes

The execution phase is then described, covering procurement, permitting, PV plant installation, commissioning, grid connection, administrative compliance, platform activation, and stakeholder training. This phase represents the transition from planning to operation and is critical for ensuring technical reliability, regulatory conformity, and long-term operability of the REC or SCS.

Finally, the chapter presents an integrated economic, social, and environmental assessment, including investment sustainability, payback analysis, social impact evaluation, and CO_2 emissions reduction. It also identifies key risk factors, such as energy price volatility, policy and incentive changes, variations in self-consumption levels, and long-term degradation of PV system productivity, emphasizing the need for resilient business models and adaptive operational strategies.

Overall, the chapter demonstrates that the successful development of Renewable Energy Communities requires a holistic approach, integrating regulatory compliance, sound governance, robust technical design, economic viability, social inclusiveness, and environmental sustainability.

ToR for implementing NBS to support REC integration in Energy-Positive, Climate-Resilient Neighborhoods

This chapter presents a comprehensive and structured methodology for the planning, design, implementation, and evaluation of NBS aimed at mitigating the Urban Heat Island (UHI) effect within REC contexts and dense urban areas, particularly next-to-port districts.

The development of a common ToR offers a structured and replicable framework for the integration of NBS into the planning and implementation of RECs or SCSs. As illustrated in Figure 59, this framework follows a step-by-step approach starting with problem localization, regulatory analysis, and stakeholder engagement, progressing through feasibility studies and impact evaluation, and culminating in implementation and long-term maintenance. This shared methodology allows pilot cities to align strategies and scale up effective solutions for achieving energy-positive and climate-resilient urban neighborhoods. The process begins with internal alignment among project partners, including engineers, planners, climate experts, and municipal stakeholders, to establish shared objectives, technical criteria, and expected outcomes. This coordination phase ensures methodological coherence, clear role allocation, and seamless integration of NBS with complementary activities such as microclimate modeling and energy planning. Urban overheating is then conceptualized as a multi-scalar problem driven by dense urban morphology, low vegetation coverage, and heat-retaining materials such as asphalt, concrete, and photovoltaic (PV) panels with low albedo. This conceptual framework supports the identification of suitable NBS typologies capable of reducing thermal stress, improving microclimatic conditions, and lowering cooling energy demand.

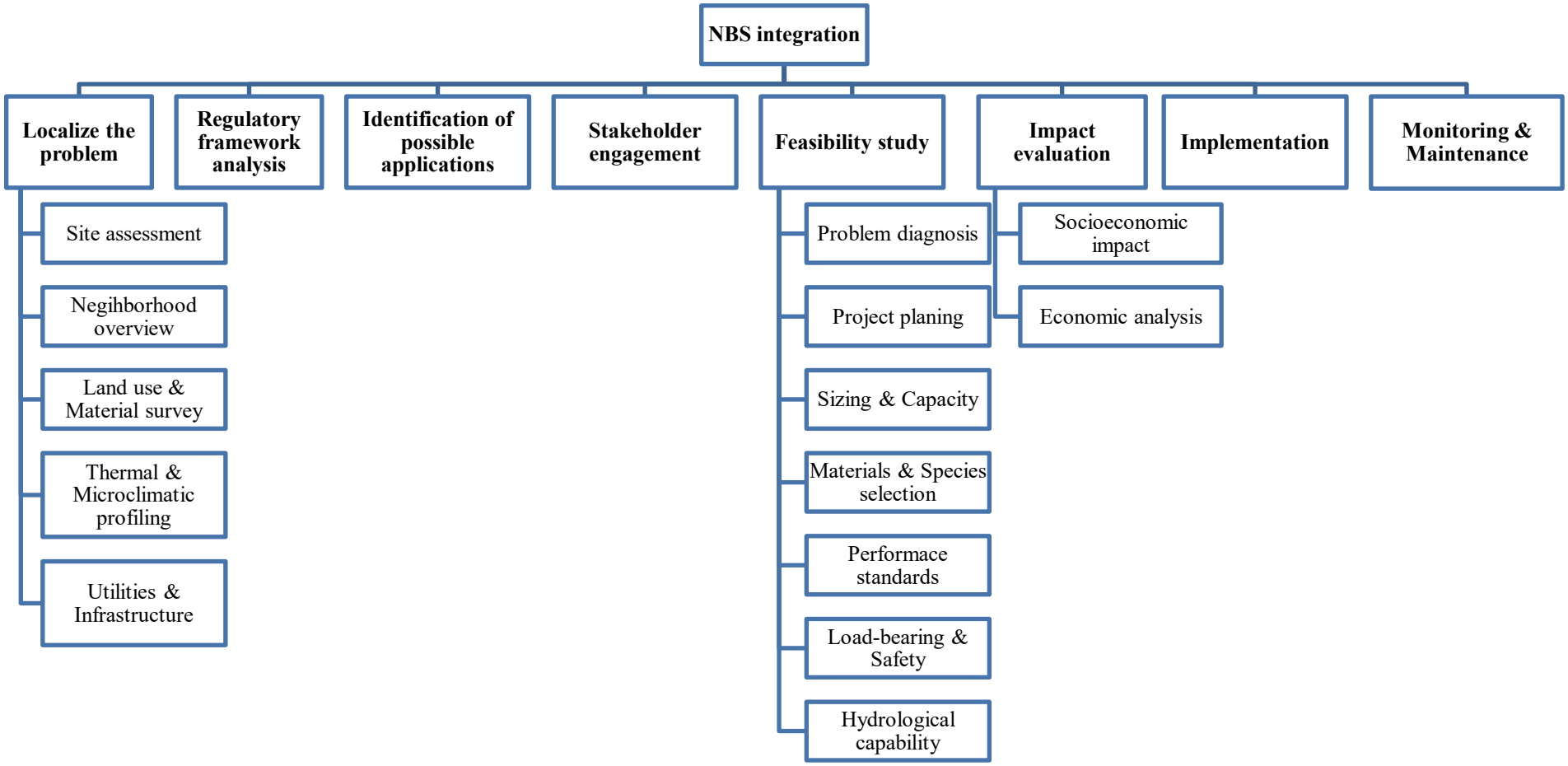

Figure 59. Scheme for the NBS Integration to support REC integration in Energy-Positive, Climate-Resilient Neighborhoods

The methodology advances through a localized diagnostic phase, translating the conceptual problem into site-specific analyses. This includes detailed site assessments covering urban morphology, land use, surface materials, vegetation distribution, and climatic variables such as solar radiation, wind, and temperature. Thermal and microclimatic profiling supported by GIS, remote sensing, and in-situ data where available enables the identification of heat hotspots and priority intervention areas. Parallel mapping of underground utilities and infrastructure ensures technical feasibility and avoids conflicts during implementation. A dedicated regulatory and spatial planning analysis evaluates municipal and regional planning instruments, zoning rules, and environmental regulations affecting NBS deployment. This step identifies legal enablers, constraints, and permitting requirements for green roofs, facades, blue-green infrastructure, and permeable surfaces, ensuring regulatory compliance and alignment with broader urban development strategies.

Based on the diagnostic results, a preliminary screening of appropriate NBS is carried out. Potential interventions, such as green roofs and façades, urban tree planting, bioswales and permeable pavements, are evaluated in terms of technical effectiveness, spatial and functional compatibility, maintenance requirements, regulatory feasibility and the provision of co-benefits, including biodiversity enhancement and stormwater and flood mitigation.

The methodology emphasizes a multi-stakeholder and participatory planning approach, involving public authorities, technical services, local communities, and vulnerable groups. Co-design processes ensure that proposed NBS are technically sound, socially accepted, and aligned with local needs, strengthening long-term stewardship and effectiveness.

A structured feasibility study framework follows, encompassing problem diagnosis, project planning, sizing and capacity calculations, materials and species selection, performance standards definition, and structural, hydrological, and safety assessments. Quantifiable Key Performance Indicators (KPIs) are defined to evaluate cooling performance, stormwater management, energy savings, biodiversity gains, and social benefits. Where applicable, PV heat impact analyses are included to assess interactions between photovoltaic systems and urban microclimates.

Alternative NBS scenarios are compared through cost–benefit and multi-criteria analyses, supporting evidence-based selection of optimal solutions. The chapter concludes with guidance on impact evaluation, action planning, implementation, and long-term monitoring and maintenance. Continuous performance assessment and adaptive management ensure durability, replicability, and contribution to climate-resilient, energy-positive urban environments.

3.1.3 Checklist

This subchapter presents four checklists corresponding to the Terms of Reference (ToR), designed as verification tools to support project managers in assessing compliance with defined activities and requirements. Applied at key project milestones, they cover regulatory, technical, organizational, and operational aspects of RECs and SCSs integrated with NBS. Their use ensures traceability, supports quality assurance, and enables early identification of gaps throughout the project lifecycle.

Checklist 1: Social Engagement of the Vulnerable Population

Checklist for the Social Engagement of the Vulnerable Population		
Contextual understanding of the vulnerable population	**Yes/No**	**Comments**
Does the demographic analysis include key data such as age distribution, population size, household structure, and population density?		
Are key socioeconomic indicators covered (e.g., income levels, employment status, education levels, housing conditions, access to basic services)?		
Does the assessment consider cultural, ethnic, or social characteristics relevant for inclusive energy planning?		
Are the specific needs, challenges, and vulnerabilities of the target population in relation to the energy transition clearly identified?		
Does the analysis identify opportunities for engagement and participation in the energy transition (e.g., local initiatives, existing actors)		
Has the analysis identified and described the key cultural values, traditions, or practices relevant to the target communities?		
Has the analysis been validated or informed by direct input from community members or local stakeholders?		
Forms of Social Engagement **Promoting Knowledge, Tailored Outreach and Support**	**Yes/No**	**Comments**
Are outreach and awareness-raising activities described, using accessible and culturally appropriate formats (e.g., workshops, community radios)?		
Do the materials and methods clearly explain RECs or Self-Consumption schemes, including their benefits for vulnerable populations?		
Are the communication strategies tailored to the specific needs and capacities of the target population (e.g., literacy, language, technology access)?		
Inclusion in Decision-Making	**Yes/No**	**Comments**
Are mechanisms described for involving vulnerable groups in planning and implementation (e.g., participatory workshops, local forums)?		

Is there a plan to ensure that community input influences decisions at governance or operational levels of RECs or energy schemes?		
Are efforts described to build trust and ensure transparency in decision-making processes involving the target population?		
Empowerment through Collective Action		
Are models of collective action or community ownership (e.g., energy cooperatives) proposed to engage vulnerable groups in RECs?		
Does the strategy emphasize community empowerment through roles in management, operation, or governance of energy projects?		
Are examples or pathways provided that show how collective action can build social cohesion and reduce energy vulnerability?		
Social Benefits	**Yes/No**	**Comments**
Are specific social benefits identified (e.g., reduced energy bills, improved housing, stronger community ties)?		
Does the analysis demonstrate how RECs contribute to broader social inclusion and community resilience in marginalized areas?		
Is there a focus on long-term benefits such as reduced energy poverty, improved quality of life, and increased local capacity?		
Monitoring, Evaluation, Feedback	**Yes/No**	**Comments**
Are there defined performance indicators (e.g., participation rates, satisfaction levels, behavior changes) to monitor engagement impact?		
Are feedback mechanisms described (e.g., surveys, community meetings, digital platforms) to refine engagement activities over time?		
Are both quantitative and qualitative tools proposed for evaluation (e.g., data analytics, interviews, behavioral tracking)?		
Integration with National and Regional Policies	**Yes/No**	**Comments**
Does the engagement strategy align with relevant national/regional policies on energy, social inclusion, and sustainability?		
Are references to specific policy frameworks, funding programs, or legal instruments provided to demonstrate alignment?		
Is there a rationale showing how policy alignment supports long-term viability, legitimacy, and institutional support for the REC initiatives?		

Checklist 2: Energy Community Technical Design & Digitalization

Checklist for Energy Community Technical Design and Digitalization		
Legal and Regulatory context for RECs	**Yes/No**	**Comments**
Has the EU Renewable Energy Directive (RED II and RED III) been fully transposed into national law, and what provisions are made for Renewable Energy Communities (RECs) and self-consumption schemes?		
Have specific national laws or regulations been established to facilitate the implementation of RECs, including eligibility criteria, support mechanisms, and operational guidelines?		

Are there any provincial or municipal regulations that modify or adapt national REC frameworks?		
Do existing regulations that enable or hinder citizen participation in RECs, and what regulatory barriers exist that may limit collective self-consumption and decentralized energy production at local levels?		
Identification of the REC or Self-Consumption scheme Members: Producers/Prosumer and Consumer	**Yes/No**	**Comments**
Have all members (producers, prosumers, and consumers) of the REC or Self-Consumption scheme been clearly identified and categorized based on legal eligibility, geographical proximity, and technical compatibility		
Does the membership plan include vulnerable households, public bodies, and local enterprises, in alignment with EU objectives for an inclusive energy transition?		
Has the potential for adding additional participants to the REC or Self-Consumption scheme been evaluated for future expansion?		
Identification of Economic Resources	**Yes/No**	**Comments**
Have various economic resources, such as grants, loans, strategic partnerships, and private investments, been identified to support the establishment and sustainability of the REC or Self-Consumption scheme?		
Has a diverse range of financial support mechanisms been considered to ensure the project's long-term sustainability and expansion?		
Technical Feasibility and Energy Modelling	**Yes/No**	**Comments**
Have national, provincial, and municipal regulations regarding photovoltaic (PV) plants been thoroughly reviewed, particularly in terms of spatial planning, permitting procedures, and integration with local energy strategies?		
Has the installation area for the PV plant been clearly defined, including the type of terrain (flat or inclined) and the characteristics of surrounding buildings or land (e.g., roof type, land usage)?		
Have key environmental factors (solar radiation, temperature, wind speed, humidity, and precipitation) been gathered for the identified installation area?		
Have the installation area's landscape, architectural, and archaeological restrictions been checked, in accordance with heritage protection regulations?		
Have potential conflicts with critical infrastructure that may affect the installation been assessed?		
Has the local solar potential been fully assessed?		
Have the necessary permits and authorizations for the PV plant installation been identified, taking into account the plant's size, location, and area-specific restrictions?		
Has the electricity consumption profile been defined?		
Has the peak power installed been evaluated?		
Has the producibility of the PV system been evaluated?		

Have different scenarios been considered?		
Has a detailed electrical schematic been created, including all plant components, connections, and mapping to evaluate energy losses and system layout, up to the primary cabin?		
Has the environmental impact of RES installations been evaluated (if required)?		
Are done the verification of the weight capacity of the roof or consistency of the terrain?		
Have the most suitable supporting elements been chosen for the PV panels, considering the roof or terrain type, and ensuring structural integrity and waterproofing?		
Are all the necessary permissions defined for the installation of the PV plant?		
Territorial & Landscape Regulations	**Yes/No**	**Comments**
Are energy installations compliant with local zoning and land-use regulations?		
Has the visual and ecological impact of the REC been assessed?		
Are all installations compliant with local building codes and regulations?		
Has stakeholder consultation been conducted with local authorities and communities?		
Additional requirements	**Yes/No**	**Comments**
Has the necessary documentation been submitted to the municipality, and has it been verified whether additional permissions (e.g., environmental impact evaluation, fire protection, or safety regulations) are required?		
Have the applicable incentives for energy fed into the grid been identified?		
Have potential installers and service providers near the installation site been identified and evaluated, with a focus on local inclusion and regional economic development?		
Has an ordinary maintenance program been developed, tailored to the site's characteristics and environmental conditions, and have contracts been prepared with selected service providers for regular monitoring and diagnostics?		
Economic Evaluation of the PV Plant	**Yes/No**	**Comments**
Has a comprehensive economic evaluation been conducted for the PV plant, covering design authorization costs, installation, maintenance, and estimated payback period?		
Grid System & Smart Meters	**Yes/No**	**Comments**
Has all required project documentation, including details about the PV plant's capacity, location, and applicable regulations, been prepared and submitted to the Energy Services Manager?		
Have suitable grid connection points been identified for the REC?		

Are smart meters correctly installed and integrated for real-time monitoring?		
Is the grid system capable of handling the energy output from the REC?		
Are energy storage systems included in the design for managing surplus energy?		
Will the measurements from the installed devices be available to the management tools?		
Is there any system considered to ensure data quality?		
Management Tools	**Yes/No**	**Comments**
Are data management systems in place for monitoring REC operations?		
Are data governance mechanisms properly defined?		
Do REC members have access to user-friendly tools for monitoring energy consumption?		
Are billing and payment systems automated and integrated into the REC platform?		
Do REC members have clear protocols to report issues and request assistance?		
Have cybersecurity measures been included to protect data and system integrity?		
Does the REC manager have tools to incentivize and maintain REC members in the community?		
General Verification of Technical Parameters	**Yes/No**	**Comments**
Have the energy production capacities been verified?		
Is there an alignment between energy production and consumption in the REC?		
Are smart metering systems calibrated and functional?		
Have all technical systems (grid, storage, metering) been tested for compliance?		

Checklist 3: Energy Community Legal, Administrative and Management structure

Checklist for Energy Community Constitution		
National Regulatory Assessment	**Yes/No**	**Comments**
Has the national legislation on Renewable Energy Communities (RECs) been analyzed and updated?		
Have any implementing decrees or secondary regulations still pending been identified?		
Are there dedicated incentives or tariffs (CAPEX/OPEX, premium tariff, collective self-consumption, etc.) compatible with the project?		
Do the timelines of the incentives match the REC implementation schedule?		
Contextualization of the Configuration Model	**Yes/No**	**Comments**
Has the collective energy profile (load vs RES production) been simulated?		
Has the best scheme been chosen among: collective self-consumption,		

diffused self-consumption, multi-site REC, etc.?		
Have options for storage, demand response or virtual PPAs been assessed?		
Governance Set-up	**Yes/No**	**Comments**
Has a promoter group been established with representation from all stakeholders (citizens, SMEs, public authorities, etc.)?		
Have roles, responsibilities and decision-making processes (e.g. simple majority, qualified majority, consensus) been defined?		
Is the appointment of a Technical-Administrative Manager (Energy/Community Manager) foreseen?		
Definition of the Juridical Entity	**Yes/No**	**Comments**
Has the most suitable legal form (cooperative, association, consortium, benefit corporation, etc.) been selected?		
Does the founding act include participation limits and voting rights consistent with the legislation?		
Preparation of Statute and Internal Regulations	**Yes/No**	**Comments**
Does the Statute cover: corporate purpose, admission/exit procedures, quorum for assemblies, allocation of profits?		
Is there a Technical Regulation defining energy-sharing criteria (sharing key, dynamic coefficient, etc.)?		
Are mechanisms for transparency, reporting and periodic review provided?		
Identification of the Management Platform	**Yes/No**	**Comments**
Has a digital platform for monitoring, billing and user support been selected?		
Does the platform comply with GDPR, cybersecurity and interoperability with DSO/TSO?		
Do members have a user-friendly interface for consumption data and economic benefits?		
Preparation of Contracts and Administrative Documents	**Yes/No**	**Comments**
Has the grid connection and exchange contract with the DSO been prepared?		
Has the internal service/energy supply contract between REC and members been drafted?		
Are price-adjustment clauses, exit strategy and force majeure included?		
Supplier and Partner Selection	**Yes/No**	**Comments**
Has a tender or comparative procedure been carried out for EPC, O&M and legal consultancy?		
Do the award criteria include quality, price, references and ESG requirements?		
Are framework agreements or service-level agreements foreseen for post-installation?		
Permitting	**Yes/No**	**Comments**
Have all necessary building and landscape permits been obtained?		
Does the project comply with power, distance and primary substation limits imposed by regulation?		
Has compliance with any constraints been verified?		
Photovoltaic Plant Installation	**Yes/No**	**Comments**

Has the executive design been drafted in conformity with CEI/UNI standards?		
Have load calculations and structural verifications of the roof been performed?		
Is a site safety plan and works schedule defined?		
Management Phase	**Yes/No**	**Comments**
Is there a preventive and corrective maintenance (O&M) contract with clear KPIs?		
Are procedures for meter reading, billing and benefit redistribution established?		
Is a reserve fund for technological renewal and contingencies planned?		
Estimation of the Social Impact	**Yes/No**	**Comments**
Has the number of vulnerable households involved and the expected average saving (€/year) been assessed?		
Have awareness and training sessions been planned for users?		
Is periodic measurement of member satisfaction (surveys, focus groups) foreseen?		
Estimation of the Environmental Impact	**Yes/No**	**Comments**
Has the annual CO_2 reduction (tCO_2/y) and other local pollutants been calculated?		
Does the initiative contribute to local climate/SECAP targets?		
Are synergies with Nature-Based Solutions or energy-efficiency measures on buildings foreseen?		
Risk Evaluation	**Yes/No**	**Comments**
Has a Risk Register covering regulatory, financial, technical and reputational risks been drafted?		
Are adequate insurance policies in place (third-party liability, indirect damage, business interruption)?		
Is a mitigation and business continuity plan (BCP) defined in case of faults or regulatory changes?		

Checklist 4: Nature-Based Solutions (NBS) Integration in REC Neighborhoods

Checklist for Nature-Based Solutions (NBS) Integration in REC Neighborhoods		
Context & Diagnosis	**Yes/No**	**Comments**
Is urban heat stress recognized as an issue within the neighborhood?		
Have environmental and social challenges been identified using available data?		
Is the role of NBS in reducing heat and increasing resilience clearly understood?		
Site-Specific Analysis	**Yes/No**	**Comments**
Have hot spots and land surface features been identified through mapping or field surveys?		
Is vegetation cover, surface reflectivity, and PV panel influence assessed per zone?		
Have possible places for NBS been mapped, considering land use and space?		
Are existing utilities and underground infrastructure mapped for		

conflict prevention?		
Legal & Planning Compliance	**Yes/No**	**Comments**
Do the proposed NBS follow local building, planning, and environmental regulations?		
Have existing legal or administrative barriers to NBS implementation been identified?		
Are incentives or supportive policy instruments for green infrastructure available?		
Feasibility & Technical Assessment	**Yes/No**	**Comments**
Has the building or site been checked to make sure it can support the NBS?		
Have local soil, water availability, and climate been considered for the design?		
Are the chosen materials and plants suitable for the local climate and long-lasting?		
Has the interaction with solar panels and possible heat effects been accounted for?		
Have risks, technical, environmental, or social, been identified and plans made to reduce them?		
Stakeholder Involvement	**Yes/No**	**Comments**
Have all relevant groups (community, authorities, experts) been identified and involved?		
Is there a clear process to include community ideas and feedback in planning?		
Are responsibilities and communication channels for stakeholder engagement defined?		
Are plans in place to educate and raise awareness about NBS benefits?		
Design Standards & KPIs	**Yes/No**	**Comments**
Are clear goals set for performance (e.g., temperature drop, water retention)?		
Has a cost-benefit or full lifecycle analysis been done for each NBS?		
Are key performance indicators (KPIs) aligned with project goals and measurable?		
Is there a plan to evaluate before and after impacts on environment and community?		
Implementation Readiness	**Yes/No**	**Comments**
Are roles, timelines, and resources clearly defined and agreed?		
Have construction steps, safety measures, and compliance checks been planned?		
Is contractor guidance aligned with technical design specifications for NBS systems?		
Monitoring, Maintenance, and Replicability	**Yes/No**	**Comments**
Is there a clear plan to monitor progress, including who collects data, how often, and reporting?		
Are there ways to adjust and improve NBS based on monitoring results?		
Are local communities or authorities involved in maintenance of NBS?		
Are lessons learned recorded to help expand or replicate in other areas?		

3.1.4 App Implementation of ToR Guideline for REC and NBS Creation

To validate the Guideline developed within WP1 and to facilitate the transition from a conceptual framework to an operational deployment action plan, a dedicated application has been developed in which the Guideline is fully implemented. The application enables all users (the Pilots), with the support of the KFI team, to systematically input the required information using country-specific and site-specific data. The data collected through the application cover all procedural and technical steps necessary for the establishment of Renewable Energy Communities (RECs) and the integration of Nature-Based Solutions (NBS), as defined in the ToR Guideline. As a result, the scope and nature of the required inputs vary according to the pilot's national regulatory framework and local site characteristics.

The application was developed using the Glide platform, which offers a free-tier solution supporting up to ten users. This platform was selected for its flexibility, ease of configuration, and suitability for managing structured data entry workflows. Glide enables the organization of complex information into a clear and intuitive interface, facilitating systematic user interaction.

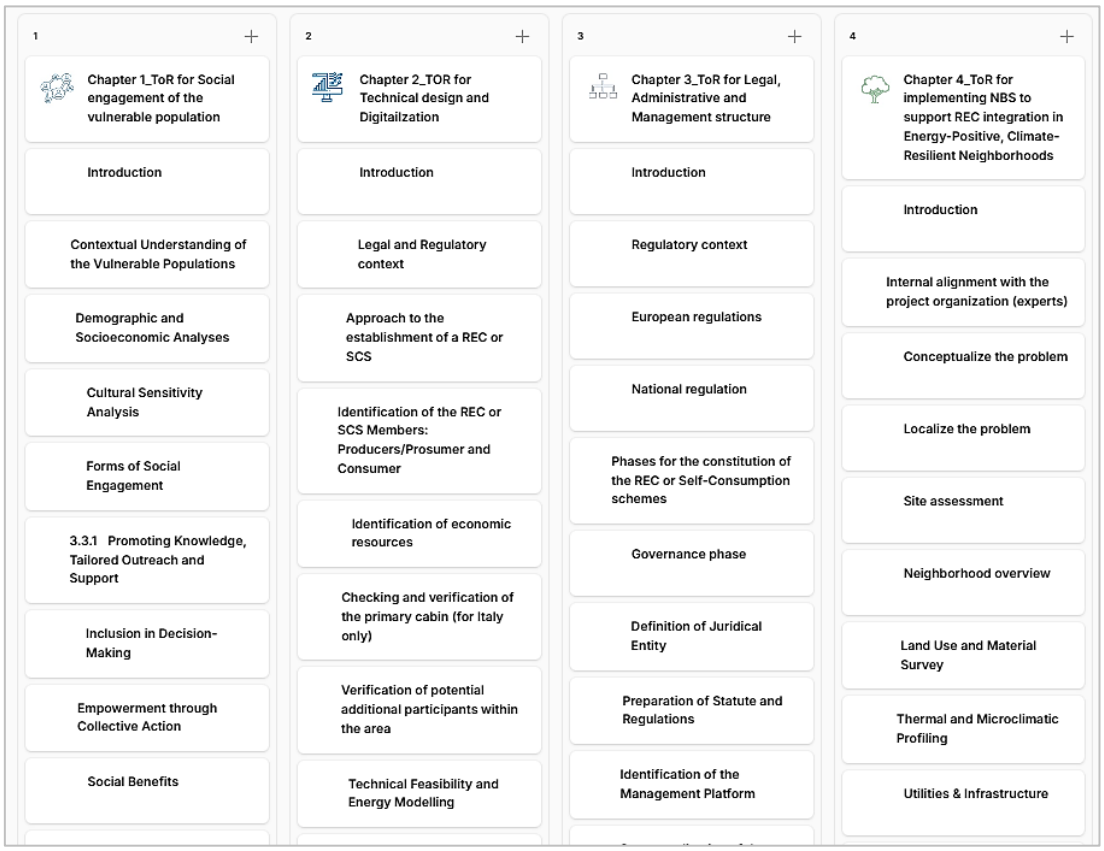

Figure 60. Screenshot of the information organization inside the application

Figure 60 illustrates the organizational logic and hierarchical structure of the application, highlighting how the different components of the Guideline are integrated and presented to users in a coherent and navigable manner.

For each chapter and subchapter, users are requested to provide a detailed response to the assigned task, with a maximum length of 20,000 characters. In cases where the response exceeds this limit, a supporting document may be attached. Furthermore, users are required to indicate if a task is not applicable, providing a justification when relevant, suggest any proposed modifications, and confirm when their responses are considered final as shown in Figure 61.

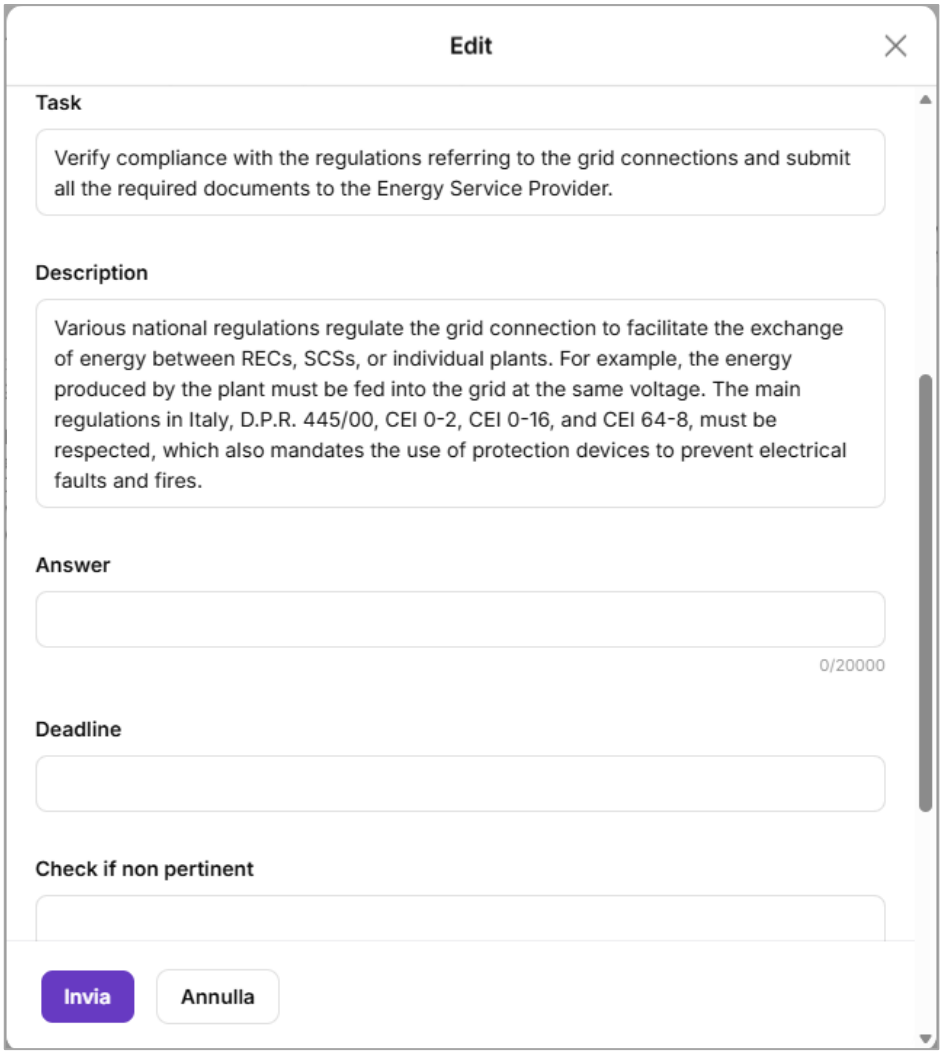

Answer	Attachments	Deadline	Check if non pertinent	Motivation	Proposed modification	Check when completed
		10/01/2026, 12:00	☐			☐

Figure 61. Screenshot of the App structure

Figure 62 presents the interface of the application, illustrating its overall layout and key features. It highlights how the information is organized, the main navigation elements, and the sections where users can input data, attach supporting documents, indicate task relevance, propose modifications, and confirm finalized responses.

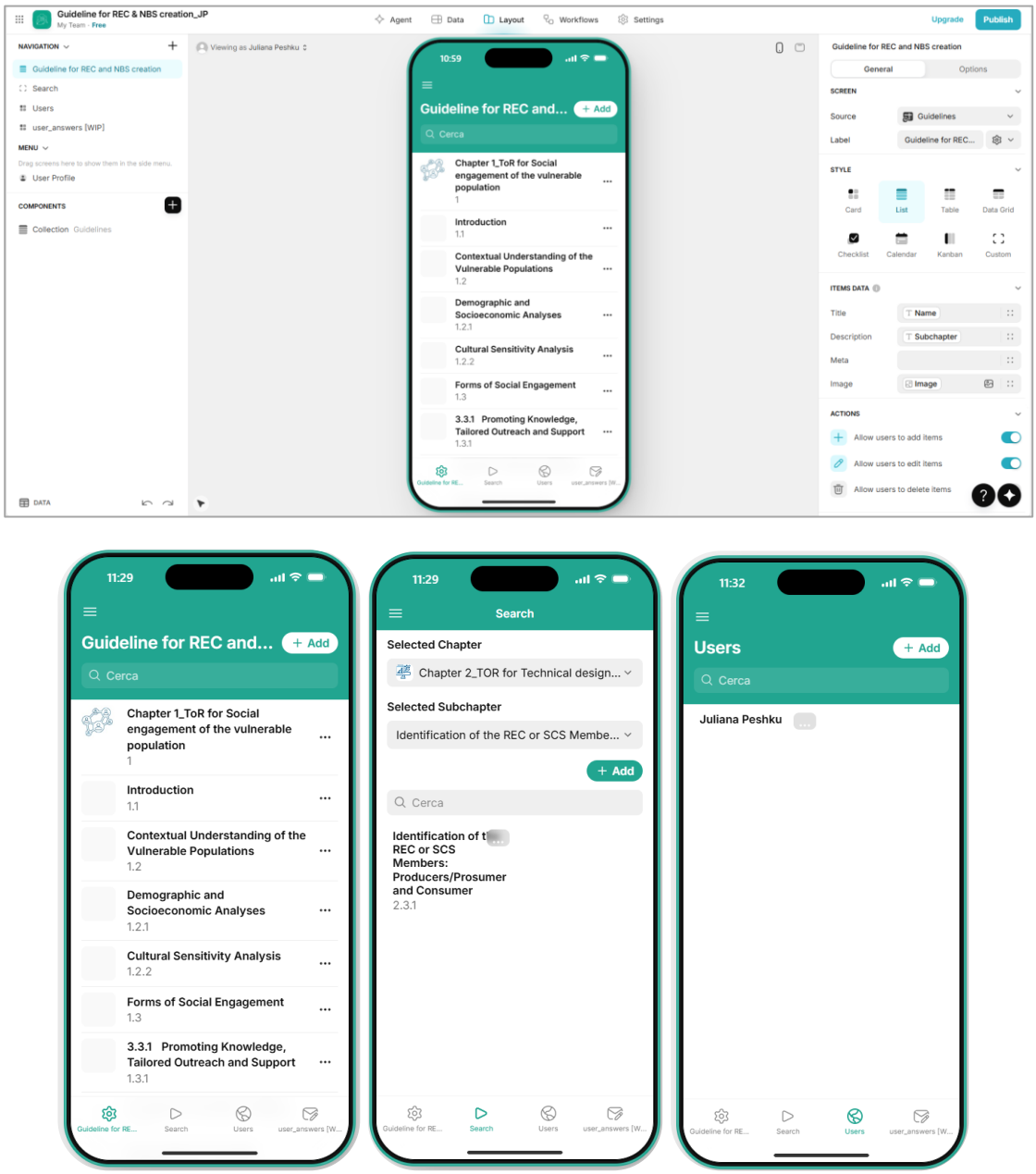

Figure 62. App interface

Upon completion by all pilots, the application will produce four country- and site-specific deployment plans for additional RECs to be implemented in the same regions as the EnerCmed pilots. Moreover, the App is designed to be further extended to support the replication program encompassing 15 additional following pilots, thereby enabling the

consolidation of their data. Altogether, the App will encompass 19 deployment plans, forming a robust basis for the development of a subsequent application aimed at providing concise and actionable deployment projects.

3.2 Energy Performance Assessment and PV Integration: Case Study of the Alessandro Volta School

3.2.1 Building description and geographic localization

One of the pilots of the EnerCmed project is the Alessandro Volta (A.Volta) school, located at 9 Cornigliano Street, CAP 16152**,** Genova, in the western urban area of the city of Genoa (see Figure 63).

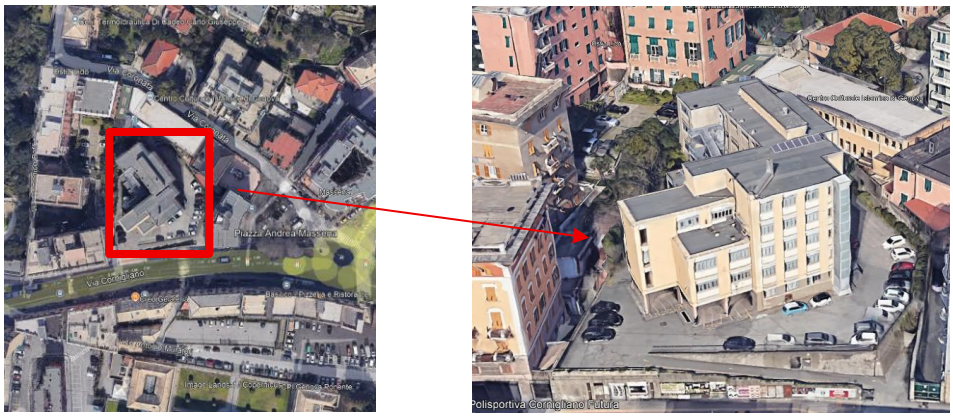

Figure 63. School identification

Locality: Cornigliano, Genova
Latitude: 44°25’00”
Longitude: 08°53’00”

It is a public secondary school facility accommodating a total of 13 classes, with an overall population of 321 students, corresponding to an average of approximately 24.7 students per class. The school activities are distributed across five floors, with a functional layout that reflects typical organizational patterns of Italian educational buildings. The ground floor hosts the main administrative and support functions, including administrative offices, a medical room, a staff lounge, and a dedicated video room. The upper floors accommodate the core educational spaces, including classrooms and a variety of specialized laboratories, such as the science laboratory, music room, art and computer laboratories, a robotics laboratory, and the school library. Additional rooms are designated for study and educational support activities.

As is common for Italian school buildings constructed prior to the widespread adoption of high-performance energy standards, the facility is characterized by relevant energy

consumption, mainly associated with space heating, lighting, and the operation of electrical equipment serving both teaching and administrative functions.

From a climatic perspective, the site is located in Italian climatic zone D, with 1,435 heating degree days (base temperature 20 °C), according to the national classification defined by D.P.R. 412/1993 [157]. This climatic context results in significant heating demand. While space heating demand is covered by a natural gas boiler system and therefore lies outside the primary scope of this research, the climatic conditions also imply non-negligible cooling requirements during the warm season, particularly in educational buildings with high internal heat gains associated with occupant density, lighting, and equipment typical of educational buildings.

In Table 15 are reported the non-occupancy days of the school, considering weekends together with the winter and summer holiday schedules.

School inoccupancy (excluding gyms):

Table 15. School inoccupancy (excluding the gyms)

Months	Public Holidays / All Closures	Weekend Days
September 2025	14 (1 to 14)	4
October 2025	0	8
November 2025	1 (1)	8
December 2025	10 (22–31)	8
January 2026	6 (1 to 6)	8
February 2026	2 (16, 17)	8
March 2026	0	9
April 2026	6 (2 to 6;+ 25)	8
May 2026	1 (1)	10
June 2026	21 (1, 2; 12 to 30)	8
July 2026	31 (1 to 31)	8
August 2026	31 (1 to 31)	10

So based on Table 15, the occupation profile for the whole school, excluding the gyms is given in Figure 64:

Figure 64. Occupation profile for the whole school

Instead, the occupancy profile for the gyms, which will remain open even during July and August, is given in Figure 65:

Gen	Feb	Mar	Apr	Mag	Giu	Lug	Ago	Set	Ott	Nov	Dic
12	10	9	12	11	19	0	1	18	8	9	16

Figure 65. Occupancy profile of the gyms

These inoccupancy profiles will then be then translated into open studio occupancy, activity, equipment, and lighting schedule profiles.

3.2.2 Energy system context and research scope

The Alessandro Volta School is analyzed as a pilot case within the EnerCmed project to assess the integration of photovoltaic (PV) systems and the development of Renewable Energy Community configurations in public buildings.

Within this context, the study defines an analysis framework combining dynamic energy modelling, PV system design under regulatory constraints, and energy balance evaluation. A physics-based model is used to estimate the building's electricity demand, with particular focus on cooling, lighting, and internal equipment, enabling the reconstruction of time-resolved demand profiles.

The PV system is sized according to technical and regulatory requirements, and its performance is evaluated through an energy balance approach, comparing electricity production and consumption over time. This allows the assessment of key indicators such as self-consumption, self-sufficiency, and surplus energy injection.

The analysis is first conducted at the single-building scale, through a self-consumption scheme, and subsequently extended to a multi-building configuration. Additional municipal buildings, characterized by different points of delivery (PODs) and heterogeneous demand profiles, are included to evaluate the potential benefits of energy sharing.

Different REC configurations are then assessed, with particular emphasis on the inclusion of stakeholders who are economically, socially, or regulatorily constrained and therefore unable to directly access renewable energy systems. The framework evaluates how their integration influences energy redistribution and overall system performance. Finally, the analysis aims to identify the optimal REC configuration in terms of economic performance, by defining revenues and overall social and environmental benefits across different scenarios including collective energy management strategies.

Overall, the proposed approach enables the assessment of PV integration strategies under near future operating conditions, including the introduction of a new cooling system, and supports the identification of configurations that enhance local energy use, reduce grid dependency, and promote a more efficient and inclusive energy transition in urban contexts.

3.2.3 Data availability and monitoring infrastructure

At the time of the analysis, no complete energy audit documentation was available for the building. In addition, access to historical electricity and natural gas bills was not possible, preventing the direct characterization of the building's energy demand based on measured consumption data. Moreover, it is necessary to perform the energy modelling to simulate the new cooling system that will be installed in the building. As a result, a physics-based energy model of the building was developed in order to estimate energy needs and to support the subsequent analyses.

Information regarding the building geometry, construction period, and envelope stratigraphies was partially retrieved from technical documentation available through the municipal archives, which represent the only accessible non-invasive source of information. Due to the public function of the building and the absence of authorization for invasive investigations, destructive or intrusive testing of the building components was not feasible. Consequently, the characterization of the building envelope was carried out using available documentation, complemented by standardized assumptions consistent with construction practices of the reference period and with national technical standards.

According to the cartographic maps area most of the buildings were constructed after the Second World War [158], more precisely, the reference building was built in 1961 (see Figure 66). The construction techniques used in that period consisted of reinforced concrete frames made of reinforced concrete slabs and cavity walls.

Figure 66. Cartographic maps indicating the construction year of the reference building and the other buildings in the area [158]

Based on the data reported in Figure 67, since its construction, the A. Volta School has undergone only one restoration, which involved the heating system, and no interventions have been made to improve the thermal performance of the building envelope, including both transparent and opaque elements.

Elenco Pratiche Edilizie

Interno	Protocollo	Autorizzazione	Protocollo Edilizia	Oggetto	Note
	9295/2014	S.U.I. S.C.I.A.	11/12/2014	S.U.464/2014 MODIFICA ED INTEGRAZIONE CENTRALE TERMICA	-
	PROGETTO 507/1961	PROGETTO	17/06/1961	SCUOLA "A.VOLTA"	-

Figure 67. Summary of Building Permits and Construction Interventions of the school from construction to the present [158]

Concerning monitoring infrastructure, the building is currently equipped with limited energy monitoring systems, which do not provide high-resolution end-use disaggregation. Therefore, the energy model plays a central role in reconstructing heating and cooling demand profiles and electricity consumption patterns associated with space cooling, lighting, and internal equipment. The modelling framework allows the generation of time-resolved demand profiles, which are subsequently used for the assessment of energy balance with reference to the energy production by PV generation adequacy and REC configuration scenarios. Despite these data limitations, the adopted approach ensures a transparent and reproducible methodology, representative of real-world conditions often encountered in existing public buildings, where detailed energy data and invasive diagnostic campaigns are frequently unavailable.

3.2.4 Energy building model: Open Studio software

Overview of the Modeling Approach

This research adopts a physics-based building energy modeling (BEM) approach implemented using OpenStudio 3.9.0 SDK software, an open-source software development kit and graphical user interface that operates as a front end for the EnergyPlus simulation engine [159]. The modeling framework enables a consistent representation of building geometry, thermal zoning, envelope characteristics, internal loads, schedules and HVAC systems within a unified simulation environment.

The building model was developed following a modular workflow, in which each modeling phase, namely geometric modeling, thermal zoning, construction characterization, internal load definition, HVAC representation, and simulation setup, is addressed separately. This structure ensures model transparency and reproducibility, which are essential for scenario-based energy analyses.

The integration between OpenStudio and the SketchUp plug-in [160] was used to translate architectural geometry into an energy simulation–ready model compliant with EnergyPlus requirements. EnergyPlus computes heating and cooling energy need by

solving the transient sensible and latent heat balance of each thermal zone, determining at each time step the thermal power required to maintain the indoor setpoint temperature.

The fundamental equation applied by OpenStudio/EnergyPlus is:

$$\rho_{air}\, c_p\, V_z\, \frac{dT_z}{dt} = \sum \dot{Q}_{surf} + \dot{Q}_{int} + \dot{Q}_{solar} + \dot{Q}_{vent} + \dot{Q}_{inf} + \dot{Q}_{HVAC} \quad (24)$$

where:

ρ_{air} = air density
c_p = specific heat of air
V_z = zone air volume
T_z = zone air temperature
$\dot{Q}_{surf}$ = convective heat transfer from internal surfaces
$\dot{Q}_{int}$ = internal sensible gains (people, lights, equipment)
$\dot{Q}_{solar}$ = solar gains through windows
$\dot{Q}_{vent}$ = sensible load due to ventilation
$\dot{Q}_{inf}$ = sensible load due to infiltration
$\dot{Q}_{HVAC}$ = heating or cooling supplied by HVAC
So, below is given the formula for obtaining the thermal power required to maintain the indoor setpoint.

$$\dot{Q}_{need} = -\left(\sum \dot{Q}_{surf} + \dot{Q}_{int} + \dot{Q}_{solar} + \dot{Q}_{vent} + \dot{Q}_{inf}\right) \quad (25)$$

Setpoint control logic:

- Heating demand:

$$T_z < T_{set,heat} \Rightarrow \dot{Q}_{need} > 0 \quad (26)$$

- Cooling demand:

$$T_z > T_{set,cool} \Rightarrow \dot{Q}_{need} < 0 \quad (27)$$

The total heating or cooling energy need is obtained by time integration:

$$Q_{need} = \sum_{t=1}^{N} | \dot{Q}_{need,t} | \cdot \Delta t \quad (28)$$

Geometric Modelling and Spatial Definition

The first step consisted of developing a three-dimensional representation of the building geometry using SketchUp integrated with the OpenStudio plug-in. The ground floor (see Figure 68) was modelled based on the available building plans and the defined floor-to-

floor height, after which the complete building geometry was generated to represent the overall volumetric configuration of the structure as shown in Figure 69.

Within SketchUp, building spaces were modeled as closed planar volumes, ensuring that all surfaces (walls, floors, roofs, and ceilings) formed a watertight enclosure. Each space was explicitly drawn following OpenStudio's surface-matching requirements to allow for proper boundary condition recognition during simulation.

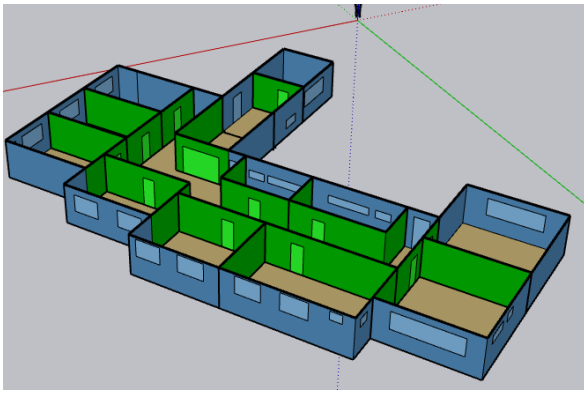

Figure 68. Ground floor plan which also represents the boundary conditions

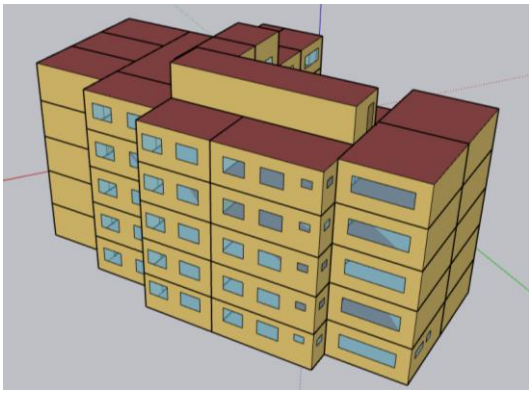

Figure 69. Completed building geometry

Site weather file and Design days

The site weather data are based on the file "Statistics for ITA_Genova-Sestri.161200_IGDG", referring to the Genova-Sestri weather station (WMO 161200), located at 44°25′ N, 8°51′ E, at an elevation of 3 m above sea level (GMT +1.0). The climatic data source is IGDG. The main data regarding the midseason, external and yearly temperatures and heating days are given in Table 16.

Table 16. Heating degree days [161]

Zone	City	Medium seasonal temperature	Heating days	T_e	Annual medium temperature
Zone D	Genoa	11,24 ˚C	166	0 ˚C	16,5 ˚C

Pursuant to Article 3 of DPR 412/93, which establishes the classification of buildings based on their use destination, the analyzed school building is classified under category E.7 – Buildings used for educational activities at all levels and similar uses [161].

Based on the intended use of the building and in compliance with UNI/TS 11300-1:2014 [162], the design indoor temperatures adopted for the energy and HVAC calculations are 20 °C for the winter heating season and 26 °C for the summer cooling season [162].

Furthermore, pursuant to Article 2, Annex A (Part 2) of DPR 412/93 [161], the municipality of Genoa is classified in climatic zone D, corresponding to 1,435 degree days. In accordance with UNI/TS 11300-1:2014 [162], the applicable heating season start and end dates are defined as reported in Table 17. Regarding the summer season, the standard does not give any indication for the cooling days.

Table 17. Start and ending date of the winter season

Climatic Zone	Start Date	End Date
A	1 December	15 March
B	1 December	31 March
C	15 November	31 March
D	1 November	15 April
E	15 October	15 April
F	5 October	22 April

Construction Assemblies and Material Properties

Within the OpenStudio environment, the building envelope materials were explicitly created by defining the individual layers composing each construction assembly. For each material layer, the relevant thermo-physical properties, such as thermal conductivity, density, and specific heat capacity, were assigned based on reference values provided by UNI EN ISO 10456 [163], which specifies declared and design values for building materials in the absence of product-specific laboratory data.

The resulting layered constructions were assembled in accordance with the calculation methodology prescribed by UNI EN ISO 6946 [164], ensuring consistency with the standard approach for the evaluation of thermal resistances and overall thermal transmittance of opaque building elements. Surface thermal resistances were defined according to the same standard.

This approach allows for a physically consistent and norm-compliant representation of the building envelope within the energy model, while explicitly accounting for the limitations associated with the lack of invasive testing and detailed construction documentation. In Figure 70 and Figure 71 are presented how construction elements are created inside OpenStudio software. Instead in Table 18 are summarized the transmittance values of the construction elements inside the software.

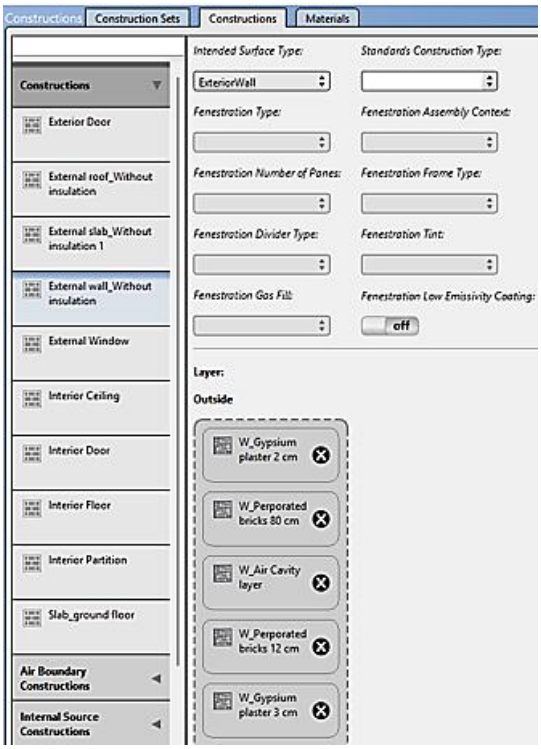

Figure 70. Exterior wall stratigraphy

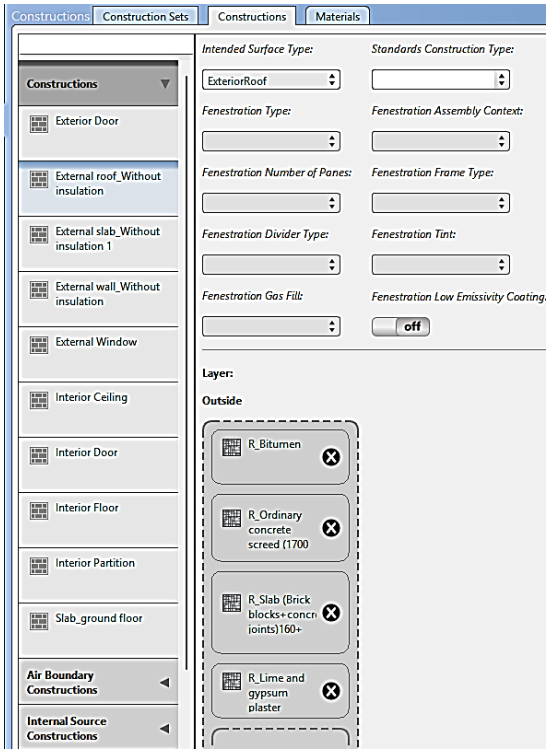

Figure 71. Exterior roof stratigraphy

Table 18. Thermal transmittance values of external opaque and transparent elements

Construction	Reflectance	U-Factor with Film [W/m2-K]	U-Factor no Film [W/m2-K]
External wall_without insulation	0.30	1.113	1.335
Slab_Ground floor	0.30	1.177	1.455
External Roof_without insulation	0.30	1.629	2.099
External Slab_without Insulation	0.30	1.748	2.632
External window	-	1.417	-

Assignment of Space Types and Thermal Zoning

Following the definition of the geometric volumes, each modeled area was converted into an OpenStudio Space object and associated with a dedicated thermal zone, establishing a one-to-one correspondence between spaces and zones. This zoning strategy allows the model to reflect variations in internal gains, occupancy patterns and usage schedules across the different functional areas of the building.

Such a detailed spatial discretization is particularly suitable for educational buildings, where rooms have diverse functions, variable occupancy levels and distinct comfort requirements. Although this approach increases computational effort, it provides a more accurate representation of indoor thermal behaviour and cooling demand dynamics.

Space types were then assigned to each zone to define internal load densities related to occupants, lighting and plug-in equipment (see Figure 72). These were selected from the OpenStudio standards libraries or custom-defined to match the specific functional programme of the building, ensuring consistency between space usage, internal heat gains and operational schedules, and thus supporting a reliable estimation of cooling-driven electricity demand.

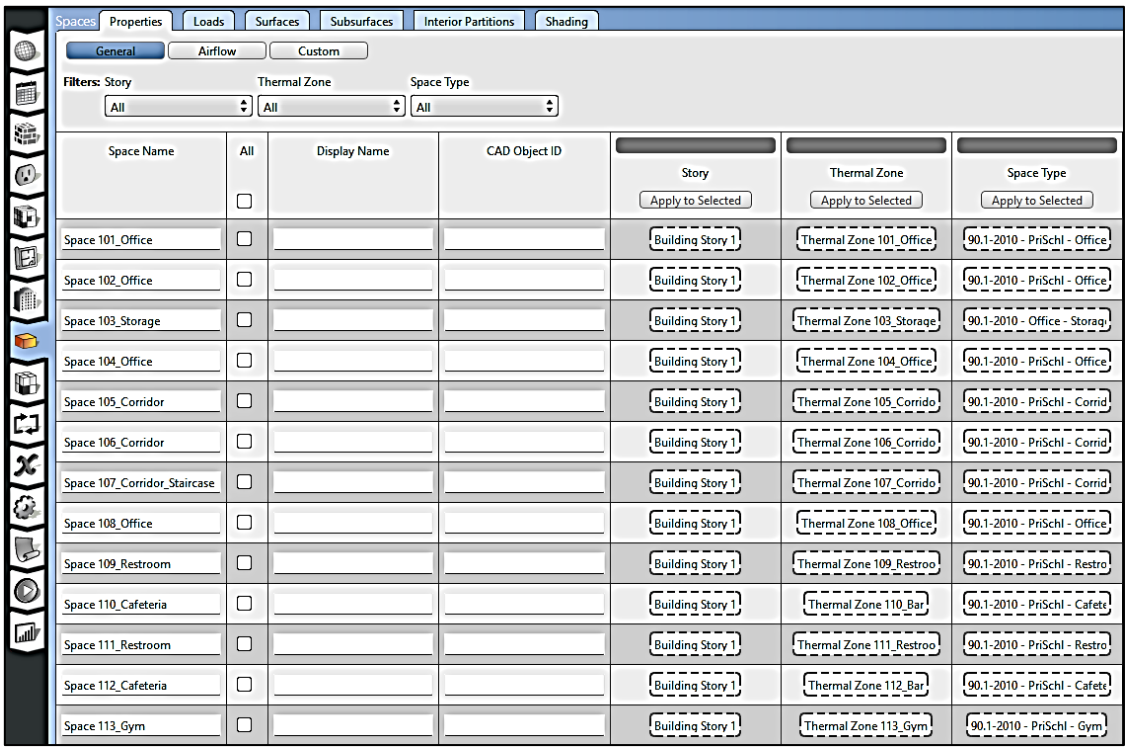

Figure 72. Assignment of the Space type and Thermal zone

Internal Loads

Internal heat gains were modeled by defining occupant densities, lighting power densities, and equipment loads at the space or space-type level.

Occupancy

According to the UNI/TS 11300-1:2014 [162], the Internal gains by occupants can be determined as a function of the intended use of the spaces, based on the values reported in Table 19. This table provides the global values of internal heat gains from occupants for non-residential buildings, expressed as a function of occupancy density.

Table 19. Occupancy density and heat gain values

Occupancy Density Class	Useful Floor Area per Person [m²/person]	Occupancy Density [persons/m²]	Simultaneity Factor f_a	Average Heat Gain from Occupants Φint,oc / Af [W/m²]
I	1.0	1.00	0.15	15
II	2.5	0.40	0.25	10
III	5.5	0.18	0.27	5
IV	14	0.071	0.42	3
V	20	0.050	0.40	2

The appropriate occupancy density class is determined according to the functional use of the spaces. For example:

- Class I–II: low density spaces (assembly rooms, classrooms, retail)
- Class III: medium-density spaces (offices, restrooms, labs)
- Class IV–V: high-density spaces (corridors, storage areas, workshops)

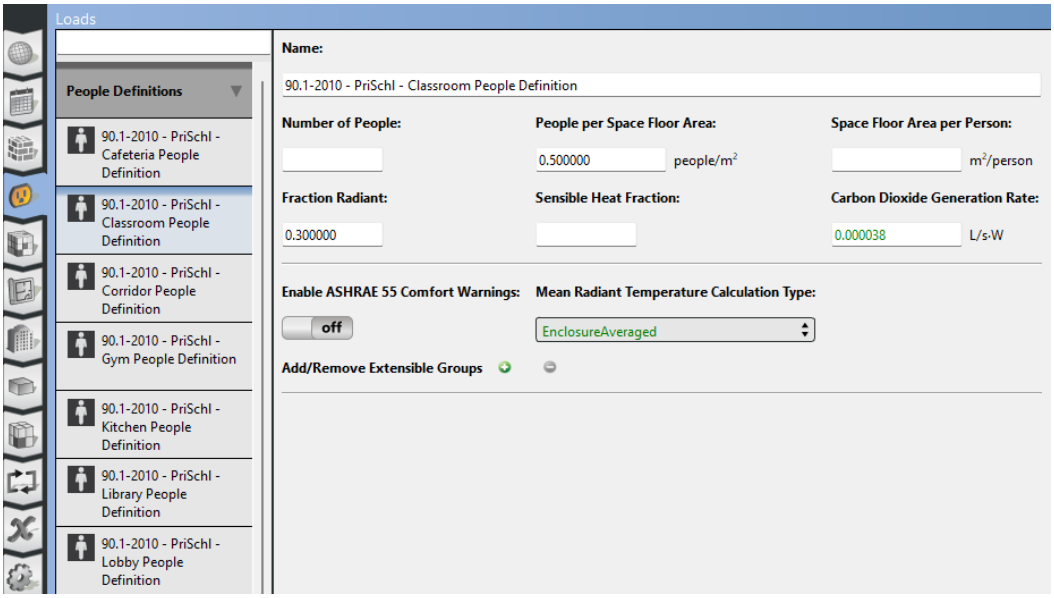

Figure 73. Definition of the occupation density in the OpenStudio software

Figure 73 shows an example of how the occupancy density for a classroom is defined within the OpenStudio software.

Lighting

As an on-site energy audit could not be carried out, the total installed lighting power for each individual space was calculated based on the requirements of UNI EN 12464-1:2021 [165] shown in Table 20.

Table 20. Lighting Requirements – General Areas Inside Buildings (UNI EN 12464-1:2021) [165]

Ref.	Area / Activity	Ēm required [lx]	Utilization Factor (u)	Specific Requirements
44.1	Classroom – general activities	500	0.55	Lighting adjustable for different activities; dimming required
44.4	Black, green and white boards	500	0.60	Vertical illuminance required; avoid veiling reflections
44.14	Practical rooms and laboratories	500	0.55	Task-dependent lighting
44.16	Teaching workshop	500	0.55	Adjustable lighting
44.17	Preparation rooms and workshops	500	0.55	–
44.18	Entrance halls	200	0.50	Horizontal illuminance
44.19	Meeting areas, corridors	100	0.45	Floor level
44.20	Corridors	100	0.45	–
44.21	Student common rooms / assembly halls	200	0.50	–
44.22	Teacher rooms	300	0.55	Office-type work
44.23	Library, bookshelves	200	0.60	Shelf lighting – see libraries
44.24	Library reading areas	500	0.60	See libraries
44.25	Stock rooms for teaching materials	100	0.45	–
44.26	Sports halls, gymnasiums, swimming pools	300	0.50	EN 12193 applies
44.27	School canteens	200	0.55	–
44.28	Kitchen	500	0.55	–

Lighting Calculation Methodology

Step 1 – Total Luminous Flux

The total luminous flux required to achieve the target illuminance on the working plane is calculated using:

$$\Phi_{tot} = \frac{E \cdot A}{u \cdot m} \tag{29}$$

Where E is the required illuminance based on the space type (see Table 20), A the area, u the utilization factor (accounting for room geometry and reflectance), and m the maintenance factor (accounting for lumen depreciation and dirt).

Step 2 – Installed Electrical Power

The required installed electrical power is obtained by dividing the total luminous flux by the average luminous efficacy of the luminaires:

$$P = \frac{\Phi_{tot}}{\eta} \tag{30}$$

where η is the luminous efficacy of the light sources.

Result

The calculated power (see Table 21) represents the total lighting power required and can be achieved through an appropriate combination of luminaires that ensures compliance with lighting performance and energy efficiency requirements.

Table 21. Results of the lighting power for each space

Room	Floor Area	Illuminance (Standard)	Lighting Power (W)
Office	30 m²	300 lux	140 W
Classroom	30 / 31 / 32 / 35 / 48 m²	300 lux	186–298 W
Laboratory	50 m²	500 lux	517 W
Corridor	100 m²	100 lux	284 W
Lobby / Atrium	29 m²	200 lux	132 W
Gym	50 m²	300 lux	341 W
Kitchen	18 m²	500 lux	234 W
Restrooms	20 m²	200 lux	101 W
Storage	19 m²	100 lux	48 W

Figure 74 shows the compilation of the lighting definition for an office inside the software.

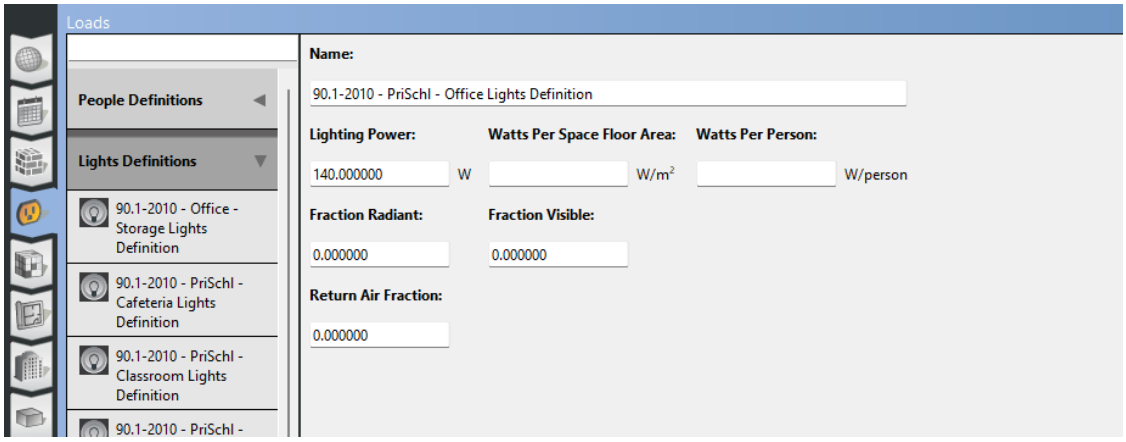

Figure 74. Lighting definition for the office

Equipment

The average internal heat gains generated by the operation of equipment can be determined as a function of the intended use of spaces. Table 22 provides global values of internal heat gains from equipment, expressed as a function of the building category, for non-residential buildings.

Table 22. Equipment heat gain

Building Category	Equipment Heat Gain during Operating Period Φint,A / Af [W/m²]	Simultaneity Factor *fA*	Average Equipment Heat Gain Φint,A / Af [W/m²]
Offices	15	0.20	3
Educational activities	5	0.15	1
Healthcare (non-clinical activities)	15	0.20	3
Supply services	10	0.25	3
Assembly spaces	5	0.20	1
Sports facilities	4	0.25	1

In the Figure 75 is shown how the heat gains are assigned to each space within the OpenStudio software.

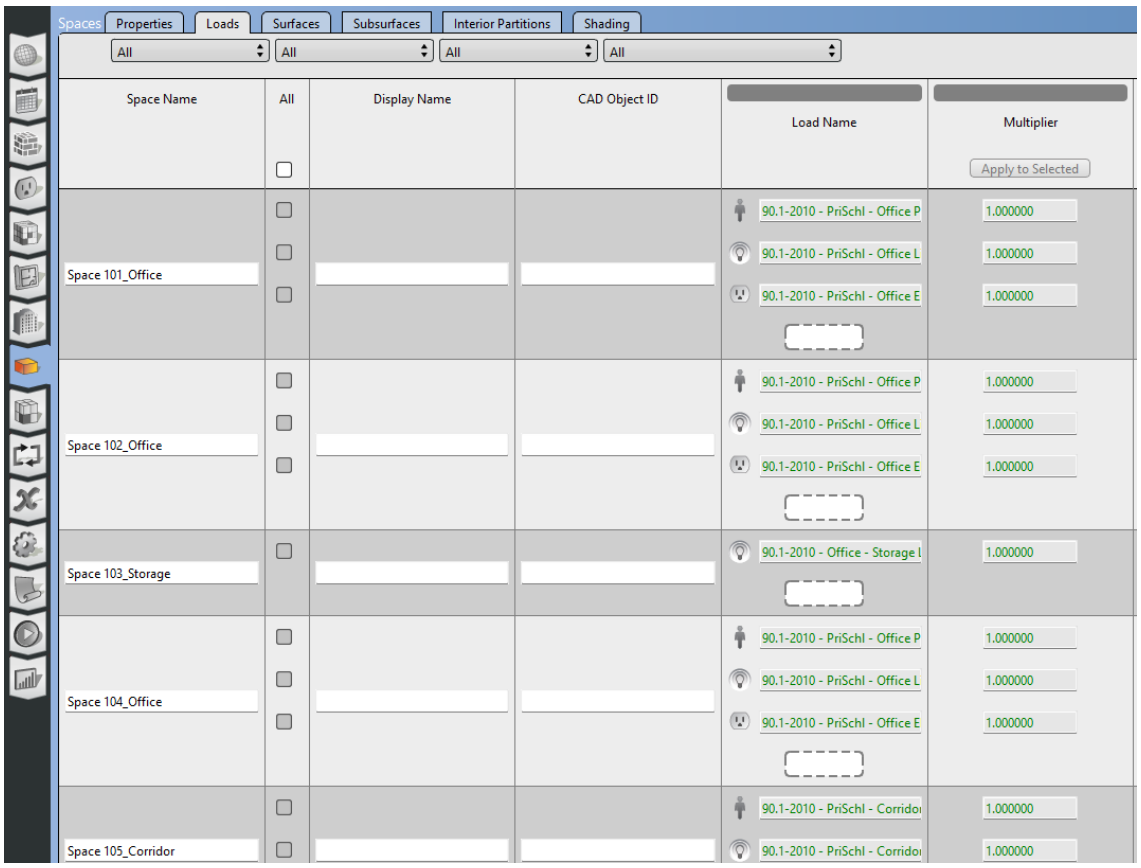

Figure 75. Assignment of the equipment heat gains to each space

Operational Schedules

Operational schedules governing occupancy, lighting usage, equipment operation, and thermostat setpoints were assigned using hourly profiles.

Schedules were developed based on either standardized reference schedules (e.g., typical weekday/weekend patterns, heating plant) or assumed operational data relevant to the

building type. This step ensured that temporal variations in internal gains and building operation were accurately represented in the simulation. The most representative schedules are given in the Figure 76.

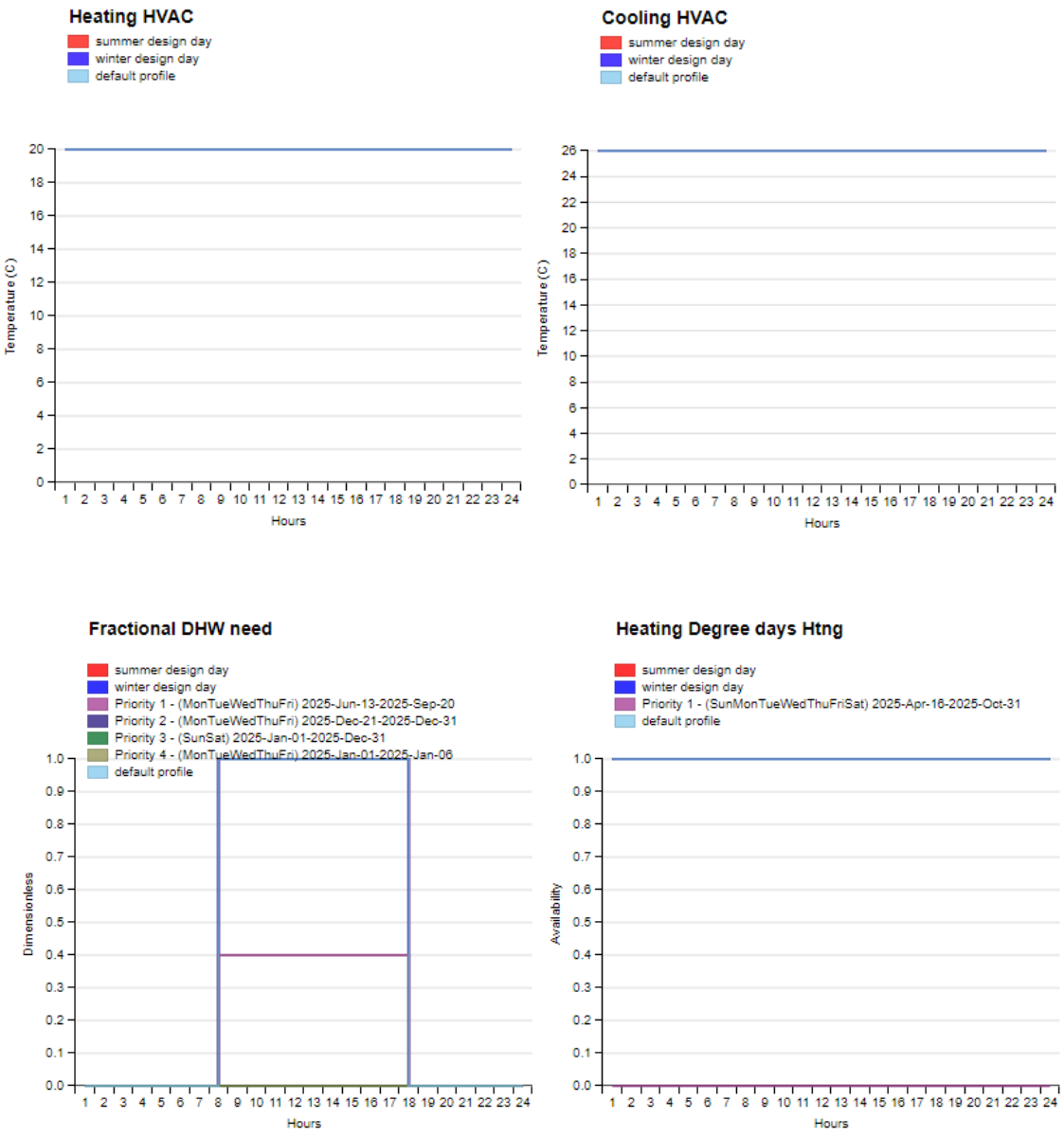

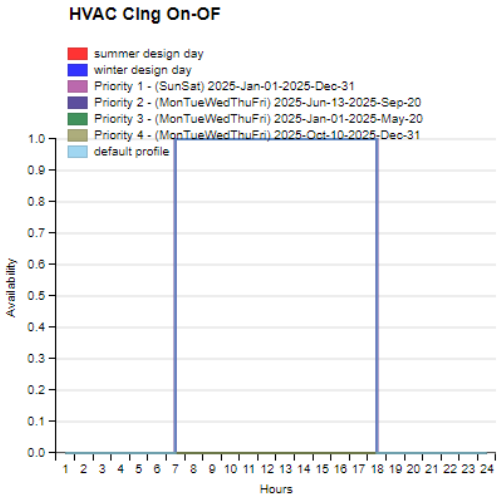
HVAC Clng On-OF
summer design day
winter design day
Priority 1 - (SunSat) 2025-Jan-01-2025-Dec-31
Priority 2 - (MonTueWedThuFri) 2025-Jun-13-2025-Sep-20
Priority 3 - (MonTueWedThuFri) 2025-Jan-01-2025-May-20
Priority 4 - (MonTueWedThuFri) 2025-Oct-10-2025-Dec-31
default profile
Availability
Hours

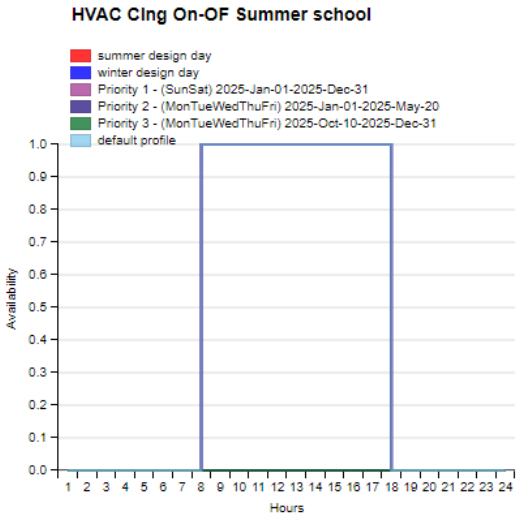
HVAC Clng On-OF Summer school
summer design day
winter design day
Priority 1 - (SunSat) 2025-Jan-01-2025-Dec-31
Priority 2 - (MonTueWedThuFri) 2025-Jan-01-2025-May-20
Priority 3 - (MonTueWedThuFri) 2025-Oct-10-2025-Dec-31
default profile
Availability
Hours

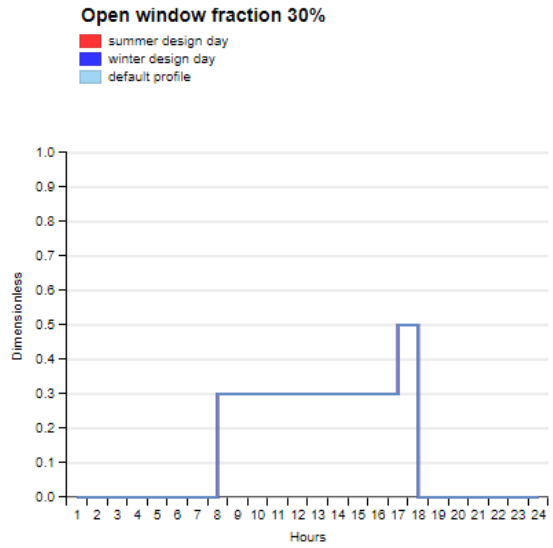
Open window fraction 30%
summer design day
winter design day
default profile
Dimensionless
Hours

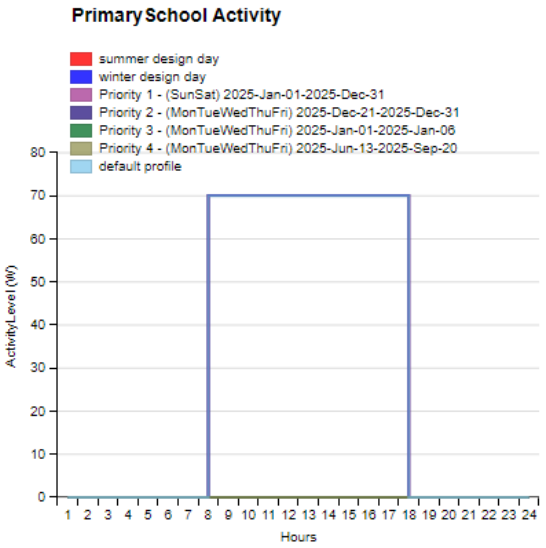
Primary School Activity
summer design day
winter design day
Priority 1 - (SunSat) 2025-Jan-01-2025-Dec-31
Priority 2 - (MonTueWedThuFri) 2025-Dec-21-2025-Dec-31
Priority 3 - (MonTueWedThuFri) 2025-Jan-01-2025-Jan-06
Priority 4 - (MonTueWedThuFri) 2025-Jun-13-2025-Sep-20
default profile
ActivityLevel (W)
Hours

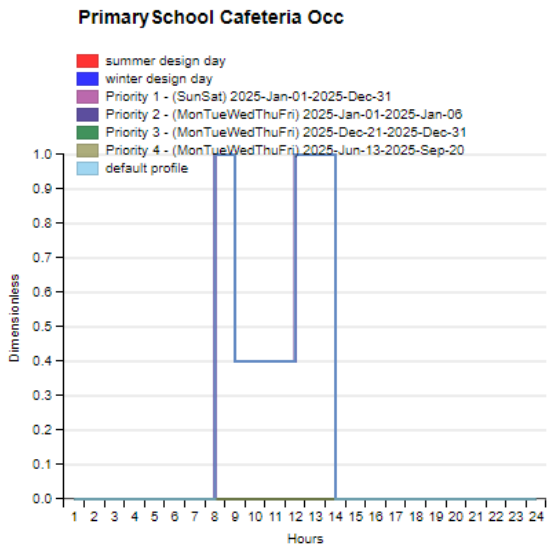
Primary School Cafeteria Occ
summer design day
winter design day
Priority 1 - (SunSat) 2025-Jan-01-2025-Dec-31
Priority 2 - (MonTueWedThuFri) 2025-Jan-01-2025-Jan-06
Priority 3 - (MonTueWedThuFri) 2025-Dec-21-2025-Dec-31
Priority 4 - (MonTueWedThuFri) 2025-Jun-13-2025-Sep-20
default profile
Dimensionless
Hours

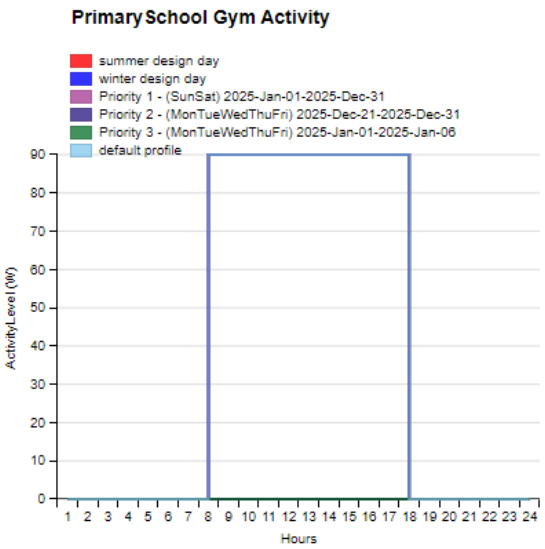
Primary School Gym Activity
summer design day
winter design day
Priority 1 - (SunSat) 2025-Jan-01-2025-Dec-31
Priority 2 - (MonTueWedThuFri) 2025-Dec-21-2025-Dec-31
Priority 3 - (MonTueWedThuFri) 2025-Jan-01-2025-Jan-06
default profile
ActivityLevel (W)
Hours

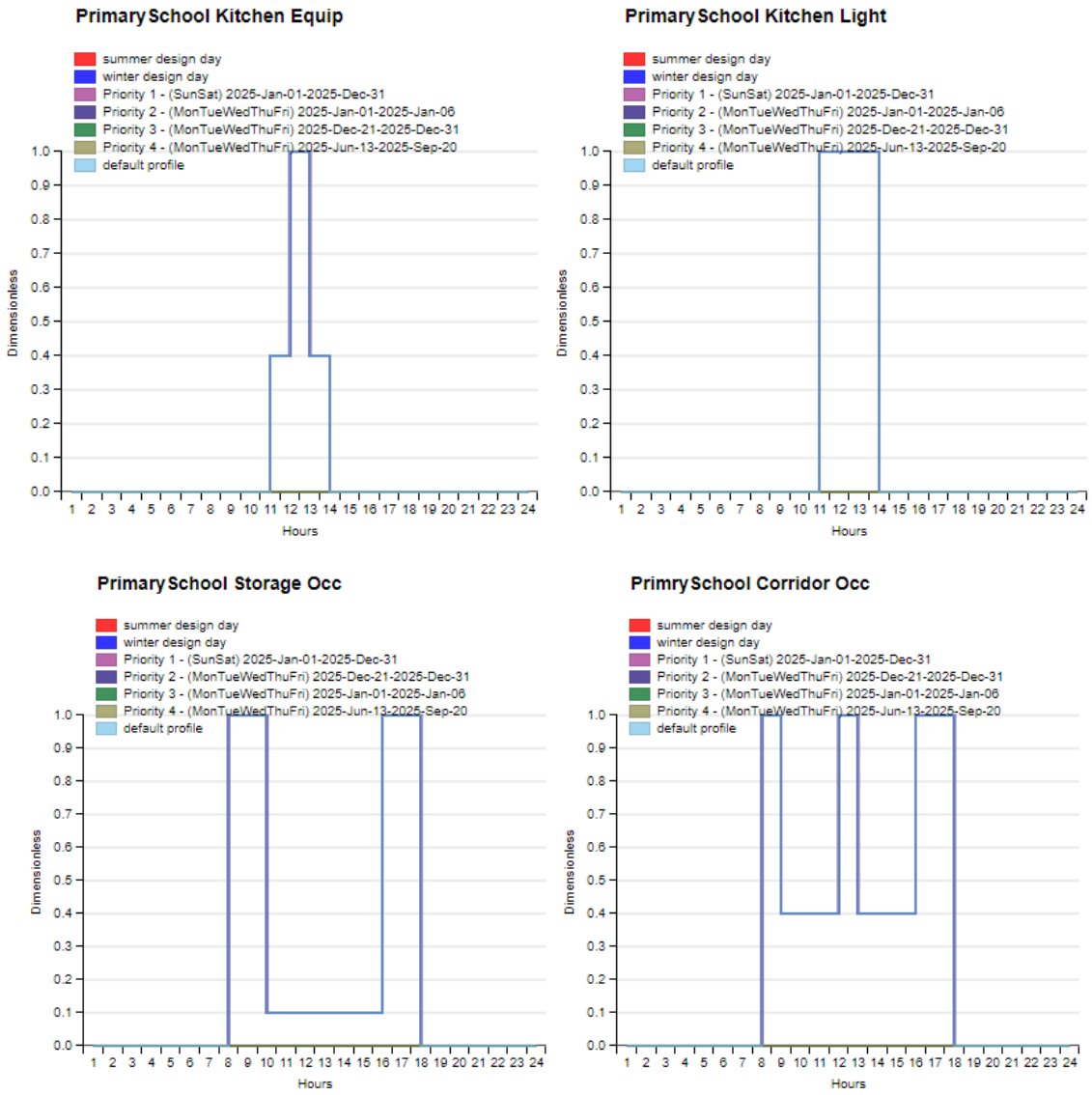

Figure 76. Representation of the most representative schedules imposed within the OpenStudio software

All schedules try to represent the actual usability, excluding weekends, hours of inoccupancy, summer and winter holidays, etc.

HVAC System

At the preliminary stage, the simulations were carried out using an Ideal Loads Air System, with no explicit HVAC equipment modeled. This approach was adopted to verify the correctness and consistency of the input data and modeling assumptions, and to identify any potential setup errors at an early stage. Under this configuration, the simulation outputs represent the heating and cooling loads required at zone level to maintain the prescribed indoor setpoint temperatures. The use of ideal loads is particularly

suitable for early-stage analyses, including envelope performance assessment, comparison of design alternatives, and sensitivity analyses of internal gains.

As described in the building characterization section, the existing heating system consists of a gas-fired boiler supplying radiators, while the school building is currently not equipped with a mechanical cooling system. However, in order to comply with the cooling setpoint temperatures required by current regulations and to improve thermal comfort conditions for both students and staff, the local municipality is evaluating the opportunity to install a cooling system. In this study, the cooling system is therefore modelled hypothetically to assess its potential impact on energy demand and indoor comfort conditions. The proposed intervention is mainly intended for the gyms, which are actively used during the months of July and August for summer school programs dedicated to students from economically disadvantaged backgrounds. The system operation is scheduled according to the heating degree days-based schedule previously reported. Figure 77 and Figure 78 illustrates the system configuration and the corresponding control system implemented in OpenStudio.

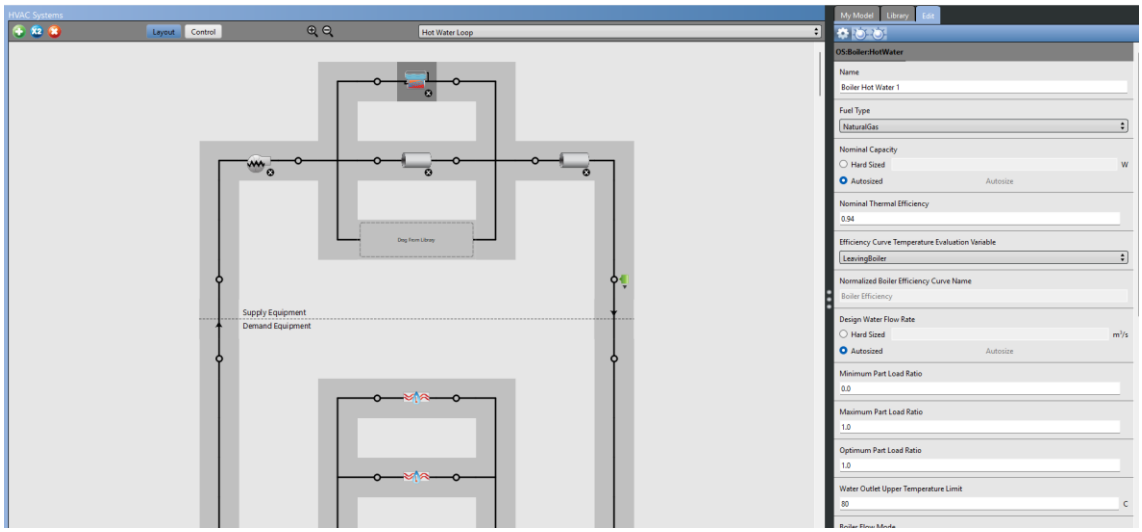

Figure 77. Heating system scheme

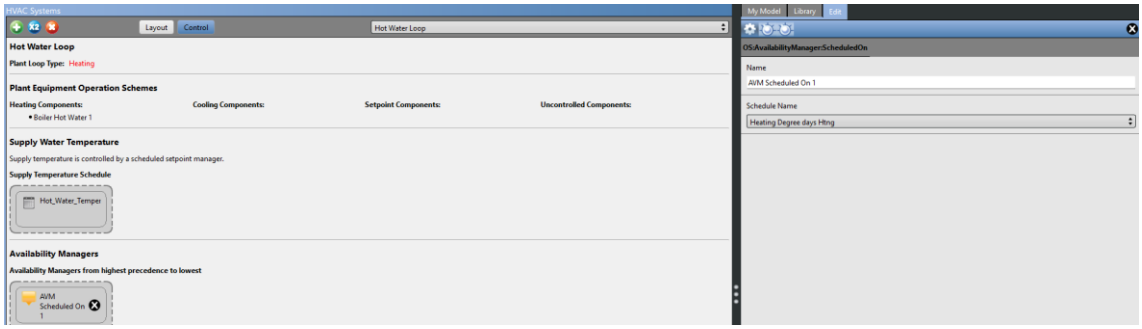

Figure 78. Heating control system

DHW system

Domestic hot water (DHW), intended for sanitary uses within the school building, is produced by a dedicated gas-fired boiler in combination with a storage tank, as illustrated in the Figure 79.

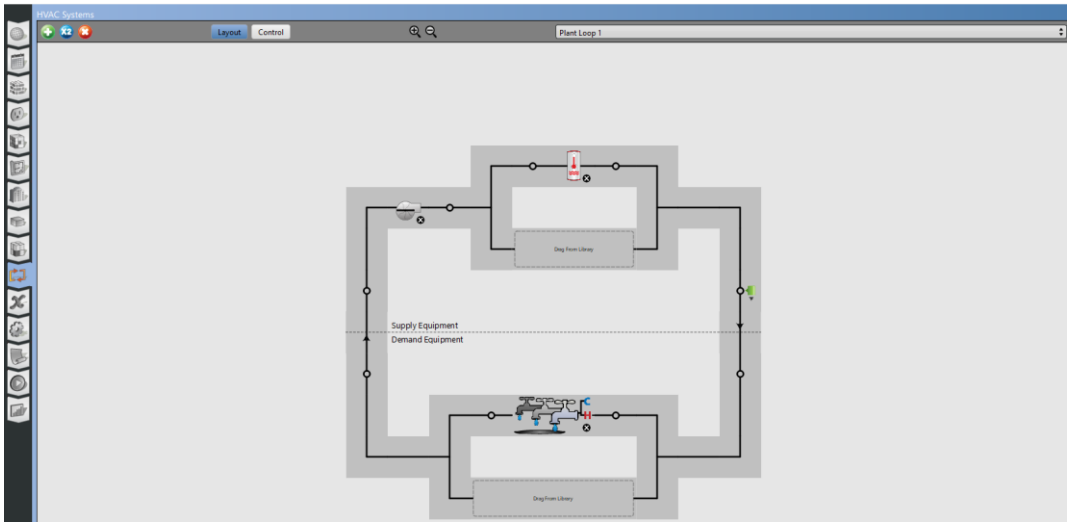

Figure 79. DHW scheme

Cooling system

Since a cooling system is currently not installed, a non-invasive solution is being considered for near-future implementation, such as split or multi-split systems. Accordingly, for the purpose of the simulations, a unitary single-speed direct expansion (DX) cooling system is assumed with a COP of 3 (see Figure 80).

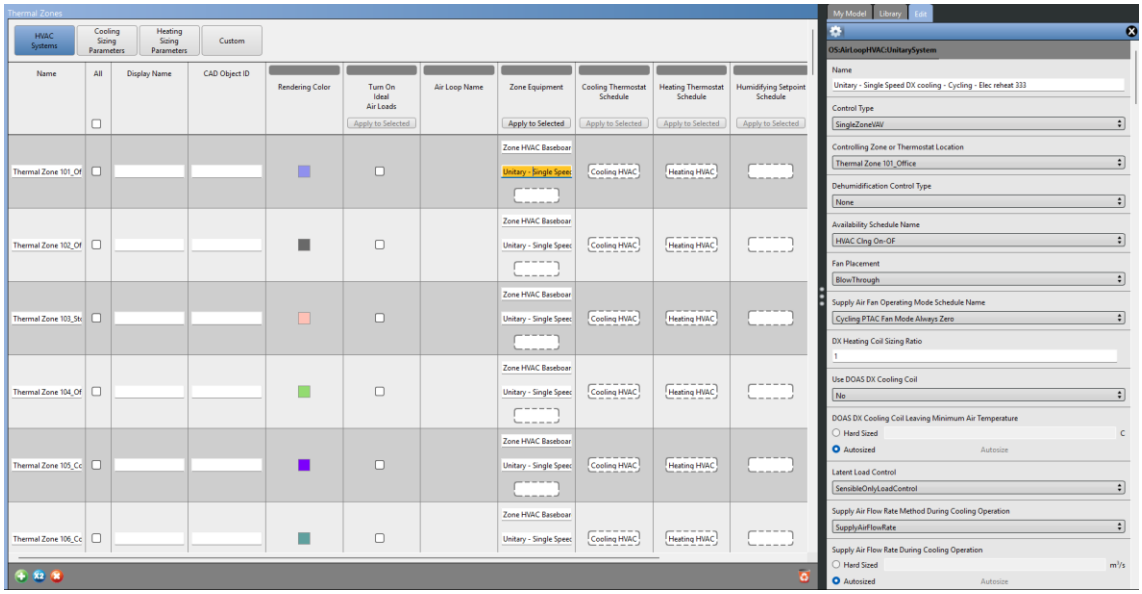

Figure 80. Cooling system configuration

Critical Issues and Modeling Limitations

- Ground–floor slab heat exchange

In OpenStudio, the heat exchange between the ground-floor slab and the soil is modeled using a constant ground temperature, set by default to 18 °C. However, this simplification does not accurately represent the seasonal variability of ground temperatures. To address this limitation, an additional plugin *Set Ground Temperatures-Monthly* was implemented, allowing the definition of average monthly ground temperatures, thereby improving the physical consistency of the model.

- Ventilation modeling

OpenStudio accounts for air infiltration through the building envelope, but it does not explicitly model natural ventilation as defined by national standards. To partially overcome this limitation, a dedicated plugin was adopted *Add Wind and Stack Open Area*. Nevertheless, this approach does not allow ventilation rates to be differentiated according to the area or use of individual spaces. Instead, ventilation is estimated using a single value based on the percentage of window opening, combined with a control schedule dependent on internal and external temperature thresholds and wind speed limits. As a result, this method may deviate from the actual ventilation requirements prescribed by UNI/TS 11300-1.

- Thermal bridges

A further limitation concerns the treatment of thermal bridges, which are entirely excluded from the building energy demand in the OpenStudio model. This represents a significant simplification, as thermal bridges are explicitly addressed by UNI EN ISO 10211 [166] and are mandatory to be considered according to the Minimum Energy Performance Requirements, as reinforced by D.M. 28/10/2025 [167]. The exclusion of thermal bridges may therefore lead to an underestimation of the building's heating energy demand.

Results

The building energy model predicts a total annual final energy consumption of 242,900 kWh, with a distribution that is strongly dominated by thermal end uses. As shown in Figure 81, space heating accounts for the largest share of energy demand, with 174,508 kWh, corresponding to 71.3% of total consumption. This result confirms that heating requirements are the primary driver of the building's energy performance.

Domestic hot water (DHW) represents 18,756 kWh (7.7%), while pumping energy amounts to 18,892 kWh (7.7%), reflecting the relevance of hydronic distribution systems in supporting thermal services. Combined, these end uses underline the strong coupling between thermal demand and auxiliary system operation.

Among the remaining end uses, interior lighting is the most significant, with an annual consumption of 23,692 kWh (9.7%), followed by cooling, which accounts for only 3,933 kWh (1.6%). The relatively low cooling demand indicates a heating-dominated building behavior, influenced by climatic conditions, envelope characteristics, and operational patterns. Interior equipment and fans contribute marginally to the overall energy balance, with shares of 1.1% and 0.1%, respectively. Their limited impact suggests that non-thermal electrical loads play a secondary role compared to space conditioning and lighting demands.

Overall, the end-use breakdown demonstrates that building energy consumption is overwhelmingly governed by heating-related demand, while electrical consumption is primarily driven by lighting and system auxiliaries. These results indicate that strategies aimed at reducing total energy use should prioritize reductions in heating demand and associated distribution losses, followed by targeted improvements in lighting efficiency.

End Use	Consumption [kWh]
Heating	175,733
Interior Lighting	24,108
Pumps	22,269
(DHW)	24,917
Cooling	2,861
Interior Equipment	2,778
Fans	230.64
Total	

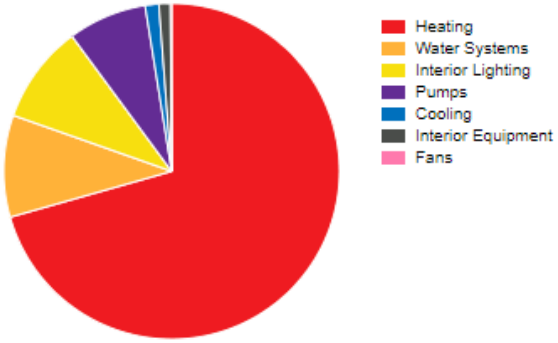

Figure 81. Annual energy consumption by end use for the case-study building

The modeled annual energy consumption totals 254,186 kWh, with a clear predominance of natural gas, which accounts for 204,364 kWh (80,40%) of the total. Electricity consumption amounts to 49,822 kWh, representing 19,60% of overall energy use (see Figure 82).

Fuel	Consumption [kWh]
Electricity	52,247
Natural Gas	200,650

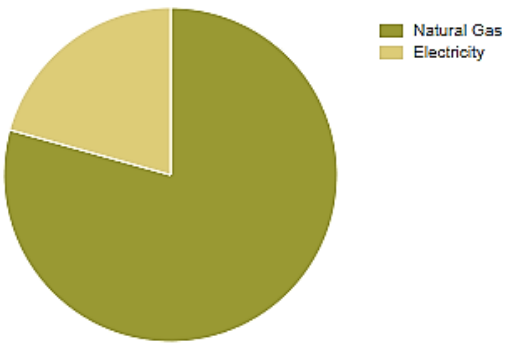

Figure 82. Annual energy consumption by end use for the case-study building

The building's annual electricity (see Figure 83) consumption of 49,636 kWh is mainly associated with interior lighting, which accounts for 47.76% of total electrical demand, followed by pumps at 38.07%. Cooling represents a limited share (7.93%), while interior equipment (5.56%) and fans (0.72%) contribute marginally to overall electricity use.

End Use	Consumption [kWh]
Interior Lighting	24,108
Pumps	22,268
Cooling	2,861
Interior Equipment	2,778
Fans	231

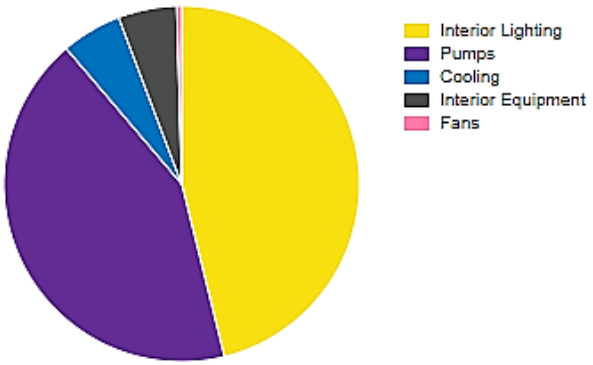

Figure 83. Annual Electricity usage by end use

Figure 84 shows the monthly electricity demand broken down by end use, highlighting a clear seasonal variation. Electricity consumption is highest during the winter months, driven mainly by pumps and interior lighting, while demand drops significantly in summer, when only lighting, minor equipment loads, and limited cooling are present. Cooling electricity use appears primarily during late spring and early autumn, whereas fans and interior equipment remain negligible throughout the year. While Figure 85 shows the monthly natural gas consumption, the results indicate a strong seasonal pattern dominated by space heating, with peak demand occurring in the winter months and negligible heating use during summer, when gas consumption is almost exclusively associated with domestic hot water.

Category	Jan	Feb	Mar	Apr	May	Jun	Jul	Aug	Sep	Oct	Nov	Dec	Total
Cooling					653.96	1,010.71	171.71	108.48	568.93	347.56			2,861.34
Interior Lighting	2,518.87	2,651.44	2,784.00	2,916.58	2,916.58	1,279.55	165.60	151.20	1,036.00	3,049.17	2,651.44	1,988.58	24,109.01
Interior Equipment	296.40	312.00	327.60	343.20	343.20	140.40			109.20	358.80	312.00	234.00	2,776.80
Fans					53.49	82.3	16.62	8.68	45.09	27.46			230.64
Pumps	4,222.64	4,455.19	4,312.94	1,528.86	5.20	4.96	5.43	4.96	5.20	5.43	4,462.08	3,256.47	22,269.36
Total	7,037.91	7,418.63	7,424.54	4,788.64	3,972.43	2,517.92	356.36	273.32	1,764.41	3,788.42	7,425.52	5,479.05	52,247.15

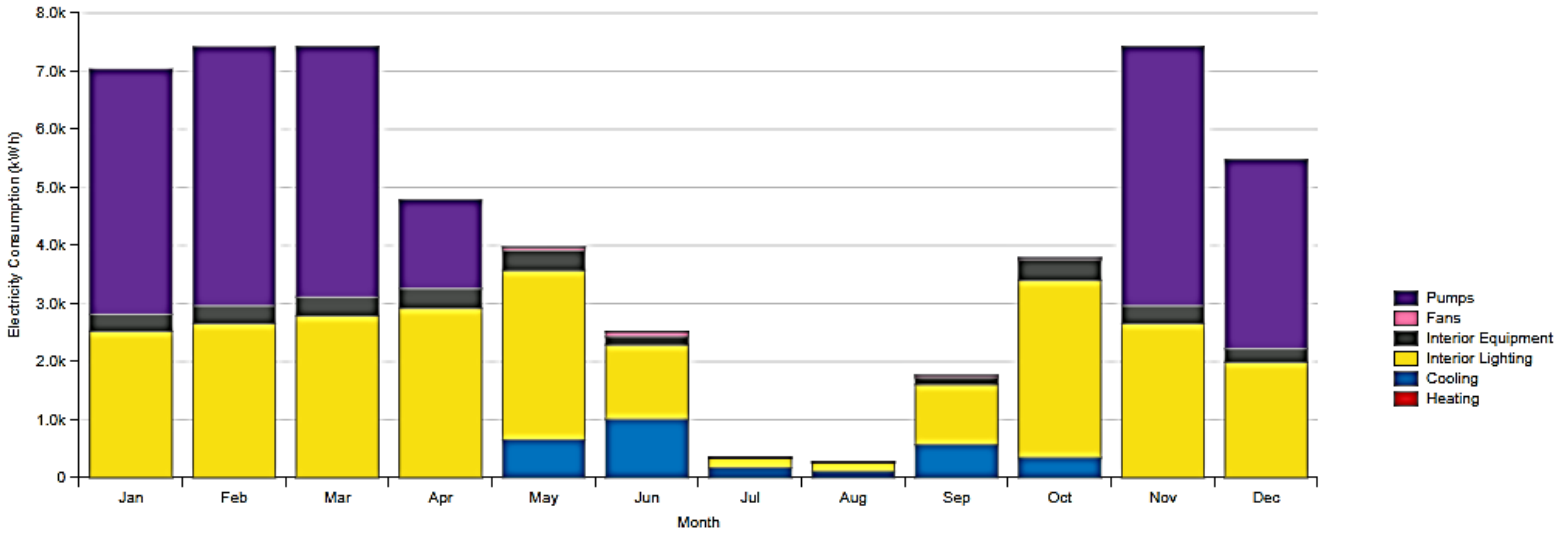

Figure 84. The monthly electricity demand [kWh] broken down by end use

Category	Jan	Feb	Mar	Apr	May	Jun	Jul	Aug	Sep	Oct	Nov	Dec	Total
Heating	38,238.61	36,570.00	33,812.50	9,902.44							32,233.06	24,975.42	175,732.03
Water Systems	2,272.49	2,363.66	2,492.89	2,594.97	2603.59	1,704.4	1,214.97	1,127.05	1,619.51	2,711.13	2,377.24	1,835.76	2,4917.67
Total	**40,511.10**	**38,933.66**	**36,305.39**	**12,497.42**	**2,603.59**	**1,704.4**	**1,214.97**	**1,127.05**	**1,619.51**	**2,711.13**	**34,610.30**	**26,811.18**	**200,649.69**

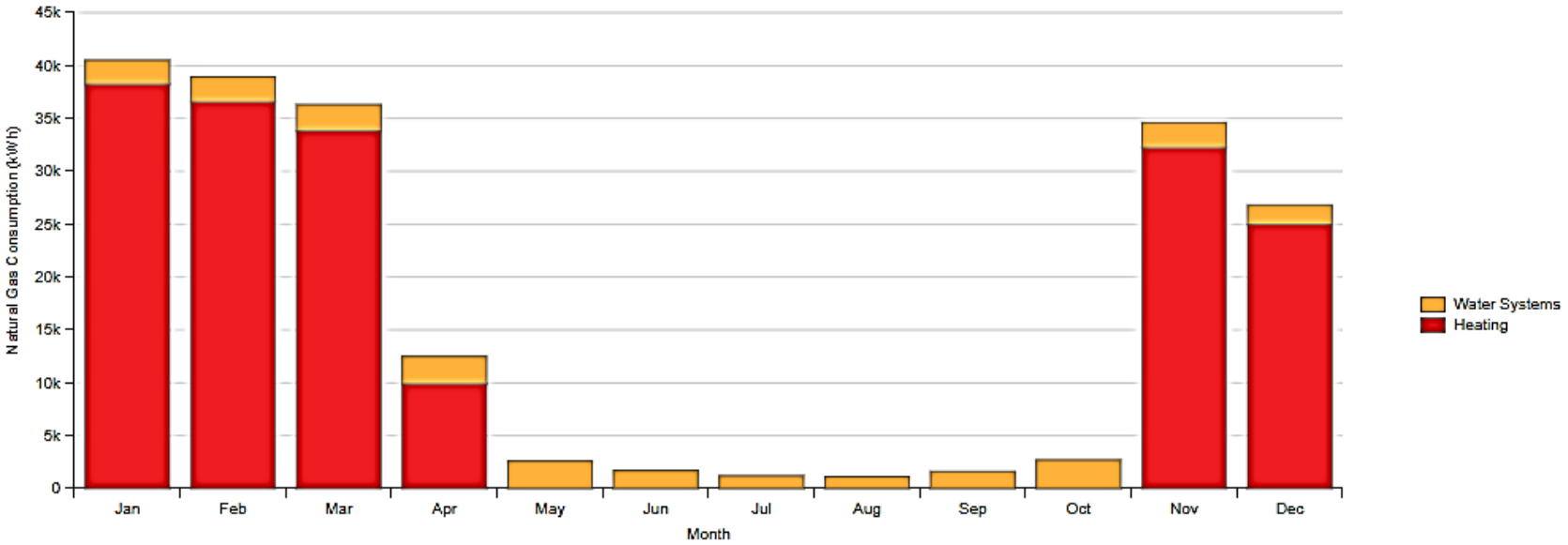

Figure 85. Monthly natural gas consumption [kWh broken down by end use

Figure 86 illustrates the relationship between heating and cooling demand and the average outdoor air dry-bulb temperature, highlighting a strong seasonal dependence. Heating demand increases significantly as outdoor temperatures decrease, with peak values observed during the winter months, whereas cooling demand remains limited overall. During July and August, cooling energy use is minimal and is mainly attributable to the gym areas, which remain operational in these months, while cooling requirements in the remaining spaces are 0.

Metric	Jan	Feb	Mar	Apr	May	Jun	Jul	Aug	Sep	Oct	Nov	Dec
Average Outdoor Air-Dry Bulb [°C]	7.4	8.0	10.5	13.8	17.4	20.2	23.6	23.0	20.8	17.0	11.3	9.2
Cooling Load [kWh]	0.00	0.00	0.00	0.00	653.96	1010.71	171.71	108.48	568.93	347.56	0.00	0.00
Heating Load [kWh]	38,238.61	36,570.00	3,3812.50	9,902.44	0.00	0.00	0.00	0.00	0.00	0.00	32,233.06	24,975.42

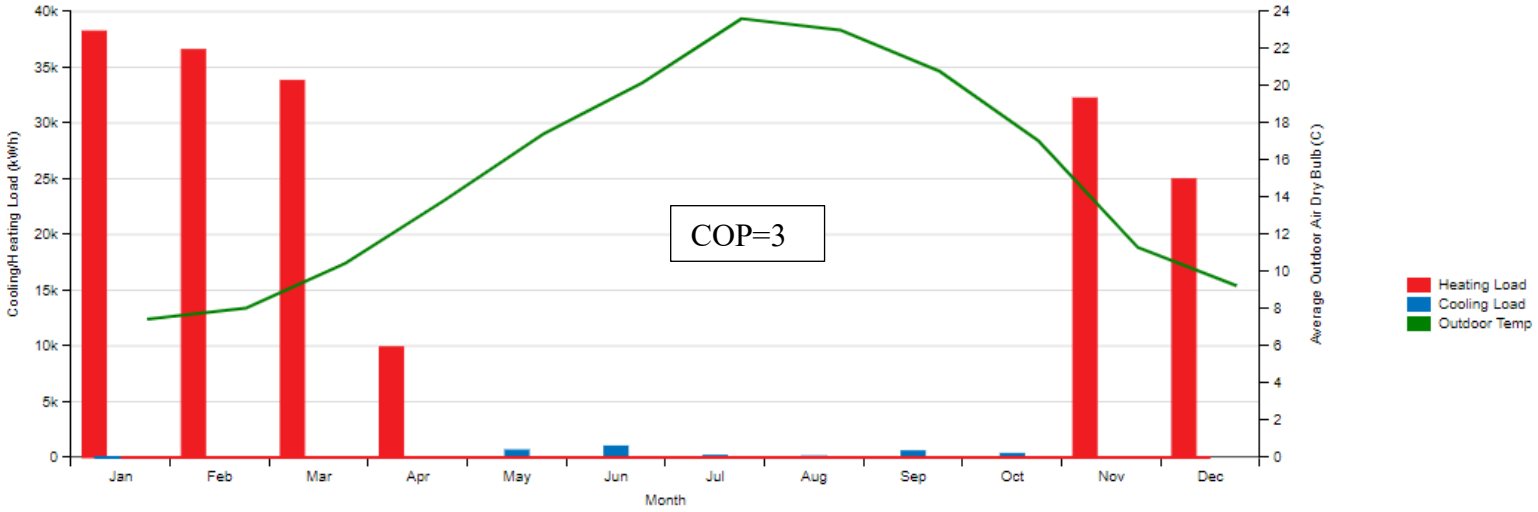

Figure 86. Relationship between heating and cooling demand and the average outdoor air dry-bulb temperature

Instead Figure 87 represents the heating and cooling demand on a different cooling scale to highlight the cooling demand more clearly.

Months	OS_QH,nd (kWh)	OS_QC,nd (kWh)
Jan	38,238.61	
Feb	36,570.00	
Mar	33,812.50	
Apr	9,902.44	
May		653.96
Jun		1,010.71
Jul		171.71
Aug		108.48
Sep		568.93
Oct		347.56
Nov	32,233.06	
Dec	24,975.42	

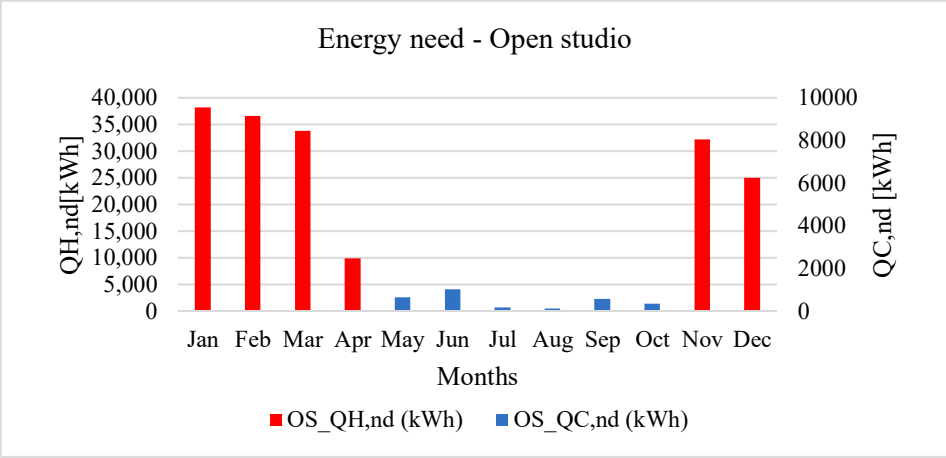

Figure 87. Heating and cooling demand (on a different scale)

The results shown in Figure 88 illustrate the heating and cooling demand for a cooling plant with COP = 1, which will subsequently be compared with the energy needs derived from another simulation software for the same reference building. The Figure 89 additionally displays the representative daily consumption profiles for each month. Consistently with the previously discussed results, Figure 90 shows the daily electricity demand broken down by different end uses over the year. The seasonal trend is mainly driven by the operation of the circulation pumps, whose consumption is higher during the winter months due to the increased heating demand and lower during the summer period. Transitional periods in spring and autumn show intermediate peaks, reflecting the intermittent overlap between heating and cooling requirements, whereas the contribution of constant electricity end uses remains relatively stable throughout the year. During some days between mid-June and the end of August, a very low or negligible cooling demand is observed due to a temporary decrease in outdoor temperature, as shown in the detail of the Figure 90.

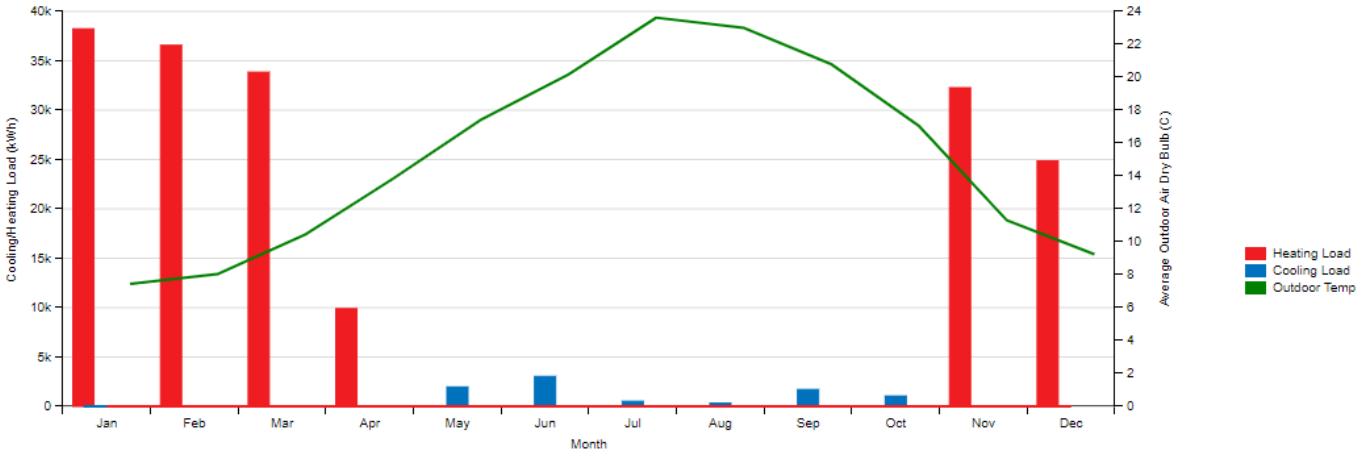

Months	OS_QH,nd (kWh)	OS_QC,nd (kWh)	Average Outdoor Air Dry Bulb (°C)
Jan	38,238.61		7.4
Feb	36,570.00		8.0
Mar	33,812.50		10.5
Apr	9,902.44		13.8
May		1,961.89	17.4
Jun		3,032.11	20.2
Jul		515.14	23.6
Aug		325.44	23.0
Sep		1,706.77	20.8
Oct		1,042.68	17
Nov	32,233.06		11.3
Dec	24,975.42		9.2

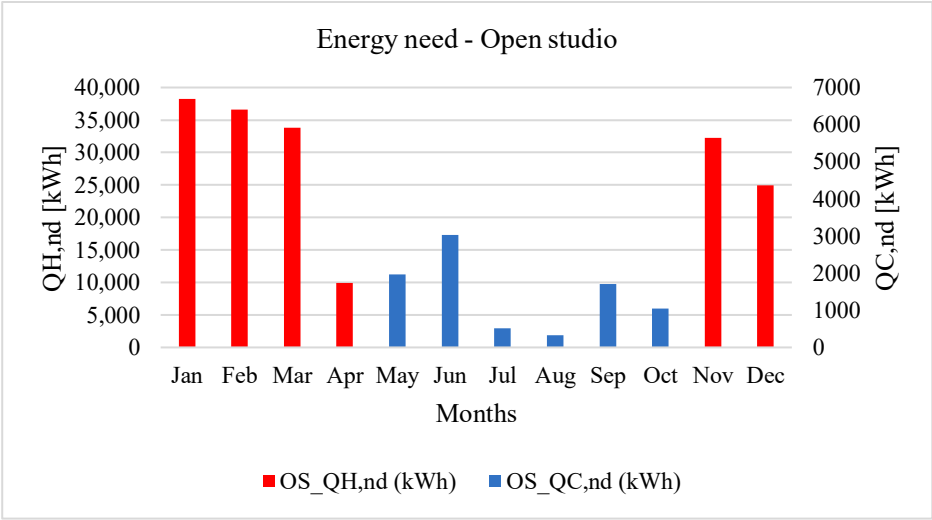

Figure 88. Relationship between heating and cooling demand and the average outdoor air dry-bulb temperature

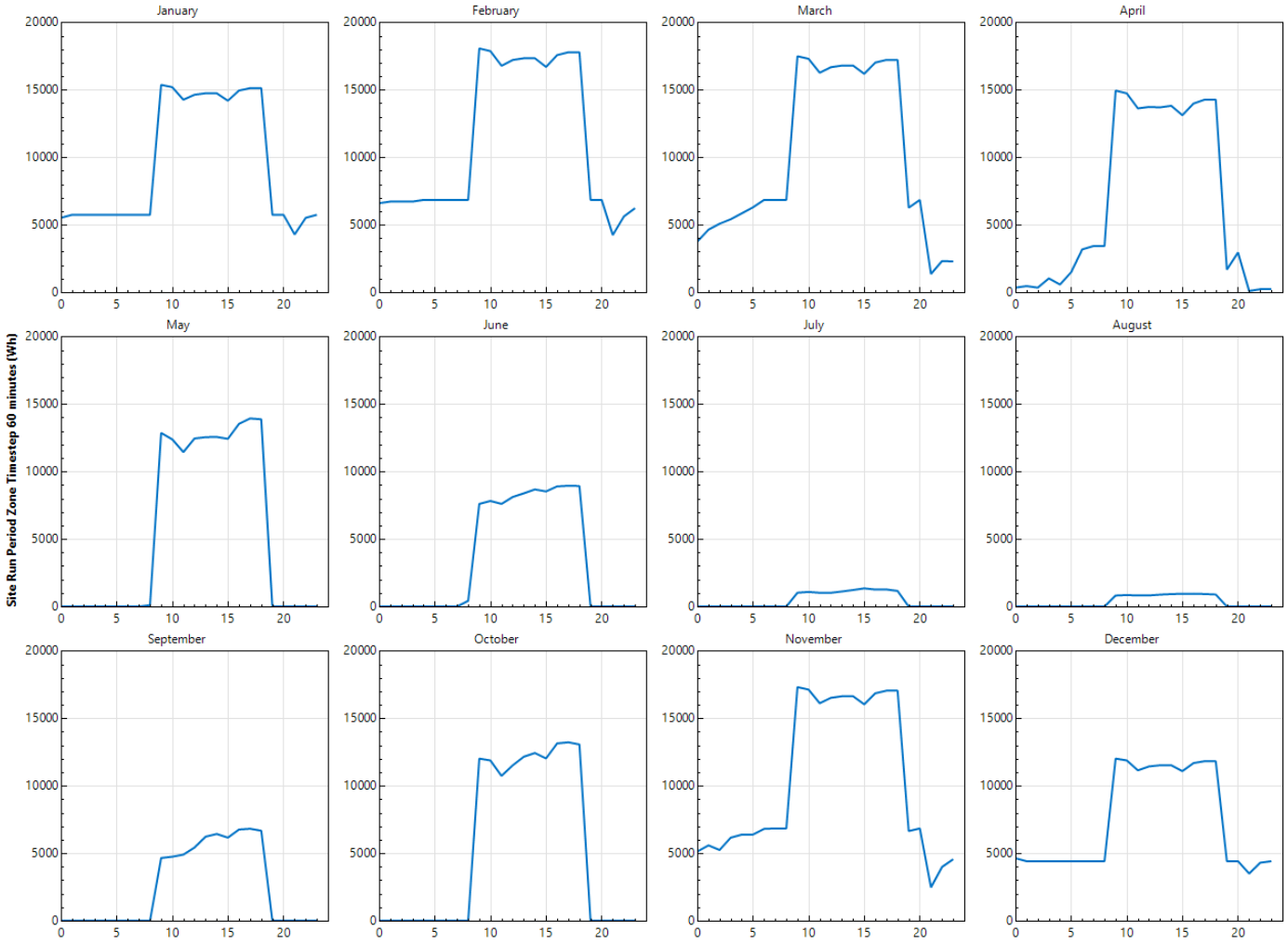

Figure 89. Representative daily energy need profile in kWh for each month

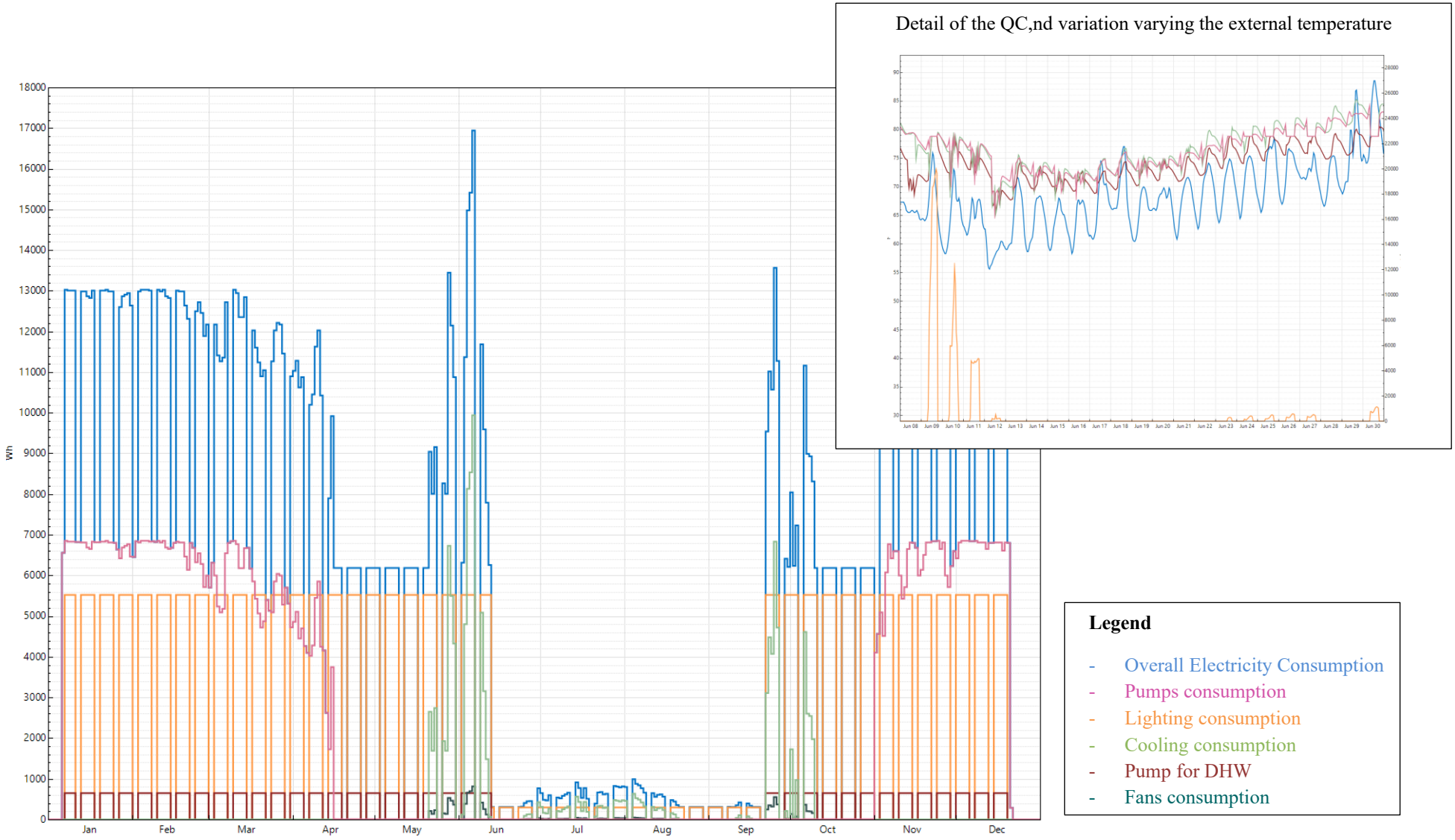

Figure 90. Daily Electric Energy need [Wh] broken for different end uses

3.2.5 Energy building model: Termo v.6.5 software

The calculation of the energy needs for heating and cooling is carried out using licensed technical software Termo v.6.5 [168], compliant with the current Italian regulatory framework. The software is updated in accordance with the DM 26/06/2015 (Minimum Energy Performance Requirements) and the latest national guidelines, and it computes the global energy performance index (EP_{gl}) following the UNI/TS 11300 series. In particular, the calculation procedures comply with UNI/TS 11300 Parts 1–4 [162], [169], [170], [171], covering energy needs, system efficiencies, summer air conditioning, and the contribution of renewable energy sources. This modelling setup was specifically adopted to allow a direct comparison between the results obtained from the open-source simulation tool and those provided by a licensed, regulation-compliant software for the same reference building.

Thermal losses and system performance are evaluated consistently with the updated Minimum Energy Performance Requirements (D.M. 28/10/2025) [167], including the mandatory consideration of thermal bridges. The TERMO software interfaces with Clima Impianti for the sizing of heat emission and distribution systems, such as radiators, convectors, fan coils, and radiant panels.

Certified by the CTI, the software enables the assessment of the energy performance of residential and non-residential buildings, accounting for all regulated energy services, including heating, cooling, domestic hot water, ventilation, lighting, and transport systems.

A comprehensive presentation of the methodology and input data definition is reported in the scientific paper by D. Borelli et al. [172], to which the author of this work contributed as a co-author.

Results

After completing the building modelling phase (see Figure 91 and Figure 92), the reference geometry and zoning of the case-study building were defined. In particular, the ground floor layout and the finalized three-dimensional geometry used for the simulations are illustrated in the aforementioned figures.

The monthly heating and cooling energy needs calculated with the licensed software are summarized in Figure 93. The results show a pronounced heating demand during the winter months (January, February, March, November, and December), while cooling needs are mainly concentrated in the summer period, with a peak in July and significant values also in June and August.

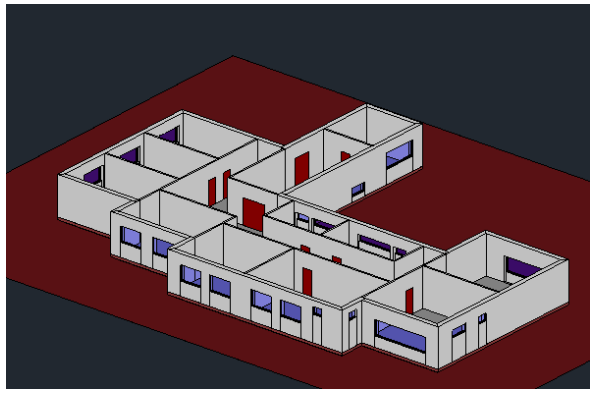

Figure 91. Ground floor plan

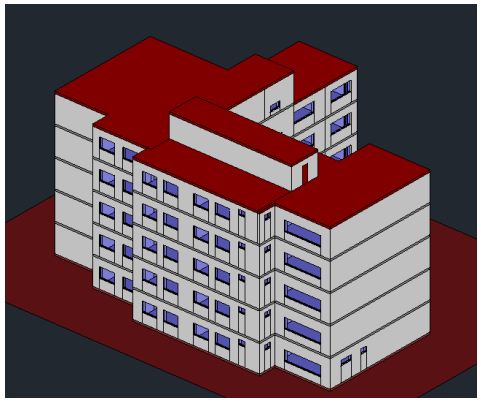

Figure 92. Completed building geometry

Months	QH,nd [kWh]	QC,nd [kWh]
January	37,856.70	
February	34,444.70	
March	31,576.70	
April	12,275.60	
May		55.70
June		332.90
July		895.10
August		321.70
September		56.90
October		
November	29,841.20	
December	29,175.40	

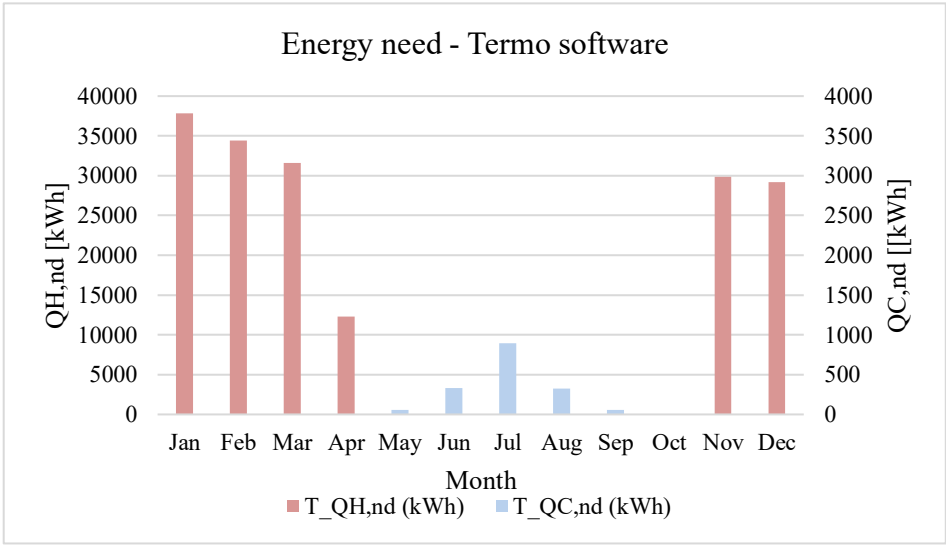

Figure 93. The monthly energy needs

Comparison: OpenStudio versus Termo Software

As we can see from the Figure 94, there are differences in the energy need for heating and cooling obtained from OpenStudio (OS) software and Termo software (T).

Months	T_QH,nd (kWh)	T_QC,nd (kWh)	OS_QH,nd (kWh)	OS_QC,nd (kWh)
Jan	37,856.70		38,238.61	
Feb	34,444.70		36,570.00	
Mar	31,576.70		33,812.50	
Apr	12,275.60		9,902.44	
May		55.70		1,961.89
Jun		332.90		3,032.11
Jul		895.10		515.14
Aug		321.70		325.44
Sep		56.90		1,706.77
Oct				1,042.68
Nov	29,841.20		32,233.06	
Dec	29,175.40		24,975.42	

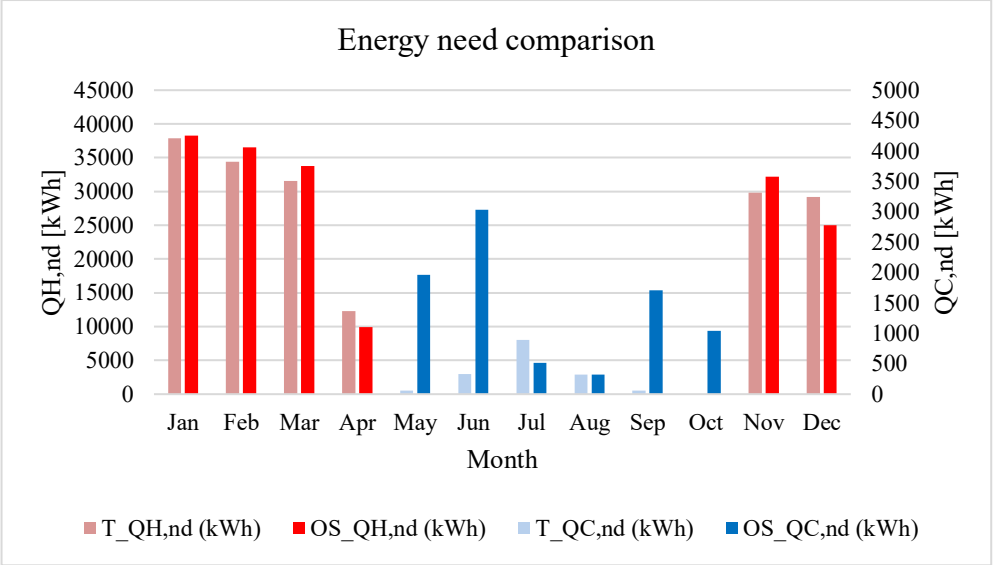

Figure 94. Monthly energy need comparison, OpenStudio vs Termo software

Figure 94 compares monthly heating (red) and cooling (blue) demand obtained with the two calculation approaches, where the lighter bars represent the results from Termo software and the solid bars those from OpenStudio. While both methods show similar seasonal patterns, OpenStudio predicts more pronounced peaks, higher heating demand in winter and higher cooling demand in the summer months, whereas Termo provides smoother and generally lower values, indicating a more averaged representation of the building's thermal behaviour over the year.

The reasons behind these incompatibilities are:

- Ventilation modelling

OpenStudio software: accounts for air infiltration through the building envelope, but it does not explicitly model natural ventilation as defined by UNI/TS 11300-1. To partially overcome this limitation, a dedicated plugin was adopted. Nevertheless, this approach does not allow ventilation rates to be differentiated according to the area or use of individual spaces. Instead, ventilation is estimated using a single value based on the percentage of window opening, combined with a control schedule dependent on internal and external temperature thresholds and wind speed limits.

Termo (UNI/TS 11300-1): For buildings where only natural ventilation is provided, the average effective ventilation airflow rate coincides with the ventilation airflow rate under reference conditions, calculated using the equation below:

$$\dot{q}_{ve,k,m} = \dot{q}_{ve,0,k} \cdot f_{ve,k} \tag{31}$$

where:

$\dot{q}_{ve,0,k}$ is the minimum design outdoor air flow rate, expressed in m³/s;

$f_{ve,k}$ is a correction factor accounting for the operating time and airflow rate. This factor includes the effects of air infiltration which, although not generated by intentional aeration, contributes to the overall ventilation. The values of $f_{ve,k}$ are reported in Table E.2 as a function of the building use category. For use categories other than residential buildings and industrial or artisanal buildings, the minimum design outdoor air flow rate $\dot{q}_{ve,0}$ is calculated according to Equation 32.

In particular, the minimum design outdoor air flow rate $\dot{q}_{ve,0}$, determined according to the building use category, is used as an input parameter and calculated using the following equation:

$$\dot{q}_{ve,0} = \sum_{k} n_{per,k} \cdot \dot{q}_{ve,0,p,k} + \sum_{k} A_k \cdot \dot{q}_{ve,0,s,k} \cdot \frac{C_8}{\varepsilon_{ve,c}} \cdot (C_1 \cdot C_2) \tag{32}$$

where:

$\dot{q}_{ve,0,p,k}$ is the specific outdoor air flow rate per person in sub-zone k (m³/s), as defined in UNI 10339 [173];
$\dot{q}_{ve,0,s,k}$ is the specific outdoor air flow rate per unit of ventilated floor area in sub-zone k (m³/s·m²), as defined in UNI 10339;
$n_{per,k}$ is the number of occupants in sub-zone k;
$n_{s,k}$ is the conventional occupancy density per unit floor area (m⁻²), referring to design conditions;

A_k is the usable floor area of sub-zone k served by the ventilation system (m²);
$\varepsilon_{ve,c}$ is the conventional efficiency of the ventilation system (assumed equal to 0.8 in the absence of specific data);
C_1 is the correction coefficient for mixed systems (conventionally assumed equal to 1);
C_2 is the correction coefficient as a function of altitude, as specified in UNI 10339.

- Thermal bridges.

OpenStudio: Thermal bridges are excluded entirely from the building energy demand in the OpenStudio model. This represents a significant simplification, as thermal bridges are explicitly addressed and mandatory by DM 26/06/2015 'The Minimum Requirements Decree 2015' in force from 1 October 2015 to 2 June 2015 [174] and after will be substituted by (D.M. 28/10/2025) [167].

Termo software: In this software the thermal bridges are considered accurately.
Thermal Bridges is the new Termo module for the numerical calculation of thermal bridges using the Finite Element Model (FEM) (see Figure 95) and for assessing the risk of mould growth, in compliance with UNI EN ISO 10211 [166] and UNI EN ISO 13788 [175].

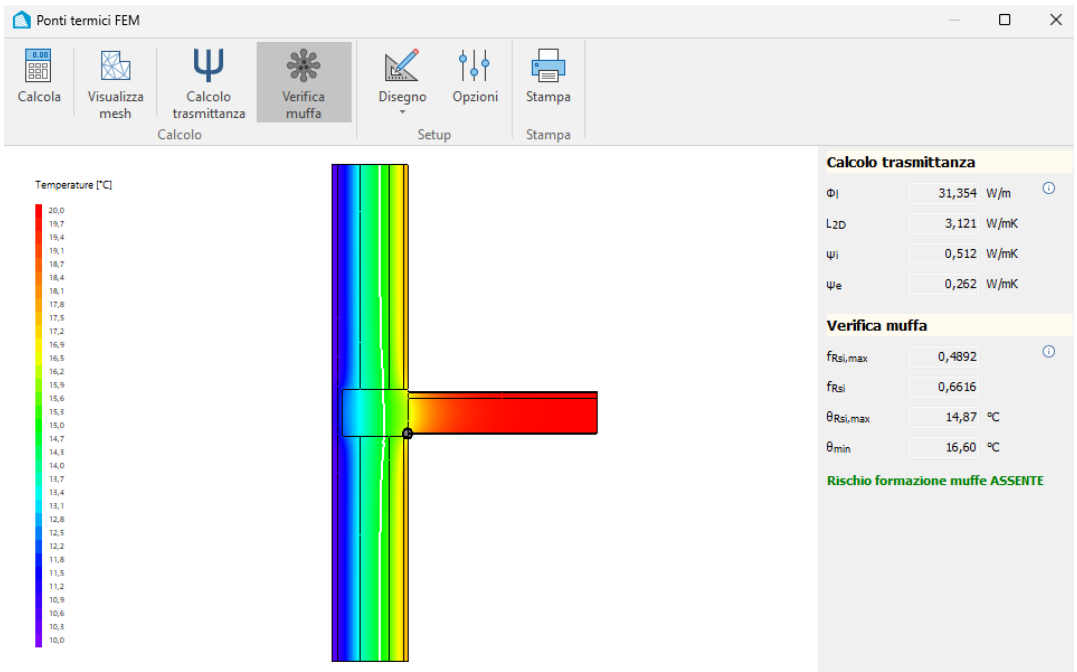

Figure 95. Example of a thermal bridge simulated by FEM methodology

- Calculation of the energy need for cooling

OpenStudio: the methodology implemented in OpenStudio is fully dynamic: the heat balance is solved at each timestep using hourly weather data, and indoor temperature evolves continuously as a function of instantaneous gains, losses and thermal mass.

Cooling demand is therefore generated only when the simulated indoor temperature exceeds the setpoint, without relying on predefined utilization factors or monthly averaging.

Termo software: Evaluate the cooling need on bases:

For each thermal zone, the start and end of the actual cooling period are determined in accordance with method b described in Section 7.4.1.2 of UNI EN ISO 13790:2008 [176]. The cooling season is identified as the set of days for which the dimensionless ratio between heat losses and heat gains in cooling mode, $1/\gamma_C$ reaches its limiting value:

$$\left(\frac{1}{\gamma_{C,\text{day}}}\right) = \left(\frac{1}{\gamma_C}\right)_{\text{lim}} = \frac{A_C + 1}{A_C} \tag{33}$$

where A_C is a dimensionless parameter depending on the thermal time constant of the thermal zone.

The cooling season is extended to all days for which:

$$\frac{1}{\gamma_{C,\text{day}}} < \left(\frac{1}{\gamma_C}\right)_{\text{lim}} \tag{34}$$

If this condition is satisfied for all months of the year, the cooling season is assumed to extend over the entire year.

So, Termo software defines the cooling energy need through a quasi-steady monthly balance between heat gains and losses, where gains (solar and internal) are partially utilized according to a utilization factor that accounts in a simplified way for the building's thermal inertia, and the indoor temperature is assumed to be maintained at the cooling setpoint.

The comparison between OpenStudio and Termo results (Figure 94) highlights systematic discrepancies in energy demand estimates, despite consistent input data, due to differences in the physical modelling approaches.

In OpenStudio, ventilation is dynamically driven by window opening and boundary conditions, resulting in time-varying and partially uncontrolled airflow rates, which increase heat losses in winter and introduce additional heat gains in summer. In contrast, Termo adopts a quasi-steady ventilation model based on UNI/TS 11300, with airflow rates defined by occupancy and space typology. OpenStudio also uses hourly schedules for internal and solar gains, while Termo relies on simplified temporal profiles. Furthermore, thermal bridges are explicitly accounted for in Termo but neglected in OpenStudio, affecting transmission losses. In addition, the temperature control tolerance

is narrower in OpenStudio (±0.2 °C) than in Termo (±0.5–1 °C), leading to longer system operation times.

These combined effects influence both heating and cooling, but are significantly amplified in summer conditions, where dynamic ventilation and time-resolved gains result in substantially higher cooling demand in OpenStudio. The observed differences are therefore consistent with the underlying modelling assumptions.

OpenStudio results are adopted for subsequent analyses, as they enable a hourly representation of energy demand, which is essential for evaluating PV performance, self-consumption, and REC configurations.

3.2.6 PV plant dimensioning and definition of the energy balance

Methodology for Grid-Connected Photovoltaic System

The photovoltaic system considered in this work is modeled as a grid-connected installation using PVsyst software, which performs a time-resolved simulation of PV electricity generation based on physical models and system-specific parameters. The simulation is conducted with an hourly time step to capture the variability of both solar irradiance and system performance.

The PVsyst simulation methodology begins with the definition of the site location and associated meteorological dataset, including global horizontal irradiance and ambient temperature. These data are transposed to the plane of array to determine the effective irradiance $G_{POA}(t)$ incident on the PV modules as a function of time.

The DC power output of the PV generator is calculated as:

$$P_{DC}(t) = G_{POA}(t) \cdot A_{PV} \cdot \eta_{mod}(G_{POA}(t), T_c(t)) \quad (34)$$

where $A_{PV}$is the total active module area and $\eta_{mod}$is the module efficiency, which depends on irradiance level and cell temperature $T_c(t)$. The cell temperature is estimated using a thermal model accounting for ambient temperature and operating conditions.

System losses, including optical losses, shading losses, electrical mismatch, and DC wiring losses, are applied sequentially to obtain the net DC energy delivered to the inverter. The AC power injected into the grid is then determined through the inverter efficiency model:

$$P_{AC}(t) = P_{DC}(t) \cdot \eta_{inv}(P_{DC}(t)) \quad (35)$$

where η_{inv} represents the inverter efficiency as a function of operating power and voltage.

The resulting hourly AC energy production $E_{PV}(t)$ constitutes the final output of the grid-connected PV simulation.

Energy Balance Between PV Production and Building Demand

The energy balance analysis is performed by comparing the simulated PV electricity production with the electrical demand of the building. The building load is represented by an hourly demand profile $E_{load}(t)$, derived from measured data or detailed building energy modeling.

At each time step, the energy balance is expressed as:

$$E_{bal}(t) = E_{PV}(t) - E_{load}(t) \tag{36}$$

When $E_{bal}(t) > 0$, the PV generation exceeds the building demand and the surplus energy is exported to the grid. Conversely, when $E_{bal}(t) < 0$, the energy deficit is supplied by grid imports.

The self-consumed PV energy is defined as:

$$E_{self}(t) = \min\left[E_{PV}(t),\, E_{load}(t)\right] \tag{37}$$

From this formulation, key performance indicators are derived over the evaluation period T:

- **Self-consumption ratio**:

$$SCR = \frac{\sum_{t\in T} E_{self}\,(t)}{\sum_{t\in T} E_{PV}\,(t)} \tag{38}$$

- **Demand coverage ratio**:

$$DCR = \frac{\sum_{t\in T} E_{self}\,(t)}{\sum_{t\in T} E_{load}\,(t)} \tag{39}$$

These indicators quantify the degree to which PV generation is utilized on-site and the extent to which the building's electrical demand is met by the PV system.

This methodology establishes a consistent and time-resolved framework for evaluating grid-connected photovoltaic systems in the context of building energy demand, enabling rigorous assessment of system sizing, load matching, and the contribution of PV generation to overall building energy performance.

PV plant dimensioning

The dimensioning of a grid-connected photovoltaic power plant is carried out through a structured and sequential methodology aimed at ensuring technical feasibility, performance optimization, and reliable energy yield estimation. The process begins with the characterization of the installation site, including geographical location, climatic conditions, and solar resource availability. Based on this information, the main design parameters of the PV system are defined, encompassing system topology, orientation, installed capacity, and component selection.

The orientation of the photovoltaic system is defined by identifying the optimal tilt and azimuth angles, considering the site's geographical location and the presence of obstructions, and evaluating deviations relative to the optimal configuration in terms of incident solar energy. The orientation of the PV modules represents a critical step in the dimensioning process, as it governs the transposition of horizontal solar irradiation to the plane of the array and directly influences the incident energy available for conversion. This geometric definition forms the basis for the calculation of plane-of-array irradiance and constitutes a prerequisite for accurate modeling of PV energy production.

Figure 96 illustrates the definition of the photovoltaic array orientation within PVsyst for a grid-connected system. The PV generator is modeled as a fixed tilted plane with a tilt angle of 30° and an azimuth of −35.3°, corresponding to a deviation toward the west from due south. The base tilt angle is set to 30°, indicating installation on a flat reference surface.

The interface confirms that the defined orientation is correctly linked to the system layout, with a total module area of 114 m², corresponding to 48 PV modules, and consistency between the system definition and the 3D scene representation. The graphical elements on the right side of the figure provide a schematic visualization of the module plane relative to the cardinal directions, facilitating verification of the geometric configuration.

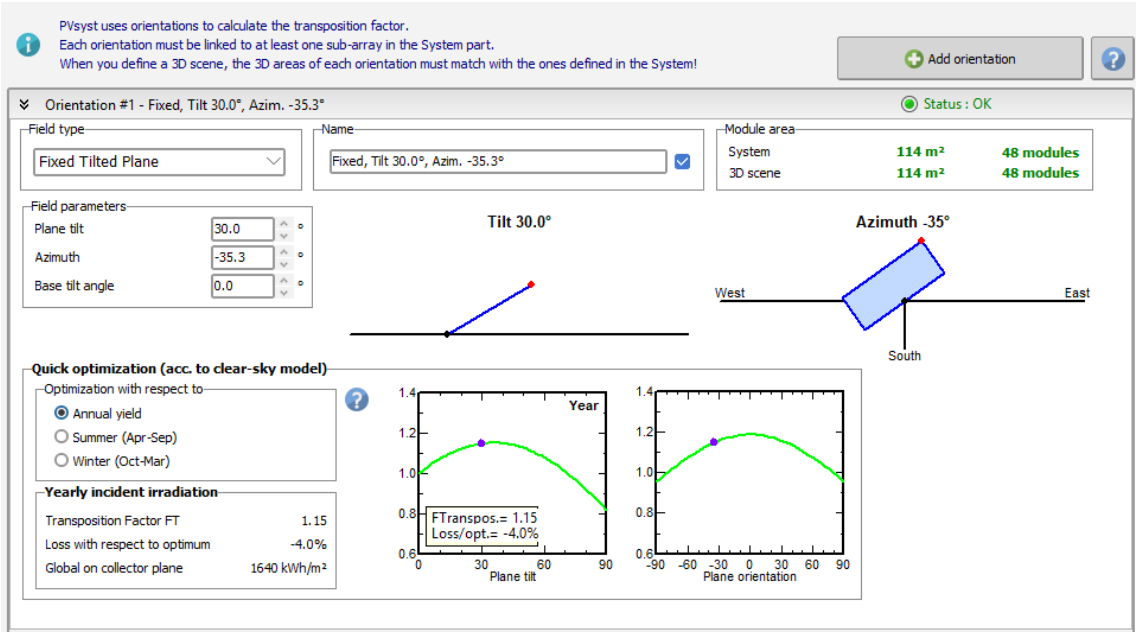

Figure 96. System configuration

The lower section of the figure presents the yearly incident irradiation analysis and the associated transposition factor (FT). For the selected orientation, a transposition factor of 1.15 is obtained, indicating that the global irradiation on the plane of array is 15% higher than the global horizontal irradiation. The deviation from the optimum orientation results in an estimated loss of 4.0% relative to the maximum achievable annual yield. The corresponding global irradiation on the collector plane is calculated as 1640 kWh/m²/year.

Additionally, the embedded plots illustrate the sensitivity of annual irradiation to variations in tilt angle and azimuth, providing a visual assessment of how the selected configuration compares to the optimal orientation under clear-sky conditions. This orientation definition serves as a key input for subsequent PV energy production simulations and directly influences the calculated plane-of-array irradiance used in the energy balance analysis.

Subsequently, the system configuration of the PV generator is established, including the choice of panels, inverter and array layout as shown in the Figure 97. It illustrates the selection of the PV module and inverter models, along with the electrical layout of the array, consisting of 48 PV modules arranged in 16 modules per string and 3 parallel strings, connected to a 30 kW AC inverter. The interface summarizes key system parameters, including installed DC power (24.0 kWp), nominal AC power (30.0 kWac), module area (114 m²), and DC/AC power ratio (0.80), while verifying operating voltage and current limits under standard and extreme conditions.

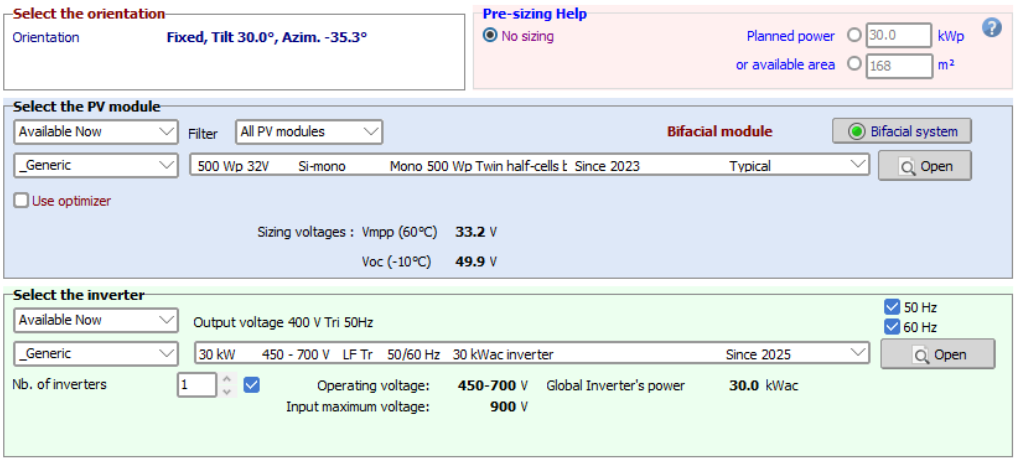

Figure 97. PV system composition

Photovoltaic System Losses

The electrical energy produced by a photovoltaic system can be expressed as the result of the available solar resource reduced by a sequence of loss mechanisms occurring at different stages of energy conversion. Losses are modeled as multiplicative derating factors applied to the theoretical energy yield and are evaluated on a time-resolved basis.

The DC energy produced by the PV array at time $t$can be written as:

$$E_{DC}(t) = E_{POA}(t) \cdot \eta_{STC} \cdot \left(\sum_{i=1}^{n} (1 - L_i(t)) \right) \tag{40}$$

where:

$E_{POA}(t)$ is the plane-of-array irradiance energy,
η_{STC} is the module efficiency at standard test conditions,
$L_i(t)$ represents the individual fractional losses applied at the DC side.

Typical DC-side losses include: Optical and incidence angle losses L_{opt}, Soiling losses L_{soil}, Thermal losses due to cell temperature L_{therm}, Shading losses L_{shad}, Module quality and degradation losses L_{qual}, Electrical mismatch losses $L_{mismatch}$ and DC wiring and diode losses L_{DC}.

Thus, the DC energy expression becomes:

$$E_{DC}(t) = E_{POA}(t) \cdot \eta_{STC}(1 - L_{opt})(1 - L_{soil})(1 - L_{therm}(t))(1 - L_{shad}(t))(1 - L_{mismatch})(1 - L_{DC}) \tag{41}$$

The AC energy delivered at the point of connection is obtained by applying inverter-related losses and system availability:

$$E_{AC}(t) = E_{DC}(t) \cdot \eta_{inv}(t) \cdot (1 - L_{AC}) \cdot (1 - L_{avail}) \quad (42)$$

where:

$\eta_{inv}(t)$ is the inverter efficiency as a function of load and voltage,
L_{AC} represents AC wiring and transformer losses,
L_{avail} accounts for system downtime and curtailment.

The total system loss over the evaluation period $T$is then defined as:

$$L_{total} = 1 - \frac{\sum_{t \in T} E_{AC}(t)}{\sum_{t \in T} E_{POA}(t) \cdot \eta_{STC}} \quad (43)$$

This formulation provides a transparent and physically consistent framework for quantifying the contribution of individual loss mechanisms to the reduction in PV system energy yield. It enables loss attribution, sensitivity analysis, and comparison of different system configurations under identical climatic conditions.

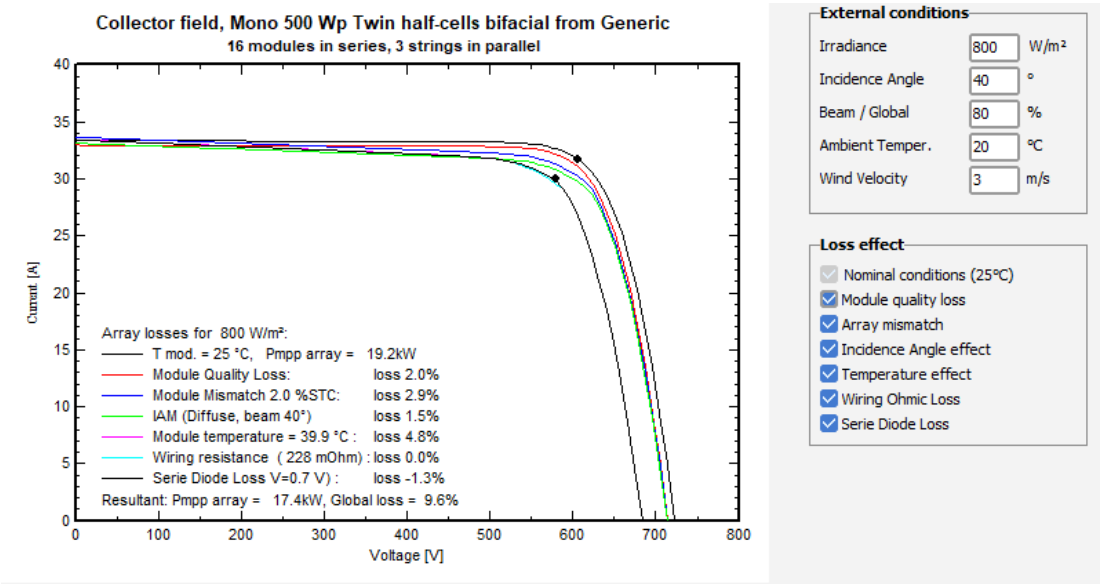

Figure 98. PV system losses configuration

Figure 98 summarizes the cumulative impact of electrical and thermal loss mechanisms on the PV array performance as modeled in PVsyst. Under an irradiance of 800 W/m² and elevated module temperature, successive losses primarily due to temperature effects, array mismatch, incidence angle, and wiring resistance, overall power loss of 9.6% relative to nominal conditions. This synthesis highlights the dominant role of operating conditions and internal electrical losses in determining the effective PV array output.

Far shading

The horizon analysis indicates that far-shading effects are limited to low solar elevation angles.

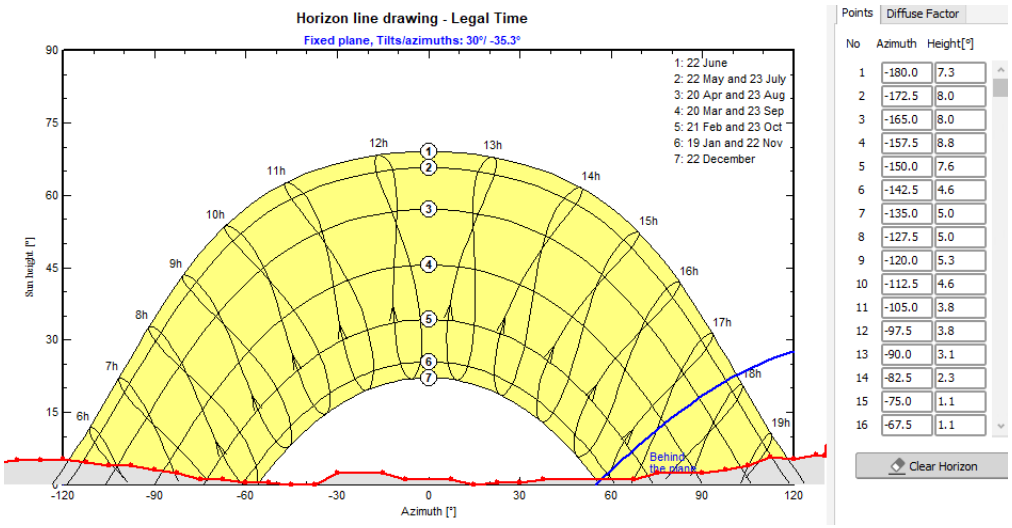

Figure 99. Horizon losses

For this specific site, as shown in Figure 99 the horizon shading is represented with the red line for different elevation angles. The diffuse factor, which is the attenuation of the diffuse irradiation part, due to the horizon shading, is 0.99. Consequently, horizon losses do not significantly influence the overall performance of the photovoltaic system.

Instead, particular attention must be paid to near-shading effects, which can have a significantly greater impact on system performance and therefore require an accurate definition of the three-dimensional shading scene.

Near shading

In order to draw the 3D scene, the SketchUp software is used, in which the terrain topography is imported, and all the 3D buildings are designed, with particular attention to the reference building, where the PV panels will be placed, and the other buildings, which can provide shading to the panels. The 3D scene in SketchUp is shown in Figure 100. PV panels have also been added to the school building roof.

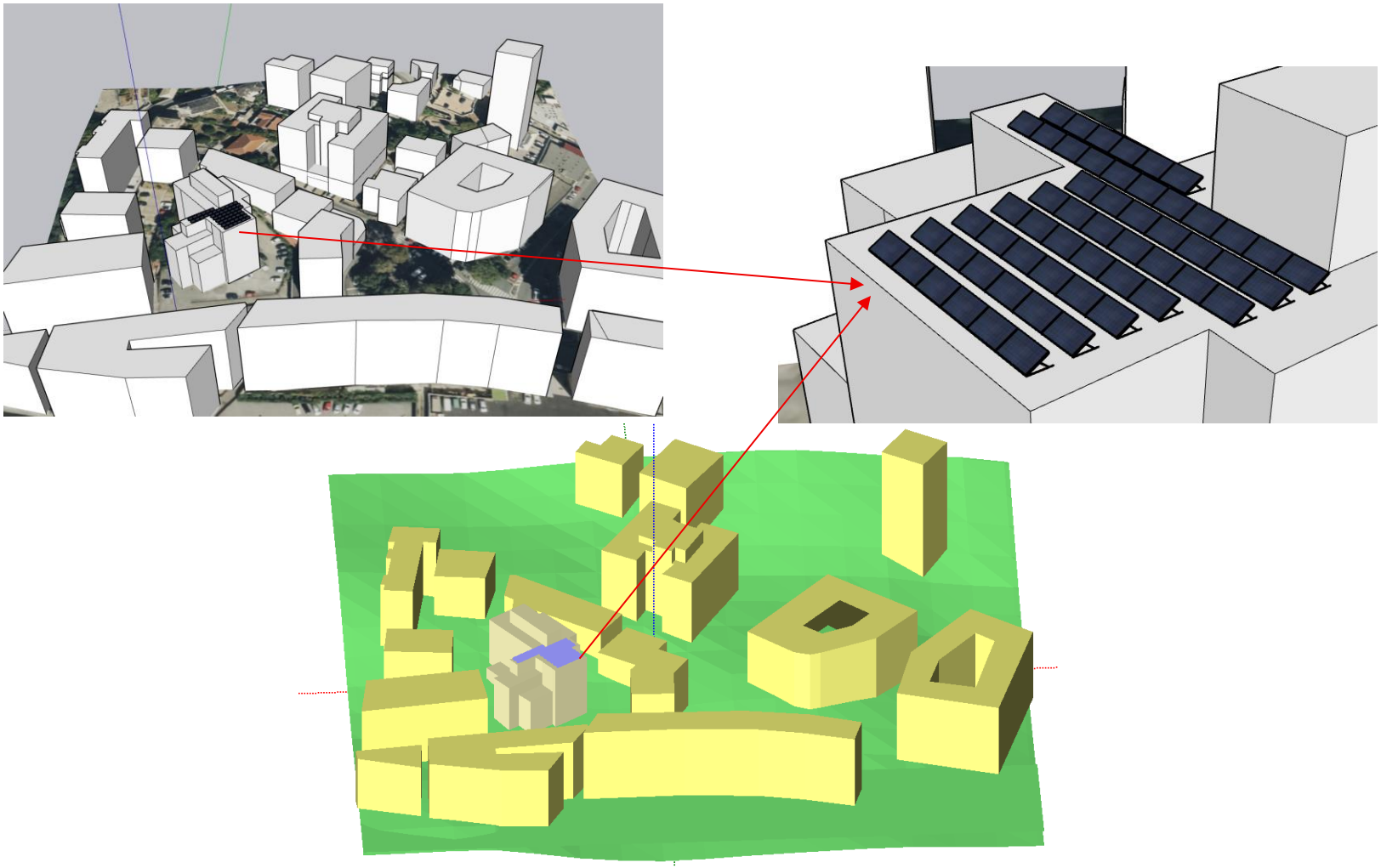

Figure 100. 3D near shading scene

The three-dimensional model developed in SketchUp is subsequently imported into PVsyst and converted into a PVsyst 3D scene. During this process, each element of the imported geometry is assigned the appropriate physical and optical properties required by PVsyst. In particular, since PVsyst represents photovoltaic modules as surfaces rather than individual panels, the PV areas must be explicitly selected and defined with the corresponding PV surface properties to enable accurate near-shading and electrical impact calculations. The same procedure is applied to surrounding shading elements, including nearby buildings and terrain features, which are defined as shading objects and assigned the appropriate geometrical properties within PVsyst. This ensures an accurate representation of near-shading effects and their impact on the incident irradiance and electrical behavior of the photovoltaic system.

In Figure 101, the shading loss is shown for a typical day and hour in the winter and summer seasons.

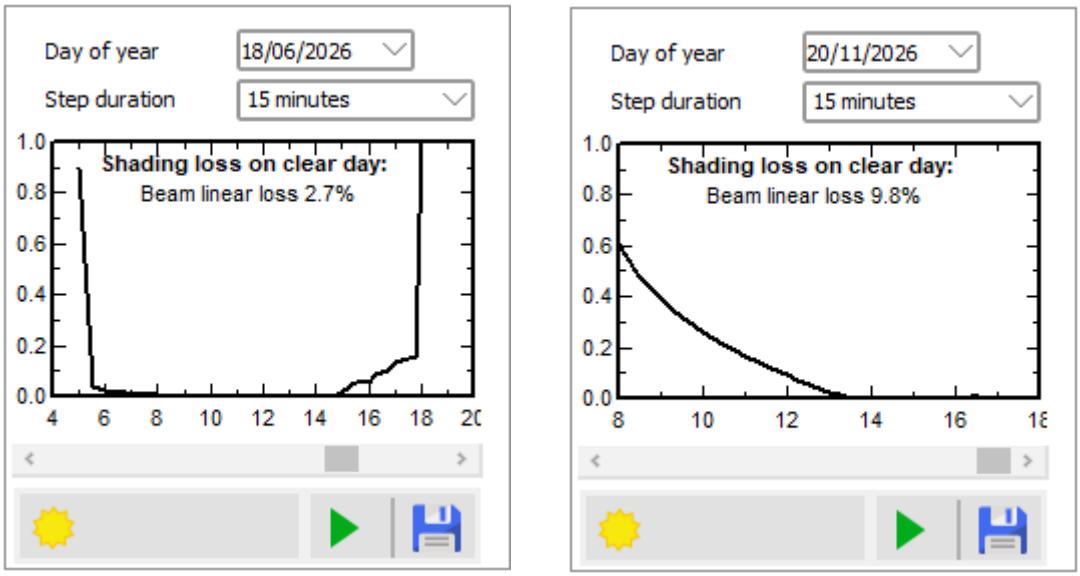

Figure 101. Shading loss factor during a) the summer and b) winter season

Instead, in Figure 102 is shown the shading provided by the interrow space during the winter and the summer seasons. During the winter season, in the afternoon, when the sun is at a lower altitude, the inter-row spacing causes increased shadowing of the panels. In contrast, during the summer season, the higher solar altitude significantly reduces shading effects.

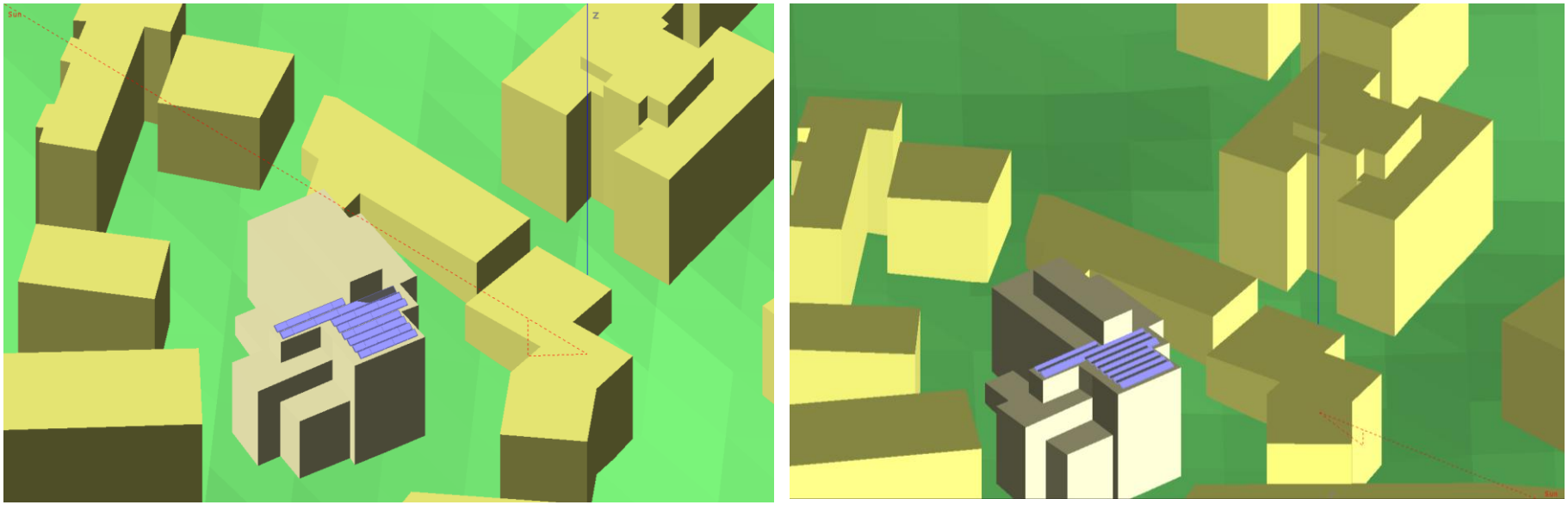

Figure 102. Shading provided by the inter-row space during a) the summer and b)winter seasons

Results

The simulated grid-connected photovoltaic system installed on the building as shown in Figure 103, produces an annual electrical energy of 26.6 MWh, corresponding to a specific yield of 1109 kWh/kWp/year. This value is consistent with a medium solar resource and reflects the combined influence of system orientation, shading conditions, and operating temperatures.

Results overview

System kind	Tables on a building	
System Production	**26.6**	MWh/yr
Specific production	**1109**	kWh/kWp/yr
Performance Ratio	**0.692**	
Normalized production	**3.04**	kWh/kWp/day
Array losses	**1.06**	kWh/kWp/day
System losses	**0.29**	kWh/kWp/day

Figure 103. Results overview

The performance ratio (PR) of 0.692 (see Figure 104) indicates that approximately 69% of the theoretically available energy at standard test conditions is effectively converted into usable AC electricity.

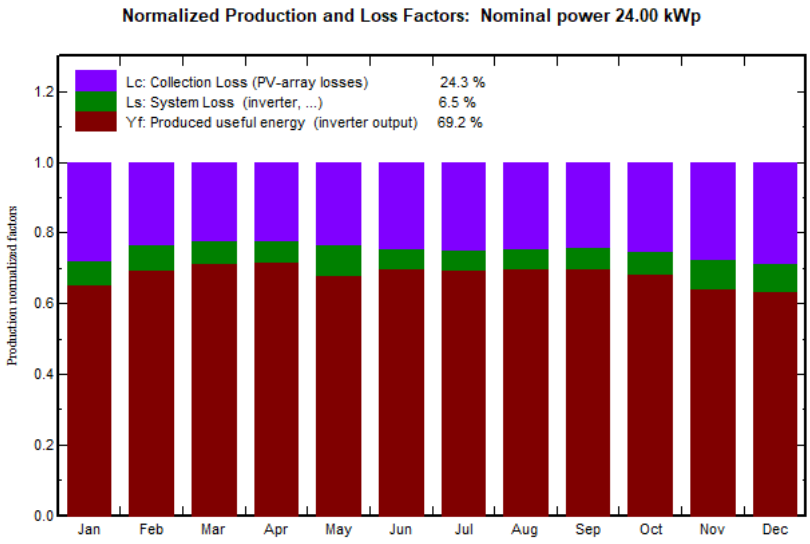

Figure 104. Monthly Performance losses

This PR value suggests the presence of moderate system losses, which are typical for building-integrated PV installations where shading, suboptimal orientation, and thermal effects are more pronounced.

The normalized production of 3.04 kWh/kWp/day confirms stable average daily performance over the year. The breakdown of normalized losses highlights that array losses (1.06 kWh/kWp/day) including temperature effects, shading, and electrical mismatch represent the dominant contribution to total losses, while system losses (0.29 kWh/kWp/day) associated with inverter conversion and AC-side components are comparatively limited.

Overall, the results indicate a technically sound system whose energy performance is primarily constrained by array-level effects rather than conversion or grid-interface inefficiencies, highlighting potential opportunities for performance improvement through

enhanced shading mitigation or thermal management. But in this configuration, the array distribution is constrained due to limited available roof space, which prevents increasing the inter-row spacing between photovoltaic panels.

Figure 105 shows the daily useful energy output of the photovoltaic system over the course of a year. A clear seasonal trend is observed, with lower daily energy production during the winter months and progressively higher values from spring to summer, reaching peak outputs between May and July. The significant day-to-day variability reflects the influence of changing meteorological conditions, such as cloud cover and solar irradiance, while the overall pattern highlights the strong dependence of photovoltaic performance on seasonal solar availability.

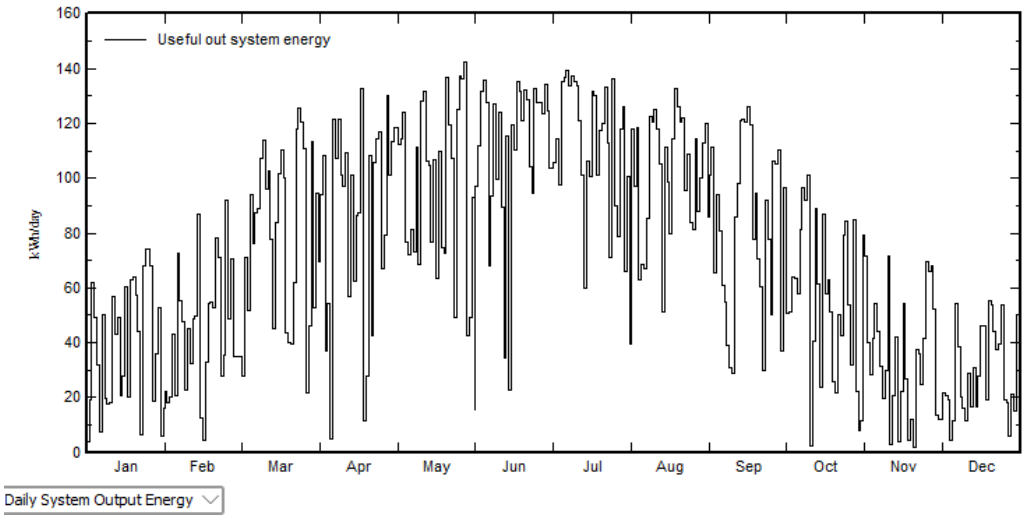

Figure 105. Daily output energy production

Self-consumption

Within PVsyst, the electrical demand can be defined using yearly, monthly, daily, or hourly consumption profiles. Since the energy modeling performed in OpenStudio provides hourly electricity consumption data, the load profile imported into PVsyst is implemented as an hourly consumption profile. This profile is used to model the interaction between the photovoltaic system and the electrical load. The hourly data csv file is imported into the software and assigned as the reference load profile, defining the electricity demand for each hour of the year. This approach enables PVsyst to perform a time-resolved energy balance by comparing photovoltaic energy generation with load consumption on an hourly basis, allowing the quantification of self-consumption, energy exported to the grid, and energy deficits. The use of hourly consumption data ensures that daily and seasonal variations in electricity demand are accurately captured in the simulation results.

Figure 106 shows the correct configuration and import of the CSV file within PVsyst, while Figure 107 presents the resulting monthly electricity consumption derived from the uploaded hourly data.

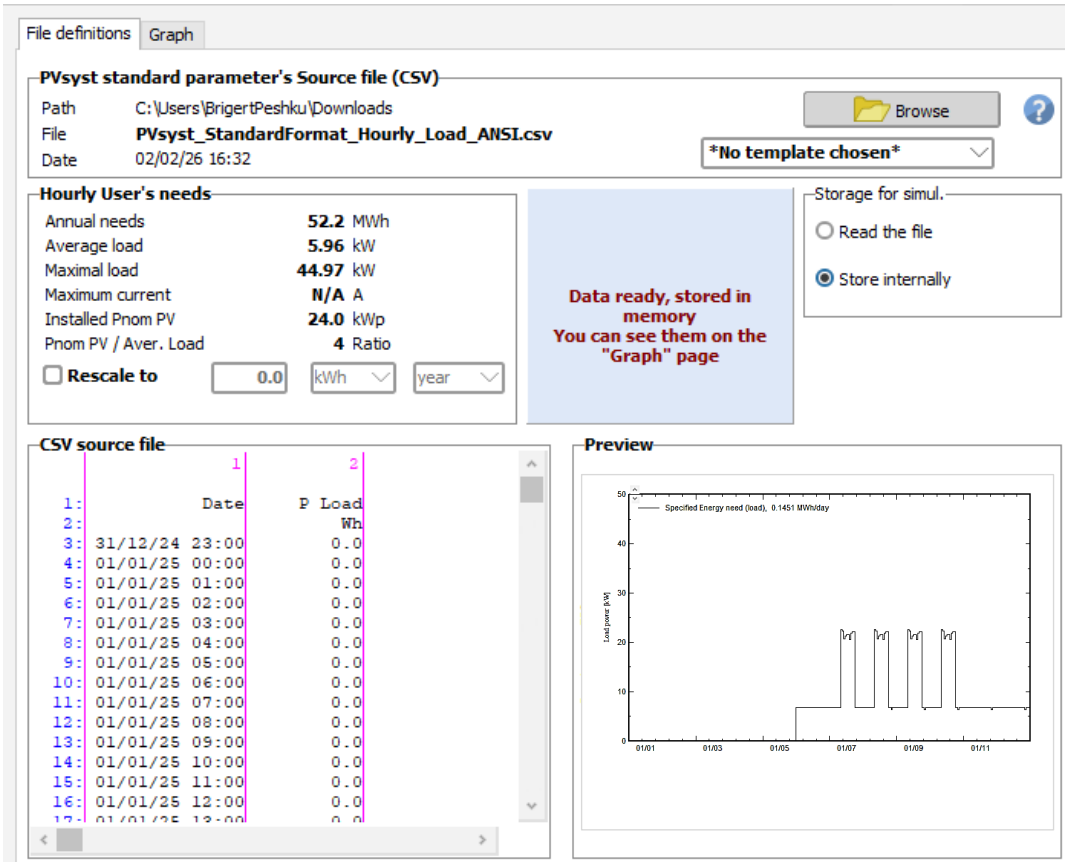

Figure 106. Hourly consumption profile configuration

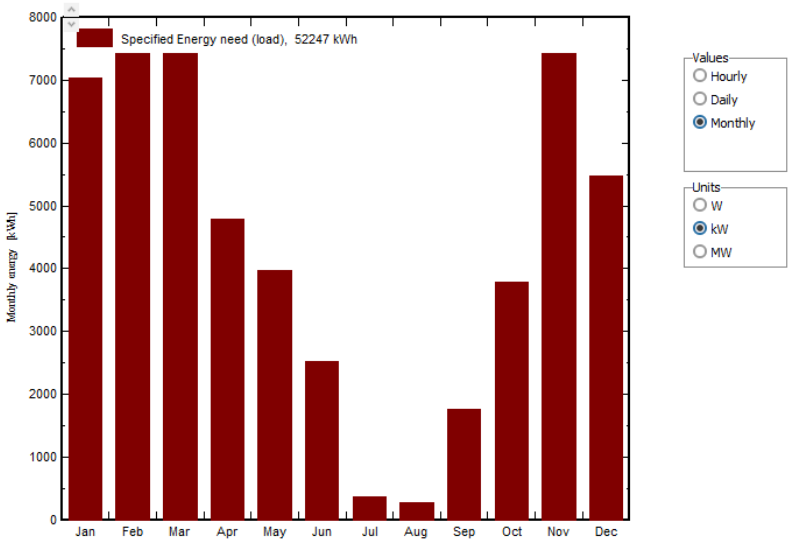

Figure 107. Monthly consumption profile configuration

Results of the energy balance

After completion of all required input data, PVsyst generates the annual loss diagram shown in Figure 108, which summarizes the overall energy balance of the photovoltaic system. The diagram illustrates the energy flow from the available solar irradiation through the various optical, thermal, electrical, and inverter-related losses, resulting in an available energy at the inverter output of 26,734 kWh per year. This value represents the net electrical energy produced by the photovoltaic system under the simulated operating conditions.

Of the total available energy, 13,304 kWh are directly self-consumed on site, while 13,290 kWh are exported to the electrical grid as surplus generation. When photovoltaic production is insufficient to satisfy the load demand, 38,943 kWh are imported from the grid. This energy balance provides a quantitative assessment of system performance, self-consumption levels, grid interaction, and the remaining dependency on grid-supplied electricity.

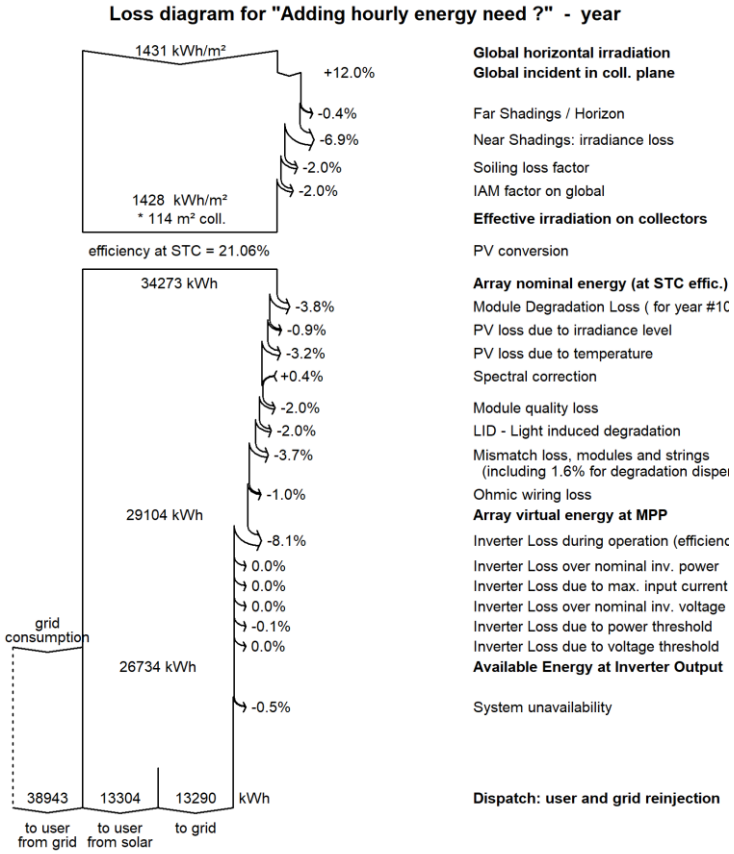

Figure 108. Loss Diagram

To better exploit the energy balance distribution, Table 23 presents the monthly values of the available energy (E_Avail), the user's electricity demand (E_User), and the amount

of energy exported to the grid (E_Grid). The highest amount of energy exported to the grid occurs during the summer season, when the school is partially closed and electricity consumption is mainly associated with the operation of the air-conditioning systems, lighting in gyms and restrooms, and pumps serving the domestic hot water system.

Table 23. Monthly energy balance

Energy use and User's needs

	E_Avail	E_User	E_Grid	SolFrac	PR
	kWh	kWh	kWh	ratio	ratio
January	1207	7038	273	0.133	0.653
February	1256	7419	30	0.165	0.694
March	2494	7425	381	0.285	0.716
April	2620	4789	550	0.432	0.717
May	2962	3972	1056	0.480	0.680
June	3328	2518	2341	0.392	0.699
July	3430	356	3074	1.000	0.695
August	3155	273	2883	0.996	0.701
September	2467	1764	1861	0.344	0.699
October	1731	3788	417	0.347	0.683
November	1045	7432	46	0.134	0.644
December	898	5472	377	0.095	0.636
Year	26594	52247	13290	0.255	0.692

The three figures below, Figure 109, Figure 110 and Figure 111 illustrate how the energy balance varies on an hourly basis.

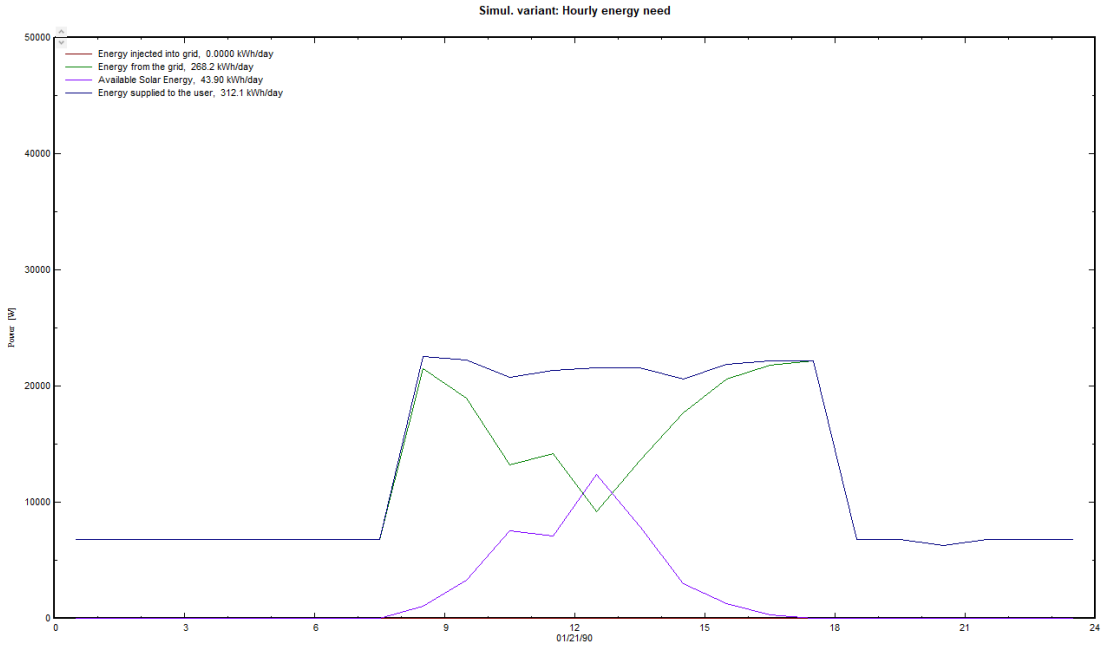

Figure 109. Energy balance for a representative winter day

The hourly energy balance is analyzed for three representative days. A typical winter day, 21 December (see Figure 109) is characterized by low energy availability from the photovoltaic system and high electricity withdrawal from the grid. In contrast, during a typical summer day, 7 August (see Figure 110), the electrical demand is very low and nearly 90% of the energy produced by the PV system is exported to the grid. For a representative day in October, as shown in Figure 111, a significant portion of the electricity demand is supplied by the photovoltaic system, while grid electricity is mainly required during the early morning hours and in the late afternoon.

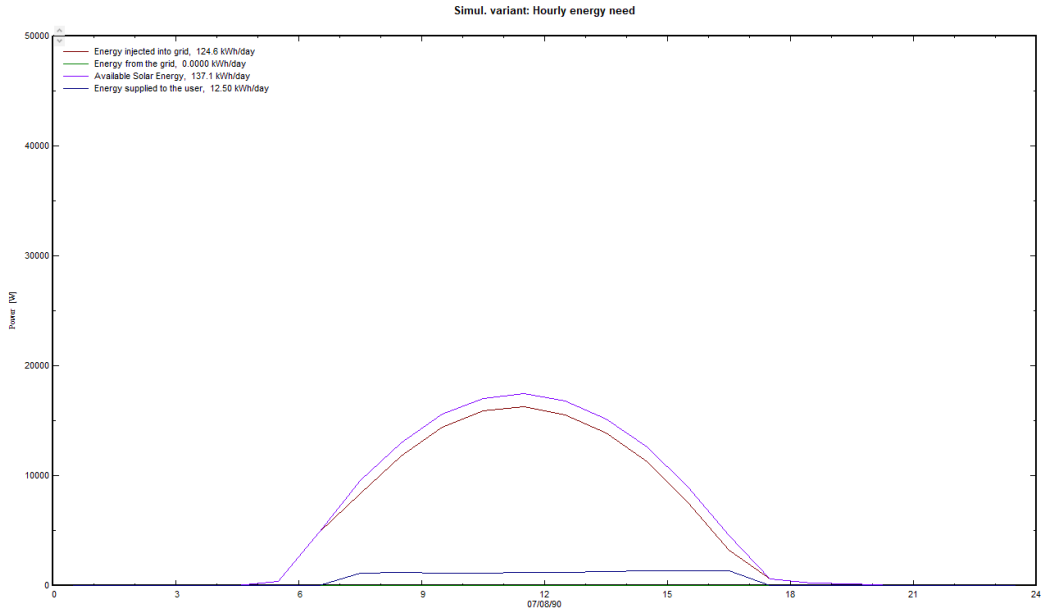

Figure 110. Energy balance for a representative summer day

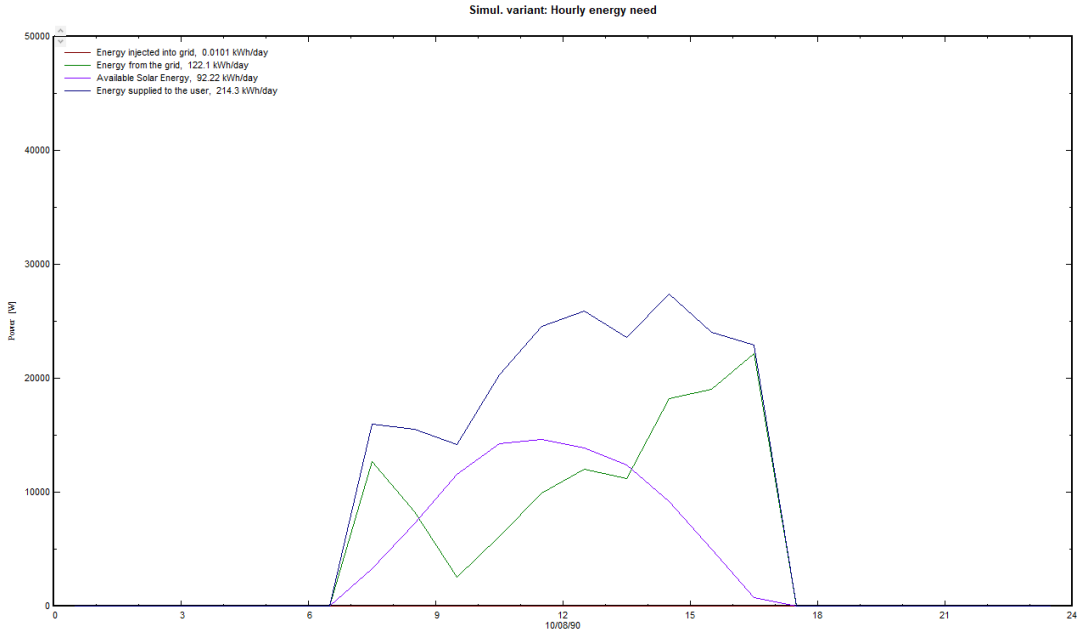

Figure 111. Energy balance for a representative autumn day

Economic evaluation

Although the total investment cost of the photovoltaic plant is fully covered by European funding within the EnerCmed project, a simplified economic assessment is carried out to evaluate the economic feasibility of the system. The cost structure implemented in PVsyst, reported in Figure 112, includes the principal capital expenditure components of the installation. The total installation cost is €24,329.44, comprising €8,809.44 for photovoltaic modules, €2,900.00 for inverters, €5,200.00 for studies and technical analyses, and €7,420.00 for installation works. Additional cost items, such as insurance, land acquisition, taxes, and financing charges, are assumed to be negligible.

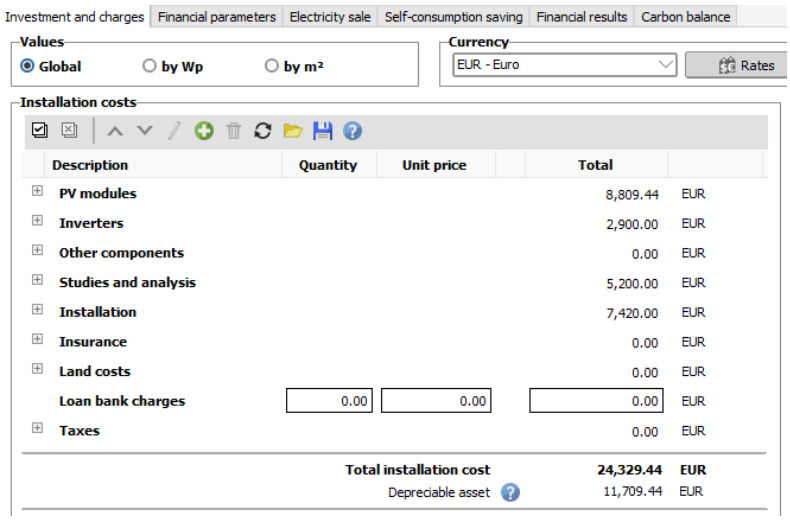

Figure 112. PV plant installation costs

In contrast, the operating costs are limited to routine maintenance and insurance expenses, resulting in a total annual operating cost of €2,480/year (see Figure 113).

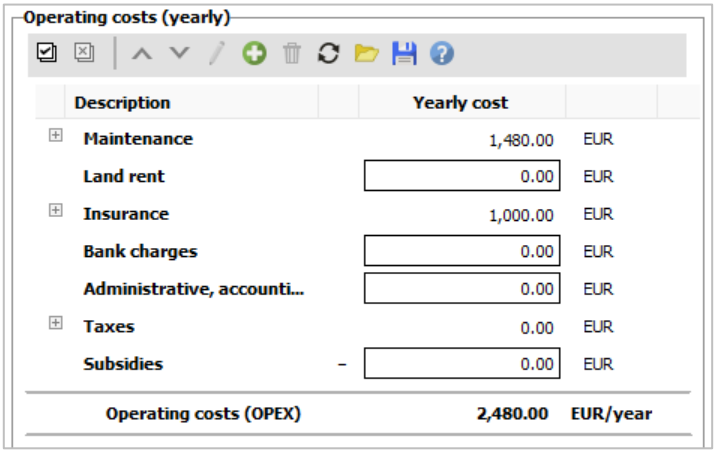

Figure 113. Operating costs

As shown in Figure 114, the cumulative cash flow analysis indicates a payback period (PBP) of approximately 9.4 years. The economic evaluation is based on an electricity consumption tariff of 0.30 €/kWh, used to quantify the economic benefit of self-consumed energy, and an electricity sale tariff of 0.08 €/kWh applied to the surplus electricity exported to the grid through the Dedicated Withdrawal (Ritiro Dedicato) mechanism. Under these assumptions, the cumulative cash flow becomes positive after the payback period and continues to increase over the remaining lifetime of the system (considering a lifespan of 20 years), confirming the long-term economic feasibility of the photovoltaic installation.

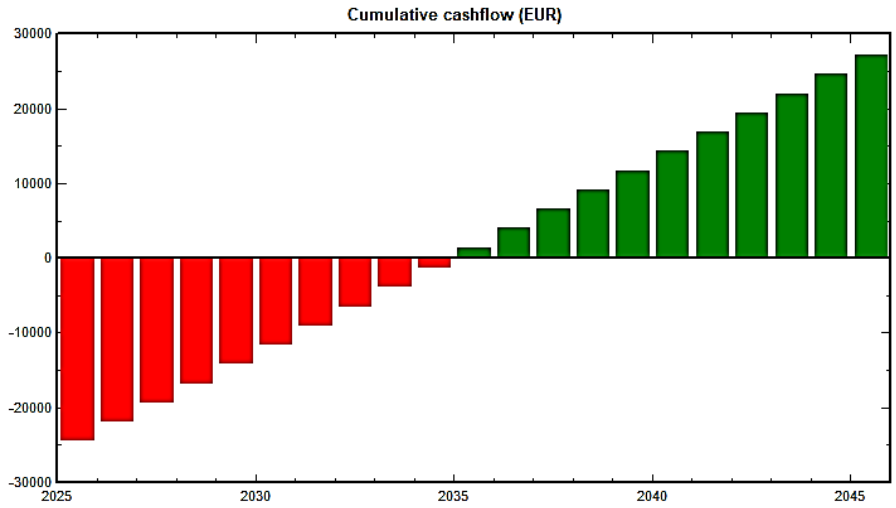

Figure 114. Cumulative cash flow

CO2 emission reduction

Figure 115 presents the carbon balance analysis performed in PVsyst for the photovoltaic system over a project lifetime of 20 years, assuming an annual module degradation rate of 1.0%. The analysis compares the electricity produced by the PV system with the Italian grid electricity mix, characterized by a carbon intensity of 423 gCO_2/kWh.

The life cycle emissions associated with the PV system amount to 37.8 tCO_2, while the cumulative avoided emissions due to the displacement of grid electricity reach 167.033 tCO_2 over the system lifetime. This corresponds to an average annual CO_2 savings of 8.352 tCO_2/year. The resulting carbon balance, illustrated by the cumulative curve, becomes positive after the initial years of operation and increases steadily over time, confirming the significant environmental benefit of the photovoltaic installation in terms of greenhouse gas emission reduction.

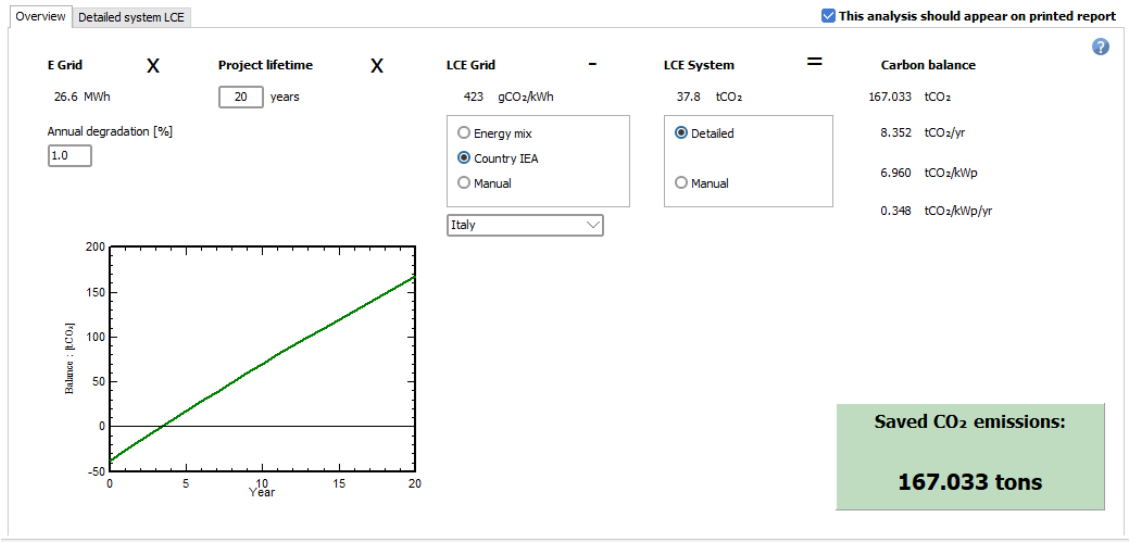

Figure 115. Average annual CO_2 savings

3.2.7 Remote Individual Self Consumption Scheme Model

In the case of Genoa, the Municipality selected the remote Individual Self-Consumption (ISC) configuration enabled by MASE Decree 414/2023 [177] to avoid the establishment of a new legal entity and to minimize administrative complexity, allowing all administrative procedures including grid connection, system registration, and incentive applications to be managed directly by the Municipality. This choice allowed the Municipality to proceed rapidly with the deployment of photovoltaic systems while maintaining its existing ownership and governance structure.

The ISC configuration requires at least two grid connection points: one or more consumption PODs owned by the same subject and a separate connection point to which a renewable energy production plant is connected. Through the distribution network, the energy produced and simultaneously consumed across the consumption PODs is virtually shared and is eligible for the incentives provided by the applicable regulatory framework, together with savings from reduced electricity withdrawals from the grid.

Relational scheme

As shown in Table 24, energy community model chosen by the municipality is based on the Italian ISC configuration under the CACER framework, with the Municipality of Genoa acting as the sole producer and consumer. The photovoltaic system installed at Scuola A. Volta, owned by the Municipality, supplies electricity primarily to the school's on-site loads, while any surplus energy is injected into the grid and, following GSE validation, virtually shared with other municipal consumption points within the same primary substation area. No new legal entity is established, as all administrative, technical, and incentive-related responsibilities are managed directly by the Municipality, ensuring a centralized governance structure and direct access to ISC incentives.

Table 24. Individual self-consumption scheme actor's role

Stakeholder	Legal Form	Role	Resources	Configuration Membership	Notes
Municipality of Genoa	Municipality	ISC Scheme Holder, investor	Full budgetary control	Yes (sole member)	Manages all infrastructure and incentive applications, it benefits from the reduced energy costs
A.Volta school	Public Educational Body	Building Operator	Operational control	No	It has the higher influence role, trough facility operations and families information
GSE	National Agency	Regulator	Administrative oversight	No	Approves ISC and issues incentives
E-Distribuzione	Private DSO	Grid Operator	Infrastructure access	No	Manages metering and connectivity

GSE (Energy Service Manager) oversees the verification of shared energy volumes and the allocation of incentives, while E-Distribuzione (Distributor) ensures technical compliance and metering accuracy. This centralized and simplified relational structure enables efficient implementation, legal clarity, and administrative coherence, providing a replicable model for municipalities seeking to deploy renewable energy systems without complex governance arrangements.

Business Model

From a business model perspective, the ISC configuration is chosen for its simplicity, cost-effectiveness, and ease of replication across the municipal building portfolio. The

model prioritizes on-site self-consumption to reduce electricity procurement costs, while surplus energy is sold to the grid through the Dedicated Withdrawal mechanism (see Table 25). Although incentive tariffs under the CACER scheme are not applicable to this ISC configuration due to prior financing arrangements *(The limitation has been introduced with the Decree of the Ministry of Environment end Energy Security 7th December 2023, n. 414 (Decreto CACER), after EnerCmed project writing design)* [177], the model remains economically viable and is presented as a scalable reference for future municipally funded deployments. By avoiding the creation of a new legal entity, the ISC approach minimizes governance, administrative, and operational costs, enabling centralized management and streamlined implementation.

Table 25. Dedicated withdrawal costs

Prezzi 2025 (Euro/MWh)												
Fascia	F1											
Zona	gen.	feb.	mar.	apr.	mag.	giu.	lug.	ago.	set.	ott.	nov.	dic.
Centro Nord	150,07	148,65	114,42	85,02	79,65	108,84	107,27	101,64	102,61	108,79	117,66	123,58
Centro Sud	147,44	146,48	106,61	81,30	74,75	108,77	107,44	101,55	102,38	106,53	109,10	120,34
Nord	149,27	146,95	113,44	84,18	78,91	109,22	106,86	101,19	102,76	108,83	121,11	124,66
Sardegna	131,68	129,10	99,47	51,51	56,77	106,17	84,59	78,33	94,29	91,35	107,07	121,94
Sicilia	141,53	147,51	99,56	82,20	76,39	108,63	99,68	103,02	103,91	75,85	104,12	118,99
Sud	143,83	148,02	101,78	80,89	76,43	108,98	100,49	102,14	103,60	80,81	105,18	119,34
Calabria	142,13	144,93	101,56	80,21	77,44	108,94	100,81	102,20	103,10	78,54	104,04	119,24
Fascia	F2											
Zona	gen.	feb.	mar.	apr.	mag.	giu.	lug.	ago.	set.	ott.	nov.	dic.
Centro Nord	145,75	149,50	118,63	74,22	62,22	93,85	104,97	92,99	84,59	86,94	115,86	109,76
Centro Sud	141,62	142,95	116,11	64,30	57,47	91,70	102,28	90,57	81,57	83,66	111,81	105,77
Nord	146,17	147,69	116,61	76,45	68,43	98,59	107,32	92,40	90,36	95,61	117,68	111,55
Sardegna	139,53	137,12	92,62	59,30	61,45	105,54	106,39	85,99	99,28	90,58	114,41	106,49
Sicilia	138,74	143,46	100,22	56,27	57,62	88,41	103,94	88,80	90,22	82,49	108,95	104,66
Sud	142,47	145,46	117,69	70,48	61,89	89,60	104,78	93,13	86,49	83,45	115,65	108,11
Calabria	143,14	146,16	116,16	67,12	60,90	89,67	103,89	92,37	91,51	84,82	112,28	106,82

No energy storage systems are planned. Surplus electricity not self-consumed on-site will be injected into the grid, but not virtually allocated to municipal consumption points within the same substation area, per GSE validation, for the reasons explained above.

Revenues

For this specific case of the Remote Individual Self-Consumption scheme model, the revenues to be considered are the following:

- Avoided costs on purchased electricity for the buildings hosting PV systems (self-consumption savings).
- Dedicated withdrawal/Ritiro Dedicato (GSE) for any residual energy fed into the grid not matched under ISC. (Market sale revenue estimations not yet available.)

**Note: In the general case: Incentive tariff on virtually shared energy from GSE (ISC under CACER) instead in the specific case of the EnerCmed pilot the public financing of the PV plant exclude it from obtaining energy sharing incentives.*

The revenues from physical self-consumption can be considered reasonably reliable, as the school's hourly electricity demand profile was incorporated into the PVsyst simulation.

The total annual electricity demand of the school is 52,247 kWh. Based on the analysis of the hourly load profile, the photovoltaic system achieves a direct self-consumption of 13,304 kWh/year. As reported in Table 26, the economic value of physical self-consumption amounts to 3,991.2 €/year, calculated using an electricity reference price of 0.30 €/kWh. The residual surplus energy, equal to 13,290 kWh/year, is not shared within the configuration and is injected into the grid, generating additional revenues of 1,063.2 €/year, assuming a unit value of 0.08 €/kWh. Overall, the combined annual revenues from self-consumption and surplus energy injection reach 5,054.4 €/year.

Table 26. Revenues of the individual self-consumption scheme

Revenues	**Total energy need**		**Amount**		**Price**		**Value**	
Physical self-consumption	52247	kWh/year	13304	kWh/year	0,30	€/kWh	3991.2	€/year
Energy surplus not shared	13290	kWh/year	13290	kWh/year	0,08	€/kWh	1063.2	€/year
Total							**5054.4**	**€/year**

3.2.8 REC Configuration – Scenario evaluation

Overall benefits of RECs

Renewable Energy Communities represent a key instrument in the European energy transition, as promoted under the RED II and RED III Directives, by integrating environmental, social, economic, and technological objectives. They contribute to greenhouse gas emission reduction and increased renewable energy deployment, while fostering social inclusion, energy awareness, and the mitigation of energy poverty. At the same time, Renewable Energy Communities support local economic development, innovation, and the digitalization of decentralized energy systems, in line with the Fit for 55 framework, as summarized in Figure 116.

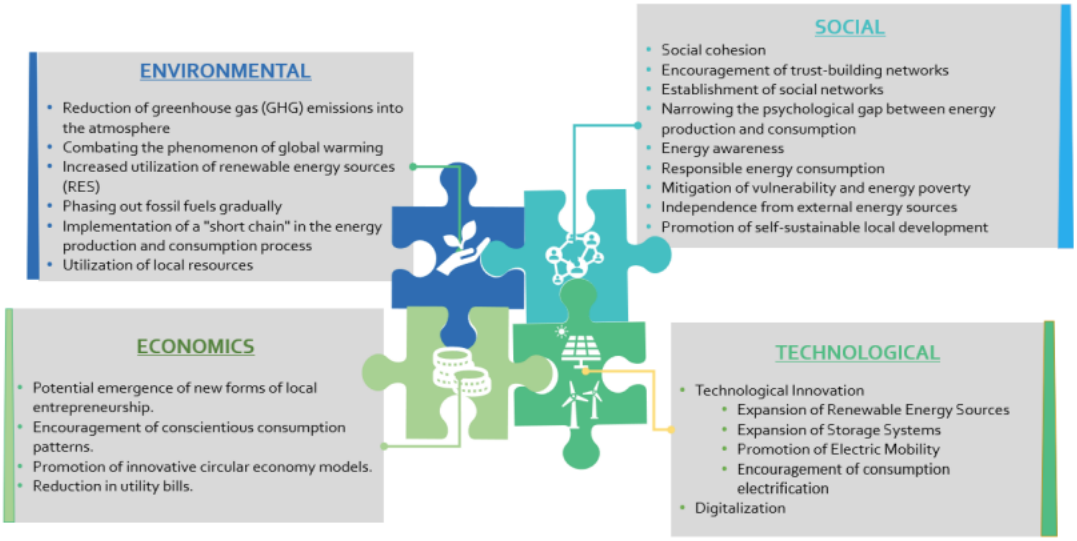

Figure 116. REC benefits [178]

As shown from the remote Individual Self consumption model, the surplus energy not shared which is paid by Dedicated Withdrawal corresponding to a medium value of 0.08, which is low compared to the energy paid for the one drawn from the grid 0.30 €/kWh.

The incentive scheme for Renewable Energy Communities in Italy provides a premium tariff for shared self-consumed electricity, composed of a fixed component linked to plant size and a variable component dependent on electricity market prices (see Table 27). The fixed component decreases with increasing installed capacity, while the variable component ranges from 0 to 40 €/MWh, increasing as market prices decline. To account for regional differences in photovoltaic productivity, additional tariff uplifts are applied, amounting to +10 €/MWh for Northern Italy. In addition to the GSE incentive, for each REC the GSE also determines an ARERA valorization fee based on the quantity of shared self-consumed electricity. This fee reflects avoided grid costs and is updated annually according to values established by ARERA [179].

Table 27. Incentives established by ARERA

Installed capacity	**Incentive tariff**
Power < 200 kW	80 €/MWh + (0–40 €/MWh)
200 kW < Power < 600 kW	70 €/MWh + (0–40 €/MWh)
Power > 600 kW	60 €/MWh + (0–40 €/MWh)

Based on Table 27 and what previously described, the economic benefits for passing from the remote Individual Self Consumption Scheme model to a REC model are summarized in the Table 28, adding the revenues from the REC incentives.

Table 28. Overall incentives for REC

Energy Destination	REC Incentive (Fixed + Variable)	Additional Revenue	Total Economic Value
Self-consumed (instantaneous)	-	Retail electricity cost savings	€200-300 / MWh
Shared within the REC	80€/MWh + (0-40 €MWh) (GSE)	Valorization €10/ MWh (GSE)	€80-130 / MWh
Exported to the grid	-	Dedicated withdrawal (RID)/ wholesale market €8/MWh) (ARERA)	€70–150 / MWh

Methodology

In order to start with the evaluation of the possible scenarios of the Renewable Energy Community, it is necessary to check for the areas served by the same primary cabin, accessing the website of the GSE [180].

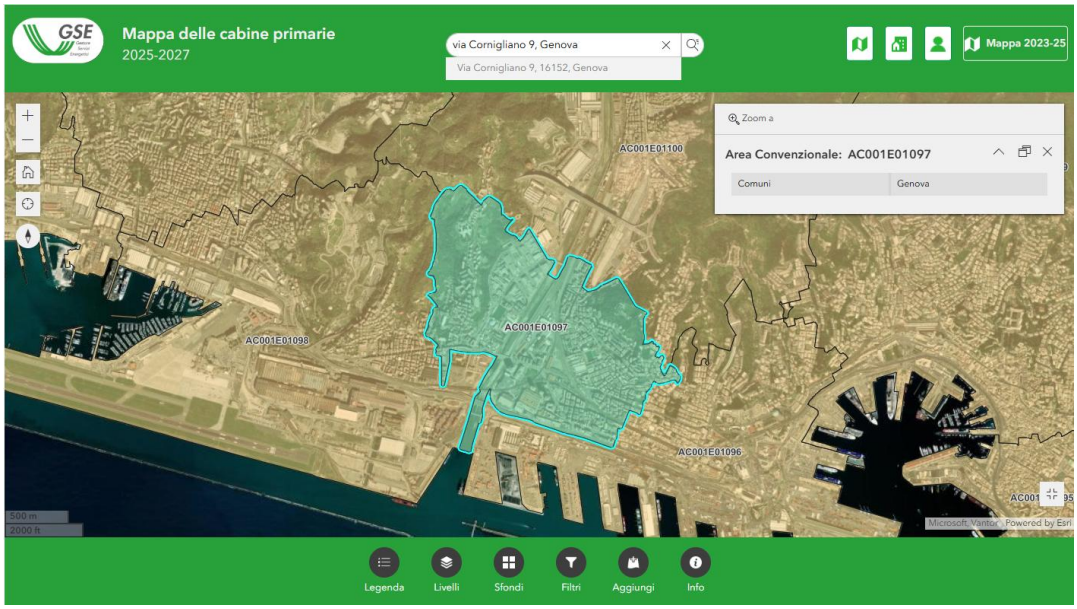

Figure 117. Map of the Primary cabins [180]

As illustrated in Figure 117, the school building is supplied by the AC001E01097 primary substation, and the reference area includes the Cornigliano and Sampierdarena districts. All entities considered as potential members of the REC are therefore located within this geographical area.

In order to enhance the economic and social benefits of the investment, several alternative configurations of the REC are analysed. In all scenarios, the Municipality of Genoa acts as the owner of the photovoltaic system and as a prosumer, in accordance with the Italian regulatory framework for RECs established by Legislative Decree 199/2021 [141] and implemented through the CACER provisions [181]. The Municipality is responsible for

electricity generation and for part of the electricity consumption associated with multiple municipal buildings connected through distinct PODs. Although the photovoltaic plant is physically installed on the rooftop of the A. Volta school building, the Municipality, as owner of the school and of other municipal facilities, retains ownership of the generated electricity. In line with ARERA regulations and GSE operational rules, the electricity produced is first used to cover the on-site consumption associated with the school POD, while any surplus energy is injected into the distribution grid and, based on hourly temporal coincidence, is virtually shared among all REC participants. These include other municipal PODs as well as residential users and small and medium-sized enterprises (SMEs), each modelled as consumers connected through separate PODs within the same primary substation area, as required by the CACER eligibility criteria.

Within the analysed configurations, all incentives associated with shared renewable energy are allocated exclusively to the Municipality of Genoa, in its role as plant owner and prosumer. This allocation reflects the fact that the Municipality fully bears the investment costs of the photovoltaic system as well as all operation and maintenance expenses. The remaining REC participants do not directly receive incentive payments; however, they benefit indirectly through reduced electricity procurement costs and increased energy cost savings resulting from access to locally generated renewable electricity.

For each scenario, the analysis is limited to the evaluation of annual revenues, without performing a detailed cost benefit analysis or assessing payback periods for 20 years life span. This methodological choice is justified by the fact that both the capital expenditure and the operation and maintenance costs of the photovoltaic system are fully covered by European funding under the EnerCMed project. Consequently, the scenarios are assessed exclusively in terms of maximizing photovoltaic self-consumption and energy sharing within the REC, consistent with the incentive allocation mechanism defined by ARERA and administered by GSE, with the objective of maximizing the associated revenues and improving the overall utilization of locally generated renewable electricity.

Furthermore, the REC configurations analyzed are designed to be scalable and open to future expansion. The progressive integration of new prosumers equipped with renewable generation systems and, consequently, new consumers represent key opportunities explicitly encouraged by the CACER framework to increase shared energy volumes, strengthen local participation, and enhance the long-term economic, social, and environmental performance of the Renewable Energy Community.

Figure 118 illustrates a three-dimensional representation of the A. Volta school building and the surrounding urban context, highlighting the location of the photovoltaic installation on the rooftop. The model provides a spatial overview of the building within the neighborhood and supports the definition and interpretation of the REC configuration.

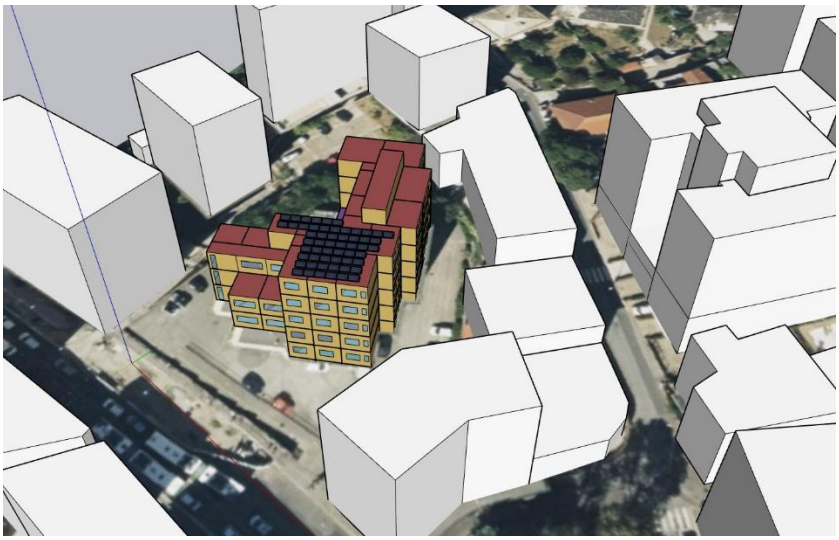

Figure 118. Example of a 3D REC representation

Scenario 1. MGE Prosumer (A. Volta POD)) + Municipality building + Residential building

The REC model simulations were carried out using the HexErgy application version 2.12.28, available at [182]. The free-licensed version of the software enables the development and comparison of multiple scenario configurations by implementing monthly energy profiles. The Renewable Energy Community is composed of one prosumer, represented by the Municipality of Genoa, whose prosumer point of delivery (POD) corresponds to the A. Volta School building, and two consumers: a multi-story residential building consisting of 80 apartments and an additional municipal building owned by the Municipality, each connected through a dedicated POD, as illustrated in Figure 120.

Electricity consumption data for the REC members, with the exception of the A. Volta School, whose energy demand was simulated through a detailed building energy model, were derived from datasets published by ARERA. Specifically, residential consumption data in Table 29 were obtained from the "Prelievi di energia elettrica dei clienti domestici" database and are reported in the table below [183].

For residential users, the electricity consumption in the F1 time band (F1 includes the energy consumption from Monday to Friday from 8:00-19:00) represents an average value of 31% of the total annual consumption per apartment, in accordance with typical residential load profiles.

Table 29. Residential consumption profiles [183]

Year-Month	Average Withdrawal
Jan 2024	133
Feb2024	108
Mar2024	122
Apr 2024	110
May 2024	109
Jun 2024	104
Jul 2024	129
Aug2024	142
Sept 2024	109
Oct 2024	117
Nov 2024	119
Dec 2024	135

Year-Month	Avg. F3 (%)
Jan 2024	38.85%
Feb2024	34.53%
Mar2024	36.52%
Apr 2024	39.68%
May 2024	37.48%
Jun 2024	38.53%
Jul 2024	36.90%
Aug2024	39.75%
Sept 2024	39.10%
Oct 2024	34.30%
Nov 2024	36.62%
Dec 2024	41.43%

For the Municipality of Genoa, electricity consumption data were obtained from the ARERA dataset "Analisi dei consumi dei clienti non domestici in BT (Bassa Tensisone – Low Voltage)", which was used to represent the consumption profile of the municipal prosumer and is reported in Figure 119. The dataset is publicly available at [184].

Figure 119. Consumption profile for public administration [184]

For the municipal building included as a consumer within the REC, the electricity consumption in the F1 time band was assumed to represent approximately 65% of the total annual consumption. This assumption reflects the typical operating schedule of municipal office buildings, whose activities are largely concentrated during standard working hours on weekdays, corresponding predominantly to the F1 time band. Evening, night-time, and weekend electricity uses are comparatively limited and mainly associated with base loads such as lighting, standby equipment, and security systems.

After collecting the electricity consumption profiles of all REC members, the modelling phase can be initiated within the HexErgy application. The model includes the main characteristics of the photovoltaic plant, such as location and installed peak power,

together with the electricity consumption profiles of the community members, costs and incentives, in order to define the overall REC configuration. The app interface after completing the data is shown in Figure 120.

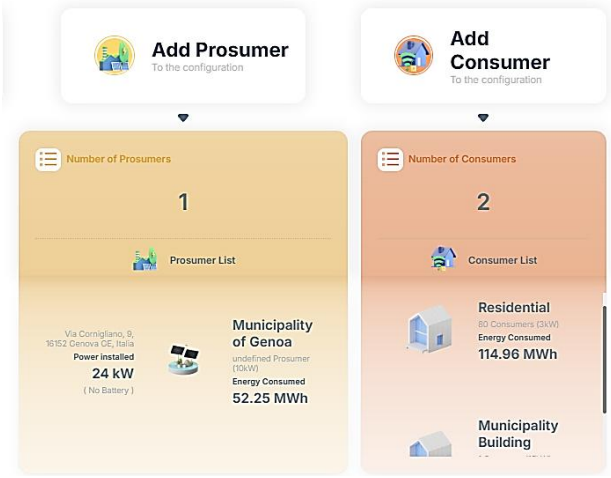

Figure 120. HexErgy app interface after data completing

The results obtained for this scenario ensure 99.87% consumption (see Figure 121) of the energy produced by the PV plant which means that it maximizes the revenues compared to the (SCS).

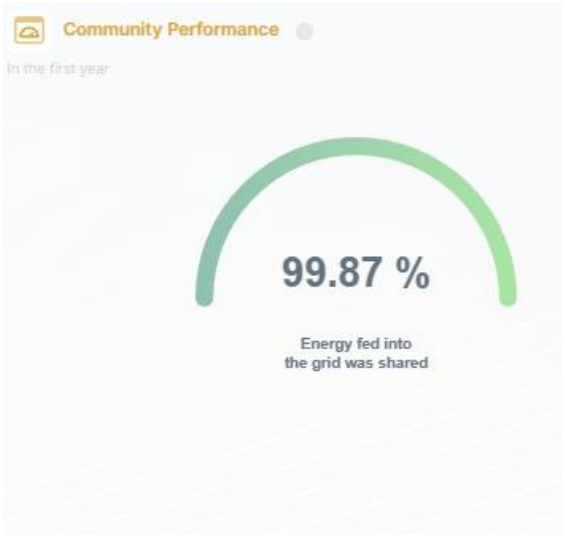

Figure 121. Percentage of the Energy consumed within the REC configuration

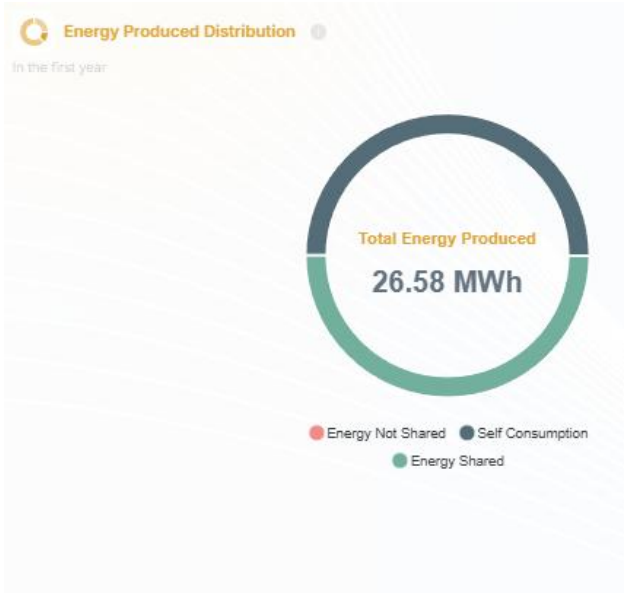

Figure 122. Energy balance within the REC configuration

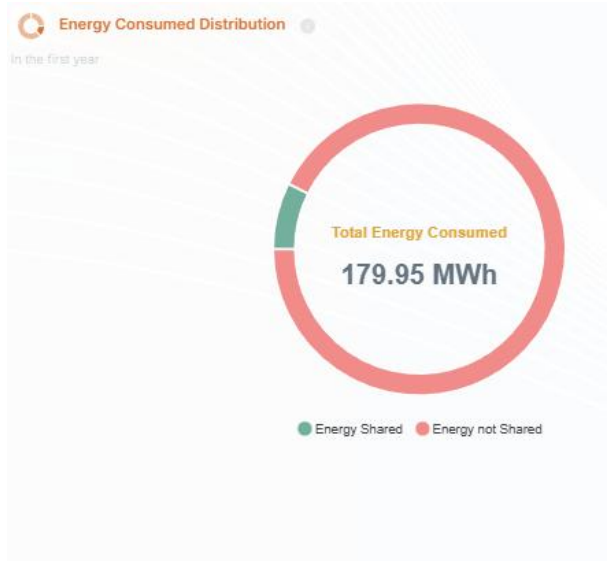

Figure 123. Energy consumed distribution

As shown in Figure 122, the photovoltaic plant produces a total of 26.58 MWh in the first year. Almost the entirety of this production is either self-consumed or shared within the Renewable Energy Community, with only a negligible fraction of energy remaining unshared 17.82 kWh. This confirms the very high level of PV generation utilization achieved under the REC configuration. At the same time, Figure 123 highlights that the total electricity demand of the REC amounts to 179.95 MWh in the first year. Although the overall demand is significantly higher than local generation, the share of energy supplied through the REC, currently 7.38%, still replaces electricity that would otherwise be entirely

purchased from the external grid. This result is consistent with the significant difference between local demand and PV generation capacity and indicates that the available photovoltaic energy is fully absorbed by the community without curtailment.

Figure 124 represents the monthly energy distribution of the REC during the first year of operation, showing the relationship between energy produced by the photovoltaic plant, energy self-consumed, energy shared within the community, and energy not shared. It shows that the non-shared energy is negligible.

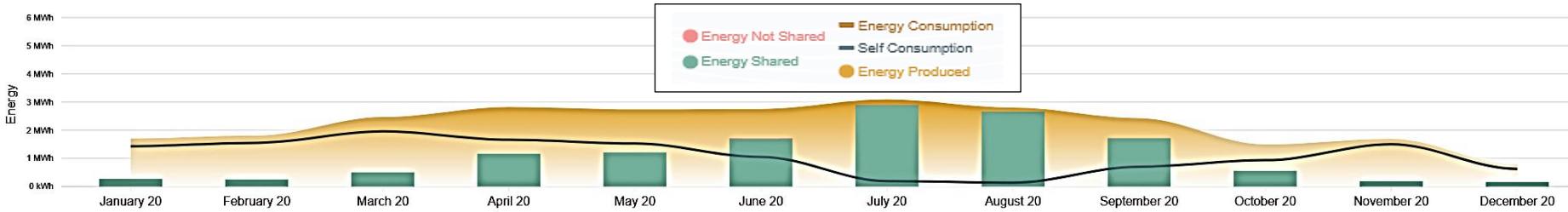

Figure 124. Monthly energy consumed distribution of the REC configuration

Figure 125 provides an overview of the energy flows within the Renewable Energy Community during the first year of operation. The diagram highlights the distribution of electricity between production, self-consumption, sharing among community members, and exchanges with the external grid, as well as the balance between local generation and aggregated demand. Overall, the figure visually supports the effectiveness of the REC configuration in integrating photovoltaic generation into a demand-dominated context.

Based on the energy shared within the Renewable Energy Community of 13.28 MWh, the performance indicators reported in show that, during the first year of operation, an estimated CO_2 emission reduction of 14.09 kt CO_2e. This indicator provide a concise measure of the environmental benefit associated with the REC configuration.

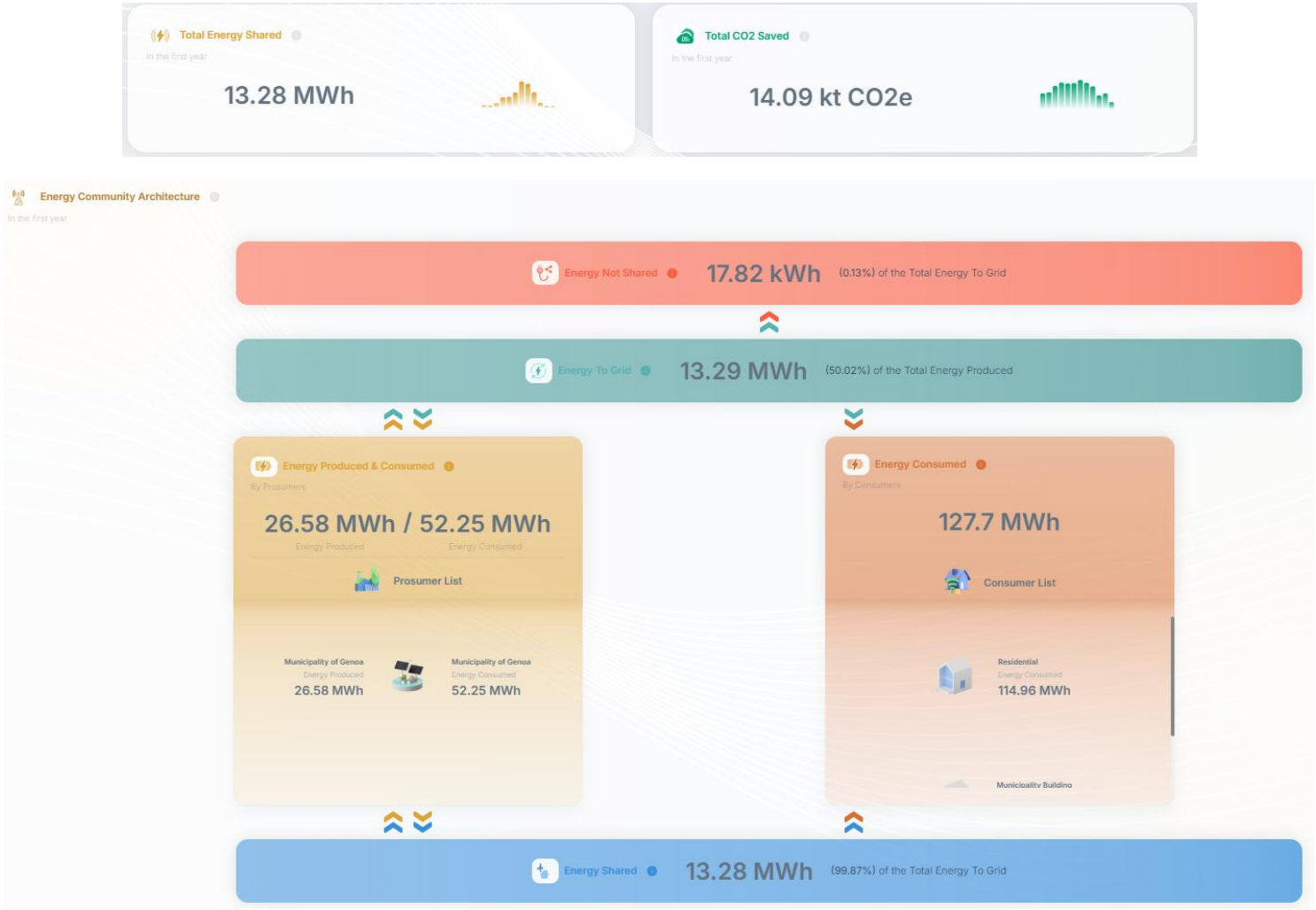

Figure 125. Energy profile of the community for the first year

This dashboard in Figure 126 provides a general overview of energy distribution within a system. It highlights the total energy produced and shows how that energy is divided between self-consumption, energy sent to the grid, and the portion that was shared or not shared. Overall, it gives a quick summary of how the generated energy is used and distributed.

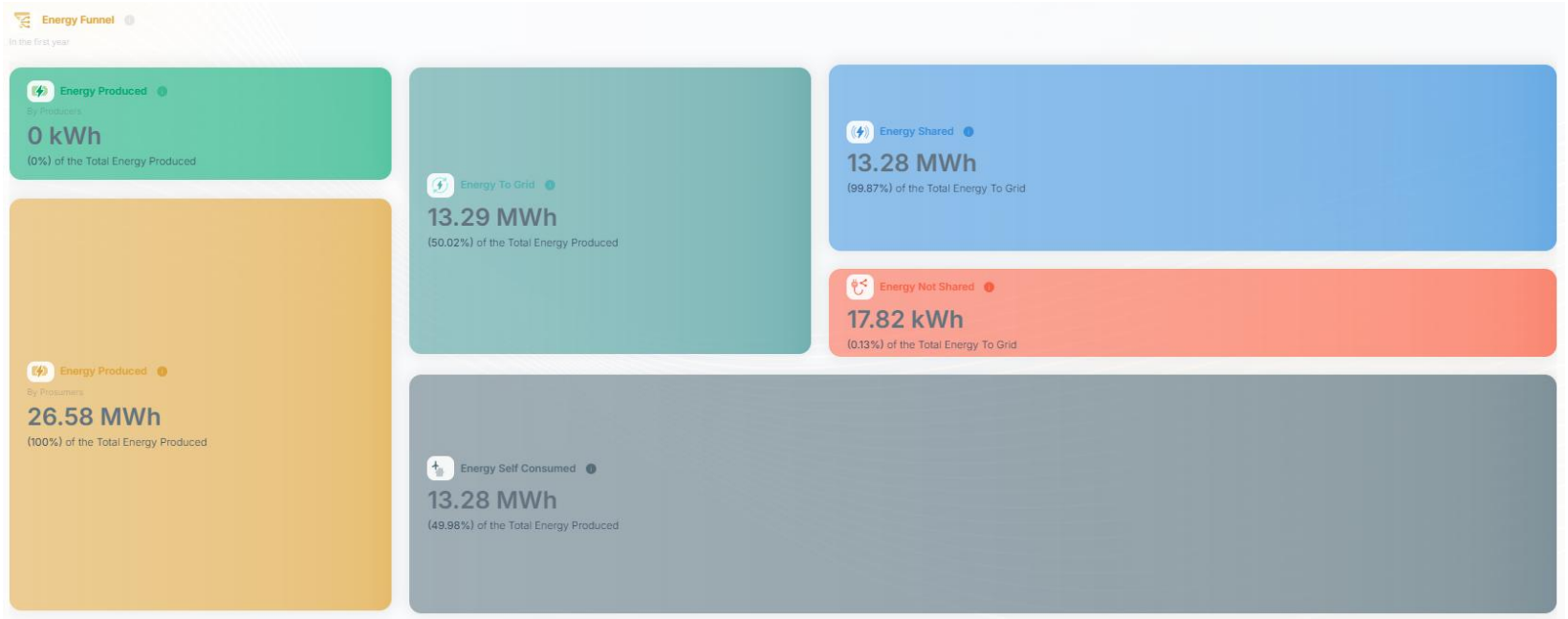

Figure 126. Energy flows inside the community

Revenues

The results reported in Table 30 indicate that the total annual revenues of the REC configuration amount to 5,711.83 €/year, which is significantly higher than the revenues achievable under a remote Individual Self consumption scheme. While physical self-consumption remains the dominant revenue component (3,984.00 €/year), the REC framework enables additional revenues through virtually consumed energy, amounting to

1,726.40 €/year. This increase is primarily driven by the inclusion of residential consumers within the community, whose electricity demand profiles are relatively continuous over the year and extend across all time periods, including weekends and holiday periods.

Table 30. Revenues definition

Revenues	**Amount**		**Price**		**Value**	
Physical self-consumption	13,280.00	kWh/year	0.30	€/kWh	3,984.00	€/year
Energy virtually consumed	13,280.00	kWh/year	0.13	€/kWh	1,726.40	€/year
Energy surplus not shared	17.82	kWh/year	0.08	€/kWh	1.43	€/year
Total					**5,711.83**	**€/year**

As a result, surplus photovoltaic energy that would otherwise be injected into the grid during periods of reduced activity at the school or municipal buildings, such as summer and winter holidays or weekends, can be effectively shared within the REC.

Since energy shared within the community is remunerated through dedicated incentives managed by GSE at more favorable conditions than those applied to non-shared surplus energy injected into the grid, which generates a negligible contribution (1.43 €/year), the presence of residential consumers significantly enhances overall revenues. These results demonstrate that the maximization of energy sharing enabled by diversified and complementary consumption profiles is a key factor in improving the economic performance of the REC model compared to a simple self-consumption scheme.

Scenario 2. MGE Prosumer (A. Volta POD) + Municipality build. + Assisted Living Facility < 4kW + Assisted Living Facility < 6kW + Non-Profit organization: Progetto 80 Sampierdarena

Also in this REC scenario, the Municipality of Genoa acts as a prosumer through the A. Volta School POD, but it supplies to a set of consumers with high social relevance. In addition to a municipal building, the configuration includes assisted living facilities with contracted power levels ranging from 4 to 6 kW, as well as a non-profit organization. This scenario is explicitly designed to maximize not only the economic performance of the REC but also its social impact by directing the benefits of locally generated renewable electricity towards facilities serving fragile and vulnerable individuals.

From an economic perspective, the presence of assisted living facilities, which exhibit continuous, essential electricity demand, increases the temporal overlap between photovoltaic generation and consumption, thereby enhancing energy sharing within the community and maximizing the revenues associated with shared energy. At the same time, the reduction in electricity procurement costs improves the financial sustainability of socially oriented services, which typically operate under constrained budgets. From a

social standpoint, the participation of assisted living facilities and a non-profit organization allows the REC to act as a tool for mitigating energy costs for vulnerable users, strengthening social inclusion, and supporting essential services. Overall, this scenario highlights the potential of REC to simultaneously deliver economic efficiency and tangible social benefits, reinforcing their role as instruments for a just and inclusive energy transition.

The following elderly care and assisted living facilities are included as consumers within the REC configuration:

- Villa Maria Residential Care Centre (RSA)
- Aurora Assisted Living Facility
- Coronata Residential Care Facility (RSA), 6 kW
- Villa Coronata Residential Care Facility (RSA), 6 kW
- Casa Famiglia Anziani Assisted Living Community for the Elderly
- Casa di Riposo "Casa Montano"
- Quadrifoglio Assisted Living Community for the Elderly
- Casa Carlotta

The consumption profiles for each consumer, derived from ARERA, are shown in the Figure 127 and Figure 128, with the main data summarized in Table 31.

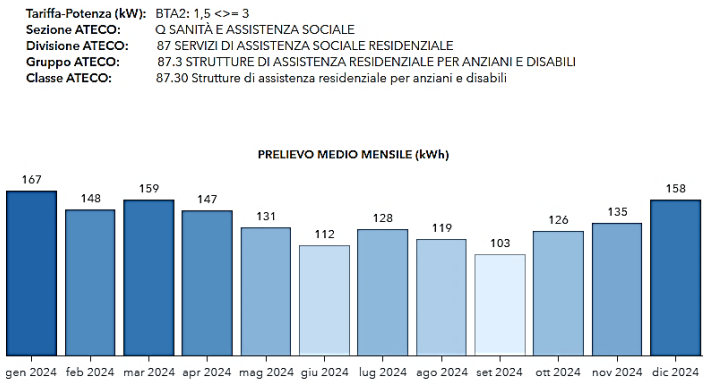

Figure 127. Consumption profile for Assisted facility

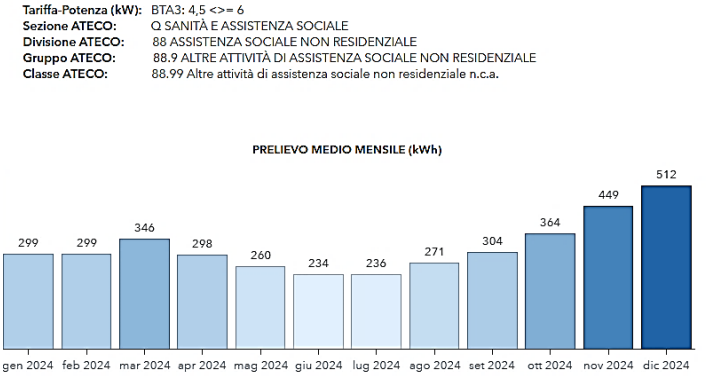

Figure 128. Consumption profile for nonresidential Social Assisted facility

Table 31. Summary of the consumption profiles for the REC members

Month	Assisted Living Facility < 4 kW	Assisted Living Facility < 6 kW	Non-Profit Organization
Jan	158	341	299
Feb	88	266	299
Mar	82	281	346
Apr	66	351	298
May	62	316	260
Jun	97	290	234
Jul	167	276	236
Aug	178	395	271
Sep	138	315	304
Oct	150	352	364
Nov	197	479	449
Dec	278	349	512

Although this scenario achieves a high level of social impact by prioritizing facilities serving fragile and vulnerable groups, the economic performance of the REC remains constrained. Despite a relatively high share of energy being effectively shared within the community (64.1% of the energy fed into the grid), the limited number and scale of consumers restrict the overall capacity to absorb surplus photovoltaic production (see Figure 129).

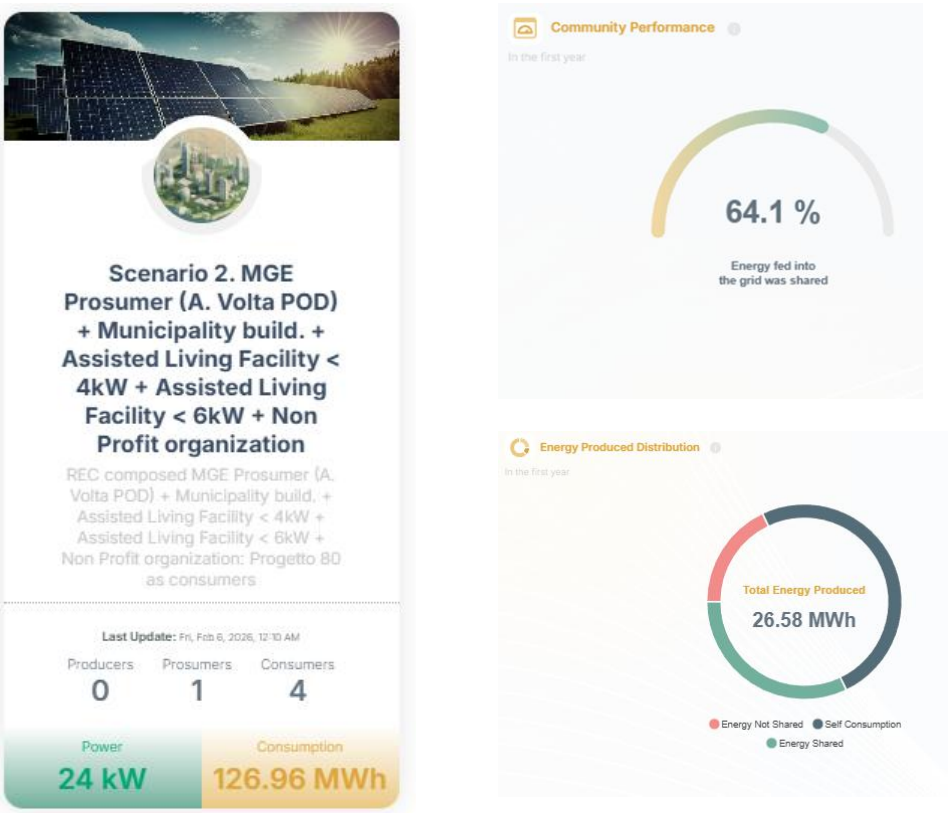

Figure 129. REC performance and energy produced distribution

Figure 130 illustrates the monthly distribution of photovoltaic energy within the REC during the first year of operation. While energy sharing increases during the spring and summer months due to higher photovoltaic production, the figure also shows that a substantial share of the generated energy remains unshared during the summer season and is therefore injected into the grid. This occurs when photovoltaic production exceeds the aggregated demand of the community members, highlighting the limited capacity of the current configuration to fully absorb surplus energy during peak generation periods.

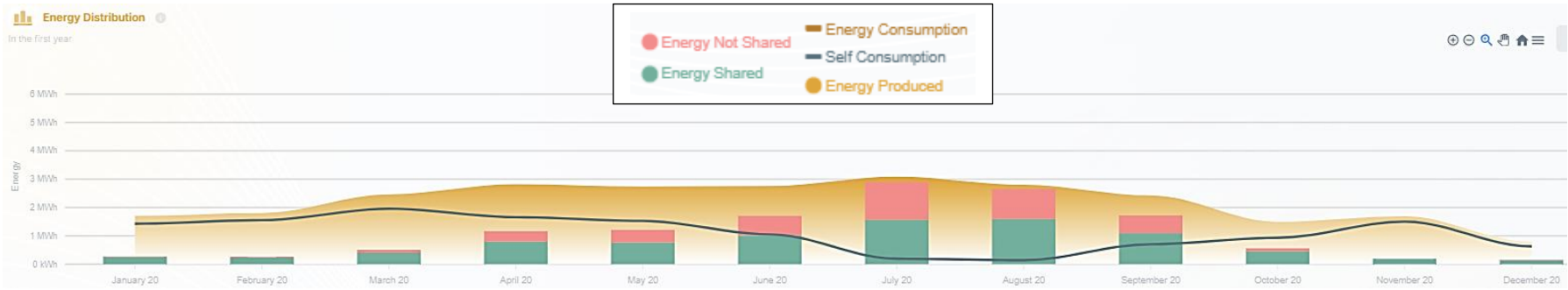

Figure 130. Monthly energy consumed distribution of the REC configuration

Revenues

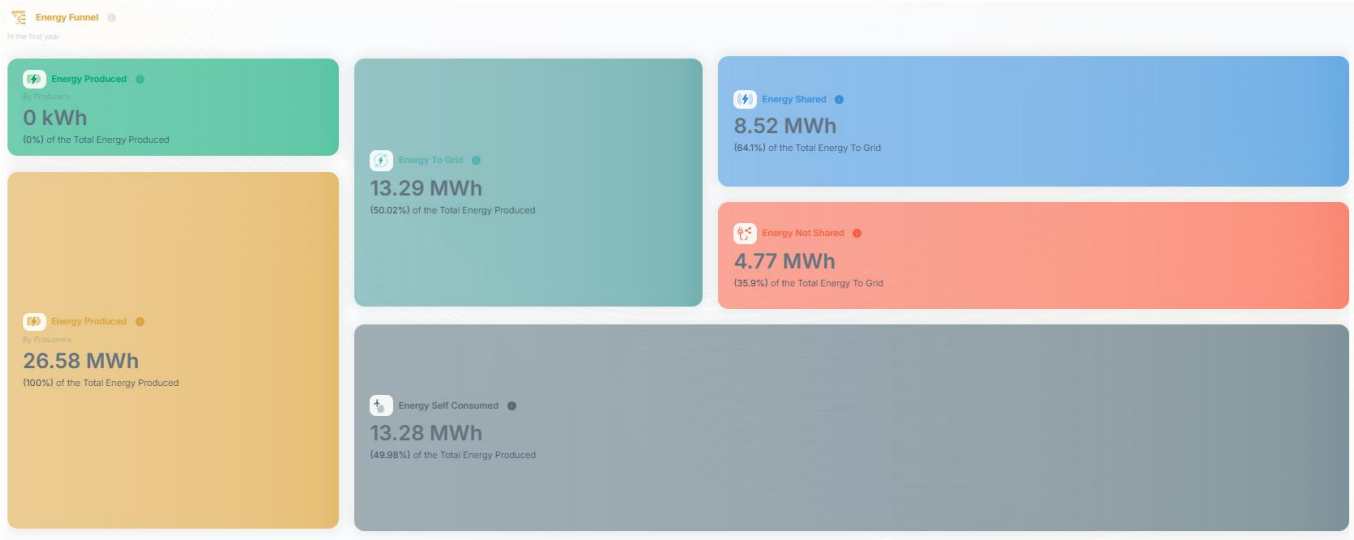

Figure 131. Energy flows inside the community

Based on the results of the energy profile of the community for the first year (see Figure 131) is possible to define the revenues for this scenario (see Table 32).

Table 32. Revenues definition

Revenues	**Amount**		**Price**		**Value**	
Physical self-consumption	13,280.00	kWh/year	0.30	€/kWh	3,984.00	€/year
Energy virtually consumed	8,520.00	kWh/year	0.13	€/kWh	1,107.60	€/year
Energy surplus not shared	4,770.00	kWh/year	0.08	€/kWh	381.60	€/year
Total					**5,473.20**	**€/year**

So, as part of the generated energy continues to be injected into the grid unless shared, led to less favorable economic conditions. These findings indicate that, while socially effective, the configuration would require the inclusion of additional consumers with complementary demand profiles to further increase energy sharing and improve the economic convenience of the REC.

Scenario 3. MGE Prosumer (A. Volta POD) + Municipality build. + Assisted Living Facility < 4kW + Assisted Living Facility < 6kW + Non-Profit organization: Progetto 80 Sampierdarena + Listed buildings

This scenario extends the previous Renewable Energy Community configuration by enlarging the group of participating consumers in order to further increase energy sharing and improve the overall economic performance of the community. The Municipality of Genoa continues to act as a prosumer through the A. Volta School POD, while the consumer base is expanded to include, in addition to a municipal building, assisted living facilities with contracted power levels below 4 kW and between 4 and 6 kW, a non-profit organization (Progetto 80 Sampierdarena), and two listed buildings. These include a school and a residential building subject to architectural and heritage protection constraints, for which the installation of photovoltaic systems on rooftops is either prohibited or entails lengthy and complex authorization procedures.

The inclusion of buildings subject to architectural constraints plays a crucial role in the configuration of the REC. Such buildings are often excluded from direct participation in renewable energy generation despite having significant and continuous electricity demand. By integrating them as consumers within the REC, it becomes possible to overcome structural and regulatory barriers while allowing these buildings to actively benefit from locally generated renewable electricity. This approach not only increases the absorption of surplus photovoltaic energy during periods of high generation but also promotes a more inclusive energy transition, ensuring that heritage-protected buildings are not left behind. Overall, this scenario highlights the strategic importance of Renewable Energy Communities as instruments capable of reconciling energy efficiency objectives with urban heritage preservation constraints.

The identification of buildings subject to architectural, archaeological, and landscape protection constraints was carried out by consulting the "*Mappa dei Vincoli Architettonici, Archeologici e Paesaggistici"* provided by the Liguria Region through the "Vincoli" web portal [185] as shown in the Figure 132.

Figure 132. Map of Restrictions for Liguria Region [185]

By overlaying the *Mappa dei Vincoli Architettonici, Archeologici e Paesaggistici* [185] with the map of the primary substation coverage area [180], it was possible to identify an elementary school building and a multi-storey residential building located within the REC boundary that

are subject to Point architectural constraints and collective heritage protection (bellezze di insieme) (see Figure 133). These constraints limit or complicate the installation of photovoltaic systems on the buildings, thereby justifying their inclusion in the REC exclusively as consumers.

Figure 133. Overlapping maps for the REC member evaluation [185], [180]

In the Figure 134, the electricity consumption profile representative of the consumption profile of the Eugenio Montale elementary school is given.

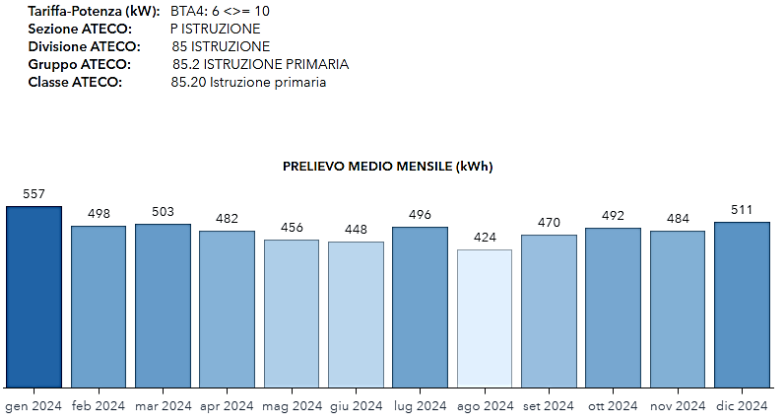

Figure 134. Consumption profile for a primary school [186]

After completing the REC configuration, as shown in Figure 135, it results that 99.89% of the energy fed into the grid is shared within the community, supported by a total annual electricity consumption of 193.26 MWh.

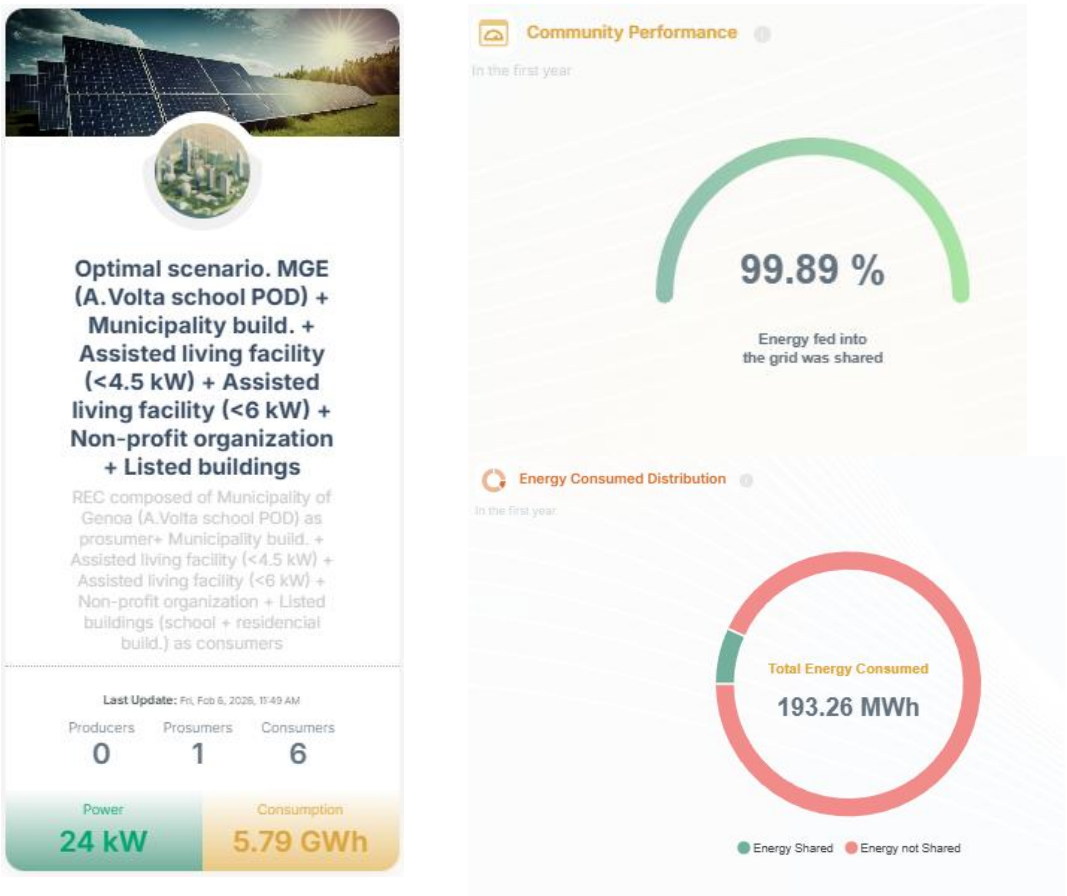

Figure 135. REC performance and energy produced distribution

Figure 136 illustrates the monthly distribution of photovoltaic energy within the REC during the first year of operation.

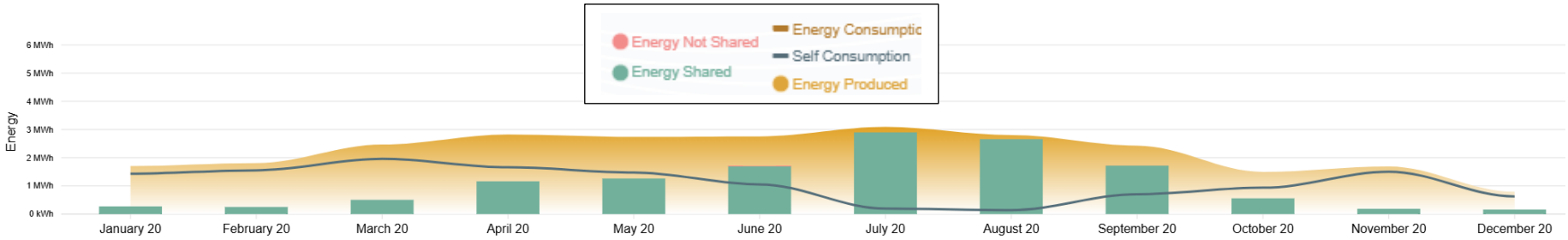

Figure 136. Monthly energy consumed distribution of the REC configuration

The weekly electricity consumption heatmap shows higher demand during daytime and early evening hours on weekdays, reflecting the operating schedules of municipal building, assisted living facilities, and non-profit activities (see Figure 137). Lower consumption occurs during night-time hours and weekends, while a stable baseline demand persists due to residential users and essential services. This diversified demand profile improves the temporal alignment with photovoltaic generation and supports higher levels of energy sharing within the REC.

Figure 137. Energy consumption for the first year, segmented by day and hour

Revenues

Based on the results of the energy profile of the community for the first year (see Figure 138) is possible to define the revenues for this scenario (see Table 33).

Figure 138. Energy flows inside the community

This configuration represents the best-performing scenario, as it maximizes energy sharing within the REC, with almost all surplus photovoltaic energy absorbed by community members, resulting in total annual revenues of 5,711.58 €/year, primarily driven by physical self-consumption and virtual energy sharing. Beyond its economic performance, the scenario delivers substantial social and institutional benefits by supporting vulnerable groups through assisted living facilities and non-profit organizations.

Table 33. Revenues definition

Revenues	Amount		Price		Value	
Physical self-consumption	13,280.00	kWh/year	0.30	€/kWh	3,984.00	€/year
Energy virtually consumed	13,280.00	kWh/year	0.13	€/kWh	1,726.40	€/year
Energy surplus not shared	14.77	kWh/year	0.08	€/kWh	1.18	€/year
Total					**5,711.58**	**€/year**

Moreover, it enables buildings subject to architectural and heritage protection to actively participate in the energy transition, despite the fact that the installation of photovoltaic systems on such buildings typically requires lengthy, complex, and uncertain authorization procedures. By including these listed buildings as consumers within the REC, the configuration provides them with access to locally generated renewable energy without the need for direct on-site installations, demonstrating the potential of Renewable Energy Communities to reconcile energy transition objectives with regulatory, cultural heritage, and urban planning constraints.

To provide a comprehensive comparison of the analyzed configurations, Table 34 summarizes the main energy, economic, and sustainability indicators derived from the Sustainable Development Goals (SDGs) for Scenarios 1–3.

Table 34. Summary of REC Scenario Performance (Scenarios 1–3)

Scenario	SDG11 Economic Benefit [€]	SDG1 – Vulnerable Users [-]	SDG1 – Inclusion [%]	SDG7 – Local RES Use [%]	SDG11 – Shared Energy [%]	SDG13 -CO_2 Savings [tCO_2/y]
ICS	5054.40	-	-	25.46%	0%	4.39
Scenario 1	5711.82	-	-	14.76%	50.0%	8.76
Scenario 2	5473.20	3	60%	25.10%	32.0%	7.19
Scenario 3	5711.58	5	71%	13.74%	50.0%	8.76

SDG indicators are introduced to complement the energy and economic analysis. SDG7 (Local RES Use), calculated as the ratio between self-consumed and shared energy and total electricity demand, reaches up to 25.10% in Scenario 2, while decreasing to 13.74% in Scenario 3, highlighting the strong influence of total demand. SDG11 (Shared Energy), defined as the share of PV production redistributed within the community, attains approximately 50% in the most effective configurations, indicating a high level of energy exchange. SDG13 (CO_2 savings), computed from locally utilized PV energy and the grid emission factor, nearly doubles from 4.39 tCO_2/y in the baseline ISC scheme model to about 8.76 tCO_2/y in REC configurations, demonstrating the environmental benefit of local energy use. SDG1 reflects social inclusion, expressed as the share of vulnerable users, reaching up to 71% in Scenario 3, which represents the highest level of inclusiveness.

Overall, Scenario 3 provides the most balanced performance, combining high energy sharing, economic benefits, and social inclusion, while maintaining CO_2 savings comparable to the best-performing configurations (8.76 tCO_2/y). Although its SDG7 value is lower (13.74%), this is primarily due to the significantly higher aggregated electricity demand in the configuration, which reduces the relative share of demand covered by local renewable energy. In absolute terms, however, Scenario 3 achieves one of the highest levels of locally utilized PV energy, indicating that the lower SDG7 value reflects a scaling effect rather than reduced system performance.

3.3 Conclusions

Within the broader framework of sustainable energy transitions in port hinterlands, this work is embedded in the context of the EnerCmed project, which promotes the development of Renewable Energy Communities (RECs) and self-consumption schemes coupled with Nature-Based Solutions in marginalized urban areas affected by energy poverty. The thesis contributes to the project by supporting the technical planning and implementation of REC pilot actions. In particular, the author contributed to the development of the Terms of Reference (ToR) guidelines for REC and NBS creation, the Knowledge Sharing Helpdesk Platform for disseminating best practices, and the Digital Application designed to operationalize the ToR framework and support the replication of REC deployment strategies.

Building on this framework, the chapter demonstrated how detailed building-level energy modelling can effectively support the design and evaluation of Renewable Energy Communities. The use of OpenStudio enabled the definition of hourly heating, cooling, and electricity demand profiles, providing representation of building energy behaviour when no data are available and new plants are considered to be integrated (in this case cooling plant), allowing the analysis of the interaction between demand and photovoltaic generation.

The results confirmed the strong seasonal variability of photovoltaic production, with higher outputs in spring and summer and reduced generation in winter. This variability emphasizes the importance of matching renewable generation with diversified and complementary demand profiles. The time-resolved modelling approach proved essential for estimating self-consumption, surplus energy, and sharing potential within the REC.

The scenario-based analysis demonstrated that progressively expanding the range of participating users significantly improves the economic performance of the REC. The inclusion of residential users, assisted living facilities, non-profit organizations, and

buildings serving vulnerable groups led to increased energy sharing and reduced surplus energy exported to the grid due to continuous consumption profiles. Among the analysed configurations, Scenario 3 emerged as the most balanced solution, achieving near-complete utilization of surplus energy and the highest economic performance. These results highlight that REC effectiveness depends not only on installed renewable capacity, but also on the diversity, continuity, and complementarity of demand profiles, which determine the coincidence factor between generation and consumption.

From a sustainability perspective, the integration of SDG-based indicators enables a multi-dimensional evaluation of the scenarios. Configurations maximizing the local use of photovoltaic energy achieve the highest contribution to SDG 13, with CO_2 savings increasing from 4.39 tCO_2/y in the baseline to about 8.76 tCO_2/y in REC configurations. In contrast, SDG 7 ranges between 13.74% and 25.10%, as it reflects the share of demand covered by local renewable energy and is therefore influenced by the scale of electricity demand. The inclusion of vulnerable users improves SDG 1, reaching 71% in Scenario 3, while energy sharing enhances SDG 11, with values close to 50% of total PV production in the most effective configurations.

Overall, the combined integration of EnerCmed project tools, dynamic energy modelling, and scenario-based REC analysis provides a comprehensive, replicable, and transferable methodological framework for enhancing renewable energy sustainability in port-city hinterlands and not only. The findings confirm that RECs centered on public buildings can maximize local renewable energy use, improve economic viability, and deliver relevant social and environmental benefits, thereby supporting inclusive and climate-resilient energy transitions.

However, the results also indicate that the performance of REC configurations is strongly influenced by the temporal distribution of electricity demand. Changes in building energy behaviour may affect the alignment between photovoltaic generation and consumption, altering the interaction between energy production and use across different periods of the year. For this reason, the following chapter investigates the impact of demand-side modifications on the energy balance, with the aim of analysing how variations in consumption profiles influence the relationship between photovoltaic production and electricity demand, without assuming a priori improvements in system performance.

3.4 Limitations

The results presented in this chapter are subject to several modelling and methodological limitations.

The building energy demand is derived from dynamic simulation based on assumptions related to occupancy schedules, which may not fully reflect real user behaviour, while internal gains and system operation are defined according to standard values and typical modelling practices. In particular the natural ventilation is modelled through the an external plug in which may not fully represent real airflow conditions. This limitation is also evident when compared with commercial tools such as Termo, leading to potential deviations in the estimation of energy needs. In addition, thermal bridges are not explicitly considered, which may affect the accuracy of heat transfer through the building envelope.

The REC configuration scenarios are developed based on a specific case study and real implementation constraints, including the absence of energy storage systems. As a result, alternative configurations involving batteries or advanced energy management strategies are not explored, which may limit the generalization of the results. Furthermore, the economic assessment is based on incentive tariff structures representative of the Italian regulatory context, which may differ from those in other countries and affect the transferability of economic results.

Finally, the SDG-based evaluation relies on a selected set of quantitative indicators, which capture key environmental, economic, and social aspects, but may not fully represent the broader multidimensional impacts of Renewable Energy Communities.

3.5 Future Work

Future work should address the identified modelling limitations by improving the representation of thermal bridges and natural ventilation, in order to achieve a more accurate definition of building energy demand profiles.

The analysis could be further extended by integrating energy storage systems and demand response strategies, with the aim of enhancing the temporal alignment between electricity demand and photovoltaic generation within REC configurations.

Further developments should also consider the application of the methodology to different urban contexts, building typologies, and regulatory frameworks, to assess its robustness and transferability.

4. Sustainability of ports and port hinterlands in terms of Energy Efficiency

4.1 Introduction

As highlighted in Chapter 3, the performance of Renewable Energy Communities is strongly influenced by the temporal distribution of electricity demand and its interaction with photovoltaic generation. However, the modification of demand profiles is not only relevant for REC performance, but also represents a central aspect of current European energy policies. In particular, energy efficiency in buildings is a key priority within the European Green Deal and the Renovation Wave Strategy, which aim to decarbonize the building stock and achieve zero-emission targets by 2050. In this context, improving the thermal performance of building envelopes plays a fundamental role in reducing energy demand and associated costs. Among the available measures, thermal insulation is one of the most effective strategies, as it directly affects both heating and cooling requirements and their seasonal distribution. The evaluation of the optimal insulation thickness is therefore a critical aspect in building design and retrofitting, as it allows the minimization of annual energy costs while ensuring efficient energy performance.

A previous study [172] has shown that, for residential buildings, the optimal insulation thickness typically ranges between 12 and 14 cm, independent of building geometry. However, such results cannot be directly extended to other building typologies, such as educational buildings, which are characterized by different occupancy patterns, internal loads, and operating schedules.

For this reason, this chapter investigates the optimal insulation thickness for a school building, evaluating its impact on annual energy demand and energy costs. Subsequently, the analysis explores how the resulting modifications in the consumption profile influence the interaction between electricity demand and photovoltaic generation, and their implications for the performance of Renewable Energy Communities.

4.2 State of the art on optimal insulation thickness

Energy consumption in the building sector remains one of the primary contributors to global energy use and greenhouse gas emissions, particularly due to space heating and cooling demands. In Europe and specifically in Italy, residential and service-sector buildings account for a significant share of final energy consumption, with space heating historically dominant. National and European policy frameworks, such as the National Energy and Climate Plan (NECP) and the Energy Performance of Buildings Directive (EPBD), have established increasingly stringent requirements for building envelope performance and energy efficiency [187-188]. This has spurred efforts to improve thermal insulation and reduce energy demand in the built environment.

Thermal insulation of building envelopes has long been recognized as an effective strategy for reducing heating energy consumption. Early studies on optimal insulation thickness, mainly developed during the 1970s–1990s, focused predominantly on heating-dominated climates and relied on simplified steady-state methods, such as degree-day approaches, to determine energy performance [189-191]. These works demonstrated that while increasing insulation generally reduces heating demand, the marginal benefits diminish beyond a certain threshold, leading to the identification of optimal ranges for insulation thickness.

More recent research has expanded the analysis by considering not only heating energy but also cooling loads, particularly in warm and Mediterranean climates where cooling demand has increased significantly in recent decades [172], [192-194]. Several studies have observed that excessive insulation can inadvertently increase cooling demand and cause overheating, especially in buildings with high internal gains, highlighting the need for annual energy balance methods that account for both heating and cooling [172], [194-195]. As a result, the determination of optimal insulation thickness now often involves both heating and cooling considerations rather than heating alone.

Within this context, Borelli et al [172] proposed a methodology to evaluate optimal insulation thickness for reinforced concrete buildings with cavity walls across different climatic zones by analyzing total annual energy demand, including both heating and cooling loads.

That study extended traditional approaches by including cooling energy and showed that the optimal insulation range can vary significantly with climate and building characteristics, often lower than regulatory limits in mild climates.

Alongside these developments, there has been a notable shift toward the use of dynamic whole-building simulation tools such as EnergyPlus and OpenStudio to evaluate building performance and insulation strategies. Dynamic simulation environments allow for detailed transient heat transfer modeling, incorporation of occupancy schedules, HVAC system interactions, and realistic weather data, which are essential for accurate assessment in both heating and cooling seasons. Works by Brackney et al [196] and An at al [197] used EnergyPlus and OpenStudio to explore building envelope optimization and energy performance, demonstrating that simulation-based approaches provide more nuanced insights into insulation effects under actual operating conditions [198, 199]. Similarly, Li et al. [200] employed an Energy-Plus-based framework to optimize insulation for a typical rural residential building in a severe cold region, highlighting the need for high insulation thickness. Other studies employed an Energy-Plus to simulate the energy saving by considering different green roof solutions [201, 202].

Recent studies underline that the optimal insulation thickness should be defined not only by regulatory limits but also by energy, economic, and environmental performance [203]. Özturan at al. [204] shows that orientation and solar radiation significantly affect the optimal thickness by influencing both heating and cooling demand. Likewise, Dylewski in his study demonstrates that the optimal thickness represents a compromise between economic and ecological benefits and varies with energy prices, material costs, climatic conditions, and environmental impacts, highlighting the importance of integrated decision-making in thermal retrofitting [205].

Building on this evolving body of work, the present thesis continues the research initiated in Borelli et al [172] by adopting a dynamic simulation methodology using OpenStudio/EnergyPlus to evaluate the influence of insulation thickness in a non-residential context. Unlike the previous study, which focused on residential buildings and followed standardized procedures aligned with Italian regulations, the current analysis employs OpenStudio/EnergyPlus to simulate the annual energy performance of a municipal school building characterized by distinct occupancy patterns, internal loads, and operating schedules. This approach enables a more comprehensive evaluation of insulation strategies under realistic conditions and contributes further insight into the role of envelope optimization in enhancing energy efficiency and sustainability.

4.3 A Methodology to evaluate the optimal Insulation thickness for heating and cooling needs in different climatic zones for buildings made of r.c and cavity walls

The study summarized in this section was carried out during the PhD program, with the author acting as one of the main contributors and was published in a peer-reviewed journal [172]. The work is included in this thesis as it represents a foundational contribution upon which the subsequent analyses are developed.

Specifically, the study presented in Borelli et al [172] proposed a methodology for determining the optimal insulation thickness for residential buildings made of reinforced concrete with cavity walls of different geometry (see Figure 139) and across different climatic zones. The analysis was based on the evaluation of the total annual energy demand, explicitly accounting for both heating and cooling needs, thereby extending traditional approaches that focus primarily on heating performance.

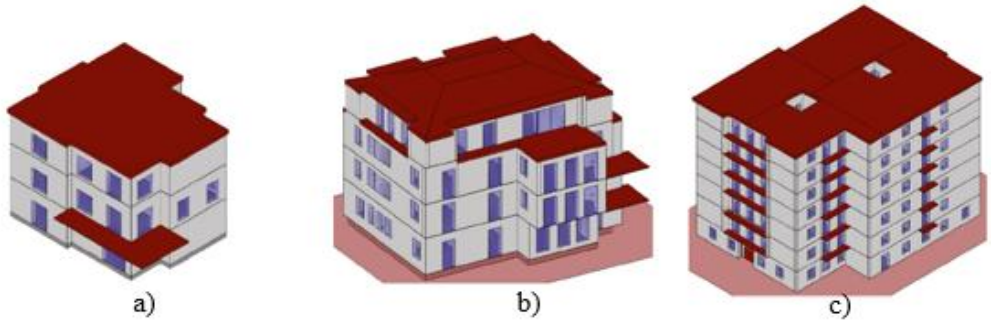

Figure 139. 3D model of the single-family building (a), semi-detached building (b) and a multistorey apartment building (c) used for the study.

The adopted methodology relies on an annual energy balance and demonstrates that, while increasing insulation thickness consistently reduces heating demand, it may also lead to an increase in cooling demand in certain climatic conditions. As a result, the total annual energy demand exhibits a minimum at specific insulation thickness ranges, beyond which additional insulation provides only marginal benefits. This behavior highlights the importance of considering both seasonal effects when defining insulation strategies, particularly in mild and Mediterranean climates.

The study identified optimal insulation thickness ranges as a function of climatic zone and building compactness, expressed through the surface-to-volume ratio (S/V). As reported in Table 35, the optimal insulation thickness generally increases with colder climatic conditions, while remaining consistently lower than or comparable to the thickness required to meet legislative transmittance limits in several zones.

Table 35. Comparison between the optimal insulation thickness carried out in the study and the range of thickness mandatory to respect the limit transmittance.

Climatic zone	Insulation range to respect legislative limits (U=0.027 W/m²K)	Single-family building (a) (S/V=0.818 1/m)	Semi-detached building (b) (S/V=0.504 1/m)	Apartment building (c) (S/V= 0.359 1/m)
B	7–12	8–10	8–10	8–10
C	9–12	10–12	10–12	10–12
D	10–15	12–14	12–14	12–14
E	11–17	14–16	14–16	14–16
F	12–18	14–16	14–16	14–16

For climatic zone D, which is of particular relevance to the present work, the optimal insulation thickness was found to lie in the range of 12–14 cm, largely independent of building geometry. This trend is further confirmed by the correlation between optimal insulation thickness and heating degree days (HDD), illustrated in Figure 140.

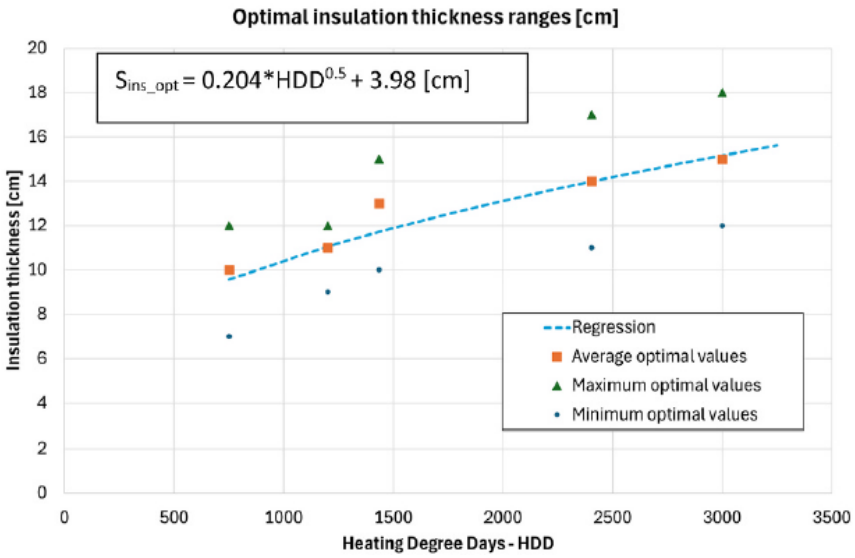

Figure 140. Optimal insulation thickness according to the heating degree days (HDD). Simulated values and the regression line.

Overall, the results demonstrate that excessive insulation does not necessarily lead to proportional reductions in total energy demand and that optimal insulation thickness should be defined by balancing heating and cooling requirements rather than by regulatory constraints alone. These findings provide a consistent methodological and conceptual basis for the present study, which further investigates insulation performance using a dynamic simulation approach and applies the analysis to a different building typology.

4.4 Evaluation of optimal insulation thickness in the A. Volta school

This section describes the methodology adopted to evaluate the optimal insulation thickness for the A. Volta school building. In this study, the term '*Optimal insulation thickness'* is defined as the thickness that minimizes the annual energy cost, derived from simulated heating and cooling energy needs and corresponding energy prices.

So, the assessment is based on the variation of energy demand as a function of insulation thickness and its impact on annual operating costs. The optimal value is identified as the point at which further increases in insulation thickness do not yield additional reductions in total annual energy cost. This definition does not rely on a cost–benefit or life-cycle analysis and excludes capital investment and payback considerations, focusing solely on operational energy performance.

This approach is consistent with the regulatory and policy framework adopted at both national and European levels, where building envelope interventions are primarily driven by the need to comply with minimum thermal transmittance requirements rather than by

purely economic optimization criteria. In Italy and other EU countries, envelope refurbishment measures are often mandatory to meet the targets established by the European Green Deal, which aim to progressively decarbonize the building stock.

Within this context, insulation is not treated as an optional investment subject to cost–benefit evaluation, but as a necessary measure to achieve required energy performance levels. Therefore, the present analysis focuses on identifying the insulation thickness that minimizes annual energy costs once the intervention is assumed, rather than evaluating its economic feasibility. A full cost–benefit or life-cycle analysis could represent an additional layer of assessment; however, it falls outside the scope of this study, which is primarily aimed at analyzing the impact of insulation on energy demand and consumption profiles.

The definition of the building energy model, occupancy schedules and HVAC systems, and photovoltaic system sizing has been presented in a previous chapter 3.2.4 and will be not repeated here.

The reference envelope configuration was defined based on available design documentation and consists of the existing, uninsulated construction stratigraphies of the external walls and the flat roof, summarized in Figure 141 and Figure 142, respectively. The external wall is composed of a double-layer perforated brick masonry with an internal air cavity and lime and gypsum plaster finishes, resulting in an overall thickness of 40 cm and a thermal transmittance of 1.08 W/m²K (see Figure 141). The flat roof consists of bituminous waterproofing, concrete screed, a slab with brick blocks and concrete joists, and an internal plaster layer, with a total thickness of 30 cm and a thermal transmittance of 1.51 W/m²K (see Figure 142).

External wall

N	Description from internal to external	Thickness [cm]	R [m²K/W]
1	Lime and gypsum plaster	2,0	0,029
2	Perforated bricks (800 kg/m³) thickness 80 mm	8,0	0,200
3	Air cavity horizontal flow 150 mm	15,0	0,184
4	Perforated bricks (800 kg/m³) thickness 120 mm	12,0	0,310
5	Lime and gypsum plaster	3,0	0,033
Total thickness		40,0	
Thermal transmittance [W/m²K]		1,080	

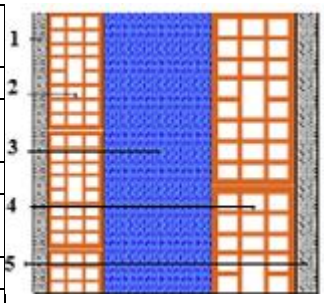

Figure 141. Stratigraphy and thermal properties of the external wall

Flat roof

N	Description from up to down	Thickness [cm]	R [m²K/W]
1	Bitumen	2,0	0,118
2	Ordinary concrete screed (1700 kg/m³)	8,0	0,075
3	Slab (brick blocks + concrete joists) 160 mm + cement mortar 20 mm	18,0	0,300
4	Lime and gypsum plaster	2,0	0,029
Total thickness		30	
Thermal transmittance [W/m²K]		1,511	

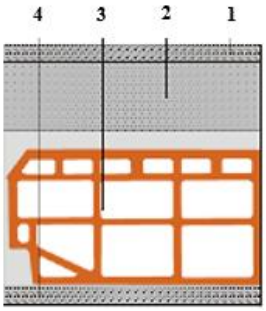

Figure 142. Stratigraphy and thermal properties of the flat roof

To ensure consistency with the previous study [172], the same insulation material has been selected for this analysis, specifically the Siferite insulation material. The Stiferite Class SK is a thermal insulation material composed of rigid polyisocyanurate (PIR) foam, faced on both sides with saturated fiberglass.
The thermal conductivity of this insulation, reported in Table 36, varies according to the material thickness. For thicknesses between 80 and 100 mm, the conductivity decreases to 0.026 W/mK, while for thicknesses ranging from 120 to 200 mm, it further decreases to 0.025 W/mK.

Table 36. Conductivity values varying the thickness

d [mm]	λ_D [W/m·K]	R_D [m²·K/W]	U_D [W/m²K]
20	0.028	0.71	1.40
30		1.07	0.93
40		1.43	0.70
50		1.79	0.56
60		2.14	0.47
70		2.50	0.40
80	0.026	3.08	0.33
100		3.85	0.26
120	0.025	4.80	0.21
140		5.60	0.18
160		6.40	0.16
180		7.20	0.14
200		8.00	0.12

In terms of reaction to fire, the material is classified as Euroclass E. In addition, it exhibits good resistance to water vapour diffusion. The thermal conductivity of the material has been tested in accordance with UNI EN ISO 14025 [206] and UNI EN 15804 [207] standards.

The evaluation was performed through a parametric analysis by progressively increasing the insulation thickness applied to the opaque envelope components. Insulation thicknesses ranging from 2 cm to 18 cm were investigated, with an increment of 2 cm

between consecutive configurations. For each insulation level, the thermal resistance of the envelope was updated accordingly, while all other building parameters were kept unchanged. The impact of insulation thickness on building performance was assessed by extracting the annual heating and cooling energy demand from the simulations, which were subsequently used to identify the insulation thickness range associated with minimum total annual energy demand and to support the evaluation of energy consumption costs.

4.4.1 Results of the Insulation Thickness Parametric Analysis

Heating and cooling energy demand

This section presents the results of the parametric analysis carried out to evaluate the influence of insulation thickness on the energy performance of the A. Volta school building. The analysis focuses on the variation of annual heating and cooling energy demand as a function of the insulation thickness applied to the opaque envelope components.

The results show that the annual heating energy demand decreases monotonically with increasing insulation thickness. The most significant reductions in heating demand occur at low insulation thicknesses because the initial increase in thermal resistance strongly reduces heat losses through the envelope. As insulation thickness increases, the overall heat transfer coefficient decreases, but at a progressively lower rate, leading to diminishing reductions in heat losses and, consequently, smaller energy savings.

In contrast, the annual cooling energy demand increases with increasing insulation thickness. This behaviour is associated with the reduced heat transfer through the building envelope, which limits the dissipation of internal and solar heat gains during the summer period. Higher insulation levels reduce the ability of the building to release accumulated heat, particularly during night-time, leading to a greater retention of internal gains and higher indoor temperatures. As a result, the cooling demand increases, especially under conditions characterized by significant internal loads and occupancy patterns typical of school buildings.

The quantitative results of the parametric analysis are reported in Table 37, which presents the annual heating and cooling energy demand corresponding to each insulation thickness configuration. These results provide the basis for identifying the insulation thickness range that ensures the best compromise between winter and summer performance and for the subsequent evaluation of energy consumption costs.

Table 37. Heating and cooling need in kWh

Building type		**School building ANTE**		**School building POST**									
Insulation thickness		No insulation		Stiferite = 2cm		Stiferite = 4cm		Stiferite = 6cm		Stiferite = 8cm		Stiferite =10 cm	
Clim. zone	Months	QH,nd	QC,nd	QH,nd	QC,nd	QH,nd	QC,nd	QH,nd	QC,nd	QH,nd	QC,nd	QH,nd	QC,nd
Zone D, Genoa	Jan	38,238.61		28,141.11		24,627.67		22,468.72		20,046.78		19,723.86	
	Feb	36,570.00		26,080.59		22,869.31		20,929.81		19,120.17		18,785.06	
	Mar	33,812.50		25,666.11		22,464.36		20,524.94		19,274.00		18,990.75	
	Apr	9,902.44		7,855.42		7,197.36		6,730.39		6,383.72		6,369.14	
	May		653.96		967.36		1,279.06		1,469.42		1,655.44		1,665.12
	Jun		1,010.71		1,308.70		1,619.16		1,665.83		1,740.79		1,823.98
	Jul		171.71		168.07		168.88		173.35		175.03		186.24
	Aug		108.48		124.43		140.25		148.26		156.40		162.47
	Sep		568.93		683.86		1,063.25		1,307.19		1,567.17		1,660.56
	Oct		347.56		409.88		483.89		555.36		688.72		734.89
	Nov	32,233.06		23,899.11		21,480.69		19,679.56		18,311.03		18,133.72	
	Dec	24,975.42		17,526.28		14,945.47		13,394.08		12,341.44		12,040.67	
TOTAL		**175732.03**	**2861.35**	**129168.62**	**3662.30**	**113584.86**	**4754.49**	**103727.50**	**5319.41**	**95477.14**	**5983.55**	**94043.20**	**6233.26**

School building POST							
Stiferite = 12cm		Stiferite = 14cm		Stiferite = 16cm		Stiferite = 18cm	
QH,nd	QC,nd	QH,nd	QC,nd	QH,nd	QC,nd	QH,nd	QC,nd
19,419.03		19,114.19		19,003.83		18,893.47	
18,505.24		18,225.42		18,096.12		17,966.81	
18,892.89		18,795.03		18,757.91		18,720.78	
6,354.43		6,339.72		6,301.57		6,263.42	
	1,801.73		1,938.33		1,935.23		1,932.13
	1,793.93		1,763.88		1,880.72		1,997.56
	186.23		186.21		191.76		197.30
	166.78		171.08		174.72		178.35
	1,756.73		1,852.89		1,899.79		1,946.68
	866.95		999.00		1,107.62		1,216.24
17,538.81		16,943.89		16,286.20		15,628.50	
11,962.10		11,883.53		11,819.61		11,755.69	
92672.49	**6,572.33**	**91,301.78**	**6,911.39**	**90,265.23**	**7,189.83**	**89,228.67**	**7,468.26**

These results provide the basis for identifying an insulation thickness range that ensures a balanced performance between heating and cooling energy demand. The implications of this balance are further analyzed in terms of energy consumption and associated costs in the following subsection.

Insulation Thickness Analysis and Energy Cost Implications

The results of the heating and cooling demand presented previously in the Table 37 are reported now in the Figure 143, where the cooling demand is reported with negative values to facilitate the visualization of its variation in relation to heating demand, allowing a clearer comparison of the opposite trends without ambiguity. The parametric analysis highlights the dependence of heating and cooling energy demand on insulation thickness. As expected, the results show that the heating energy demand decreases with increasing insulation thickness, with the most significant reduction occurring within the first 2 cm of insulation.

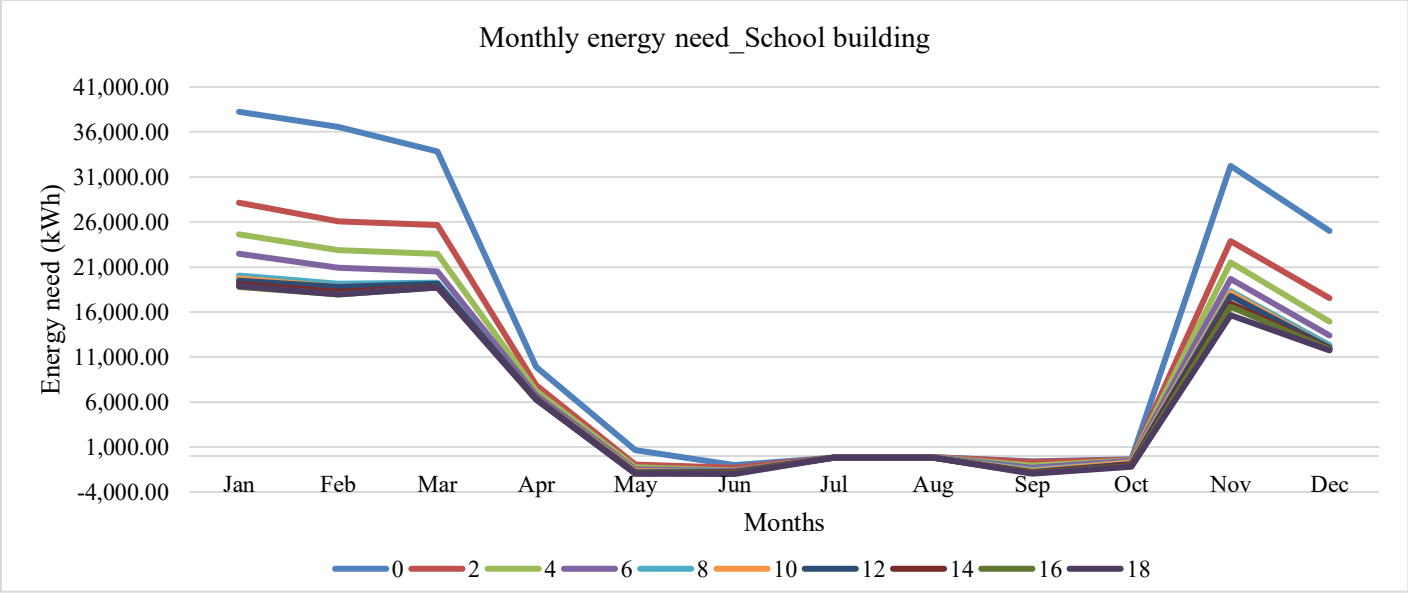

Figure 143. Monthly energy need varying the insulation thickness

Beyond the initial range, further increases in insulation thickness lead to progressively smaller reductions in heating demand, as the additional thermal resistance provides a decreasing contribution to the reduction of heat losses through the envelope. During the heating season, it is evident that beyond insulation thicknesses of approximately 8–10 cm, the heating energy demand curves tend to overlap, indicating that transmission losses have already been substantially reduced and that further increases in insulation thickness have a limited impact on heat transfer. In contrast, the cooling energy demand increases continuously with increasing insulation thickness. This behaviour is physically associated with the reduced heat transfer through the envelope, which limits the dissipation of internal and solar gains and leads to greater heat retention within the building.

This opposite trend highlights the trade-off between winter and summer performance and reinforces the need for a combined assessment of heating and cooling energy use when defining an optimal insulation thickness.

To better identify the insulation thickness that minimizes overall energy expenditure, the calculated heating and cooling energy demands were converted into annual energy costs by applying current energy prices of 0.10 €/kWh for natural gas and 0.30 €/kWh for electricity. The resulting annual energy costs for climatic zone D, as a function of insulation thickness, are reported in Figure 144. The results clearly indicate that annual energy costs decrease significantly up to an insulation thickness of about 8–10 cm, while further increases lead to only negligible additional savings. In particular, beyond 10 cm, the reduction in annual energy cost becomes marginal, with variations below 0.3% for subsequent thickness increments. This confirms that insulation thicknesses greater than 10 cm do not provide substantial economic benefits in terms of energy cost reduction for the analyzed climatic conditions.

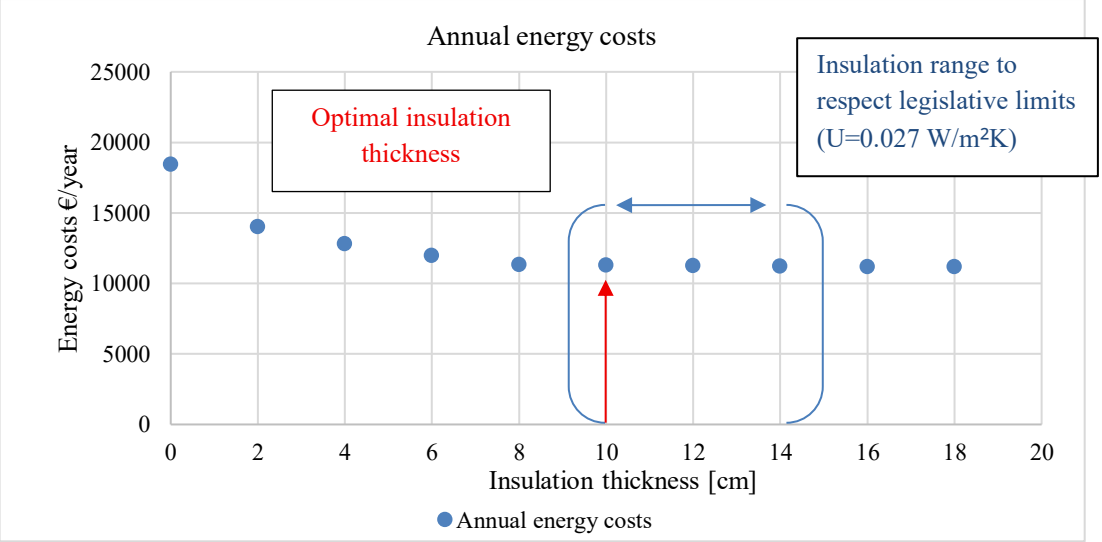

Figure 144. Annual energy costs varying the insulation thickness

It is therefore important to emphasize that the identification of this insulation thickness as *"optimal"* is based exclusively on the criterion of annual energy cost reduction (see 4.4). As discussed in 3.2.4, the simulations were performed using OpenStudio, which does not explicitly account for thermal bridges and provides a simplified representation of natural ventilation. In addition, the model does not include Italian regulatory compliance checks, such as those required under Law 10 [208] or under the updated Minimum Energy Performance Requirements introduced by D.M. 28 October 2025 [167], published in the *Gazzetta Ufficiale* on 5 December 2025 and entering into force on 3 June 2026, which updates and integrates D.M. 26 June 2015 [174]. Consequently, the results should be interpreted as a performance-based assessment, rather than as a verification of compliance with current or forthcoming regulatory frameworks.

4.4.2 Discussion and implications

The results obtained for the A. Volta school building are consistent with the insulation thickness ranges required to comply with maximum transmittance limits for opaque envelope components. The optimal insulation thickness identified in this study (≈10 cm) is slightly lower than the 12–14 cm range typically found for residential buildings.

The parametric analysis confirms the presence of diminishing returns with increasing insulation thickness. While heating demand continues to decrease for higher insulation levels, the associated energy cost reduction becomes progressively smaller. At the same time, the increase in cooling demand becomes dominant, progressively outweighing the marginal savings in heating energy cost and leading to an increase in total annual energy cost beyond the optimal range.

The lower optimal insulation thickness observed in this case is therefore mainly attributable to the higher sensitivity of the building to cooling demand. Increased thermal resistance limits heat transfer through the envelope, reducing the dissipation of internal and solar gains and leading to greater heat retention during occupied periods. This effect is particularly relevant for school buildings, characterized by high internal loads and daytime operation, which amplify cooling requirements and shift the balance between winter and summer performance.

The adoption of a dynamic simulation approach enables the explicit representation of hourly variations in heating and cooling demand, allowing a detailed assessment of seasonal trade-offs. This is particularly relevant for educational buildings, where occupancy patterns and internal gains significantly influence cooling demand.

The modelling framework adopts simplified representations of natural ventilation and does not explicitly account for thermal bridges, which may affect absolute energy demand values. Nevertheless, the analysis provides a robust assessment of relative trends,

enabling the identification of the insulation thickness range associated with minimum annual energy cost.

Overall, the results provide a reliable basis for the preliminary evaluation of insulation strategies in educational buildings, highlighting the importance of considering both heating and cooling effects. However, any retrofit solution should be subsequently verified in accordance with the Italian regulatory framework, including Law 10 [208] and the minimum energy performance requirements defined by D.M. 28 October 2025 [167].

4.5 Incentive Framework for Public Administrations

Italy's energy efficiency and renewable energy policies are framed within the broader European Union climate strategy, which aims to reduce net greenhouse gas emissions by at least 55% by 2030 compared to 1990 levels and to achieve climate neutrality by 2050, as established by the European Climate Law. Within this framework, particular emphasis is placed on the building sector, which represents a significant share of final energy consumption and associated emissions, especially due to space heating and cooling.

While the European Commission defines the overarching regulatory framework and climate objectives, the implementation of incentive mechanisms is delegated to Member States. In this context, the Italian Government has introduced national support schemes to promote energy efficiency improvements and the integration of renewable energy systems in buildings, with a specific attention also to the public sector. These measures are intended to translate European decarbonization targets into concrete actions at the local level, addressing both energy consumption reduction and emission mitigation.

Among the national instruments currently in force, the Thermal Energy Incentive Scheme 'Conto Termico 3.0' [209] represents one of the main incentive schemes dedicated to Public Administrations. The scheme provides capital grants for energy efficiency interventions on building envelopes and energy systems, with incentive rates typically ranging from 40% to 65% of eligible costs. For specific categories of buildings, such as schools, hospitals, and buildings owned by municipalities with fewer than 15,000 inhabitants, the incentive may cover up to 100% of eligible costs, including expenses related to energy audits and Energy Performance Certificates directly connected to the incentivized interventions. Applications must be submitted through the GSE Portale Termico within 90 days from the completion of the intervention, in accordance with the procedures defined in the scheme's application rules.

In this context, the insulation strategies analyzed in the present study can be coherently discussed with respect to the objectives of the Thermal Energy Incentive Scheme 3.0. Although the analysis does not include an assessment of investment costs, it identifies an

insulation thickness range that minimizes annual energy demand and energy consumption costs, highlighting the presence of diminishing returns beyond a certain insulation level. This outcome is fully aligned with the rationale of the incentive framework, which aims to promote technically efficient and non-over-dimensioned retrofit solutions capable of delivering substantial energy savings without unnecessary increases in material use.

Therefore, the results of this study can support preliminary design decisions by Public Administrations, providing a technical basis for selecting envelope insulation measures that are consistent with both energy performance objectives and the structure of national incentive schemes. Final design choices and implementation, however, must be accompanied by the required regulatory verifications under the Italian normative framework, including Law 10 [208] and the Ministerial decree regarding the Minimum Requirements D.M. 28 Ottobre 2025 [167].

4.6 Implications for Renewable Energy Community (REC) Scenarios

The reduction in building energy demand resulting from the insulation measures has direct implications for Scenario 3, which represents the most balanced REC configuration identified in the previous analysis. In this scenario, the electricity demand of the A. Volta school constitutes a significant share of the local load, directly affecting the level of PV self-consumption and the amount of energy available for sharing within the community.

The insulation intervention modifies the building's electricity demand profile, primarily through a reduction in heating-related electricity consumption. This effect is mainly associated with the decrease in operating hours of the heating circulation pumps during the winter season, which represents the dominant contribution to the reduction in annual electricity demand, as shown in Table 38.

Table 38. Annual electricity consumption by end use for the baseline and insulated building configurations

End use	Annual electricity – no insulation (kWh)	Annual electricity – 10 cm insulation (kWh)	Variation (%)
Cooling	2,861.34	6,233.32	**+117.8%**
Interior lighting	24,109.01	24,109.01	**0.0%**
Interior equipment	2,776.80	2,776.80	**0.0%**
Fans	230.64	504.92	**+118.9%**
Pumps	22,269.36	17,227.67	**−22.6%**

Conversely, the increase in thermal resistance leads to higher cooling-related electricity consumption compared to the baseline configuration. This effect is particularly evident during the summer and early autumn months, where the reduced heat transfer through the envelope limits the dissipation of internal and solar gains, resulting in greater heat

retention and increased cooling demand, as reflected in the monthly electricity consumption reported in Table 39.

Despite this seasonal redistribution of electricity demand profile, Table 39 shows an overall reduction in annual electricity consumption, decreasing from 52,247.15 kWh in the baseline configuration to 50,851.71 kWh after the insulation intervention. From the perspective of Scenario 3 of the REC configurations discussed in 3.2.8, this reduction in annual demand implies that, for a fixed installed PV capacity, a larger share of the building's electricity demand can be met by on-site PV generation. As a consequence, a greater share of PV electricity becomes available for intra-community sharing, particularly during periods of high solar production or when there is a mismatch between electricity demand and PV generation in terms of timing and magnitude.

Table 39. Monthly energy consumption by end use for the baseline and insulated building configurations

Month	Total electricity – no insulation (kWh)	Total electricity – 10 cm insulation (kWh)	Variation (%)
Jan	7,037.91	6,406.99	−9.0%
Feb	7,418.63	6,504.99	−12.3%
Mar	7,424.54	6,448.66	−13.1%
Apr	4,788.64	4,529.79	−5.4%
May	3,972.43	5,066.07	+27.6%
Jun	2,517.92	3,397.11	+34.9%
Jul	356.36	371.80	+4.3%
Aug	273.32	331.58	+21.3%
Sep	1,764.41	2,945.81	+66.9%
Oct	3,788.42	4,206.75	+11.0%
Nov	7,425.52	5,976.80	−19.5%
Dec	5,479.05	4,665.38	−14.9%
Annual	**52,247.15**	**50,851.71**	

This reduction in annual electricity demand enhances the operational flexibility of the REC configuration, enabling a more efficient allocation of locally generated renewable energy. In particular, it allows either an increase in intra-community energy sharing among existing members or the integration of additional consumers without modifying the installed PV capacity, thereby supporting more inclusive REC configurations.

Based on these considerations, Scenario 4 is defined by adopting the post-intervention electricity demand profile while maintaining the same community structure as Scenario 3. The updated hourly demand profile is implemented in PVsyst to simulate the energy balance between photovoltaic generation, on-site self-consumption, and grid export.

The resulting system performance is illustrated through the loss diagram and summarized by the energy balance indicators reported in the corresponding Loss diagram in Figure 145 and better exploited in Table 40.

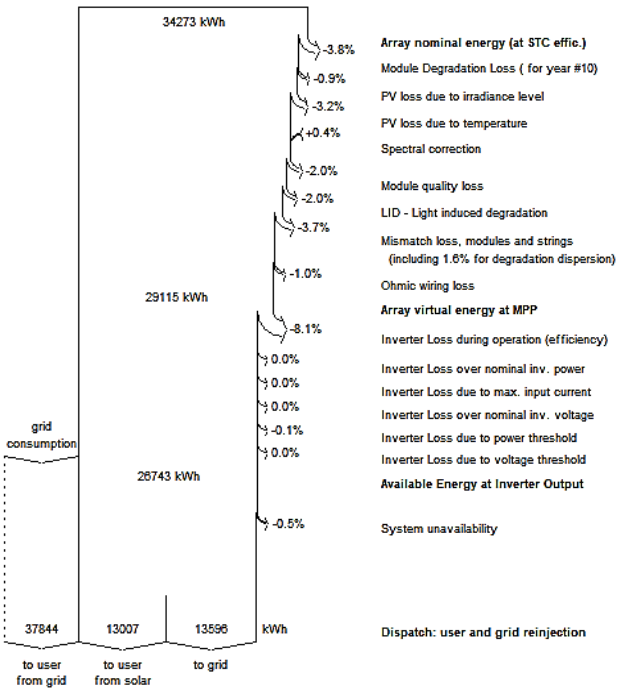

Figure 145. Loss diagram considering the new consumption profile after the insulation

Month	E.Avail [kWh]	E.User [kWh]	E.Self-cons. [kWh]
Jan	1,207	6,407	1,029
Feb	1,256	6,505	1,113
Mar	2,495	6,449	1,878
Apr	2,621	4,530	1,700
May	2,963	5,066	1,946
Jun	3,330	3,397	1,066
Jul	3,432	372	336
Aug	3,156	332	281
Sept	2,468	2,946	1,084
Oct	1,732	4,207	1,240
Nov	1,045	5,977	840
Dec	899	4,665	495
Year	**26,604**	**50,852**	**13,007**

Table 40. Monthly energy balance

The updated demand profile results in a reduction in electricity consumption during the winter season, due to lower heating-related loads, which leads to a decrease in on-site self-consumption in winter months (see Figure 146, and Figure 147). Conversely, during the summer season, the increase in cooling-related electricity demand leads to higher on-site self-consumption, as a larger share of photovoltaic generation is directly matched by the building demand.

Figure 146. Monthly energy consumed distribution of the Base case REC configuration

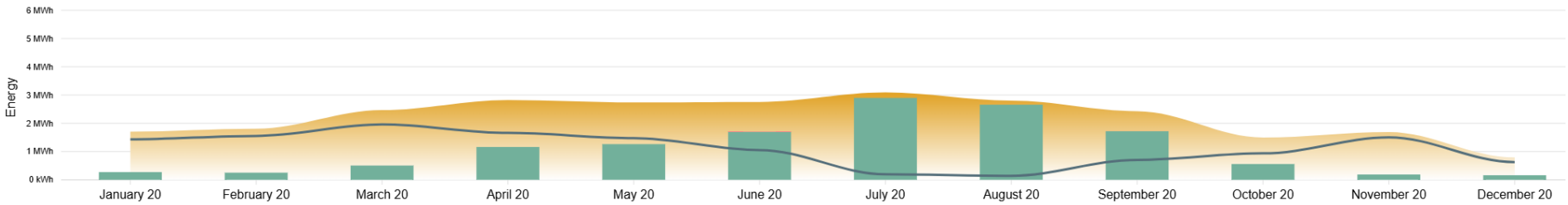

Figure 147. Monthly energy consumed distribution after the insulation intervention

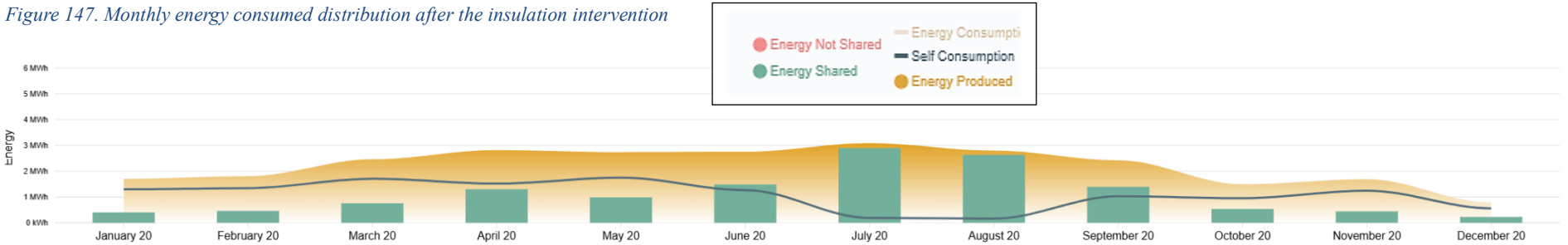

Revenues

Based on the energy profile of the REC shown in Figure 148, the annual revenues obtained for the updated configuration are slightly lower than those of the reference Scenario 3 or "Optimal scenario" presented in 3.2.8, decreasing from 5,722.22 €/year to 5,672.37 €/year (see Table 41).

Table 41. Revenues definition

Revenues	**Amount**		**Price**		**Value**	
Physical self-consumption	13,040.00	kWh/year	0.30	€/kWh	3,912.00	€/year
Energy virtually consumed	13,540.00	kWh/year	0.13	€/kWh	1,760.20	€/year
Energy surplus not shared	2.13	kWh/year	0.08	€/kWh	0.17	€/year
Total					**5,672.37**	**€/year**

This variation is mainly attributable to the reduction in self-consumed energy following the insulation intervention. Since the incentive associated with self-consumed energy is higher than that granted for shared energy, the shift from self-consumption toward increased energy sharing results in a marginal decrease in total annual revenues, despite a more efficient overall utilization of locally generated renewable energy.

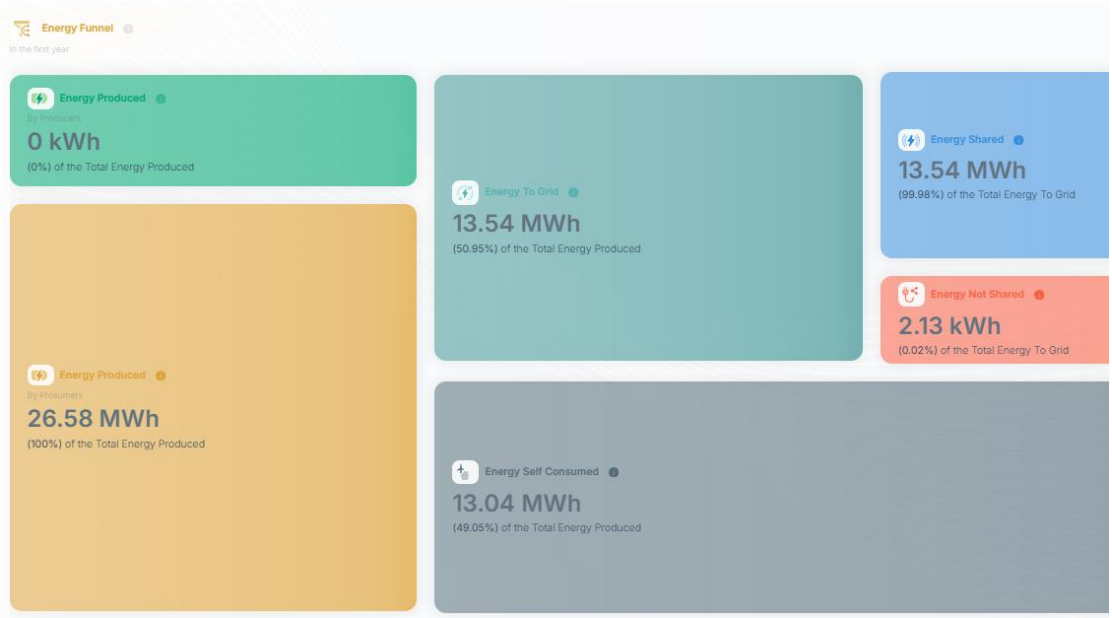

Figure 148. Energy flows inside the community

In general, within a Renewable Energy Community configuration, higher revenues are typically achieved by selecting prosumers characterized by a high and relatively continuous electricity consumption profile, as this maximizes the amount of energy that can be self-consumed. The resulting economic benefit is mainly driven by avoided electricity withdrawals from the grid, which are valued at the retail electricity tariff paid by the user and are therefore typically higher than the incentives associated with shared energy.

Referring to specific case study analyzed in this work, both the photovoltaic plant and the school building are owned by the municipality, and the choice of potential prosumers was therefore limited to PODs under municipal ownership. Within this constrained set of options, the school building emerges as the most suitable candidate due to higher consumption profile, despite its non-continuous load profile. However, this enables a substantial share of the photovoltaic generation to be effectively utilized during periods of reduced school activity (e.g., holidays and closures), which temporally align with the demand profiles of other REC members, thereby enhancing the overall utilization of locally generated energy within the community.

Accordingly, the resulting REC configuration can be considered optimal for the specific context analyzed, as it balances ownership constraints, energy demand characteristics, and effective utilization of locally generated renewable energy, while maintaining a satisfactory level of economic performance.

Table 42. Sustainability Performance of REC Configurations: Comparison of Scenarios 3 and 4 (SDG-Based Indicators)

Scenario	**SDG11 Economic Benefit [€]**	**SDG1 – Vulnerable Users [-]**	**SDG1 – Inclusion [%]**	**SDG7 – Local RES Use [%]**	**SDG7 – Energy efficiency [%]**	**SDG11 – Shared Energy [%]**	**SDG13 -CO_2 Savings PV plant [tCO_2/y]**	**SDG13 -CO_2 Savings Energy efficency [tCO_2/y]**
Scenario 3	5711.58	5	71	13.74	-	50	8.76	-
Scenario 4	5672.37	5	71	13.85	2.7	51	8.76	0.46

In particular, as shown in Table 42, Scenario 4 can be regarded as the most balanced configuration, despite a slight reduction in economic benefit of approximately 0.7% compared to Scenario 3. This configuration ensures an improved level of shared energy within the community (SDG11 ≈ 51%) and a slight increase in local renewable energy use (13.85% vs. 13.74% in Scenario 3), while maintaining comparable CO_2 savings associated with photovoltaic generation (8.77 tCO_2/y). In addition, the reduction in annual electricity demand resulting from the insulation intervention contributes to further CO_2 emission savings. This effect can be quantified as the product of the demand reduction (1,396 kWh/y) and the grid emission factor (EF = 0.33 $kgCO_2/kWh$), resulting in additional avoided emissions of approximately 0.46 tCO_2/y. This contribution highlights the role of energy efficiency as a complementary demand-side decarbonization measure.

Moreover, the social dimension remains unchanged, with the inclusion of five vulnerable users (SDG1) and an equivalent level of inclusion of 71%, confirming that the redistribution of energy within the REC does not compromise its social benefits.

Therefore, although Scenario 4 does not maximize economic returns, it represents the most sustainable solution, as it combines high levels of energy sharing (SDG11), consistent renewable energy utilization (SDG7), additional emission reductions through energy efficiency (SDG13), and stable social inclusion (SDG1).

4.7 Conclusions

This chapter evaluated the energy performance of the A. Volta school building through dynamic simulation, enabling the definition of time-resolved heating, cooling, and electricity demand profiles based on occupancy patterns and internal gains. The results show that increasing insulation thickness reduces transmission heat losses through the envelope during the heating season, while simultaneously limiting heat dissipation during the cooling season. As a consequence, the progressive increase in thermal resistance leads to a non-linear response of the annual energy balance, with decreasing heating demand and increasing cooling requirements. The optimal insulation thickness is therefore identified as the point at which the reduction in heating-related energy costs is balanced by the increase in cooling-related consumption, corresponding to the minimum of total annual energy costs. The parametric analysis indicates that this condition is reached at approximately 10 cm, beyond which additional insulation produces negligible net benefits due to the dominance of cooling-related energy use. Compared to residential buildings, the lower optimal thickness is attributable to the higher relevance of cooling demand as the increased thermal resistance limits heat dissipation, leading to greater retention of internal and solar gains and higher cooling requirements.

The identification of the optimal insulation thickness is based solely on operational energy performance and does not include a cost–benefit analysis of the investment. This approach is consistent with the regulatory framework, which imposes minimum transmittance requirements for building envelope refurbishment, making insulation measures mandatory rather than optional. In the Italian context, fiscal incentive schemes (e.g., tax deductions and public funding) can significantly influence the economic viability of such interventions by reducing upfront costs and affecting payback periods. Therefore, the analysis focuses on energy demand and system-level performance, while acknowledging that economic feasibility is partly determined by external policy conditions.

A key finding is that energy efficiency improvements do not necessarily enhance REC economic performance. Although the insulation intervention reduces electricity demand (2.7%), it alters the temporal alignment between demand and photovoltaic generation, leading to a shift from self-consumption to energy sharing (SDG11 increasing to 51%). As a result, a slight reduction in economic benefit (0.7%) is observed, despite improved intra-community energy exchange. At the same time, the intervention does not compromise system performance. Renewable energy utilization remains stable (SDG7 ≈13.8%), and social inclusion is preserved, while total CO_2 savings increase (8.77 tCO_2/y + 0.46 tCO_2/y from efficiency), reflecting the combined effect of local generation and reduced demand. Overall, these results highlight that energy efficiency acts as a complementary demand-side measure within RECs. While it may slightly reduce economic returns, it enhances environmental performance and supports a more balanced and sustainable configuration.

Overall, the results demonstrate that REC performance is governed not only by demand magnitude but also by its temporal alignment with renewable generation. Consequently, the definition of optimal insulation thickness and REC configurations should account for both heat transfer mechanisms and the time-dependent interaction between demand and energy production.

From a methodological perspective, the proposed approach is transferable to other building typologies and contexts, as it is based on the combined assessment of dynamic energy modelling, envelope performance analysis, and REC-level energy balance evaluation. By integrating time-resolved demand profiles with renewable generation and community energy sharing mechanisms, the methodology enables the systematic investigation of the interaction between energy efficiency measures and REC performance, and can be applied to different climatic conditions, usage patterns, and energy system configurations.

4.8 Limitations

The results are subject to modelling simplifications related to the representation of natural ventilation and the exclusion of thermal bridges, which may affect the accuracy of heat transfer through the building envelope as consequence the energy demand.

The analysis focuses on operational energy performance and energy savings and does not include a detailed economic evaluation of the insulation intervention. Although a cost–benefit analysis could provide additional insight, its results would be influenced by regulatory requirements and existing fiscal incentives. Therefore, it is not considered within the scope of this study, which is primarily aimed at assessing energy performance rather than investment feasibility. Furthermore, the findings are specific to the analyzed building typology and climatic context, and the interaction between energy efficiency and REC performance is evaluated under fixed system and community configurations, without considering adaptive strategies such as energy storage or demand response.

4.9 Future Work

Future work should focus on improving the representation of physical processes in the energy model, particularly through the explicit modelling of thermal bridges and a more accurate characterization of natural ventilation and airflow dynamics. The analysis should also be extended to include thermal comfort and overheating indicators, in order to assess the impact of insulation measures on indoor environmental conditions. Further developments should investigate the application of the methodology to different building typologies and climatic contexts, to evaluate its robustness and transferability.

Finally, the interaction between energy efficiency and REC performance could be further explored by integrating energy storage systems and demand response strategies, with the aim of improving the temporal alignment between electricity demand and renewable generation.

5. Overall Conclusions and Future Work

In this chapter are presented the main findings across all pillars and include (i) limitations/uncertainties, (ii) what is transferable to other ports vs site-specific, and (iii) a clear future research roadmap.

Pillar 1 – Environmental Acoustics

1.1 Source identification and characterization

The combined use of acoustic camera, phonometric measurements (short and long term) and Noise perception evaluation enables the precise identification and impact of dominant noise sources and their spatial distribution in port hinterland areas.

- *(i)* *Limitations:* the methodology is costly and time-demanding, requiring specialized instrumentation and expertise for data acquisition and interpretation, and results may vary depending on measurement duration and environmental conditions.
- *(ii)* *Transferability:* The measurement methodology is transferable, while results are site-specific.
- *(iii)* *Future work*: extend this methodology to different urban contexts beyond port areas, in order to assess its robustness and adaptability under varying environmental and operational conditions.

1.2 Dominance of traffic-related noise

When road infrastructure in port areas is located close to receptors, truck traffic becomes the dominant source, driven by tire–road interaction noise influenced by speed, axle load, and pavement characteristics.

- *(i)* *Limitations:* results are based on specific measurement conditions and do not fully capture variations.
- *(ii)* *Transferability:* the tire–road interaction mechanism is general, but its contribution depends on pavement type, road conditions, vehicle speed, and axle load, as well as local layout.
- *(iii)* *Future work:* extend the analysis to different pavement types and traffic conditions.

1.3 Noise mitigation through novel sound-absorbing materials

The results demonstrate that optimized porous and hybrid systems provide the highest acoustic performance, with absorption coefficients up to 0.95–1.0. Multilayer double-porosity materials show peak absorption in the 1500–2200 Hz range, governed by thickness-dependent dissipation mechanisms. Reticulated polyimide foams achieve α about 0.95–1.0 in the 700–1700 Hz range, due to increased pore interconnectivity. The best overall performance is obtained with perforated plates combined with porous layers, reaching α of 0.96 between 1800 and 2200 Hz and effective absorption from 1000 Hz, enabling compact and efficient mitigation solutions.

(i) *Limitations*: the acoustic performance is primarily concentrated in the mid-frequency range (700–2200 Hz), with reduced effectiveness at lower frequencies, particularly for thin multilayer and perforated configurations without optimized backing conditions.
(ii) *Transferability:* the experimental methodology (impedance tube characterization and configuration-based analysis) and the identified relationships between material structure, geometry, and acoustic performance are transferable.
(iii) *Future work:* Further optimization of perforation geometry and porous material properties is required to enhance broadband and low-frequency absorption.

1.4 Source-oriented mitigation strategies
The analysis confirms that low-noise pavements and acoustic barriers are effective mitigation solutions when designed according to source characteristics and propagation conditions.

(i) *Limitations*: mitigation performance assessed under specific boundary conditions.
(ii) *Transferability*: design principles are transferable, while performance depends on geometry and context.
(iii) *Future work*: develop multi-scale acoustic propagation models for design optimization.

Pillar 2 – Renewable Energy (PV + REC)

2.1 Temporal matching and demand diversification as key drivers of REC performance
REC performance is primarily governed by the temporal alignment between electricity demand and photovoltaic generation, as well as by the diversification of demand profiles, which improves the coincidence factor. In this context, Scenario 3 achieves high renewable energy utilization (99.8%) and significant energy sharing (50%).

(i) *Limitations:* based on deterministic demand and generation profiles.
(ii) *Transferability:* the methodology is transferable, while results depend on local demand patterns, user composition, and solar resource availability.
(iii) *Future work:* develop and assess more heterogeneous and scalable REC configurations.

2.2 Inclusiveness of REC configurations when activated by public buildings
REC configurations enable the inclusion of stakeholders constrained by economic, social,

or regulatory limitations, while maintaining high levels of energy sharing and economic performance supporting both system efficiency and social inclusion.

- *(i)* *Limitations:* based on a specific set of users and load profiles.
- *(ii)* *Transferability:* the principle is general, while effectiveness depends on community structure and local regulatory conditions.
- *(iii)* *Future work:* develop and propose targeted policy, regulatory, and financial mechanisms to incentivize private actors to implement inclusive REC models, improving access to renewable energy for vulnerable and energy-constrained users.

2.3 Multi-dimensional sustainability of REC configurations

REC scenarios presented achieve high performance across multiple dimensions, including shared energy (50–51%), renewable energy use (up to 25% of the total demand), CO_2 reduction (8.77 tCO_2/y from PV, with additional 0.46 tCO_2/y from energy efficiency), and social inclusion (up to 70%).

- *(i)* *Limitations:* SDG evaluation based on a limited set of indicators.
- *(ii)* *Transferability:* framework is transferable, while values depend on local context and policies.
- *(iii)* *Future work:* expand multi-criteria sustainability assessment.

Pillar 3 – Building Energy Efficiency and REC implication

3.1 Non-linear effect of insulation on energy demand

Increasing insulation thickness reduces heat losses but limits heat dissipation, leading to a non-linear energy balance with decreasing heating demand and increasing cooling demand.

- *(i)* *Limitations:* simplified modelling of ventilation without considering the thermal bridges.
- *(ii)* *Transferability:* the methodology is general, while results are building and site specific.
- *(iii)* *Future work:* overcome the issues of the natural ventilation and extend analysis to different climates and building types.

3.2 Definition of optimal insulation thickness

The optimal insulation thickness for the school building in climatic zone D (≈ 10 cm) is determined by the minimization of total annual energy costs (heating + cooling), resulting lower than the optimal one for the residential building at the same climatic zone due to higher internal gains and daytime occupancy.

- *(i)* *Limitations:* no cost–benefit analysis of investment included and limited accuracy of the natural ventilation calculation.

(ii) *Transferability:* methodology is transferable, while values depend on building typology and usage.

(iii) *Future work:* overcome the issues of the natural ventilation and extend analysis to different climates and building types.

3.3 Interaction between energy efficiency and REC performance

Energy efficiency reduces electricity demand (with 2.7%) and alters its temporal distribution, leading to lower self-consumption and increased shared energy, with a slight reduction in economic benefit (−0.7%).

(i) *Limitations:* based on a fixed REC configuration and tariff/incentive schemes specific to the Italian context.

(ii) *Transferability:* the observed behaviour is case-specific, as it depends on load profiles, insulation effects, and local photovoltaic generation patterns.

(iii) *Future work:* assess the reliability of this interaction across different building typologies, climates, and REC configurations, and integrate energy storage and demand response strategies to improve demand–generation alignment.

Overall, the three pillars, environmental acoustics, renewable energy systems, and building energy efficiency, contribute to a common objective: the improvement of environmental quality, energy performance, and human well-being in port–city systems. Although each domain is governed by distinct physical processes (i.e., sound propagation, heat transfer, and energy flows), the results highlight that they are inherently interconnected, as interventions in one domain can influence system performance in the others.

In this work, the acoustic pillar is primarily addressed as a parallel domain due to its specific methodologies. However, potential interactions with building energy performance cannot be excluded, as acoustic interventions may influence thermal behaviour at both buildings (sound-absorbing solutions may also affect thermal behaviour) and urban scales (acoustic barriers can modify microclimatic conditions, with possible implications for building energy demand). These cross-domain effects are not explicitly quantified in this study but represent a relevant direction for future research.

Conversely, building energy efficiency and renewable energy systems are directly coupled, as modifications in demand profiles influence REC performance, energy sharing, and economic outcomes. These findings demonstrate that sustainable port–city development requires a coordinated multi-domain approach, enabling the simultaneous optimization of environmental, energy, and social dimensions and supporting the design of resilient and integrated port hinterland systems.

References

[1] European Commission, "Ports," [Online]. Available:https://transport.ec.europa.eu/transport-modes/maritime/ports_en

[2] DNV GL, "Ports: Green Gateways to Europe," DNV, Norway, 2020. [Online]. Available: https://www.eurelectric.org/wpcontent/uploads/2024/06/ports_greengateways_executive-summary_final_29-06-2020.pdf

[3] J. Chen, W. Zhang, L. Song, and Y. Wang, "The coupling effect between economic development and the urban ecological environment in Shanghai port," vol. 841, no. 156734, 2022, doi: 10.1016/j.scitotenv.2022.156734.

[4] E. Bracker, "Shipbuilding and maritime transportation industries," in Impacts of Shipping on Environment and Climate. Cham, Switzerland: Springer, 2019, pp. 183–189.

[5] S. P. Parvasi, G. Panagakos, M. B. Barfod, and J. S. L. Lam, "Ports as energy hubs: Renewable energy integration and distribution," in Proc. 25th DNV Nordic Maritime Universities Workshop, Tech. Univ. Denmark, Kgs. Lyngby, Denmark, 2025.

[6] M. Viana, V. Rizza, A. Tobías, E. Carr, J. Corbett, M. Sofiev, A. Karanasiou, G. Buonanno, and N. Fann, "Estimated health impacts from maritime transport in the Mediterranean region and benefits from the use of cleaner fuels," Environment International, vol. 138, May 2020, doi: 10.1016/j.envint.2020.105670.

[7] L. Sun, J. Zhang, C. Ducruet, H. Itoh, and X. Liu, "The impact of shipping activities on air quality and residents' health in China's port cities," Journal of Transport Geography, vol. 123, 2025, doi: 10.1016/j.jtrangeo.2024.104099.

[8] A. Barbagallo, V. Torrisi, S. Ricci, E. Twrdy, and M. Ignaccolo, "Assessing ship emissions: An estimation approach applied to the Port of Catania (Italy)," in Proc. Int. Conf. Computational Science and Its Applications, Istanbul, Türkiye, 2025, doi: 10.1007/978-3-031-97660-5_9.

[9] L. Styhre, H. Winnes, J. Black, J. Lee, and H. Le-Griffin, "Greenhouse gas emissions from ships in ports—Case studies in four continents," Transportation Research Part D: Transport and Environment, vol. 54, pp. 212–224, Jul. 2017, doi: 10.1016/j.trd.2017.04.033.

[10] L. Fredianelli, T. Gaggero, M. Bolognese, D. Borelli, F. Fidecaro, C. Schenone, and G. Licitra, "Source characterization guidelines for noise mapping of port areas," Heliyon, vol. 8, no. 3, Mar. 2022, doi: 10.1016/j.heliyon.2022.e09021.

[11] A. K. Paschalidou, P. Kassomenos, and F. Chonianaki, "Strategic noise maps and action plans for the reduction of population exposure in a Mediterranean port city," Science of the Total Environment, vol. 654, pp. 144–153, Mar. 2019, doi: 10.1016/j.scitotenv.2018.11.048

[12] C. Ducruet, B. P. Martin, M. A. Sene, M. L. Prete, L. Sun, H. Itoh, and Y. Pigné, "Ports and their influence on local air pollution and public health: A global analysis," Science of the Total Environment, vol. 819, 2024, doi: 10.1016/j.scitotenv.2024.170099.

[13] N. E. Hassan, "Noise pollution and its effects on human health: A review," EPRA International Journal of Multidisciplinary Research, vol. 10, no. 11, Nov. 2024, doi: 10.36713/epra2013.

[14] European Environment Agency, "Environmental noise and impacts on human health," Sep. 29, 2025. [Online]. Available: https://www.eea.europa.eu/en/europe-environment-2025/thematic-briefings/environment-and-human-health/environmental-noise-and-impacts-on-human-health

[15] L. R. Iglesias, E. G. Vazquez, V. S. López, and E. Dopico, "Citizen science on maritime traffic: Implications for European eel conservation," Oceans, vol. 6, no. 50, 2025, doi: 10.3390/oceans6030050.

[16] Z. Wan, A. Nie, J. Chen, C. Pang, and Y. Zhou, "Transforming ports for a low-carbon future: Innovations, challenges, and opportunities," Ocean & Coastal Management, vol. 264, May 2025, doi: 10.1016/j.ocecoaman.2025.107636.

[17] European Commission, Greening of European Sea Ports—Final Report. Mar. 2024, doi: 10.2832/3479075.

[18] European Sea Ports Organisation, "Top 10 environmental priorities," 2025. [Online]. Available: https://www.ecoports.com/publications/top-10-environmental-priorities-2025

[19] European Sea Ports Organisation, "ESPO Environmental Report," 2025. [Online]. Available: https://www.espo.be/media/esp-0135_sustainability-report-2025.pdf

[20] European Sea Ports Organisation, "A net-zero, smart, resilient, and competitive Europe: Europe's ports are part of the solution," 2024. [Online].Available:https://www.espo.be/media/ESPO%20memorandum%20%20%20priorities%20-%20Elections%202024_3.pdf

[21] Interreg Maritime IT-FR, "CLASTER—Compatibilità e Sostenibilità Rumore portuale," [Online]. Available: https://interreg-marittimo.eu/web/claster

[22] Interreg Euro-MED Programme, "EnerCmed—Testing energy-community and climate-resilient integrated solutions," [Online]. Available: https://enercmed.interreg-euro-med.eu/

[23] D. Borelli, T. Gaggero, E. Rizzuto, and C. Schenone, "Holistic control of ship noise emissions," vol. 3, pp. 107–119, Apr. 2016, doi: 10.1515/noise-2016-0008.

[24] S. Schiavoni, G. Baldinelli, A. Presciutti, and F. D'Alessandro, "Acoustic mitigation of noise in ports: An original methodology for the identification of intervention priorities," Noise Mapping, vol. 9, pp. 211–226, doi: 10.1515/noise-2022-0159.

[25] IT-FR Interreg Maritime, "RUMBLE—Réduction du bruit dans les grandes villes portuaires dans le programme maritime transfrontalier," [Online]. Available: https://interregmaritime.eu/documents/781707/6821944/T3.4.1+Valutazione+conclusiva+_It.pdf/c1fbf43b-ec6c-474e-9b0e-1caa01984c7f?t=1643297012167

[26] Interreg Maritime IT-FR, "DECIBEL—Dépollution acoustique des centres portuaires urbains et insulaires," [Online]. Available: https://interreg-maritime.eu/documents/772201/0/T2.3.2+-+CATALOGUE+BONNE+PRATIQUE.pdf

[27] M. Economidou, V. Todeschi, P. Bertoldi, D. D'Agostino, P. Zangheri, and L. Castellazzi, "Review of 50 years of EU energy efficiency policies for buildings," Energy and Buildings, vol. 225, Oct. 2020, doi: 10.1016/j.enbuild.2020.110322.

[28] N. Skandalos and D. Karamanis, "Decarbonizing operational emissions in urban neighborhoods with the integration of rooftop photovoltaics and green infrastructure under current and future climate conditions," Energy and Buildings, vol. 329, Feb. 2025, doi: 10.1016/j.enbuild.2025.115306.

[29] M. Bera, S. Das, Gautam Chatterjee, "Advancing energy efficiency: Innovative technologies and strategic measures for achieving net-zero emissions," Carbon Footprints, vol. 4, no. 3, Jan. 2025, doi: 10.20517/cf.2024.48.

[30] European Commission, Joint Research Centre, "Delivering the EU Green Deal: Progress towards targets," 2025. [Online]. Available: https://joint-researchcentre.ec.europa.eu/publications-and-data-0_en

[31] European Environment Agency, Environmental Noise in Europe 2025. Luxembourg: Publications Office of the European Union, Jun. 2025, doi: 10.2800/2287869.

[32] World Health Organization, Compendium of WHO and Other UN Guidance in Health and Environment—Update, 2024. [Online]. Available: https://www.who.int/publications/i/item/9789240095380

[33] Eurofound, European Quality of Life Survey 2016: Quality of Life, Quality of Public Services, and Quality of Society. Luxembourg: Publications Office of the European Union, 2017. [Online]. Available: https://www.eurofound.europa.eu/en/publications/2018/european-quality-life-survey-2016

[34] European Commission, "Environmental Noise Directive," [Online]. Available: https://environment.ec.europa.eu/topics/noise/environmental-noise-directive_en

[35] European Parliament and Council, "Directive 2002/49/EC of the European Parliament and of the Council of 13 June 2002 relating to the assessment and management of environmental noise," Jun. 2002. [Online]. Available: https://eur-lex.europa.eu/eli/dir/2002/49/oj

[36] Joint Research Centre, "Common Noise Assessment Methods in Europe (CNOSSOS-EU)," Sep. 12, 2012. [Online]. Available: https://publications.jrc.ec.europa.eu/repository/handle/JRC72550

[37] "Art. 884 del Regio Decreto 16 marzo 1942, n. 262," [Online]. Available: https://www.normattiva.it/

[38] "Regio Decreto 19 ottobre 1930, n. 1398," Jul. 1931. [Online]. Available: https://www.normattiva.it/

[39] "Legge 26 ottobre 1995, n. 447—Legge quadro sull'inquinamento acustico," Dec. 1995. [Online]. Available: https://www.normattiva.it/

[40] "Decreto Legislativo 17 febbraio 2017, n. 42," Apr. 2017. [Online]. Available: https://www.normattiva.it/

[41] UNI, "UNI/TS 11844:2022—Procedure for intrusive noise measurements and analysis," Mar. 2022. [Online]. Available: https://store.uni.com/

[42] Ministero dell'Ambiente e della Sicurezza Energetica, "Decreto 5 agosto 2024—Criteri ambientali minimi per infrastrutture stradali," Aug. 2024. [Online]. Available: https://www.gazzettaufficiale.it/

[43] UNI, "UNI EN ISO 11819-2:2017—Acoustics—Measurement of the influence of road surfaces on traffic noise—Part 2," Jun. 2017. [Online]. Available: https://store.uni.com/

[44] "Decreto-Legge 1 marzo 1991, n. 60," Mar. 1991. [Online]. Available: https://www.normattiva.it/

[45] Regione Liguria, "Legge Regionale 20 marzo 1998, n. 12—Disposizioni in materia di inquinamento acustico," Mar. 1998. [Online].

[46] Regione Toscana, "Legge Regionale 1 dicembre 1998, n. 89—Norme in materia di inquinamento acustico," Dec. 1998. [Online].

[47] Regione Toscana, "Regolamento 8 gennaio 2014, n. 2/R—Attuazione della legge regionale n. 89/1998," Jan. 2014. [Online].

[48] EcoPorts, "NoMEPorts—Noise Management in European Ports," [Online]. Available: https://www.ecoports.com/

[49] Interreg Maritime IT-FR, "MON ACUMEN—Monitorage Actif Conjoint Urbain-Maritime de la Nuisance," [Online]. Available: https://interreg-maritime.eu/

[50] Interreg Maritime IT-FR, "REPORT—Rumore e porti," [Online]. Available: https://interreg-maritime.eu/

[51] C. Schenone, I. Pittaluga, D. Borelli, W. Kamali, and Y. E. Moghrabi, "The impact of environmental noise generated from ports: Outcome of MESP project," Noise Mapping, pp. 26–36, Feb. 2016, doi: 10.1515/noise-2016-0002

[52] M. Casazza, F. Boggia, G. Serafino, V. Severino, and M. Lega, "Environmental impact assessment of an urban port: Noise pollution survey in the port area of Napoli (S Italy)," Environmental Accounting and Management, vol. 6, 2018, doi: 10.5890/JEAM.2018.06.004.

[53] L. Fredianelli, M. Bernardini, F. D'Alessandro, and G. Licitra, "Sound power level and spectrum of port sources for environmental noise mapping," Ocean Engineering, vol. 306, Aug. 2024, doi: 10.1016/j.oceaneng.2024.118094.

[54] S. Schiavoni, F. D'Alessandro, D. Borelli, and L. Fredianelli, "Airborne sound power levels and spectra of noise sources in port areas," International Journal of Environmental Research and Public Health, 2022, doi: 10.3390/ijerph191710996.

[55] H. Mollenhauer et al., "Long-term environmental monitoring infrastructures in Europe: Observations, measurements, scales, and socio-ecological representativeness," Science of the Total Environment, vol. 624, pp. 968–978, May 2018, doi: 10.1016/j.scitotenv.2017.12.095.

[56] European Commission, “Advanced noise control strategies in harbour (ANCHOR LIFE project),” 2022. [Online]. Available: https://webgate.ec.europa.eu/life/publicWebsite/project/LIFE17-GIE-IT-000562.

[57] S. Schiavoni et al., “Guidelines for a common port noise impact assessment: The ANCHOR LIFE project,” Noise Mapping, vol. 9, pp. 89–108, 2022, doi: 10.1515/noise-2022-0006.

[58] R. M. Martinez et al., “A review of acoustic imaging methods using phased microphone arrays,” 2019, doi: 10.1007/s13272-019-00383-4.

[59] IEC, “IEC 61672-2:2013—Electroacoustics—Sound level meters—Part 2: Pattern evaluation tests,” 2013. [Online]. Available: https://webstore.iec.ch/

[60] IEC, “IEC 61672-3:2013—Electroacoustics—Sound level meters—Part 3: Periodic tests,” 2013. [Online]. Available: https://webstore.iec.ch/

[61] GFaI Tech GmbH, “Star48 AC Pro—48-channel system for outdoor measurements,” [Online]. Available: https://www.gfaitech.com/

[62] J. A. Bocanegra et al., “Acoustic camera measurements of moving cargo ships in the Port of Livorno,” in Proc. Int. Congress on Sound and Vibration, Amsterdam, Netherlands, 2024.

[63] J. A. Bocanegra, D. Borelli, T. Gaggero, E. Rizzuto, and C. Schenone, “A novel approach to port noise characterization using an acoustic camera,” Science of the Total Environment, 2022, doi: 10.1016/j.scitotenv.2021.151903.

[64] J. A. Bocanegra, D. Borelli, and C. Schenone, “Acoustic camera ship noise measurements during docking operations: A case study in Genoa,” in Proc. Int. Congress on Sound and Vibration, Singapore, 2022.

[65] ISO, “ISO 2922:2020—Acoustics—Measurement of airborne sound emitted by vessels on inland waterways and harbours,” 2020. [Online]. Available: https://www.iso.org/

[66] ISO, “ISO 14509-1:2008—Small craft—Airborne sound emitted by powered recreational craft,” 2008. [Online]. Available: https://www.iso.org/

[67] L. Fredianelli et al., “Source characterization guidelines for noise mapping of port areas,” Heliyon, vol. 8, no. 3, Mar. 2022, doi: 10.1016/j.heliyon.2022.e09021.

[68] J. A. B. Cifuentes, D. Borelli, E. Pallavidino, and C. Schenone, “Noise sources evaluation of a Ro-Pax ship by means of an acoustic camera: A case study in Nice,” in Proc. Int. Congress on Sound and Vibration, Prague, Czech Republic, 2023.

[69] Ministero dell’Ambiente e della Sicurezza Energetica, “Decreto 5 agosto 2024—Minimum environmental criteria for road infrastructure,” Aug. 2024. [Online].

[70] UNI, “UNI EN ISO 11819-2:2017—Measurement of the influence of road surfaces on traffic noise,” 2017. [Online].

[71] J. Ciucci, C. Detotto, C. Idda, and D. Prunetti, “The impact of port noise on residents’ willingness to pay,” in Proc. Regional Science Association International, New Orleans, USA, 2024.

[72] T. Istamto, D. Houthuijs, and E. Lebret, "Willingness to pay to avoid health risks from road-traffic-related air pollution and noise," Science of the Total Environment, vol. 497–498, pp. 420–429, Nov. 2014, doi: 10.1016/j.scitotenv.2014.07.110.

[73] ARPAL, "Agenzia Regionale per la Protezione dell'Ambiente Ligure—Rumore," [Online]. Available: https://www.arpal.liguria.it/

[74] ISTAT, "Istituto Nazionale di Statistica," [Online]. Available: https://www.istat.it/

[75] Comune della Spezia, "Piano di zonizzazione acustica comunale," Nov. 2024. [Online].

[76] C. Detotto and D. Prunetti, "CLASTER—Compatibilità e sostenibilità rumore portuale," [Online].

[77] X. Sagartzazu, L. H. Nieto, and J. M. Pagalda, "Review in sound absorbing materials," Archives of Computational Methods in Engineering, vol. 15, 2007, doi: 10.1007/s11831-008-9022-1.

[78] T. J. Cox and P. D'Antonio, "Absorption mechanisms and characteristics," in Acoustic Absorbers and Diffusers: Theory, Design and Application, 2nd ed. Boca Raton, FL, USA: CRC Press, 2009, pp. 156–159.

[79] T. J. Cox and P. D'Antonio, "Material types," in Acoustic Absorbers and Diffusers: Theory, Design and Application, 2nd ed. Boca Raton, FL, USA: CRC Press, 2009, pp. 160–169.

[80] T. J. Cox and P. D'Antonio, "Resonant absorbers," in Acoustic Absorbers and Diffusers: Theory, Design and Application, 2nd ed. Boca Raton, FL, USA: CRC Press, 2009, pp. 196–240.

[81] M. Liu, X. Wang, and F. Xin, "Sound absorption of acoustic resonant absorbers with rough oblique perforations," Applied Acoustics, vol. 217, Feb. 2024, doi: 10.1016/j.apacoust.2023.109828.

[82] J. P. Arenas, V. Marin, and R. Venegas, "Membrane sound absorber with a granular activated carbon infill," Applied Acoustics, vol. 202, Jan. 2023, doi: 10.1016/j.apacoust.2022.109180.

[83] S. Dogra and A. Gupta, "Design, manufacturing, and acoustical analysis of a Helmholtz resonator-based metamaterial plate," Acoustics, vol. 3, no. 4, pp. 630–641, Oct. 2021, doi: 10.3390/acoustics3040040.

[84] S. H. Park, "Acoustic properties of micro-perforated panel absorbers backed by Helmholtz resonators," Journal of Sound and Vibration, vol. 332, pp. 4895–4911, Sep. 2013, doi: 10.1016/j.jsv.2013.04.029.

[85] R. S. D. Amarilla et al., "Acoustic barrier simulation of construction and demolition waste: A sustainable approach to environmental noise control," Applied Acoustics, vol. 182, Nov. 2021, doi: 10.1016/j.apacoust.2021.108201.

[86] E. T. Paris, "Sound absorption coefficients measured by reverberation and stationary-wave methods," Proceedings of the Royal Society, vol. 115, pp. 407–419, 1927.

[87] P. Bonfiglio and F. Pompoli, "Caratterizzazione sperimentale dei materiali per la modellazione vibro-acustica in edilizia," 2008.

[88] UNI, "UNI EN ISO 10534-2:2024—Determination of acoustic properties in impedance tubes," Mar. 2024. [Online].

[89] J. D. McIntosh, M. T. Zuroski, and R. F. Lambert, "Standing wave apparatus for measuring acoustic material properties," Journal of the Acoustical Society of America, vol. 88, no. 4, pp. 1929–1938, Oct. 1990, doi: 10.1121/1.400216.

[90] O. Doutres, Y. Salissou, N. Atalla, and R. Panneton, "Evaluation of acoustic and non-acoustic properties using a three-microphone impedance tube," Applied Acoustics, vol. 71, no. 6, pp. 506–509, Jun. 2010, doi: 10.1016/j.apacoust.2010.01.007.

[91] F. Pompoli and P. Bonfiglio, Assorbimento acustico: Teoria, tecniche di misura e simulazione. Ferrara, Italy.

[92] K. H. Or, P. Azma, and M. Z. Selamat, "Oil palm empty fruit bunch fibres as sustainable acoustic absorbers," Applied Acoustics, vol. 119, pp. 9–16, Apr. 2017, doi: 10.1016/j.apacoust.2016.12.002.

[93] Y. Salissou, R. Panneton, and O. Doutres, "Complement to standard method for measuring normal incidence sound transmission loss," Journal of the Acoustical Society of America, 2012, doi: 10.1121/1.3681016.

[94] F. Pompoli and P. Bonfiglio, "Tecniche avanzate di caratterizzazione fisico-acustica di materiali porosi," in Associazione Italiana di Acustica, Milan, Italy, 2008.

[95] A. Nilsson, S. Baro, and E. A. Piana, "Vibro-acoustic properties of sandwich structures," Applied Acoustics, vol. 139, pp. 259–266, Oct. 2018, doi: 10.1016/j.apacoust.2018.04.039.

[96] E. Moosavimehr and A. S. Phani, "Sound transmission loss of sandwich panels with a truss lattice core," Journal of the Acoustical Society of America, vol. 141, no. 4, pp. 2921–2932, Apr. 2017, doi: 10.1121/1.4979934.

[97] C. W. Isaac, M. Pawełczyk, and S. Wrona, "Comparative study of sound transmission losses of sandwich composite double panel walls," Applied Sciences, vol. 10, no. 4, Feb. 2020, doi: 10.3390/app10041543.

[98] M. Neri, E. Levi, E. Cuerva, and F. P. Bosch, "Sound-absorbing and insulating low-cost panels from end-of-life household materials," Applied Sciences, vol. 11, no. 12, Jun. 2021, doi: 10.3390/app11125372.

[99] F. C. Sgard, X. Olny, N. Atalla, and F. Castel, "On the use of perforations to improve the sound absorption of porous materials," Applied Acoustics, vol. 66, no. 6, pp. 625–651, Jun. 2005, doi: 10.1016/j.apacoust.2004.09.008.

[100] X. Olny and C. Boutin, "Acoustic wave propagation in double porosity media," Journal of the Acoustical Society of America, vol. 114, no. 1, pp. 73–89, Jul. 2003, doi: 10.1121/1.1534607.

[101] F. Xin, X. Ma, X. Liu, and C. Zhang, "A multiscale theoretical approach for sound absorption of slit-perforated double-porosity materials," Composite Structures, vol. 223, Sep. 2019, doi: 10.1016/j.compstruct.2019.110919.

[102] M. K. Williams et al., "High-performance polyimide foams," in Fire and Polymers, 2001, pp. 49–62, doi: 10.1021/bk-2001-0797.ch005.

[103] Y. Z. Zhang et al., "Properties and microstructure of polyimide foam plastic," Cellular Polymers, vol. 29, no. 4, pp. 211–226, Jul. 2010, doi: 10.1177/026248931002900401.

[104] C. I. Cano et al., "Polyimide foams from powder: Experimental analysis of diffusion phenomena," Polymer, vol. 46, no. 22, pp. 9296–9303, Oct. 2005, doi: 10.1016/j.polymer.2005.07.056.

[105] S. Song, Y. Shi, J. Tan, Z. Wu, M. Zhang, S. Qiang, J. Nie and H. Liu, "An efficient approach to fabricate lightweight polyimide/aramid sponge with excellent heat insulation and sound absorption performance," Journal of Industrial and Engineering Chemistry, vol. 109, pp. 404-412, May 2022, doi: 10.1016/j.jiec.2022.02.027.

[106] X. Ren, J. Wang, G. Sun, S. Zhou, J. Liu and S. Han, "Effects of structural design including cellular structure precision controlling and sharp holes introducing on sound absorption behavior of polyimide foam," Polymer Testing, vol. 84, Apr. 2020, doi: 10.1016/j.polymertesting.2020.106393.

[107] X. Hou, R. Zhang, and D. Fang, "Flexible, fatigue resistant, and heat-insulated nanofiber-assembled polyimide aerogels with multifunctionality," Polymer Testing, vol. 81, Jan. 2020, doi: 10.1016/j.polymertesting.2019.106246.

[108] X. Zhang, W. Li, P. Song, B. You and G. Sun, "Double-cross-linking strategy for preparing flexible, robust, and multifunctional polyimide aerogel," Chemical Engineering Journal, vol. 381, Feb. 2020, doi: 10.1016/j.cej.2019.122784.

[109] W. Ye, G. Lin, W. Wu, P. Geng, X. Hu, Z. Gao and J. Zhao, "Separated 3D printing of continuous carbon fiber reinforced thermoplastic polyimide," Composites Part A, vol. 121, pp. 457–464, Apr. 2019, doi: 10.1016/j.compositesa.2019.04.002.

[110] W. Gu, G. Wang, M. Zhou, T. Zhang, and G. Ji, "Polyimide-based foams: Fabrication and multifunctional applications," ACS Applied Materials & Interfaces, vol. 12, no. 43, pp. 48246–48258, Oct. 2020, doi: 10.1021/acsami.0c15771.

[111] X.-Y. Liu, M.-S. Zhan, and K. Wang, "Influence of foam structure and service environment on sound absorption characteristics of polyimide foams," High Performance Polymers, vol. 24, no. 7, pp. 646–653, Nov. 2012, doi: 10.1177/0954008312448073.

[112] X.-H. Ren, G.-H. Sun, L.-C. Wang, R.-R. Chen, and J. Wang, "Facile adjusting for cells of lightweight isocyanate-based polyimide foam and operable combination between distinctive acoustic foams for higher performance," Chinese Journal of Polymer Science, vol. 39, no. 2, pp. 237–248, Feb. 2021, doi: 10.1007/s10118-020-2482-y.

[113] O. Doutres, N. Atalla, R. Wulliam, S. Ferguson, and S. Bailey, "Optimization of the acoustic performance of polyimide foams," in Proc. Inter-Noise, 2011.

[114] R. J. Silcox, R. J. Cano, B. Howerton, B. J. Stuart, and N. N. Kim, "Development of polyimide foam for aircraft sidewall applications," in Proc. AIAA Conference, 2013, doi: 10.2514/6.2013-213.

[115] O. Doutres, N. Atalla, M. Brouillette, and C. Hébert, "Using shock waves to improve the sound absorbing efficiency of closed-cell foams," Applied Acoustics, vol. 79, pp. 110–116, May 2014, doi: 10.1016/j.apacoust.2013.12.022.

[116] D. Borelli, I. Pittaluga, C. Schenone, M. Ghirlanda, and F. Stretti, "Use of innovative composite materials and foam for noise control on board ships," in Proc. International Conference on Noise Control Engineering, Jul. 2015.

[117] D. B. Callaway and L. Ramer, "The use of perforated facings in designing low-frequency resonant absorbers," The Journal of the Acoustical Society of America, vol. 24, no. 3, 1952, doi: 10.1121/1.1906897.

[118] K. P. Byrne, "Calculation of the specific normal impedance of perforated facing–porous backing constructions," Applied Acoustics, vol. 13, no. 5, pp. 377–389, 1980, doi: 10.1016/0003-682X(80)90042-0.

[119] B. Yoan, T. You, and H. Jiang, "Prediction of the sound absorption performance for micro-perforated panels based on machine learning," Engineering and Applied Science, 2025, doi: 10.1186/s44147-025-00598-9.

[120] U. Ingard, "On the theory and design of acoustic resonators," The Journal of the Acoustical Society of America, vol. 25, no. 6, 1953, doi: 10.1121/1.1907235.

[121] W. H. Chen, F. C. Lee, and D. M. Chiang, "On the acoustic absorption of porous materials with different surface shapes and perforated plates," Journal of Sound and Vibration, vol. 237, no. 2, pp. 337–355, 2000, doi: 10.1006/jsvi.2000.3029.

[122] J. W. Strutt, The Theory of Sound, vols. 1–2. New York, NY, USA: Dover Publications, 1926.

[123] I. B. Crandall, Theory of Vibrating Systems and Sound. New York, NY, USA: D. Van Nostrand Company, 1926.

[124] D. Y. Maa, "Microperforated-panel wideband absorbers," Noise Control Engineering Journal, vol. 29, no. 3, pp. 77–84, 1987, doi: 10.3397/1.2827694.

[125] N. Atalla and F. C. Sgard, "Modeling of perforated plates and screens using rigid frame porous models," Journal of Sound and Vibration, vol. 303, no. 1–2, pp. 195–208, Jun. 2007, doi: 10.1016/j.jsv.2007.01.012.

[126] A. Jadhav and V. S. Jadhav, "A review on 3D printing: An additive manufacturing technology," Materials Today: Proceedings, 2022, doi: 10.1016/j.matpr.2022.02.558.

[127] Z. Liu, J. Zhan, M. Fard, and J. L. Davy, "Acoustic properties of multilayer sound absorbers with a 3D-printed micro-perforated panel," Applied Acoustics, vol. 121, pp. 25–32, 2017, doi: 10.1016/j.apacoust.2017.01.032.

[128] Y. J. King and K. K. Teo, "Application of 3D-printed structured materials as sound absorption panels," in IOP Conference Series: Earth and Environmental Science, vol. 463, 2020, doi: 10.1088/1755-1315/463/1/012032.

[129] M. R. Khosravani and T. Reinicke, "Experimental characterization of 3D-printed sound absorbers," European Journal of Mechanics - A/Solids, vol. 89, 2021, doi: 10.1016/j.euromechsol.2021.104304.

[130] A. Arjunan, A. Baroutaji, and A. Latif, "Acoustic behaviour of 3D-printed titanium perforated panels," Results in Engineering, vol. 11, 2021, doi: 10.1016/j.rineng.2021.100252.

[131] J. A. Bocanegra, D. Borelli, E. Pallavidino, C. Schenone, J. Peshku, and others, “Effect of geometrical parameters on sound absorption in perforated plates with elliptical holes,” in Proc. Int. Congress on Sound and Vibration, 2024.

[132] J. A. Bocanegra, M. Misale, C. Schenone, and D. Borelli, “Geometric correction factor for elliptic holes in perforated plates and its role in sound absorption coefficient,” in Forum Acusticum, Lyon, France, 2020, doi: 10.48465/fa.2020.0971.

[133] F. Pompoli and P. Bonfiglio, “Tecniche avanzate di caratterizzazione fisico-acustica di materiali porosi,” in Proc. Associazione Italiana di Acustica, Milan, Italy, 2008.

[134] B. N. Algueró, “Growth in the docks: Ports, metabolic flows and socio-environmental impacts,” Sustainable Science, vol. 15, no. 3, pp. 1–20, 2019, doi: 10.1007/s11625-019-00764-y.

[135] P. Nastos and H. Saaroni, “Living in Mediterranean cities in the context of climate change: A review,” International Journal of Climatology, 2024, doi: 10.1002/joc.8546.

[136] D. Streimikiene, V. Lekavičius, T. Baležentis, G. L. Kyriakopoulos, and J. Abrhám, “Climate change mitigation policies targeting households in the European Union,” Energies, vol. 13, no. 13, 2020, doi: 10.3390/en13133389.

[137] European Commission, “The European Green Deal,” [Online]. Available: https://commission.europa.eu/

[138] European Union, “Directive (EU) 2023/2413 of the European Parliament and of the Council on the promotion of the use of energy from renewable sources,” 2023. [Online].

[139] European Commission, “Energy system integration,” [Online]. Available: https://energy.ec.europa.eu/

[140] Ministero dell’Ambiente e della Sicurezza Energetica, “Decreto CER,” Dec. 2023. [Online].

[141] Italian Republic, “Decreto Legislativo 8 novembre 2021, n. 199—Attuazione della direttiva (UE) 2018/2001,” 2021. [Online].

[142] A. Panori, N. Komninos, D. Latinopoulos, I. Papadaki, E. Gkitsa, and P. Tarani, “Blending nature with technology: Integrating nature-based solutions with renewable energy systems,” Designs, vol. 9, no. 3, 2025, doi: 10.3390/designs9030060.

[143] G. Yiasoumas, L. Berbakov, V. Janev, A. Asmundo, E. Olabarrieta, A. Vinci, G. Baglietto, and G. E. Georghiou, “Key aspects and challenges in the implementation of energy communities,” Energies, vol. 16, no. 12, 2023, doi: 10.3390/en16124703.

[144] S. R. Asl, “Re-powering nature-intensive systems: Insights from linking nature-based solutions and energy transition,” Frontiers in Sustainable Cities, vol. 4, 2022, doi: 10.3389/frsc.2022.860914.

[145] R. Mendonça, P. Roebeling, T. Fidélis, and M. Saraiva, “Socio-economic models and policy instruments for nature-based solutions,” in Sustainable City, Ancona, Italy, 2021, doi: 10.2495/SC210451.

[146] S. Rafael, L. P. Correia, A. Ascenso, B. Augusto, D. Lopes, and A. I. Miranda, "Are green roofs the path to clean air and low-carbon cities?" Science of the Total Environment, vol. 798, Dec. 2021, doi: 10.1016/j.scitotenv.2021.149313.

[147] S. Ahmed, A. Ali, and A. D'Angola, "A review of renewable energy communities: Concepts, scope, progress, challenges, and recommendations," Sustainability, vol. 16, no. 5, Feb. 2024, doi: 10.3390/su16051749.

[148] B. A. Mantegazzini, L. Wangen, and C. Clastres, "Energy communities in Europe: Regulatory and economic perspectives," Economics and Policy of Energy and Environment, pp. 5–23, 2022, doi: 10.3280/EFE2022-002001.

[149] J. A. Bocanegra et al., "EnerCmed project: Combining energy communities and nature-based solutions for Mediterranean cities," International Journal of Energy and Environment, vol. 8, no. 6, pp. 1197–1205, Dec. 2025, doi: 10.56578/ijei080607.

[150] D. Al Kez, A. Foley, C. Lowans, and D. F. Del Rio, "Energy poverty assessment: Indicators and implications," Energy Conversion and Management, vol. 307, May 2024, doi: 10.1016/j.enconman.2024.118324.

[151] T. A. de Bruin, "Optimising renewable energy communities," Feb. 2025, doi: 10.4337/9781802208870.00027.

[152] J. Peshku, J. A. Bocanegra, et al., "D1.3.1—Terms of reference for REC development," Jun. 2025. [Online]. Available: https://enercmed.interreg-euro-med.eu/what-we-achieve/

[153] J. De Zeeuw and A. Reeman, "Vulnerable people in social impact assessment," in Social Impact Assessment and Management, 2024, pp. 258–273, doi: 10.4337/9781802208870.00027.

[154] EnerCmed Project, "RECs: Technical aspects of PV plant design and installation," Mar. 2025. https://enercmed.interreg-euro-med.eu/knowledge-sharing-platform/

[155] European Parliament and Council, "Directive (EU) 2018/2001 on the promotion of the use of energy from renewable sources," 2018. https://eur-lex.europa.eu/eli/dir/2018/2001/oj

[156] European Parliament and Council, "Directive (EU) 2019/944 on common rules for the internal market for electricity," 2019. https://eur-lex.europa.eu/eli/dir/2019/944/oj

[157] Italian Republic, "Decreto del Presidente della Repubblica 26 agosto 1993, n. 412," 1993. https://www.normattiva.it/

[158] Comune di Genova, "Cartografie del Comune di Genova." https://consultazionepraticheedilizia.comune.genova.it/frontend/

[159] National Renewable Energy Laboratory (NREL), "OpenStudio v3.9.0 SDK." https://openstudio.net/

[160] Trimble Inc., "OpenStudio SketchUp plug-in." https://extensions.sketchup.com/extension/ec07ca64-fb93-4d9d-89d6-4f2dc9a1dc6c/0

[161] Italian Republic, “Decreto del Presidente della Repubblica 26 agosto 1993, n. 412—Regolamento per impianti termici negli edifici,” 1993. https://www.normattiva.it/uri-res/N2Ls?urn:nir:presidente.repubblica:decreto:1993-08-26;412

[162] UNI, “UNI/TS 11300-1:2014—Prestazioni energetiche degli edifici: Determinazione del fabbisogno di energia termica,” 2014. https://store.uni.com/uni-ts-11300-1-2014

[163] UNI, “UNI EN ISO 10456:2008—Building materials and products: Hygrothermal properties,” 2008. https://store.uni.com/uni-en-iso-10456-2008

[164] UNI, “UNI EN ISO 6946:2018—Thermal resistance and transmittance of building elements,” 2018. https://store.uni.com/en/uni-en-iso-6946-2018

[165] UNI, “UNI EN 12464-1:2021—Lighting of workplaces: Indoor workplaces,” 2021. https://store.uni.com/en/uni-en-12464-1-2021

[166] UNI, “UNI EN ISO 10211:2018—Thermal bridges in building construction,” 2018. https://store.uni.com/en/uni-en-iso-10211-2018

[167] Ministero dell’Ambiente e della Sicurezza Energetica, “Decreto 28 ottobre 2025—Aggiornamento delle metodologie di calcolo delle prestazioni energetiche degli edifici,” 2025. https://www.gazzettaufficiale.it/eli/id/2025/12/05/25A06487/SG

[168] Namirial S.p.A., “Termo v.6.5 software.” https://www.edilizianamirial.it/software-certificazione-energetica/

[169] UNI, “UNI/TS 11300-2:2019—Energy performance of buildings: Primary energy and system efficiencies,” 2019. https://store.uni.com/en/uni-ts-11300-2-2019

[170] UNI, “UNI/TS 11300-3:2010—Energy performance of buildings: Cooling systems,” 2010. https://store.uni.com/en/uni-ts-11300-3-2010

[171] UNI, “UNI/TS 11300-4:2016—Energy performance of buildings: Renewable energy systems,” 2016. https://store.uni.com/en/uni-ts-11300-4-2016

[172] D. Borelli, A. Cavalletti, P. Cavalletti, J. Peshku and L. A. Tagliafico, "A methodology to evaluate the optimal insulation thickness for heating and cooling needs in different climatic zones for buildings made of reinforced concrete with cavity walls," Heliyon, vol. 10, no. 10, 30 May 2024, doi: 10.1016/j.heliyon.2024.e30653.

[173] UNI, “UNI 10339:1995, Impianti aeraulici ai fini di benessere—Generalità, classificazione e requisiti,” 1995.

https://store.uni.com/uni-10339-1995

[174] Italian Republic, “Decreto 26 giugno 2015, schemi e modalità di riferimento per la compilazione della relazione tecnica di progetto ai fini dell’applicazione delle prescrizioni e dei requisiti minimi di prestazione energetica negli edifici,” 2015. https://www.gazzettaufficiale.it/atto/serie_generale/caricaDettaglioAtto/originario?atto.dataPubblicazioneGazzetta=2015-07-15&atto.codiceRedazionale=15A05199

[175] UNI, "UNI EN ISO 13788:2013, Hygrothermal performance of building components and building elements—Internal surface temperature to avoid critical surface humidity and interstitial condensation—Calculation methods," 2013. https://store.uni.com/en/uni-en-iso-13788-2013

[176] UNI, "UNI EN ISO 13790:2008, Energy performance of buildings—Calculation of energy use for space heating and cooling," 2008. https://store.uni.com/en/uni-en-iso-13790-2008

[177] Ministero dell'Ambiente e della Sicurezza Energetica, "Avviso di avvenuta pubblicazione del decreto n. 414 del 7 dicembre 2023, recante: 'Individuazione di una tariffa incentivante per impianti a fonti rinnovabili inseriti in REC e ISC singolo e collettivo'," 2024. https://www.gazzettaufficiale.it/eli/id/2024/02/07/24A00671/sg

[178] Gestore dei Servizi Energetici (GSE), "Appunti di Energia—REC," Apr. 2024. https://www.rse-web.it/wp-content/uploads/2024/04/06_CER-inglese.pdf

[179] Gestore dei Servizi Energetici (GSE), "Le comunità energetiche rinnovabili in pillole." https://www.gse.it/servizi-per-te/autoconsumo/le-comunita-energetiche-rinnovabili-in-pillole

[180] Gestore dei Servizi Energetici (GSE), "Mappa interattiva delle cabine primarie." https://www.gse.it/servizi-per-te/autoconsumo/mappa-interattiva-delle-cabine-primarie

[181] Gestore dei Servizi Energetici (GSE), "Decreto CACER e TIAD—Regole operative per l'accesso al servizio per l'autoconsumo diffuso e al contributo PNRR," 2022. https://www.rinnovabili.it/wp-content/uploads/2025/03/ALLEGATO-1-Regole-Operative-CACER.pdf

[182] HexErgy, "HexErgy 2.12.28." https://hexergy.app/

[183] ARERA, "Analisi dei prelievi di energia elettrica dei clienti domestici," 2024. https://reporting.arera.it/SASVisualAnalytics/?reportUri=%2Freports%2Freports%2Fff58199d-f010-4cfd-a5d1-32c1d6359c05&sso_guest=true&reportViewOnly=true&reportContextBar=false&sas-welcome=false

[184] ARERA, "Analisi dei prelievi di energia elettrica dei clienti." https://reporting.arera.it/SASVisualAnalytics/?reportUri=%2Freports%2Freports%2F4abc549e-0f55-4b56-a905-7478a58e9201&sso_guest=true&reportViewOnly=true&reportContextBar=false&sas-welcome=false

[185] Regione Liguria, "Vincoli architettonici, archeologici, paesaggistici—Regione Liguria." https://srvcarto.regione.liguria.it/geoapps/viewer/pages/apps/vincoli/

[186] ARERA, "Prelievo dei clienti non domestici in BT per provincia—Istruzione—Scuola primaria." https://reporting.arera.it/SASVisualAnalytics/?reportUri=%2Freports%2Freports%2F4abc549e-0f55-4b56-a905-7478a58e9201&sso_guest=true&reportViewOnly=true&reportContextBar=false&sas-welcome=false

[187] European Commission, “Commission Recommendation of 18 June 2019 on the draft integrated National Energy and Climate Plan of Italy covering the period 2021–2030 (2019/C 297/12),” Official Journal of the European Union, Sep. 2019. https://eur-lex.europa.eu/legal-content/EN/TXT/PDF/?uri=CELEX:32019H0903(12)

[188] European Parliament and Council, “Directive (EU) 2024/1275 of 24 April 2024 on the energy performance of buildings,” Official Journal of the European Union, May 2024. https://eur-lex.europa.eu/legal-content/EN/TXT/?uri=OJ:L_202401275

[189] P. A. Fokaides and A. M. Papadopoulos, “Cost-optimal insulation thickness in dry and mesothermal climates: Existing models and their improvement,” Energy and Buildings, vol. 64, pp. 203–212, Jan. 2014, doi: 10.1016/j.enbuild.2013.09.006

[190] X. Gong, Y. Akashi, and D. Sumiyoshi, “Optimization of passive design measures for residential buildings in different Chinese areas,” Building and Environment, vol. 58, pp. 46–57, 2012, doi: 10.1016/j.buildenv.2012.06.014.

[191] D. Mazzeo, G. Oliveti, and N. Arcuri, “Influence of internal and external boundary conditions on the decrement factor and time lag heat flux of building walls in steady periodic regime,” Applied Energy, vol. 164, pp. 509–531, Feb. 2016, doi: 10.1016/j.apenergy.2015.11.076.

[192] ISTAT, “Consumi energetici delle famiglie 2021,” 2022. https://www.istat.it/it/files/2022/06/REPORT-CONSUMI-ENERGETICI-FAMIGLIE-2021-DEF.pdf

[193] Statista, “Demand for air conditioners in Italy from 2012 to 2021,” Nov. 2025. https://www.statista.com/statistics/721653/ac-demand-units-italy/

[194] I. Ballarini and V. Corrado, “Analysis of the building energy balance to investigate the effect of thermal insulation in summer conditions,” Energy and Buildings, vol. 52, pp. 168–180, Sep. 2012, doi: 10.1016/j.enbuild.2012.06.004.

[195] L. Valentin, M. Dabbagh, and M. Krarti, “Benefits of switchable insulation systems for residential buildings in France,” Energy and Buildings, vol. 259, Mar. 2022, doi: 10.1016/j.enbuild.2022.111868.

[196] L. Brackney, A. Parker, D. Macumber, and K. Benne, Building Energy Modeling with OpenStudio, Jan. 2018, doi: 10.1007/978-3-319-77809-9.

[197] N. An et al., “From building information modeling to building energy modeling: Optimization study for efficient transformation,” Buildings, vol. 14, no. 8, Aug. 2024, doi: 10.3390/buildings14082444.

[198] T. L. Garwood, B. R. Hughes, M. R. Oates, D. O’Connor, and R. Hughes, “A review of energy simulation tools for the manufacturing sector,” Renewable and Sustainable Energy Reviews, vol. 81, pp. 895–991, Jan. 2018, doi: 10.1016/j.rser.2017.08.063.

[199] V. K. Arya, E. O. Rasheed, and D. A. S. Samarasinghe, “A simulation-based study of classroom IAQ and thermal comfort performance across New Zealand’s six climate zones,” Buildings, vol. 15, no. 12, May 2025, doi: 10.3390/buildings15121992.

[200] L. Qin, M. Zhou, W. Shi, H. Guan, and X. Fan, “Research on comprehensive energy saving of rural residential buildings in severe cold regions,” Journal of Basic Science, vol. 28, no. 1, pp. 67–80, Feb. 2020, doi: 10.16058/j.issn.1005-0930.2020.01.007.

[201] R. Zahedi, S. Daneshgar, O. N. Farahani, and A. Alireza, “Thermal analysis model of a building equipped with a green roof and its energy optimization,” Nature-Based Solutions, vol. 3, Dec. 2023, doi: 10.1016/j.nbsj.2023.100053.

[202] J. A. Bocanegra, J. Peshku, C. Schenone, P. Mouzourides, G. Alexandrou, and M. K.-A. Neophytou, “Performance of green roofs in the Mediterranean region: A numerical study based on energy balance,” in E3S Web of Conferences, vol. 654, 2025, doi: 10.1051/e3sconf/202565401003.

[203] O. Kaynakli, “A review of the economical and optimum thermal insulation thickness for building applications,” Renewable and Sustainable Energy Reviews, vol. 16, no. 1, pp. 415–425, Jan. 2012, doi: 10.1016/j.rser.2011.08.006.

[204] M. K. Özturan and A. K. Seyhan, “Determination of optimum insulation thickness of building walls according to four main directions considering solar radiation,” Energy and Buildings, vol. 304, Jan. 2024, doi: 10.1016/j.enbuild.2023.113871.

[205] R. Dylewski and J. Adamczyk, “Optimum thickness of thermal insulation with both economic and ecological costs of heating and cooling,” Energies, vol. 14, no. 13, Jun. 2021, doi: 10.3390/en14133835.

[206] UNI, “UNI EN ISO 14025:2010—Environmental labels and declarations: Type III environmental declarations,” 2010.

https://store.uni.com/en/uni-en-iso-14025-2010

[207] UNI, “UNI EN 15804:2021—Sustainability of construction works: Environmental product declarations,” 2021. https://store.uni.com/en/uni-en-15804-2021

[208] Italian Republic, “Legge 9 gennaio 1991, n. 10—"Norme per l'attuazione del Piano energetico nazionale in materia di uso razionale dell'energia, di risparmio energetico e di sviluppo delle fonti rinnovabili di energia,” 1991. https://www.gazzettaufficiale.it/eli/id/1991/01/16/091G0015/sg

[209] Gestore dei Servizi Energetici (GSE), “Conto Termico 3.0,” 2025. https://www.gse.it/servizi-per-te/efficienza-energetica/conto-termico-3-0